HELICOPTER NOISE SYMPOSIUM

SEPTEMBER 28-30, 1971

DURHAM'S HOTEL AND MOTEL

DURHAM NORTH CAROLINA

Sponsored by:

U. S. Army Research Office—Durham

American Helicopter Society, Incorporated

HELICOPTER NOISE SYMPOSIUM

Sponsored by:
U. S. Army Research Office—Durham
American Helicopter Society, Incorporated

SEPTEMBER, 1971

FOREWORD

In these days much of the interest and activity of scientists, engineers and even laymen is directed toward the elimination of those by-products of an exploding population and burgeoning technology that are detrimental to the health and well being of the populace. One hears much of the man-made perturbations of the ecology and the environment. One hears even more about those elements contributing to those perturbations; elements such as air, water and solid pollutants.

Among these problems is another which has received less attention but in terms of its insidious effects may approach the others in importance. This is the ever present intrusion upon the conscious and maybe upon the subconscious human mind of sound. Not the sound of the mountain brook or symphony but the random and raucous cacophony produced by much of our technology in action. Except when such sound evidences itself in abnormal frequencies and amplitudes, one is not conscious that we live with it continuously. What effect it has on our serenity and our ability to concentrate is probably not too well known. Nevertheless, if we are to have a well-balanced and tranquil life, it is necessary that we understand how such undesirable vibrations are initiated, how they influence our lives and what we can do to suppress or eliminate them.

This meeting devoted to the source and suppression of sounds associated with a single type of aerial vehicle is not directed toward the more general subject but it is hoped that the information evolving from these efforts will be applied to the specific case of the vehicle in question and will at the same time make a worthwhile contribution to the resolution of the larger, more comprehensive problem.

TABLE OF CONTENTS

TABLE OF CONTENTS (Continued)

INTRODUCTION

In 1968, scientists of the United States Army Research Office, Durham, North Carolina (ARO-D), and members and staff of the National Academy of Sciences and National Academy of Engineering, identified an urgent need for renewed effort toward suppression of helicopter and V/STOL noise in military operations. Academy studies also noted that short-haul commercial aviation was expected to grow rapidly over the next few years with increasing noise abatement problems.

Subsequently, a conference on the subject of helicopter and V/STOL noise generation and suppression was jointly sponsored on July 30-31, 1968 by ARO-D and the National Academy of Sciences and National Academy of Engineering. An NAS-NAE report entitled, "Helicopter and V/STOL Noise Generation and Suppression", November 1968, summarized the findings of this conference and identified important areas of research.

In response to the findings of the July 1968 assessment meeting, ARO-D initiated in July 1969, a Helicopter Noise Investigation Program with six new projects. At the inception of this program, a coordination meeting was held at ARO-D to encourage the free exchange of information between participants and to integrate the efforts of various researchers. An ARO-D report entitled, "Army Helicopter Noise Investigation Program", September 1969, gave summaries of the work to be performed on the ARO-D projects, three AVLABS projects, two other relevant ARO-D projects, and the in-house research efforts of the Army Aeronautical Research Laboratory.

Since the Helicopter Noise Program has been in operation approximately two years, it was felt that a good professional look at the whole program

was required at this time. Thus, a symposium in which recognized experts in the helicopter noise field would participate has been organized. Primary researchers from ten ARO-D-sponsored contracts and five other groups presented papers on the subject of helicopter noise. In addition, helicopter noise research at two U. S. Army Air Mobility R & D Laboratories (AAMRDL), at NASA Langley Research Center, and at the Office of the Chief of Research and Development (OCRD) was discussed.

This report includes all formal papers presented at the Helicopter Noise Symposium held in Durham, North Carolina, on September 29-30, 1971. Although much cross correlation and discussion between helicopter noise researchers was encouraged, this report was handed to each symposium attendee as the official proceedings and no discussion could be included herein.

ROTARY WING ACOUSTIC RESEARCH

AT THE AMES DIRECTORATE OF THE

U.S. ARMY AIR MOBILITY RESEARCH & DEVELOPMENT LABORATORY

The research in aircraft noise which is being conducted by the U. S. Army Air Mobility Research & Development Laboratory is almost exclusively related to rotary wing vehicle noise. Although some effort is going into lift-fan noise reduction, the majority of the work addresses aerodynamically generated rotary wing noise. The Army's primary objective (Slide 1) to be obtained through this noise reduction research program is to minimize aircraft detection time and distance on present and future V/STOL aircraft. The minimization of crew station cabin noise and the minimization of the annoyance of Army aircraft operations to the surrounding communities are two additional goals. These objectives are being achieved through efforts which are fundamental in nature and are directed primarily at understanding and reducing the noise sources.

ROTARY WING ACOUSTIC RESEARCH

PROGRAM GOAL

- UNDERSTANDING AND ELIMINATION / REDUCTION OF ROTARY WING NOISE MECHANISMS

ARMY'S DIRECT INTERESTS

- DEFINE AND MINIMIZE DETECTABILITY
- MINIMIZE CABIN NOISE
- MINIMIZE THE ANNOYANCE OF ARMY AIRCRAFT TO THE SURROUNDING COMMUNITY

Slide 1

The Ames Directorate of AMRDL is located at NASA's Ames Research Center, (Slide 2) Moffett Field, California. Under an agreement for joint participation between NASA and the Army, the staffs of both organizations perform jointly in accomplishing research of mutual interest. Exchange of manpower and fiscal resources is included.

Slide 2

The Ames Directorate has concentrated its efforts on four basic areas of acoustic research which are listed in Slide 3. They are basic acoustic theory, helicopter and V/STOL noise reduction, systems studies of noise-performance tradeoffs, and acoustic wind tunnel investigations. A quick review of each subject area will now be presented in order to outline the extent of the Ames Directorate's research effort.

ACOUSTIC RESEARCH

- BASIC ACOUSTIC THEORY
- HELICOPTER AND V/STOL NOISE REDUCTION
- SYSTEMS STUDIES OF NOISE-PERFORMANCE TRADEOFFS
- ACOUSTIC WIND TUNNEL INVESTIGATIONS

Slide 3

The first area of research, entitled "Basic Acoustic Theory," addresses the fundamentals of the generation and measurement of aerodynamic sound. Under a study contract with Stanford University, the sound produced by a vortex interacting with a rigid flat plate airfoil is being explored. A simple two-dimensional analysis of the vortex-wing interaction has been developed to assess the importance of the induced vortex's motion on the generation of noise (Slide 4).

TWO DIMENSIONAL VORTEX-AIRFOIL INTERACTION

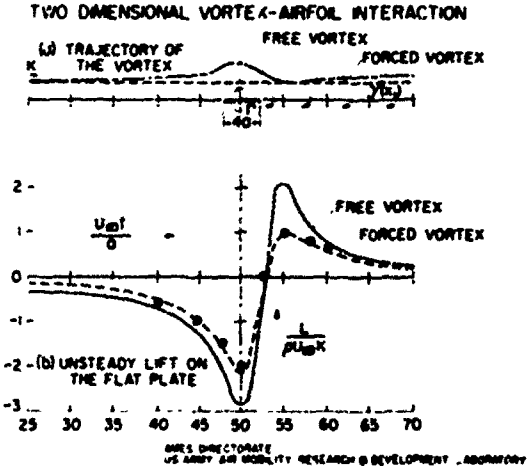

Slide 4

As the vortex passes the rigid airfoil, it is allowed to follow its own trajectory as determined by the wing-vortex interaction. In previous investigations, the motion of this vortex has been restricted to move parallel to the airfoil. Preliminary results indicate that the additional sound produced by allowing the vortex to move along its own trajectory is significant.

Another research effort has commenced to try, and develop techniques which can be used to predict the far acoustic field from selected near-field pressure measurements. This theoretical study is being performed in-house and is designed for potential application in the Ames 40X80 Foot Wind Tunnel.

The second major area of rotary wing acoustic research is helicopter and V/STOL noise prediction and reduction. Most of the programs in this area are being performed in-house.

One particularly annoying feature of helicopter flight is the occurance of impulsive noise in certain flight regimes. Theoretical and experimental programs are being pursued in an effort to try to understand the parameters which are important in the generation of this type of noise. At high advancing tip Mach numbers, significant increases in level and harmonic content of rotor noise have been noticed. Data which was gathered in the NASA-Ames 40X80 Foot Wind Tunnel in which noise was measured on a full-scale helicopter rotor showed a rapid increase in sound pressure level with increasing tip Mach number when operating in the transonic range (Slide 5). Poor correlation between theory and experiment was noted when operating in this range.

EFFECTS OF ADVANCING TIP MACH NUMBER

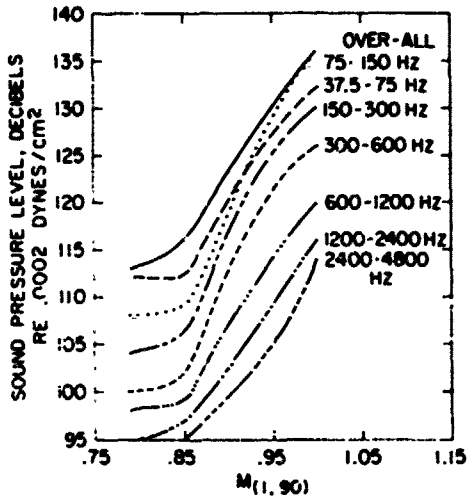

Slide 5

Including the noise due to compressibility drag, however, significantly improved the correlation between theory and experiment. (Slide 6).

CALCULATED AND MEASURED SOUND PRESSURED LEVEL VS HARMONIC NUMBER

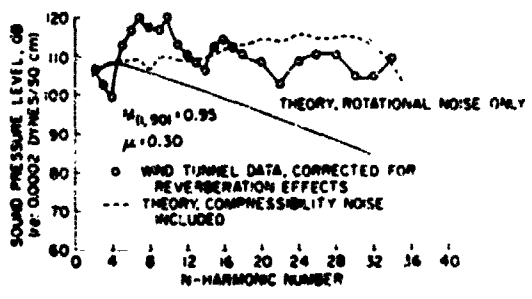

AMES DIRECTORATE
US ARMY AIR MOBILITY RESEARCH & DEVELOPMENT LABORATORY

Slide 6

Blade slap (impulsive noise) is also thought to occur when the blade of a rotor interacts with the tip vortex of the preceding blade. It was noted in data collected from previous full-scale wind tunnel investigations of helicopter noise that distinct spikes in the sound pressure level data were occurring at locations which corresponded to potential blade vortex interactions. Tests have now been conducted in the AMRDL-Ames 7X10 Foot Wind Tunnel using a 50-inch diameter model rotor. Stop-action photographs showing top and side views of several stages of vortex interaction are shown in Slide 7. The

TIP VORTEX TRAJECTORY OF A TWO-BLADED HINGELESS ROTOR

RPM=850, $\mu = 0.2$, $\theta_c = 12°$

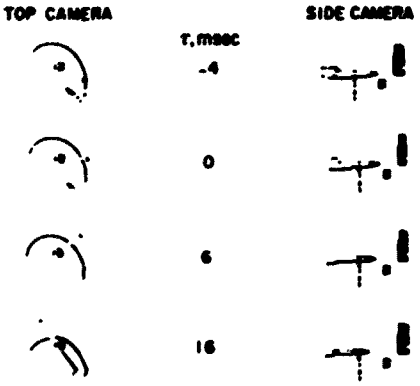

Slide 7

objectives of this test were to correlate the hypothesized blade vortex interactions with the sound pressure level recordings. Results of this investigation have not been completely satisfying. The primary problem which was encountered was correlating the sound pressure level recordings and the film data. Work is currently being conducted on obtaining better data acquisition and analysis equipment and developing more sophistic ted techniques for providing this correlation.

An in-house research effort to correlate the latest available theoretical predict' chniques with experimental noise data is being pursued. .. program related to this effort is one in which an attempt is being made to verify and extend loading laws which have been postulated previously for use in the prediction of rotary wing rotational noise. Under a previous Army supported effort, a theoretical method was developed by Lowson and Ollerhead for the purpose of predicting aerodynamically generated noise. A drawback to the developed theory was the requirement for very detailed aerodynamic loading information and this required detail is not available for rotary wing vehicles today. Recognizing this, the investigators analyzed integrated aerodynamic pressure data which was available and hypothesized a loading law to be used in lieu of the required detailed aerodynamic input. Under the current program, detailed blade loading data and far field acoustic data have been simultaneously recorded. This data was obtained from wind tunnel experiments over a wide range of operating parameters. Results from this program are just becoming available. It is anticipated that this data will yield part of the information which is required to establish blade loading laws over a wide range of operating parameters

and that this loading law information can then be used to provide more accurate predictions for the rotational component of rotary wing aerodynamically generated noise. Data from this program will be augmented with data being taken under a present NASA-Army program at the Langley Research Center. Simultaneous blade pressure data and acoustic measurements are being taken on full-scale helicopter blades operating on the NASA-Langley Whirl Tower Facility.

In cooperation with NASA, a limited effort also exists to understand and predict lift-fan noise. Some concepts actively being investigated include the use of a serrated leading edge to reduce fluctuating lift noise and stator lean to reduce rotor-stator interaction noise.

The last area of research which can be classified under the heading of helicopter and V/STOL noise prediction and reduction is entitled rotor acoustic synthesis. This program is just beginning. Its primary objective is to develop a method of synthesizing audible sound in order to a) verify analytical noise analysis by comparison of analytically produced synthetic noise and actual measured noise, and b) predict noise characteristics of future aircraft or of modifications to existing aircraft. The significance of this effort lies in the immediate elimination of existing subjective noise judgements. The ear will be given the opportunity to judge the characteristics of the analytically generated noise. Such a technique will enable quantitative evaluation of rotary wing operational and design tradeoffs to ascertain the more important acoustical characteristics of proposed designs prior to experimental testing.

Systems studies of V/STOL noise is the third area of active research. As implied previously, the most direct and effective way of alleviating the rotary wing noise problem is to eliminate the source. This, however, may not be feasible. Therefore, ways and means of reducing aircraft noise through system design and/or a judicious selection of flight paths are being investigated. The current in-house effort, which was initiated under an Army-NASA contract with Boeing-Vertol, consists of the optimization of the trajectory of a tilt-rotor aircraft

TRAJECTORY OPTIMIZATION OF A TILT-ROTOR AIRCRAFT WITH NOISE CONSTRAINTS

TASK OBJECTIVES

- EXPLORE, THEORETICALLY, MINIMUM TIME AND FUEL TRAJECTORIES OF A TILT-ROTOR AIRCRAFT DURING TAKEOFF AND LANDING WITH STRUCTURAL, AERODYNAMIC, TRAJECTORY, AND NOISE CONSTRAINTS
- BETTER DEFINE THE AREAS WHERE THEORETICAL AND/OR EXPERIMENTAL RESEARCH NEEDS TO BE CONCENTRATED
- TRY TO ESTABLISH AND MINIMIZE MEANINGFUL SUBJECTIVE NOISE CRITERIA WHICH EVALUATE TOTAL AIRCRAFT OPERATIONAL NOISE

Slide 8

with noise constraints. (Slide 8). The objectives of the initial program were to explore on a theoretical basis the minimum time and the fuel trajectories of a tilt-rotor aircraft during the takeoff and landing phases of flight with structural, aerodynamic, and noise constraints. Secondary objectives were to define areas of research where theoretical and experimental effort needs to be concentrated, as well as establish and minimize meaningful subjective noise criteria which evaluate total aircraft operational noise. Currently, the emphasis is being placed upon using this theoretical study to assess methods of reducing tilt-rotor detectability through flight path control.

This program has involved the development of both a theoretical performance and far-field acoustic model of a tilt-rotor aircraft

ACOUSTIC MODEL OF A TILT-ROTOR AIRCRAFT

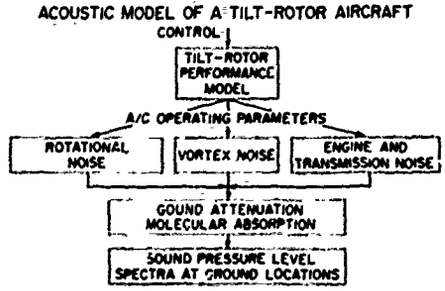

ROTATIONAL NOISE PREDICTION OF A TILTING ROTOR IN NON-AXIAL FLIGHT MODIFICATION OF OLLERHEAD & LOWSON HELICOPTER ROTATIONAL NOISE PREDICTION TECHNIQUE (HERON II). BLADE LOADING LAWS WILL BE CORRELATED WITH PERFORMANCE PARAMETERS (I.E., INFLOW)
VORTEX NOISE: EMPIRICALLY FITTED DATA
ENGINE NOISE: EMPIRICALLY FITTED DATA

Slide 9

(Slide 9). In the acoustic model, rotational noise and vortex noise were considered and found to be dominant over engine and transmission noise. The rotational noise was predicted from a modified version of Lowson and Ollerhead's method for predicting helicopter rotational noise. The program previously mentioned regarding the generation of blade loading law information is being incorporated into this model. The blade loading laws postulated by the previous investigators are not suitable for the wide range of operating conditions experienced by a tilt-rotor aircraft. In this model, vortex noise is predicted using empirically fitted data.

A typical noise abatement takeoff profile that might be flown by

EFFECTIVE PERCEIVED NOISE LEVEL VERSUS DISTANCE ALONG THE FLIGHT PATH

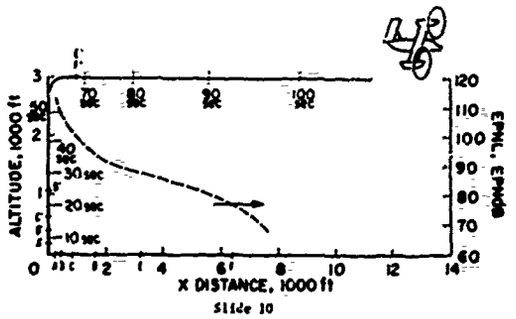

Slide 10

a commercial tilt-rotor aircraft is illustrated in Slide 10. A purely vertical takeoff trajectory is flown to an altitude of 3000 feet to reduce the noise exposure near a hypothetical takeoff site. An observer located at the three locations, A, C, and E, which correspond to distances of 200, 800, and 3200 feet from the takeoff point would hear the maximum sound pressure level curve illustrated in Slide 11. Rotational and vortex noise components are discernible in each case. The effects of atmospheric absorption included in the model are noticeable at the higher harmonics where they drop off rapidly as distance is increased.

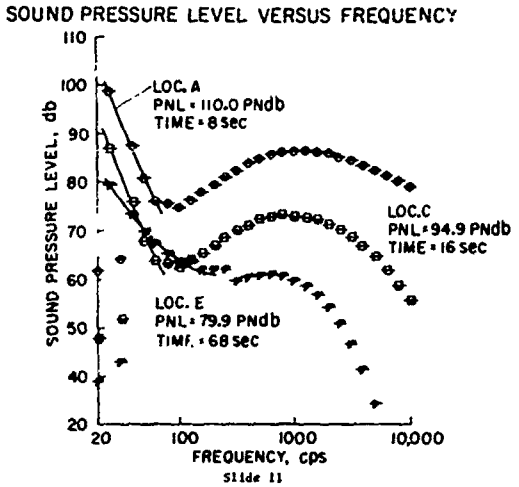

Slide 11

Although the first phase of this effort is complete, a similar in-house theoretical study of other rotary wing V/STOL configurations is planned. Emphasis will be placed upon understanding the operational tradeoffs which are possible with V/STOL aircraft through flight trajectory management.

The last area of research to be reviewed is acoustic wind tunnel investigations. The Army has embarked upon several in-house programs to determine the feasibility of using the wind tunnel to gather acoustic data. This effort is required to help develop an adequate supply of accurate V/STOL acoustic data which has been taken under carefully controlled test conditions.

Unfortunately, taking acoustic data in the confines of a wind tunnel is not an easy task. In some tunnels it may not be possible to accurately re-produce the acoustic characteristics of free-field noise. Reverberation effects, tunnel fan noise, and boundary layer noise may make it difficult, if not impossible, to distinguish model generated noise from tunnel background noise.

An in-house program to survey the acoustic properties of the Ames Directorate's own 7X10 Foot Wind Tunnel (Slide 12) is nearing

Slide 12

completion. Preliminary results indicate that the amplification factor of the tunnel is both a strong function of frequency and microphone location in the tunnel. Thus it will be necessary to acoustically treat the tunnel to make quantitative rotary wing noise measurements that can be corrected to free field conditions. At the present time, the Ames Directorate is supporting a research contract with Penn State University to explore various alternative means to improve the acoustical characteristics of the 7X10 Foot Subsonic Wind Tunnel.

The 40X80 Foot Wind Tunnel (Slide 13) is also being used to take

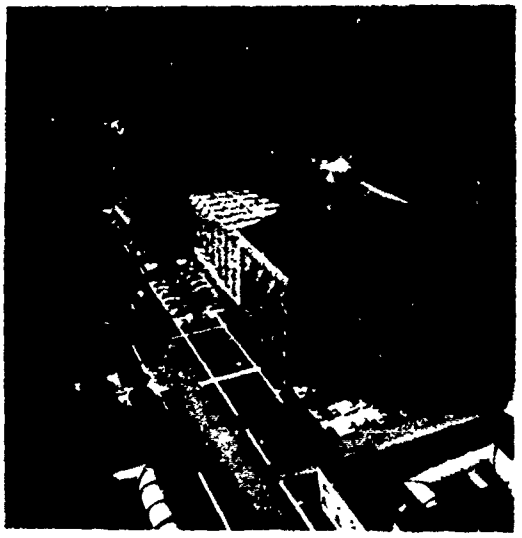

Slide 13

acoustic data on full scale aircraft. One third octave band amplification factors have been established for the tunnel and the personnel there have a policy of taking noise measurements for all tests. Meaningful quantitative acoustic data has been taken in the confines of the tunnel illustrating both broad acoustic trends and the effects of incremental design and operational changes on the acoustical characteristics of several V/STOL aircraft. Acoustic measurements will be taken by NASA on both the OV-10 (Slide 14) and XV-5 (Slide 15) aircraft in the

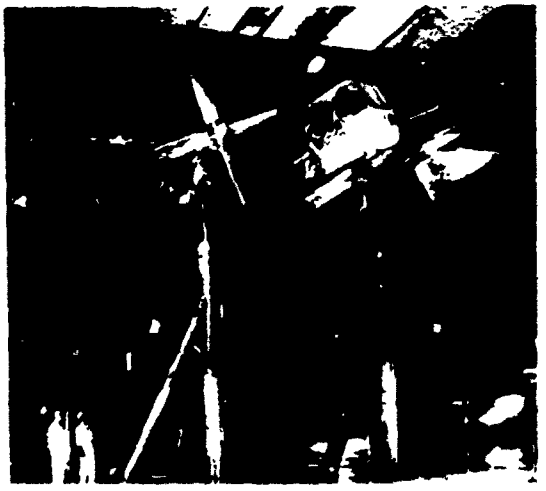

Slide 14

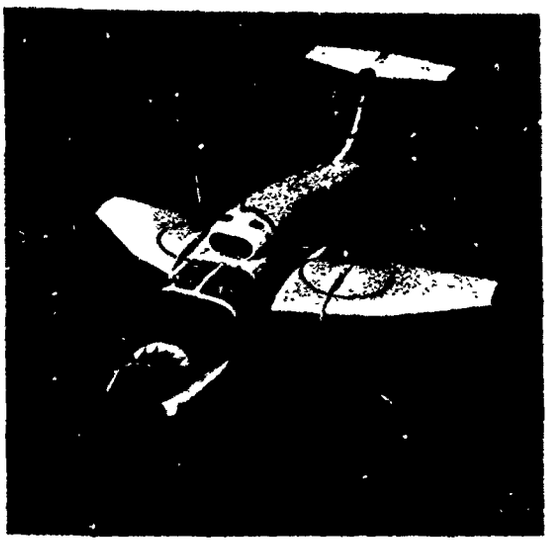

Slide 15

NASA 40X80 Foot Wind Tunnel Unfortunately, because of the amplification factor's apparent dependence upon sound source and microphone position, some uncertainty as to the validity of data which has been corrected to free-field conditions still exists

Summary of Helicopter Noise Research at Eustis Directorate,

U.S. Army Air Mobility R&D Laboratory

by:

John E. Yeates, Chief, Aeromechanics Division
William E. Nettles, Aerospace Engineer
William T. Alexander, Aerospace Engineer

Helicopter noise research has been underway at Eustis Directorate since about 1960 and numerous reports reporting the results have been published.

The present report treats only those research efforts that are just being completed or are now in progress.

Summary of the following research studies will cover five general areas.

a. Tip vortex noise

b. Shed vortex and rotational noise

c. Internal noise (transmission, engine, etc.)

d. Tail rotor noise

e. Measurement & detection of noise

1. INVESTIGATION OF THE REDUCTION OF BLADE TIP VORTICES AND NOISE DUE TO ROTOR WAKE/BLADE INTERACTION, BY AIR INJECTION AT THE BLADE TIP

Summary: Subject effort is being performed by RASA under Contract DAAJ02-71-C-0036. The program is essentially an experimental investigation to determine the practicality of introducing a mass of air into the tip vortex core of a rotating rotor blade, as a means of modifying or dissipating the vortex. Essential to the conduct of this study will be the measurement of influential parameters, and both visual and optical (photographic) recording of blade tip and vortex flow patterns in the University of Maryland 8' X 11' Wind Tunnel. Improved discernment of flow patterns is expected by application of new hydrogen bubble techniques. The test model will be a full scale helicopter blade tip with the span properly sized to fit the wind tunnel test section. A few of the parameters that will be studied are angle of attack, mass injection rate, location and size of mass injection, lift, drag, vorticity distribution, etc. Their effects on the coupling characteristics of the trailed vortices and the aerodynamic flow of the model will be investigated.

Finally, all data will be analyzed to determine if tip injection is a practical means for eliminating the vortex without compromising rotor performance.

NOTE: Completion date: January 1972.

2. INVESTIGATION OF THE VORTEX NOISE PRODUCED BY A HELICOPTER ROTOR

Summary: The objective of this program was twofold. The first part was to develop an advanced capability to accurately analyze the more subtle components of helicopter noise, in particular, the broad band or vortex noise. The second part consisted of the development of an explicit analyses to predict rotor vortex noise based on a correlation of the vortex noise components with a shed vortex analysis. That is, instead of being satisfied with empirical curves fit to what is nominally called vortex noise as had been done in the past, an attempt was made to predict vortex noise based on a specific aerodynamic source.

The effectiveness of this research required the development of a digital band pass filter for analyzing noise records. This computer program, based on Fourier transform techniques, provided a narrow digital filter which accurately calculated both amplitude and phase of the noise components. This digital technique also allowed close control of the specific sample of the noise signature selected for analysis, an item of particular importance where the noise has a transient quality.

In the second phase of this program, this filter was used to extract the vortex noise from selected signatures. The noise was examined and correlated with shed vortex calculations. The correlation results were used with existing noise analysis theory, and an analytical technique was developed for predicting the helicopter vortex noise signature.

The resulting analyses were used to study the basic character of vortex noise produced by the helicopter rotor. One point of particular interest was the ability to reproduce on magnetic tape a vortex noise pattern which could readily be identified as a helicopter noise signature although rotational noise was not present. While the results of this work have not yet been fully reported or evaluated, it is anticipated that these findings will produce a significant new capability to analyze and understand the quality of helicopter noise.

NOTE: This work has just been completed under Contract DAAJ02-70-C-0023 with Rochester Applied Sciences Associates (RASA). Final report to be distributed about December 1971.

3. DEVELOPMENT OF A TECHNIQUE FOR REALISTIC PREDICTION AND ELECTRONIC SYNTHESIS OF HELICOPTER ROTOR NOISE

Objective: Extend current analytical prediction technique for rotor broad-band noise to include rotational noise and develop a method of simulating the noise signature of a helicopter from the predicted noise force constants.

Approach:

a. Develop an acoustical data bank (controlled data, i.e., whirl tower, flight test, etc.)

b. Extract rotational noise from the broad-band noise (using method developed under Contract DAAJ02-70-C-0023)

c. Extend RASA analytical prediction technique to include rotational noise.

d. Develop technique for converting predicted noise into analog acoustic tapes.

e. Evaluate effectiveness of noise prediction and simulation methods by comparing predicted results with experimental data.

Summary: RASA, under Contract DAAJ02-70-C-0026, developed an analytical technique for predicting the acoustical signature of a helicopter rotor. This method, however, only accounted for the broad band (boundary layer) oscillatory noise. The current study is designed to expand this tool to include derivation of the force constants for rotational noise. The technique will be designed to predict noise of a rotor using such parameters as: number of blades, blade chord, blade thickness, blade twist, rotational speed, forward velocity, aircraft weight, and aircraft attitude.

In attacking this problem, the Contractor will research and catalog all noise data considered accurate and applicable to the task. Selected data will then be converted from analog to digital form to permit separation of the rotational from the broad band (vortex) noise using the extraction method developed under the above contract. The force constants derived for both noise sources (broad band & rotational) are then converted into

parametric form as functions of the above listed control parameters to form a data book.

In addition to the above, the Contractor is to investigate a means of electronically simulating rotor noise by converting the predicted digital noise signatures into analog acoustic tape. Such tapes then can be used as a design tool in subjective evaluation of a new design or planned rotor modification.

Finally, the Contractor is to test the accuracy of this design tool by correlating the predicted results with experimental data from the UH-1B and Vertol Model 347. Data will be compared as: (a) pressure time history plots, (b) noise spectrum plots, and (c) subjective evaluation of audio tapes. Further, for the HLH configuration currently under development, the Contractor will predict and provide simulated noise tapes in the same format as for above aircraft.

Upon completion of the above, the Contractor will demonstrate and instruct Army personnel in the capabilities and practical use of the design tool.

NOTE: This study is being performed under Contract DAAJ02-71-C-0064. (A 12-month effort with a completion date of June 1972)

4. INTERNAL NOISE REDUCTION (Gearbox Noise and Vibration Reduction for Rotary-Wing Aircraft

Summary: Approximately four years ago, this Directorate initiated a program with Mechanical Technology, Inc. (MTI) of New York to analytically investigate means of reducing the internal noise levels of helicopters by improved design of transmission gearing. Also, this effort was further enhanced by the possibility of achieving an extended Time Between Overhaul (TBO) as a result of reducing the dynamic force levels between drive train components. One of the achievements to result from this initial effort has been the development of analytical tools and methods of predicting noise levels of various gear trains. This Directorate now has a computer program that provides means of evaluating new transmission designs as well as proposed modifications for noise reduction.

Although some of the recommendations derived from the MTI programs have proved impractical (such as machining complicated tooth profiles) others, such as operating too near critical vibratory frequencies and having too stiff or too soft bearing supports, are proving to have merit. Many of the MTI findings are being experimentally verified through a research program now being conducted at Boeing/Vertol *(Investigation of Helicopter Transmission Noise Reduction by Vibration Absorbers).

A survey of the major airframe manufacturers and Government agencies is currently being made in-house to determine the overall status of noise reduction efforts and what is required to assure quiet helicopters of the future.

It is becoming increasingly clear and essential that a key to any successful noise reduction program is cooperative effort between the designer and acoustician during initial design and in the application of the tools now available.

*NOTE: Final Report due September 1971.

5. ADVANCED RESEARCH PROJECTS AGENCY (ARPA)-QUIET HELICOPTER PROGRAM

Summary: It is well known that the tactical use of the helicopter in Southeast Asia has been somewhat compromised by its high noise levels. That is, the element of surprise is negated by early aural detection.

In an effort to rectify this condition, ARPA recommended that three "crash" programs be initiated to prove the feasibility of quietening three operational type helicopters (the Kaman HH-43B, Sikorsky SH-3A, and Hughes OH-6A) using current technology. The Eustis Directorate, was directed to manage the technical and contractual aspects of each program. The necessity for

6

ARPA QHP

OH-6A
1 REDUCED BOTH MAIN & TAIL ROTOR RPM
2 INSTALLED LOWER SPEED TAIL ROTOR GEAR BOX
3 TWO DIFFERENT TAIL ROTORS USED (2 & 4 BLADE)

HH-43B
1 ROTOR SPEED REDUCED
2 TIP CAPS WITH SWEPT LEADING EDGES ADDED TO THE ROTOR BLADES
3 MODIFIED ENGINE TAIL PIPE
4 ADDED ACOUSTICAL BLANKETING TO REAR CABIN
5 THICKER TRANSMISSION OIL

SH-3A
1 REDUCED BOTH MAIN & TAIL ROTOR RPM
2 INCREASED MAIN ROTOR FROM 5 TO 6 BLADES
3 ADDED TRAPEZOIDAL CAPS TO MAIN ROTOR BLADE TIPS
4 INSTALLED LOWER SPEED TAIL ROTOR GEAR BOX
5 INCREASED NO OF TAIL ROTOR BLADES FROM 5 TO 10
6 TAIL PYLON WAS CAMBERED
7 LINED THE DUCTS OF ENGINE INLETS & EXHAUSTS

Figure 1

separate contracts is apparent from the responsibility given each Contractor in performing Phase I: The design, fabrication, and installation of those modifications that the Contractor felt would aid in reducing the external noise of his particular helicopter. Phase II: the evaluation phase, was the responsibility of the Government which conducted noise measurements at the Wallops Island test station "before and after" the modifications for each aircraft to determine the noise reduction achieved.

The modifications performed on each vehicle are identified in Figure 1.

Although the quantitative results of the three programs are classified, some of the conclusions that may be revealed are:

a. The tip speed of the main rotor has the most pronounced effect on the helicopter's noise signature. However, helicopter performance is compromised (forward speed, pay load, range) as a result of reducing rotor speed.

b. Mechanical sources of sound such as gearboxes, transmission, etc. are not heard until the aircraft is relatively close. Noise attenuating efforts should be directed, therefore, towards the main and tail rotors.

NOTE: A listing of papers which report on the results of the program is shown in the Appendix.

6. BASELINE NOISE MEASUREMENTS OF ARMY HELICOPTERS

Summary: The principle aims of this program are the development of a data bank of helicopter acoustic signatures and a draft specification that may be used as a standard in the test and measurement of helicopter acoustic

signatures. Initially, effort will be directed to: (1) researching current techniques employed in the measurement and analysis of acoustical data and (2) defining a total field measurement program (instrumentation, flight patterns, pertinent parameters, calibration, etc.).

The acoustic signatures were measured at Camp Pickett, Virginia for five Army helicopters, the OH-6A, UH-1B, AH-1G, CH-47B and CH-54A, during hover and flyover modes of operation. This phase is critical to the success of any measurement program because of the necessity of having reliable equipment, knowing precise position of aircraft relative to recording media, documenting all environment, instrument, aircraft descriptive data, and the recording of the aircraft noise in a manner that will assure validity and easy retrieval of the recorded data.

The data from these tests were quantitatively evaluated through narrow band analysis to define frequency distribution, harmonics, random noise, acoustic energy, etc., and identify the contributors or sources of the total aircraft noise.

Finally, the Contractor recommended procedures, equipment specs, calibrations, flight conditions, signal and recording particulars, etc., essential to the development of standardized noise data banks. The noise data, recorded on magnetic tape, will be retained in a data bank at the Eustis Directorate.

NOTE: The above effort was conducted under Contract DAAJ02-70-C-0025, with Wyle Labs. It is now complete and reported in 2 Vols, USAAMRDL TR #71-36A and 71-36B. 71-36B is classified because noise levels for the aircraft are specified.

7. HELICOPTER AURAL DETECTION

Summary: This is an analytical study designed to:

a. Determine the survivability of current tactical helicopters on the basis of their noise signatures.

b. Develop noise signature criteria for optimum helicopter survivability.

Fundamental to the analysis is that only aural detection of the helicopter will be considered as it is "flown" against hostile forces.

The program is divided into three (3) phases: Phase I, Study Definition; Phase II, Survivability Determination; and Phase III, Analysis and Results. In Phase I, those parameters that describe the tactical use of the five classes of aircraft (observation, attack, cargo, utility and heavy lift) will be defined. From this appropriate scenario/program material will be arranged to support the basic analysis. Consideration of enemy threat will be limited to aural and visual perception of the approaching helicopter by the enemy (i.e., RADAR, optical/acoustical aids are not considered in the detection).

Phase II will be devoted to the development of aural detectability contours as dictated by the helicopter noise spectra and environments. Determination of survivability will be based upon:

a. Single ground weapon vs single aircraft

b. Aircraft penetrating forward battle line

The final phase will be devoted to analyzing the helicopter aural detection patterns (contours) to determine the probability of kill from enemy fire. Recommendations will then be made as to what kill probability for each aircraft would represent an optimized survivability/mission effectiveness level. As a consequence, new optimized acoustic detectability distance contours will also be developed for each class of aircraft.

NOTE: This study is being conducted by Boeing/Vertol under Contract DAAJ02-71-C-0065. (Estimated completion date is June 1972)

Hopefully, the noise research brief presented above gives some indication of the new importance given to this area of work.

The results from the acoustics work presented above show that significant gains have been made in experimentally recording and analyzing data, the capabilities and limitations of existing instrumentation are better understood, and in many cases while new systems and techniques have evolved

In the area of theoretical analysis, major improvements have been made in defining the mechanics of the noise source. This has led to the development of aero-acoustic teams which have attacked the problem at the source and, in many cases, have demonstrated that this approach can produce significant reductions in the noise signature of a helicopter. As a result, the helicopter noise problem is no longer a secondary consideration, but is being treated by the preliminary designer in his initial conceptual layouts.

In effect, the subject of rotary wing acoustics is becoming increasingly important and is no longer simply an art, but a well defined science

APPENDIX I

Reports on the ARPA Quiet Helicopter Program

NASA-LANGLEY WORKING PAPERS:

1. #755 - Description of the Noise Measurement Program on a Standard and a Modified Kaman HH-43B Helicopter with Some Initial Results. June 6, 1969.

2. #838 - Description of the Noise Measurement Program on a Standard and Two Modified Hughes OH-6A Helicopters with Some Initial Results. Dec 23, 1969.

3. #963 - Description of the Noise Measurement Program on a Standard and the Modified Phase II Hughes OH-6A Helicopter May 26, 1971

4. #803 - Description of the Noise Measurement Program on a Standard and a Modified Sikorsky SH-3A Helicopter with Some Initial Results Sep 30, 1969.

REPORTS:

1. NASA Technical Memorandum #X-2226 - Ground Noise Measurements During Flyover, Hover, Landing and Takeoff Operations of a Standard and a Modified HH-43B Helicopter February 1971

2. Sikorsky Final Report #SER-61147A prepared under Contract DAAJ02-69-C-0020, title HUSH Final Report - Quiet Helicopter Program (S-61)

3. Hughes Final Report, HTC-AD 70-26, Contract DAAJ02-69-C-0078, title: Program to Reduce the Noise Signature of the OH-6A Helicopter

4. Kaman Final Report #R-388 of April 2, 1969, Contract DAAJ02-69-C-0019, title: Noise Reduction Program HH-43B Helicopter

NOTE: All of the above reports are classified CONFIDENTIAL.

RECENT ASPECTS OF THE ARMY'S INTEREST IN THE REDUCTION OF HELICOPTER NOISE

Richard L. Ballard
Office, Chief of Research and Development
Department of the Army

The problem of the noise signature of a helicopter is an important aspect in the consideration of the survivability of the helicopter on the battlefield. During the 1960's, the U. S. Army was involved in a war that was classified as low intensity and therefore in the area of survivability the main emphasis was placed on providing protection to the aircrews from 7.62mm (30 cal) projectiles. No real attempt was made to reduce the noise signature of the helicopter or any of the other signatures (radar, infrared, or optical). The real desire was to produce helicopters that would operate effectively against the enemy. Any changes to the design of the helicopter that reduced its ability to accomplish its main mission were not accepted. In the case of noise, no changes to reduce noise were allowed because it meant penalties in that the aircraft gross weight was increased with accompanying reduction in payload or the rotor efficiency was decreased or expensive modification to an existing fleet would be required. The Army has learned a lot about fighting with helicopters and is changing its attitudes toward survivability. The Army is now designing its aircraft (HLH, UTTAS) to operate in mid-intensity. The aircraft must be capable of withstanding hits from 12.7mm (50 cal) projectiles, and must have reduced signatures. Therefore, emphasis at the present time is to reduce noise, infrared, and radar signatures of Army aircraft.

The Army has produced a short film on the noise reduction program conducted by AFPA with the Army on the OH-6A. The research effort on the OH-6A employed a different design philosophy than previous noise reduction programs in that the design of the helicopter was for minimum noise level, regardless of the reduction in performance except that it must be able to fly.

This film showed some very remarkable results. These results are going to be used in a program for a scout helicopter. This effort brought out one very important aspect of designing helicopters for low noise signature. -- "It is possible to give the pilot the option of selecting his noise signature." For example, at home base the pilot loads the helicopter to the normal gross weight and takes off. Prior to approaching the target area, the pilot reduces the speed to that requiring the minimum horsepower and reduces the rotor RPM to about 67 percent. The noise signature is greatly reduced as well as the performance. The helicopter can continue to fly straight and level but is very limited in maneuverability. The performance has been reduced, but not the payload. When the pilot arrives in the target area and determines that he must have the performance to land or maneuver, and/or the noise signature is no longer important, the pilot can increase the rotor RPM to 100 percent. The modern Army helicopter will be using a broader definition of survivability than has previously been used, and the noise signature will be carefully considered. I am sure that in such aircraft as the HLH and UTTAS, only minor reductions in performance will be allowed for design features that will reduce the noise signature. However, in special purpose helicopters such as the aerial scout, other major changes in design may be appropriate and justified that result in significant reductions in noise signature.

VTOL NOISE RESEARCH AT THE LANGLEY RESEARCH CENTER

By

Robert J. Pegg - Langley Research Center

and

Robert M. Hosier - Langley Directorate
U. S. Army Air Mobility
Research and Development
Laboratory

SUMMARY AND ABSTRACT

A brief overview of the NASA Langley programs in VTOL noise reduction research is presented. Included are descriptions of specialized facilities relating to VTOL noise, and programs designed to explore basic theoretical concepts and to develop noise control technology for quiet vehicle designs.

INTRODUCTION

The joint NASA-USAAMRDL acoustics research program at Langley, is broadly based and diverse in nature. Included are several specific research areas relating directly to VTOL noise control, and these are outlined in figure 1. The purpose of this paper is to present brief discussions of the activities in each of these areas and in the order listed in the figure.

Specific areas of VTOL noise research include rotor blade noise reduction; the development of techniques for measuring flyover noise radiation; reciprocating engine exhaust muffling technology; human factors studies which deal primarily with the effects of noise on annoyance and task performance; and special facility developments. In this work, use is made of facilities and equipment which will be described briefly along with discussions of the associated research projects. References are made also to future facility modifications and developments now under consideration.

ROTOR BLADE NOISE REDUCTION

The sound of a rotorcraft is complex in nature since it is produced by several individual sources which may generate acoustic energy by various mechanisms. The primary emphasis in Langley VTOL noise research is centered on obtaining a more complete understanding of these generation mechanisms. An example of in-house fundamental research is the study of the effects of fluctuating blade pressures on the far field radiated noise. The significance of fluctuating forces on rotor noise has been established and is indicated in figure 2. In this figure predicted noise level due to steady rotor loads show a rapid drop off with increasing harmonic number, whereas experimental data indicate a very slow reduction. Recent theories, such as that of reference 1, which are based on fluctuating blade loads concepts, predict noise levels much closer to the experimental data. This result suggests that a prediction method based on fluctuating blade loads may be useful, particularly for the higher harmonics which are of concern for community annoyance.

The nature of the fluctuating loads theory is indicated by the formula of figure 3. The acoustic pressure harmonics, P_n, are expressed as a function of the thrust, T_n, and torque, Q_n, blade loading harmonics. The Bessel function $J_{nB\pm\ell}(nB\lambda_t \sin\theta)$ and the cosθ term define the directivity pattern associated with rotor noise whereas the term $e^{-i\ell\phi}$ represents, in complex form, the Fourier series expansion of the blade loading. The objective of one research program is the simultaneous measurement of the fluctuating loads quantities (T_n and Q_n) and the radiated noise (P_n), to validate the equation.

The above work will be carried out on the Langley whirl tower shown in figure 4. Far field noise data will be time correlated with simultaneous blade pressure measurements at several spanwise and chordwise locations. An attempt will be made to correlate the above rotary data with similar data from a two dimensional wing in a wind tunnel test at comparable Reynolds numbers. Special instrumentation of the type developed by GEN (see reference 2) will be used to measure surface pressures in the frequency range up to 1 MHz and to telemeter these data from the blade to ground based recorders. In addition to the above programs, consideration is being given to research that will evaluate the viscous dissipation of the blade core vortex and possible beneficial noise effects by means of tip air mass injection. These studies will be based on initial work performed by NASA and George Washington University (See reference 3).

FLYOVER NOISE MEASUREMENTS

Several helicopter flight test programs have been conducted at the NASA Wallops Station noise measurement range which is shown in figure 5. The range consists of an operational airstrip, located in relatively open and flat terrain. Because there is little air traffic and sparse population in the area, the ambient noise levels are generally low. All measurement procedures used at this range to measure external aircraft noise conform as closely as possible to the standards set forth in reference 4. In addition to provisions for flexible time correlated microphone arrays involving multiple mobile tape recording stations (see inset photo), there is a precision tracking radar for obtaining aircraft position, and complete meteorological facilities.

As an example of the use of this test range, a flight investigation was performed to obtain information on the noise radiation characteristics of a helicopter in forward flight and the effects of changes in aircraft operating parameters on the noise characteristics. A typical in-flight noise radiation pattern is shown in figure 6. In order to provide such results, it is necessary to time correlate all microphone channels with the helicopter position information. The helicopter used for the tests was the CH-47A single rotor, tandem powered aircraft. The results of the tests, show that the in-flight noise radiations patterns are strongly directional, the maximum noise radiation being in the direction of flight. The primary parameter that affected in-flight noise was rotor speed. Only small beneficial effects on radiated noise were associated with reduced forward speed and reduced main rotor thrust (see reference 5).

A helicopter noise measurement program sponsored by ARPA was also accomplished at the above noise measurement range. As a part of the above program the two vehicles of figure 7 were tested. The standard configuration is shown in the top photo and the modified version is shown in the bottom photo. The objective was to compare a standard helicopter with one especially modified for low external noise. It was concluded from the results of the tests that the noise reductions were substantial.

RECIPROCATING ENGINE EXHAUST MUFFLING

Piston engines have been replaced in the majority of military helicopters by less noisy gas turbine engines, but they are still used to power many small civil helicopters. Operations over congested areas by users such as police departments may require engine noise reduction.

Langley Research Center has had a sustained program to develop reciprocating engine exhaust muffler technology. The development of a muffler to a point where it can provide large noise reductions and still have acceptable weight and performance, has in the past required a lengthy "cut and try" approach. This approach has been supplemented by a newly developed, more exact, computerized muffler attenuation, evaluation, and design procedure. This program allows for such constraints as volume and size to be placed on the muffler design. The program then performs the required numerical iterations to define an expansion chamber muffler whose acoustic performance is maximized within the initial size and volume constraints.

Using the above technique, two muffler configurations shown in figure 8 have been designed and evaluated on the NASA H-13M helicopter. Typical narrow band noise spectrum results of these tests are presented in figure 9, for the hovering flight condition. The upper curve is for the basic engine, and the lower curve is representative of muffler configuration I for comparable operating conditions. A large number of noise peaks observed for the basic engine are essentially eliminated by the muffler, with an associated substantial reduction in the overall noise levels. The acoustic results for configuration II were the same as those for configuration I but the weight and back pressure were less. The results of this study also show that for the H-13 helicopter, the mufflers can be designed within acceptable size and back pressure limits, (less than 5 in. Hg).

HUMAN FACTORS

The Langley Research Center has active contractor studies in the area of human response to VTOL noise. As an example of some of this work, figure 10 illustrates the test configuration for a Sikorsky Aircraft Company study to determine the effects of combined noise and vibration stimuli on VTOL pilot performance. As is illustrated, pilots placed in a cockpit simulator are exposed to pre-recorded helicopter noise and vibrations. While being thus exposed, the pilots fly a simulated commercial air route, performing IFR navigation tasks. Pilot performance ratings are made during e" flight and post-flight questionaires are also administered. This program is still in progress and the final results are not yet available.

Another example of Langley supported psychoacoustics work is illustrated in figure 11. Shown is the test environment for a Boeing/Vertol study to determine the absolute acceptability of VTOL aircraft noise during simulated terminal area operations. Subjects are placed in the test trailer, which simulates a work and leisure environment, and asked to pursue a number of activities such as job related work, playing cards, or watching television. While the subjects are performing these activities, recorded VTOL terminal area noise records are played to them through the speaker systems for evaluation purposes. The results of this work are awaiting publication as a NASA Contractor Report.

The Langley Low Frequency Noise Facility (LFNF), shown in figure 12, provides an in-house capability to study human and structural response to VTOL noise in the frequency range below 50 Hz. Room-size structures can be placed in the noise field generated by the facility in order to evaluate the effects of low frequency noise exposure of people both inside and outside of structures.

SPECIAL FACILITIES DEVELOPMENTS

Two of the Langley subsonic wind tunnels which are ideally suited for VTOL aerodynamics research are being acoustically calibrated. Measurements are being made to determine the sound absorption treatment needed to increase the utility of the tunnels for evaluating the effects of forward velocity on rotor noise characteristics. An example of the results of this calibration work accomplished to date are shown in figures 13 and 14. Typical experimental data obtained in the evaluation of the Full Scale tunnel are shown in figure 13 where the noise levels from a calibrated acoustic source are shown as a function of distance in the tunnel test section. At the large distances, the measured noise levels approach those in the reverberant field. For the example shown, the measured values exceed those of the inverse distance law by 3 dB at a distance of about 17 feet. This is defined as the hall radius which is the limiting distance at which useable acoustic data can be obtained. A plan view sketch of the test area of this wind tunnel is shown in figure 14 and the current useable acoustics test area is shown cross hatched. Consideration is being given to the inclusion of acoustic wall treatment so that the acoustics test area can be considerably increased as indicated by the dashed lines.

Of special interest is the Aircraft Noise Reduction Laboratory now under construction at Langley and which is shown as an artists conception in figure 15. This laboratory will specifically support VTOL noise reduction research by providing for rotor noise studies at forward velocities up to 150 ft/sec. Of particular significance is the capability for testing rotor models up to 3 feet in diameter in an anechoic environment and where the tunnel noise and turbulence levels are a minimum. In addition, the laboratory will provide improved capability to quantitatively determine the effects of noise on people and for engine and exhaust noise control studies.

CONCLUDING REMARKS

The NASA/USAAMRDL research programs exploring VTOL noise from the source (rotors and engines) to the receiver (human and structural response) have been outlined. The various research facilities at which the above work is being conducted were also described. Proposed future programs were shown to provide increased emphasis on helicopter noise reduction and prediction techniques, and to include considerations of improved facility capabilities.

REFERENCES

1. Wright, S. E.: Sound Radiation From a Lifting Rotor Generated by Asymetric Disk Loading, Journal of Sound and Vibration, Vol. 9, 1969 P. 223-240.
2. Heller, Hanno H., and Widnall, Sheila E.: The Role of Fluctuating Forces in the Generation of Compressor Noise; Bolt, Beranek and Newman, NASA Contract NAS1-9083, Contractor Report to be published.
3. Rinehart, Stephen A., Balcerak, John C., and White, Richard P., Jr.: An Experimental Study of Tip Vortex Modification by Mass Flow In-

jection, Rochester Applied Science Assoc., NASA Report 71-01, ONR Contractor Report, Contract No. N00014-69-C-0169, 1971, to be published.

4. SAE Committee A-21, Aerospace Recommended Practice, ARP 796, "Measurements of Aircraft Exterior Noise in the Field, 1965"

5. Pegg, R. J.: The Effect of Various Operating Parameters on the Noise Radiation Patterns from a Helicopter in Forward Flight. Presented at the Joint AeS-University of Texas Symposium on Environmental Effects on VTOL Designs, Arlington, TX.; November 1970.

- ROTOR BLADE NOISE REDUCTION
- FLYOVER NOISE MEASUREMENTS
- RECIPROCATING ENGINE EXHAUST MUFFLING
- HUMAN FACTORS
- SPECIAL FACILITY DEVELOPMENTS

Figure 1. - Langley VTOL acoustics research.

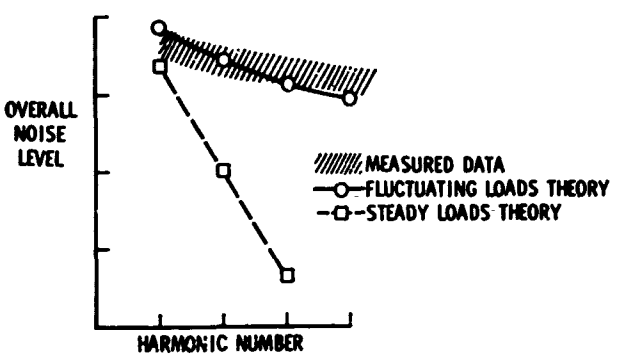

Figure 2. - Helicopter rotor rotational noise.

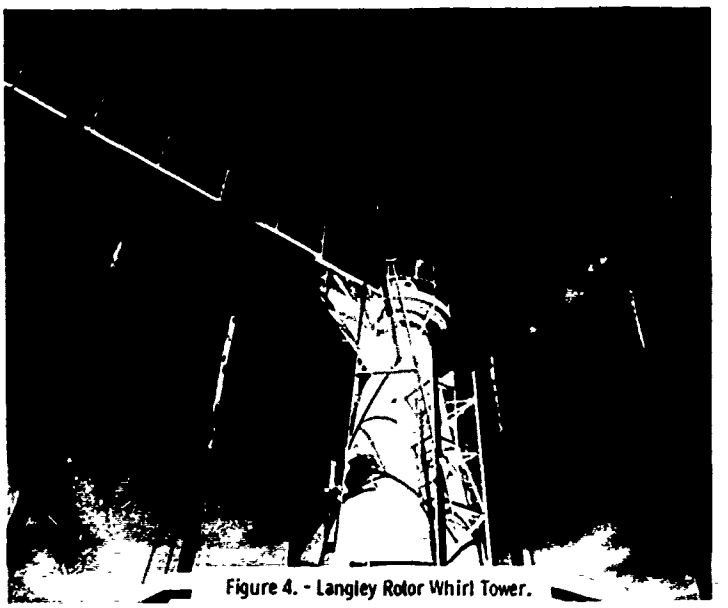

Figure 4. - Langley Rotor Whirl Tower.

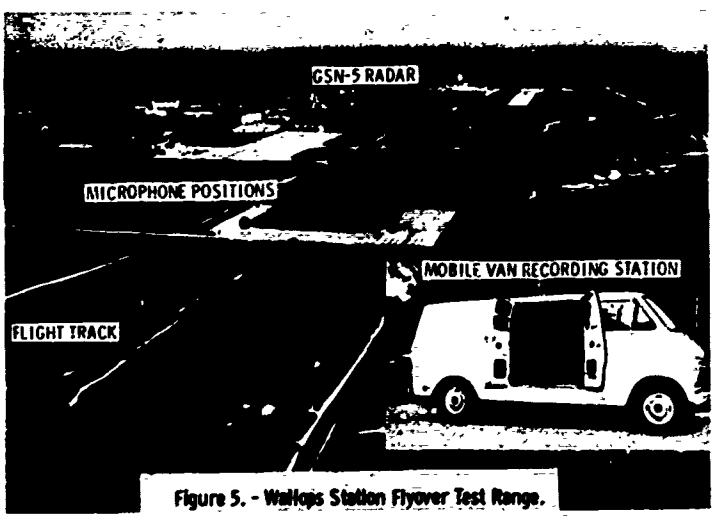

Figure 5. - Wallops Station Flyover Test Range.

WHIRL TOWER DATA

$$P_n(R,\theta,\Phi) = \frac{1}{2\pi a_0 R}\sum_{s=-\infty}^{\infty}\left[nB\Omega T_s\cos\Phi - \frac{\Omega Q_s}{M_t R_e}(nB-s)\right]J_{nB-s}(nBM_t\sin\Phi)e^{-is\theta}$$

P_n	- ACOUSTIC PRESSURE	M_t	- TIP MACH NUMBER
T_s	- THRUST	n	- ACOUSTIC MODE NUMBER
Q_s	- TORQUE	s	- LOADING HARMONIC NUMBER
a_0	- SPEED OF SOUND	R_e	- EFFECTIVE RADIUS
$B\Omega$	- BLADE PASSAGE FREQUENCY	R	- SOURCE-OBSERVER DISTANCE
θ	- AZIMUTHAL ANGLE		
Φ	- ELEVATION ANGLE		

Figure 3. - Fluctuating loads theory.

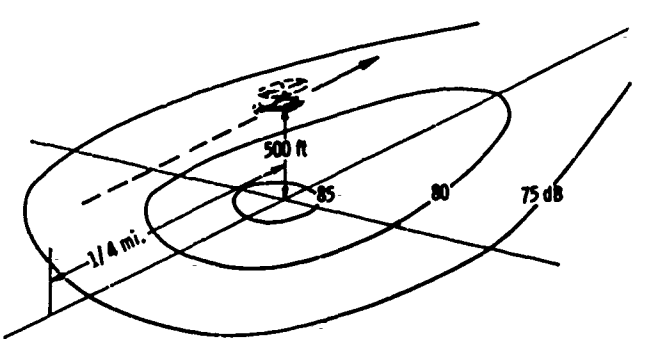

Figure 6. - Overall noise level radiation pattern.

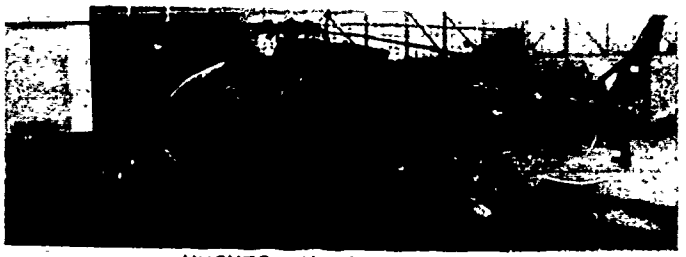

HUGHES OH-6A STANDARD

HUGHES OH-6A MODIFIED

Figure 7. - Quiet helicopter program.

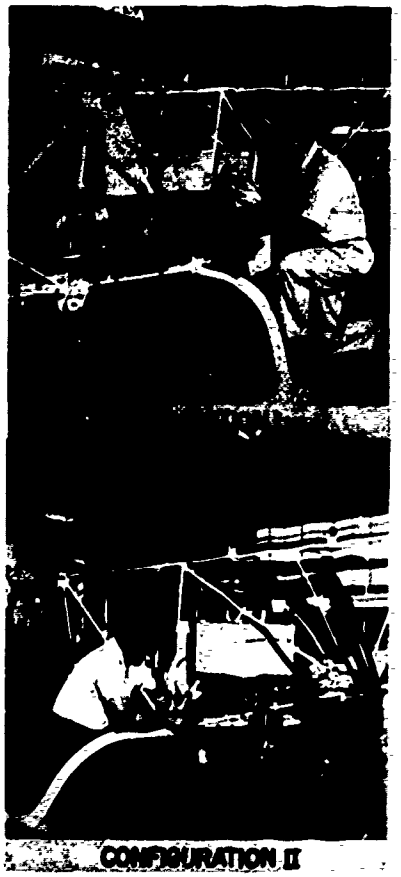

Figure 8. - H-13 muffler test configurations.

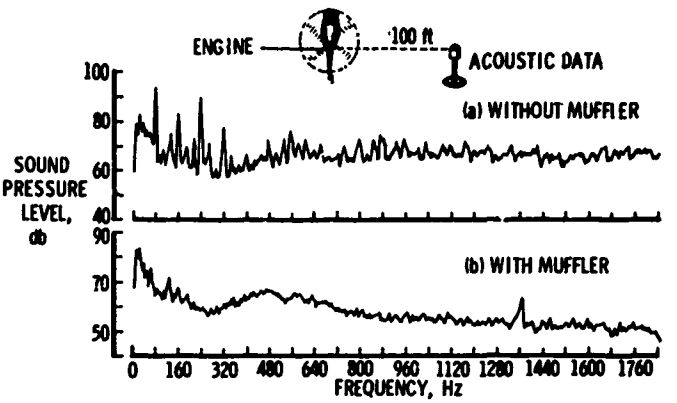

Figure 9. - Helicopter hovering noise measurements.

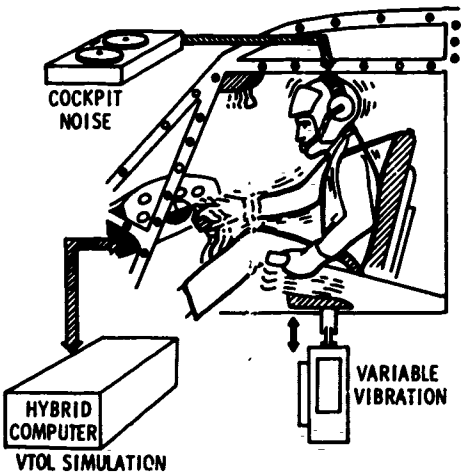

Figure 10. - Combined noise and vibration test configuration.

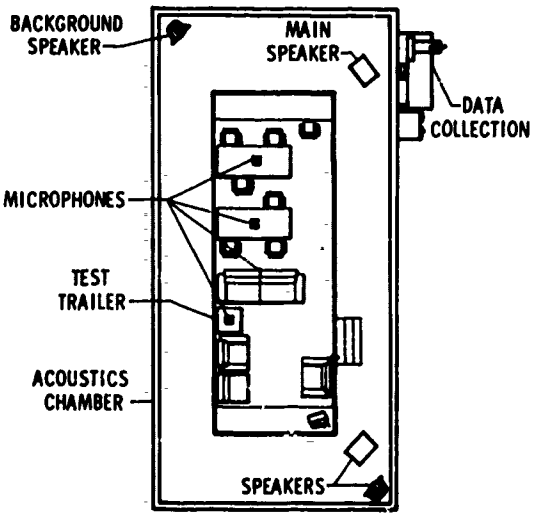

Figure 11. - Test environment for subjective reaction to VTOL aircraft noise.

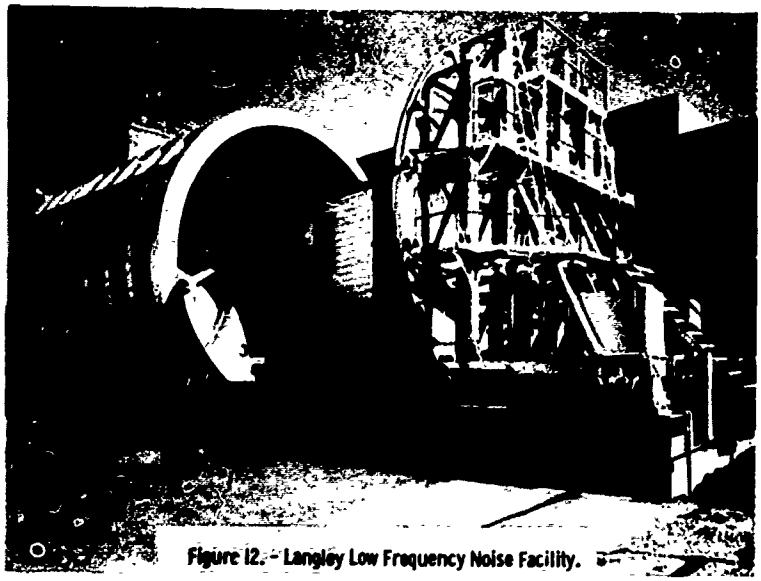

Figure 12. - Langley Low Frequency Noise Facility.

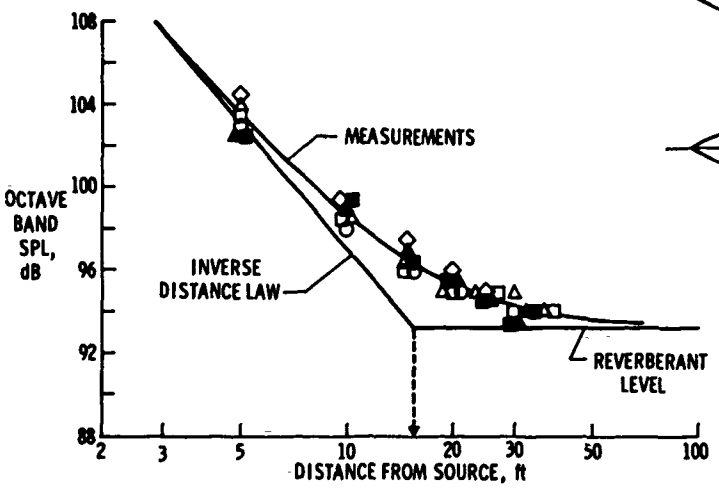

Figure 13. - Acoustic calibration data for the Langley Full Scale Wind Tunnel.

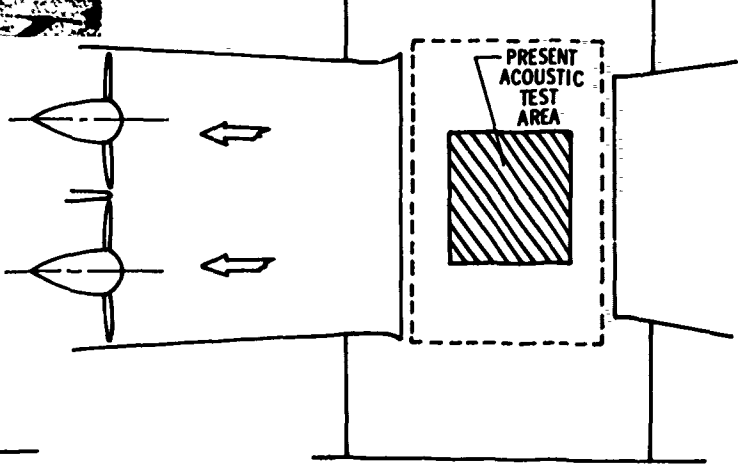

Figure 14. - Planform diagram of Langley Full Scale Wind Tunnel test section.

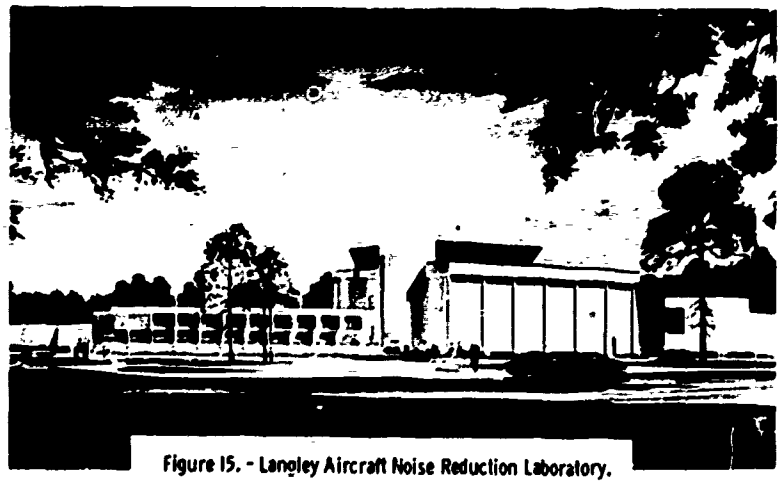

Figure 15. - Langley Aircraft Noise Reduction Laboratory.

NOISE ANALYSIS OF THE EXTERNAL AERODYNAMIC DIFFUSER APPLIED TO SHROUDED PROPELLERS

R. E. Longhouse and

J. R. Bailey

CENTER FOR ACOUSTICAL STUDIES

MECHANICAL AND AEROSPACE ENGINEERING DEPARTMENT

NORTH CAROLINA STATE UNIVERSITY

RALEIGH, NORTH CAROLINA

Abstract

It is well known that propeller performance can be improved by proper addition of a shroud. Previous investigators have shown that, attendant with the improved performance, the shroud significantly reduces the system noise, provided inlet flow separation does not occur.

External aerodynamic diffusion (EAD) of the exhaust flow provides an extension of the shrouded propeller concept. This concept, which is useful for V/STOL aircraft during hover operation, significantly improves the system thrust/power ratio compared to the conventional shrouded propeller with no diffusion. Attendant with the performance increase is a reduction in the system noise. The noise reduction is a result of a decrease in the fan blade aerodynamic loading and final exhaust velocity. EAD, therefore, provides a method of decreasing the system noise while improving system performance. Current techniques of reducing the noise of V/STOL propulsive units tend to degenerate system performance.

Introduction

For V/STOL aircraft incorporating shrouded propellers or fan-in-wing units, the system noise and thrust to power ratio can be significantly improved by using external aerodynamic diffusion during hover operation. External aerodynamic diffusion (EAD) is a process that produces aerodynamic expansion of the fan exhaust flow. EAD can be accomplished by providing a short expansion area in the exit section of a shroud and by preventing flow separation on the diffuser wall for high divergence angles, Figure 1. The effect of EAD is to increase the effective exhaust to fan disc area ratio which, in turn, reduces the final exit flow velocity, fan back pressure, and fan blade aerodynamic loading for a given thrust condition.

The noise produced by the propulsion unit is related to the magnitude of steady and fluctuating blade loading components and to the exhaust velocity. Reduced blade loading, as given by EAD, would therefore tend to reduce the intensity of sound produced. Furthermore, since jet noise depends on the 8th power of the exhaust velocity and the 2nd power of the exhaust diameter (1), lowering the exhaust velocity would materially reduce jet noise (2).

Early studies of shrouded two-blade propellors by Hubbard (1) indicated that the presence of the shroud, which decreases blade loading, reduced the sound pressure level by 6 dB at the fundamental frequency and by as much as 20 dB for the higher harmonics for smooth flow conditions. Flow separation at the inlet of the shroud caused the noise level to increase to the unshrouded values and greater with more acoustic energy concentrated at the higher frequencies. It was also noted that flow separation could be precipitated by very slight cross-winds. Inlet flow separation is an attendant problem with shrouded propeller systems. Expansion of the exhaust flow will tend to aggravate this situation since the mass flow through the system is increased. Therefore, considerable attention must be given to the inlet wall contour. Inlet boundary control methods (suction, etc.) may be required.

Since fuel requirements are about ten times greater in the hover modes compared to level flight, the increase in the thrust to power ratio that can be provided by EAD is most attractive. An operational aircraft with lift fans equipped with EAD would have increased range and payload capability and would decrease the probability of human annoyance response since less noise would be produced in the hover modes where the potential of noise annoyance is greatest. EAD, therefore, has the potential of providing a built-in noise reduction mechanism that enhances rather than degrades system performance. Current procedures under investigation (4, 5) degenerate system performance.

While early experimental investigations at Princeton (6, 7) did not establish positive benefits with EAD, more recent experimental results (8, 9, 10) indicate considerable system performance improvement can be achieved. An increase in exhaust area of 50% can be expected. The effect of this increase in exhaust area is to reduce the fan blade loading by 34% and the exhaust velocity by 50% at constant thrust.

Recognizing that the noise produced by a propulsive unit is related to the magnitudes of the steady and fluctuating blade loading forces and the exhaust velocity, the intent of this paper is to examine the potential offered by EAD for simultaneous improvement of system noise and performance.

Noise Reduction Analysis

The noise is considerably reduced by using EAD due to three effects:

(a) Reduction in steady loads

(b) Reduction in fluctuating forces on the blades

(c) Reduction in final exhaust velocity

It is important to understand that large area increases are possible. Increases of 50% in area are realizable. The following example will illustrate how this affects blade loading for the simple case of ideal, uniform flow. For a propeller (shrouded or unshrouded),

$$\frac{T_p}{T_T} = \frac{1}{2\sigma} \quad \text{, where } T_p = \text{propeller thrust (i.e., blade loading)}$$

T_T = system total thrust

Consider the cases that follow:

$$\sigma = \frac{A_2}{A_1} = \frac{1}{2}$$

and

$$\frac{T_p}{T_T} = \frac{1}{2(\frac{1}{2})}$$

or

$$T_p = T_T$$

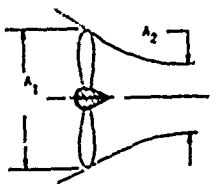

No Shroud, $\sigma = .5$

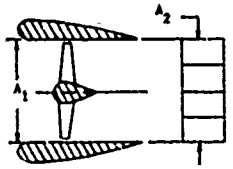

Shroud, $\sigma = 1.0$

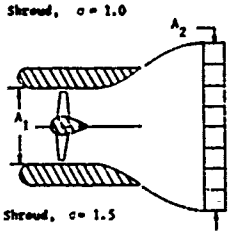

Shroud, $\sigma = 1.5$

$$\sigma = \frac{A_2}{A_1} = 1 \quad \text{and}$$

$$\frac{T_p}{T_T} = \frac{1}{2(1)} = \frac{1}{2} \quad \text{or}$$

$$T_p = \frac{1}{2} T_T$$

$$\sigma = \frac{A_2}{A_1} = 1.50 \text{ and } \frac{T_p}{T_T} = \frac{1}{2(1.50)}$$

or

$$T_p = .33\ T_T \text{ (67\% reduction in } T_p \text{ compared to no shroud condition)}$$

In the preceeding example, it is shown that a shrouded propeller with 50% diffusion will cause a decrease in blade loading of 67% in comparison to an unshrouded propeller for the same total thrust. It appears that a significant reduction in noise would therefore be expected. As demonstrated by Hubbard (3), shrouding the free propeller (doubling exhaust area) reduced the fundamental frequency noise of the system by 6 dB. This reduction is the order of magnitude that would be expected since T_p, and assuming a proportionate change in torque, was reduced by a factor of 2.0. The pressure would be reduced by the same order of magnitude. The external aerodynamic diffuser provides an extension of the use of propeller thrust relief as a means of pure tone noise reduction.

A similar comparison of a standard shrouded propeller with no diffusion to a shroud with $\sigma = 1.5$ can be made. The latter has 34% less loading on the blades. This represents approximately a 2.5 dB fundamental frequency noise reduction. Only the noise reduction due to the steady lift has been considered. The unsteady pure-tone noise is also reduced by the decreased blade loading via a decrease in the potential field interaction. This can be illustrated as follows. Since the thrust increase at constant pressure ratio is proportional to area, the system with $\sigma = 1.50$ has 50% more thrust than the system with $\sigma = 1.0$. Thus to return to comparable thrust levels, the pressure ratio of the diffuser system must be significantly reduced, i.e., the propeller must be throttled back. If the propeller was originally operating at $P_T/P_0 = 1.40$, this means the pressure ratio must be reduced to $P_T'/P_0 = 1.255$ to make a noise comparison at constant thrust. The affect of pressure ratio on noise for a typical system (7), considered here to be the General Electric lift fan LF475, is shown in Figure 2. The applicable reduction in pressure ratio indicates a 5.5 dB reduction in the fundamental frequency noise. The difference in this value and the steady lift noise is attributed to unsteady loading noise reduction and reduced exhaust velocity.

It is expected that the noise reduction achelved for a given σ will depend significantly on the characteristics of the particular propulsive unit. The numbers presented here are for the purpose of showing the order of magnitude to be expected. From a free propeller to a shrouded propeller with $\sigma = 1.5$, the order of magnitude of fundamental frequency noise reduction is 10 dB for constant thrust.

Diffuser System Performance

Use of an external aerodynamic diffuser significantly increases the system thrust to power ratio. Considering the case of the constant thrust for ideal, uniform total pressure flow, it can be shown that the performance improvement ratio is

$$\tau = \sqrt{\sigma} \text{ , where } \tau = \frac{\left(\frac{\text{Thrust}}{\text{Power}}\right)_{\text{with diffusion}}}{\left(\frac{\text{Thrust}}{\text{Power}}\right)_{\text{no diffusion}}},$$

at constant thrust. Thus, for $\sigma = 1.50$, the performance improvement factor is 1.225, so that the performance improvement is 22.5% at constant thrust.

Thus, not only has the system noise been reduced, but the hover performance has been significantly improved.

The overall performance of the EAD will be dependent on the efficiency of the means incorporated for diffuser boundary layer control. Several methods may be applied, e.g., blowing from slots, trapped vortex, suction, etc. Also the weight of the shroud must be considered. Too large of a shroud would tend to negate the performance gains.

Use of EAD for performance improvement is not without problems. Experimentation to date has indicated that the high divergence angle diffuser system tends to be unstable when subjected to disturbances (side winds, etc.). Thrust variations of 10% or more can be expected. Also, the flow will tend to separate at the inlet unless proper design is followed. Current experimentation indicates that the inherent instability of the system is the major obstacle that must be overcome before system integrity can be acheived.

Conclusions and Recommendations

Current experimental investigations substantiate theoretical claims that the system thrust to power ratio can be significantly improved. A comparable decrease in system noise is also predicted, but it remains to be shown experimentally.

EAD is not a panacea. The problems with the inherent instability remains a major obstacle in its application. Attendant with the instability would be aggravation of the noise problem.

It is believed the potential merits of EAD warrant further experimental and theoretical investigations to eliminate the instability problem and to delineate the absolute level of noise reduction.

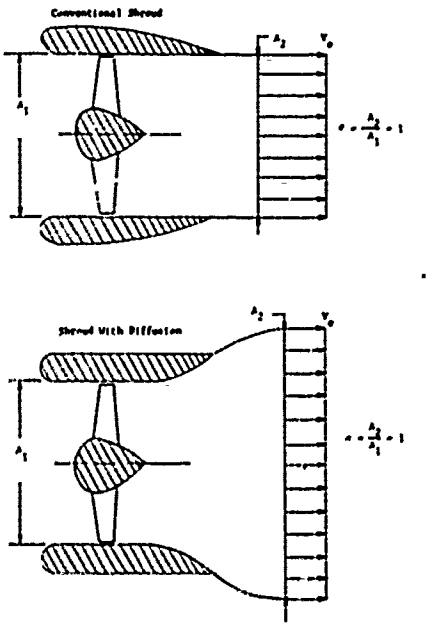

Figure 1. Comparison of Conventional and EAD Fan Configurations

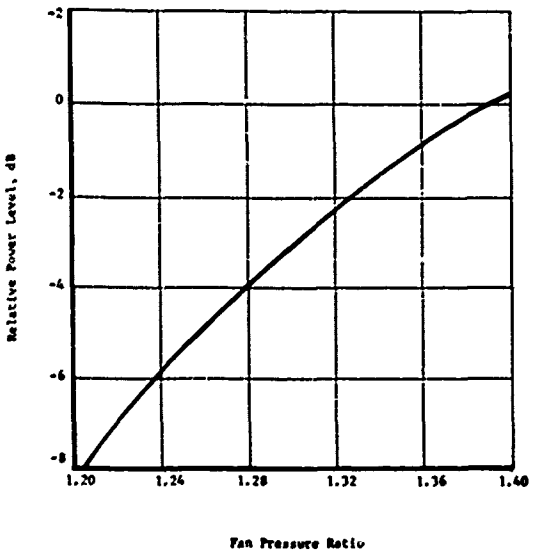

Figure 2. Power Levels at the Fundamental of Blade Passing Frequency vs. Pressure Ratio

1. Basic Aerodynamic Noise Research, NASA SP-207, Washington, D. C. July 1969.
2. Kramer, J. J. et al. Noise Reduction, Chap. 4, Aircraft Propulsion, NASA SP-259, November 1970.
3. Hubbard, H. H. Sound Measurements for Five Shrouded Propellers at Static Conditions. NACA 2024, 1950.
4. Benzakein, M. J. and L. J. Volk. Study Program for Lift Fan Noise Reduction and Suppression. NASA CR-1493, March 1970.
5. Sofrin, G. and J. McCann. P & W. Aircraft Experience in Compressor Noise Reduction. Aircraft Noise Symposium, University of Tennessee, February 1968.
6. Beatty, D. H. A Preliminary Investigation of Aerodynamic Diffusion Applied to a Shrouded Propeller. Masters Thesis, Report 481, Princeton University, March, 1959.
7. Carstens, J. P. Static Tests on a Ducted Fan Equipped with an Aerodynamically Controlled Diffuser. Masters Thesis, Report 486, Princeton University, September 1960.
8. Lazareff, M. Aerodynamics of Shrouded Propellers. AGARDOGRAPH 126, May 1968.
9. Lee, Y. A. Theoretical Investigation of an External Aerodynamic Diffuser. Masters Thesis, West Virginia, August 1970.
10. Longhouse, R. E. Experimental Investigation of an External Aerodynamic Diff .er, Masters Thesis, Aerospace Engineering Department, West Virginia University, May 1971.

THEORETICAL AND EXPERIMENTAL STUDIES OF HELICOPTER NOISE DUE TO BLADE-VORTEX INTERACTION

Sheila Widnall, Sing Chu and Albert Lee

Department of Aeronautics and Astronautics
Massachusetts Institute of Technology

ABSTRACT

The generation of impulsive sound, commonly called blade slap, due to blade-vortex interaction for helicopter rotors is discussed. Two cases are considered: first, blade-vortex interactions for which the angle between the blade and vortex is less than a critical value such that the entire length of the blade participates in efficient sound generation--likely to occur for tandem rotors only; second, blade-vortex interaction in which the unsteady interaction of the vortex with the tip of the blade is the primary cause of noise--important for the single rotor helicopter. For the first type of blade vortex interaction, the unsteady lift on the blades is calculated using an existing linear unsteady aerodynamic theory for oblique blade-vortex interactions. For the tip dominated blade-vortex interaction, unsteady slender-body theory is used to calculate the unsteady force on the blade as it encounters the vortex. A theoretical model for radiated sound due to the transient lift fluctuations is presented. Predictions of the directivity, frequency spectrum and transient acoustic signal are presented. Calculations of the transient signal are presented in comparison with recent experimental results. The agreement is good, particularly for the small angle blade-vortex interactions.

Introduction

The generation of lift by a helicopter rotor in forward flight is accompanied by the creation of an aerodynamic flow field of great complexity in both space and time. The characteristic noise signature is largely determined by the fluctuating loads on the blades due to operation in this nonuniform flow field. In many cases, the operation of the helicopter rotor produces an impulsive sound. One source of this is due to transonic flow effects at the tip on the advancing blade side. A recent paper by Lyon (1) has demonstrated that when an airfoil changes its forward speed relative to the fluid in an unsteady manner, as does a rotating blade in forward flight, sound is generated even though the flow speed is less than sonic everywhere. Another source of blade slap is the unsteady lift fluctuation on a blade due to interaction with the vortex from another blade.

Even when the helicopter operates in a condition which subjectively is described as non-banging, it is likely that blade-vortex interaction provides much of the higher harmonic content in the rotational noise spectrum. As has been noted by many authors, the boundary between blade-slap noise and rotational noise is not sharp. Below speeds for which compressible blade slap can occur, both are due to fluctuating forces acting on the blade which although very complex are nonetheless deterministic. The distinction between blade slap and rotational noise is made for convenience, usually on basis of subjective response.

In this paper, we discuss two potential-flow models for the fluctuating lift due to blade-vortex interaction and the resulting impulsive noise signature. Some recent experimental results are also presented.

If we consider the rotor flow fields sketch in Fig. 1 we see that the possible blade-vortex interactions are quite different for the single rotor as compared with the tandem rotor. As is well known, for the tandem rotor, blade-vortex interactions can take place in which the angle between the blade and vortex is small (say less than 30°) and for which a good portion of the blade will experience a fluctuating lift force. This of course gives rise to tandem-rotor blade slap which on the newer helicopters was substantially reduced by raising the aft rotor well above the forward rotor. For the single rotor helicopter it is likely that the blade tip on the advancing side is the most likely area of blade-vortex interaction although a possible interaction could occur between blade 3 and the vortex from blade 4. (See Fig. 1). Since the rotor wake is not well modeled by assuming no distortion of the vortex filaments (the rigid-wake assumption) a great deal more must be learned from flow visualization to accurately locate the vortices relative to the blades. Two potential-flow models which are appropriate for tandem-rotor blade interaction and single-rotor tip interaction will now be discussed.

If we consider the tandem-rotor flow field interaction sketched in Fig. 1 and we see that the essence of the blade-vortex interaction problem is that of a long blade passing obliquely over a vortex. Except near the blade tip, the aerodynamics of this interaction can be modeled as a two-dimensional airfoil in an oblique gust. Two recent aerodynamic theories have been developed to predict the unsteady lift fluctuations on a blade due to an oblique sinusoidal gust. Filotas (2) has considered the oblique gust interaction for incompressible flow. Johnson (3) has considered the oblique gust interaction for subsonic compressible flow. Johnson has also applied this theory to the calculation of helicopter airloads for blade-vortex interactions.

In a recent paper, Widnall (4) presented a model for sound radiation due to this type of blade-vortex interaction. The results of this analysis will be discussed and compared with experiments.

While the analytic model of blade-vortex interaction present in (4) is very suitable for the tandem-rotor interactions, it would not correctly predict the radiated noise due to blade-vortex interaction near the tip on the advancing blade side of a single-rotor helicopter. This is because the unsteady aerodynamics assumes an infinite two-dimensional blade with no tip. This aerodynamic model is not able to account for the unsteadiness as the tip of the blade rotates and moves over the vortex.

A preliminary treatment of this aspect of blade-vortex interaction, based on slender-body theory, will be discussed.

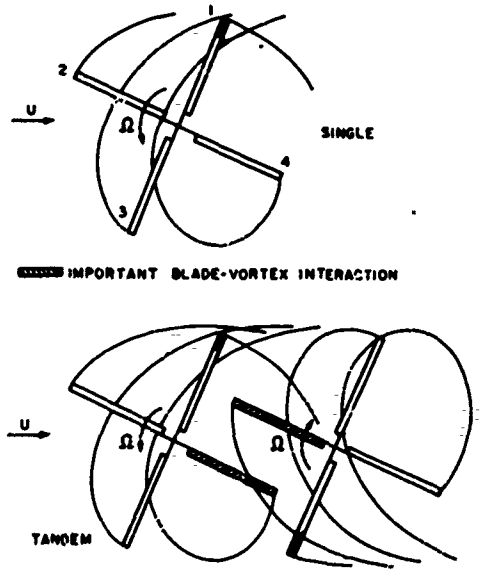

FIG.1 SKETCH OF TIP VORTEX CONFIGURATION FOR SINGLE AND TANDEM HELICOPTER ROTORS.

IMPULSIVE NOISE DUE TO BLADE-VORTEX INTERACTION -- MODEL I

The most straight forward calculation of the impulsive noise due to blade-vortex interaction is to use the model sketched in Figure 2. In this model the observer is located in the fluid at a distance r from the location of a vortex, which is taken to be at rest in the still fluid. The blade moves in the positive y direction at a speed U a distance h above the vortex, which is oblique to the leading edge by an angle Λ. The vortex height h is taken as constant along the span. The sound generated by repeated occurances of this transient, as occur for helicopter operation, is built up in a simple way from the fourier transform of the transient signal. This simplified model contains the essential features of the blade-vortex interactions which occur for tandem rotors but does not include the complexities of blade rotation, the nonuniform free stream at each blade element due to rotation, the curvature of the vortex filament and changes in distance between the blade and vortex along the length of the blade. In the calculation of the unsteady lift on the blade a two-dimensional theory is used, thus ignoring three-dimensional effects at the tip. The finite length of the blade is considered only in the acoustic calculation.

A. The Unsteady Aerodynamics Of Blade-Vortex Interaction

The unsteady lift on the blade due to blade-vortex interaction is calculated using linear unsteady aerodynamics in a manner analogous to the theory of Sears (5) developed for parallel interactions. The unsteady lift on the blade is primarily due to the interaction between the vertical velocity field of the disturbance and the solid airfoil surface. Linear theory treats this vertical velocity input as an imposed unsteady upwash field which creates the unsteady lift distribution on the airfoil surface necessary to satisfy the condition of no flow through the airfoil. Figure 3 shows the geometry of the interaction. As is standard in

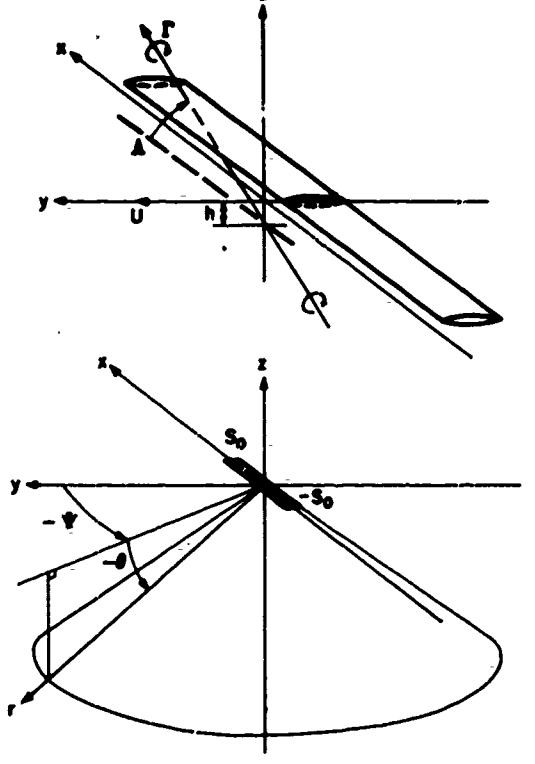

FIG. 2 MODEL FOR BLADE/VORTEX INTERACTION AND DEFINITION OF COORDINATE SYSTEM.

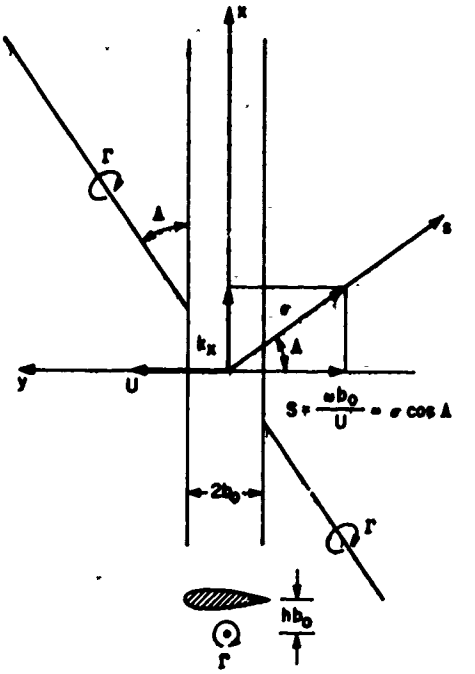

FIG. 3 GEOMETRY OF BLADE/VORTEX INTERACTIONS.

unsteady aerodynamics, the blade semichord b_0, and the blade velocity U are used as reference quantities. The nondimensional frequency is then $S=\omega b_0/U$, the Strouhal frequency.

The velocity field of a vortex of strength Γ located a distance h from the blade may be modeled as a distribution of oblique sinusoidal gusts. Using Fourier transforms, the vertical velocity field at the airfoil location due to the vortex may be written

$$w(x) = \frac{\Gamma}{2\pi}\frac{x}{x^2+h^2} = \int_{-\infty}^{\infty} W(\sigma)e^{+i\sigma x}d\sigma, \tag{1}$$

where

$$W(\sigma) = \frac{i\Gamma}{4\pi}\frac{\sigma}{|\sigma|}e^{-|\sigma|h} \tag{2}$$

is the Fourier transform of $w(x)$. For a real vortex, with a viscous core, a reasonable fit to the velocity distribution is obtained if h is replaced by $(h^2+h_c^2)^{1/2}$ where h_c is the radius of the vortex core, to the point of maximum tangential velocity.

A sinusoidal gust with this orientation will cause an unsteady lift on a blade section of frequency

$$S = \sigma\cos\Lambda \tag{3}$$

and sinusoidal variation along the span

$$L(x,S) = L_0(S,\Lambda)\exp[i\sigma x\sin\Lambda - i\Omega t), \tag{4a}$$

or alternately,

$$L(x,S) = L_0(S,\Lambda)\exp[i\sigma\sin\Lambda[x - (\cos\Lambda/\sin\Lambda)t]] \tag{4b}$$

This can be interpreted as a sinusoidal pattern of lift which is convected along the blade with convection speed

$$U_c = U/\tan\Lambda. \tag{5}$$

For the simplest acoustic model, a criterion for very efficient sound radiation would be $U_c > a$, the speed of sound. This would correspond to radiation from a disturbance moving at a supersonic speed with respect to the fluid.

The unsteady lift for such an oblique sinusoidal gust interaction is available from the incompressible flow theory of Filotas (2) or the more general subsonic theory of Johnson (3) in the form

$$L(x,S,\Lambda) = (2\pi\rho U^2 b_o)C_{L2D}(\sigma, M, \Lambda)\exp[i(k_x x - \omega t)], \tag{6}$$

where

$$k_x = \sigma\sin\Lambda$$

To obtain the spectrum of the lift due to blade-vortex interaction, $L(x,S,\Lambda)$ from Eq. 6 is multiplied by the Fourier transform of the vortex velocity, Eq. 2, expressed as a function of S. A factor $1/\cos\Lambda$ appears in the transformation $d\sigma$ to dS. Expressing the unsteady lift as a function of frequency and Λ only, we obtain

$$L(x,S,\Lambda) = (2\pi\rho U^2 b_o)C_{L2D}(S/\cos\Lambda,\Lambda,M)e^{i(k_x x - \omega t)} \cdot \frac{\Gamma}{2\pi}\left(\frac{\Gamma}{4\pi}\right)\frac{c}{2}\frac{e^{-|S/\cos\Lambda|}}{\cos\Lambda} \tag{7}$$

Filotas has developed a simple analytic expression for C_{L2D} (C_{L2D} is a complex quantity with both magnitude and phase dependent upon frequency)

$$C_{L2D}(S/\cos\Lambda,\Lambda;\ M=0) = \left[\frac{1}{\sqrt{1 + \pi\frac{S}{\cos\Lambda}(1 + \cos^2\Lambda + \pi S\tan\Lambda)}}\right]e^{-i\phi} \tag{8a}$$

where the aerodynamic phase shift between the gust input and the unsteady lift is

$$\phi(S,\Lambda;\ M=0) = S\left[1 - \frac{\pi\left(\frac{c}{2} - \Lambda\right)\left(2 + \frac{1}{2}\sin\Lambda\right)}{\cos^2\Lambda + 2\pi S\left(1 + \frac{1}{2}\sin\Lambda\right)}\right] \tag{8b}$$

This expression was used in the numerical predictions of the acoustic transient signal due to blade-vortex interaction. A more complete account of these aerodynamic theories can be found in (2) & (3).

B. Acoustic Radiation From Blade-Vortex Interaction

In developing the expression for sound generated by blade-vortex interaction, we consider the blade translating normal to its leading edge to pass over the vortex which is at rest in the still fluid, as sketched in Fig. 2. For a helicopter in forward flight, there is a flow along the blade which could be represented by sweeping back the blade. This additional complication has not been included, since the convective Mach number of flow along the blade never exceeds the forward flight speed of the helicopter. In addition, on the advancing blade side where the Mach number is the highest, the most critical condition for noise generation, the flow component along the blade is identically zero.

In (4), a detailed analysis of the acoustic field due to a single frequency component of unsteady lift was presented assuming that the blade chord is smaller than a wavelength so that the unsteady lift may be modeled as a line of acoustic dipoles, distributed along the span, moving with velocity U in the y direction.

Under these conditions the far field acoustic pressure due to a single frequency component of unsteady lift caused by the oblique sinusoidal gust was shown to be

$$|p(\theta,\psi)| = \frac{L_o}{2\pi}\frac{k\sin\theta\,\sin[ks_o[(\tan\Lambda)/M - (\cos\psi\sin\phi)/(1 - M\cos\theta\cos\psi)]]}{(1 - M\cos\theta\cos\psi)^2\, k[(\tan\Lambda)/M - \cos\theta\sin\phi/(1 - M\cos\theta\cos\psi)]} \tag{9}$$

where L_o is the amplitude of the fluctuating lift, ψ and ϕ are the elevation and azimuth angles of Fig. 2, Λ is the angle between the blade and the vortex M is the blade Mach number, k is the acoustic wave number ω/c. (Equation 9 differs from eq. 30 of ref (4) in that an error was made previously in going from acoustic power to acoustic pressure for a moving acoustic source). Equation 9 indicates that the angle Λ between the blade and vortex has a major effect on the acoustic field. This is because the angle between the vortex and blade determines the trace velocity of the interaction along the blade. If this trace velocity is subsonic, very little acoustic power is generated for the fluctuating force level which exists at the various spanwise stations along the blade. In fact, if the blade were infinitely long, exactly no sound would be generated by these fluctuating forces. (This is discussed in more detail in (4)).

Figure 4 shows the maximum amplitude of the directivity function defined as

$$D(\theta,\psi) = \frac{\sin[s_o\kappa[\tan\Lambda/M - \cos\theta\sin\psi/(1 - M\cos\theta\cos\psi)]]\,\sin^4}{s_o(1 - M\cos\theta\cos\psi)^2\,[\kappa[\tan\Lambda/M - \cos\theta\sin\phi/(1 - M\cos\theta\cos\psi)]]} \tag{10}$$

vs. elevation angle θ

for various combinations of Λ and Mach number M. The most important feature of these curves is the dependence on Λ. As the angle between the blade and vortex increases, the acoustic efficiency is greatly reduced. The results of ref.(4) also indicated a strong beaming of the signal in a direction normal to the blade (say within 20°).

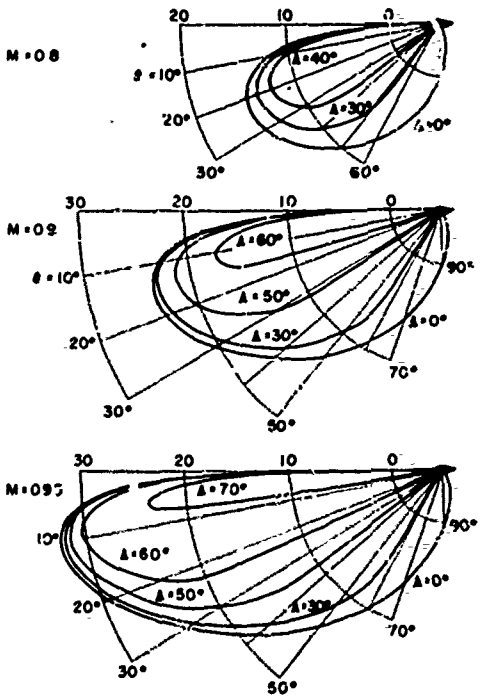

FIG. 4 MAXIMUM AMPLITUDE OF THE DIRECTIVITY FUNCTION AS A FUNCTION OF θ; $20\log D(\theta,\psi_{crit})$ FOR $ks_o >> 1$.

Since the directivity function does not contain the magnitude of the unsteady lift, a further reduction in the signal is obtained as Λ increases due to a decrease in the fluctuating lift. Fig (5) taken from (4) indicates the effect on the acoustic spectrum of the reduction in unsteady lift due to increasing blade vortex angle Λ and blade vortex spacing h. Recalling that an increase in vortex core size is equivalent to an effective increase in h, we can see a reduction in level and high frequency content would accompany an increase in vortex core size.

As Λ approaches 90° the acoustic and aerodynamic theories in this model predict no unsteady lift and no sound radiation. This is one reason why this model does not characterize blade-vortex interaction which occur near the tip for a single rotor since these interactions occur at angles very close at 90°. The complexities of the real flow which have been left out of the simplified model must then be re-examined.

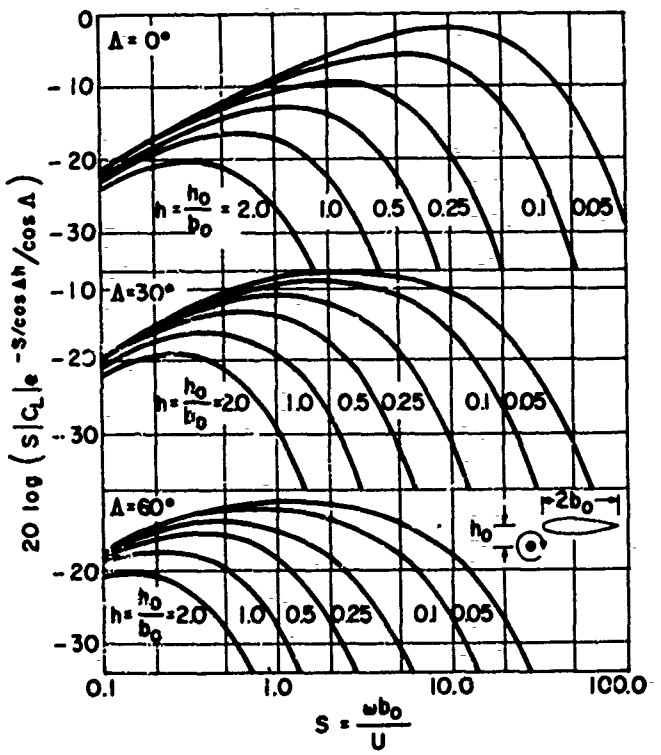

FIG. 5 NORMALIZED SPECTRA OF THE TRANSIENT BLADE/VORTEX INTERACTION AS A FUNCTION OF S; Λ = BLADE/VORTEX ANGLE, h = BLADE/VORTEX SEPARATION.

EXPERIMENTAL STUDY

Some of the earliest experimental data we had access to on the acoustic signature due to blade-vortex interaction was obtained by Boeing Vertol (6) using the model rotor of McCormick (7). The comparison between the peak to peak pressure in the transient acoustic signal as obtained from the experiment and as predicted from the theoretical model are shown in Fig. 6 and 7, taken from (4). Also shown is a sketch of the transient acoustic pulse from both the theoretical prediction and the experiment. We felt that the double pulse obtained in the experiment was the result of reflection of some nearby surface. This was later confirmed when we obtained our own experimental results. Also shown in Fig. 6 is the theoretical prediction of the effect of a change in core size on the signal. As would be expected the core size affects the level significantly for very close interactions but is unimportant if the blade passes only through the potential-flow region of the vortex.

We have now begun to obtain experimental data on radiated noise due to blade-vortex interaction in our open jet wind tunnel. Figure 8 shows a skematic of the experiment (the tunnel with the model helicopter rotor and the upstream vortex generator) as well as the transient acoustic signal due to blade-vortex interaction at an angle Λ=40°. The acoustic signature is processed on a "Waveform Educator" which extracts the repeated transient signal from the uncorrelated background noise. The lower trace shows the raw data (at a reduced scale), the upper trace the extracted blade-vortex transient signal. The left-hand curves shows the acoustic signal obtained from the model rotor without flow in the tunnel. This signal is just the rotational noise of the model rotor in hover. The right-hand curves show the acoustic signal due to blade-vortex interaction -- the vortex being generated upstream in the tunnel by a fixed vortex generator. The processing of the signal by the wave analyzer improves the clarity of the transient signal in comparison with the raw

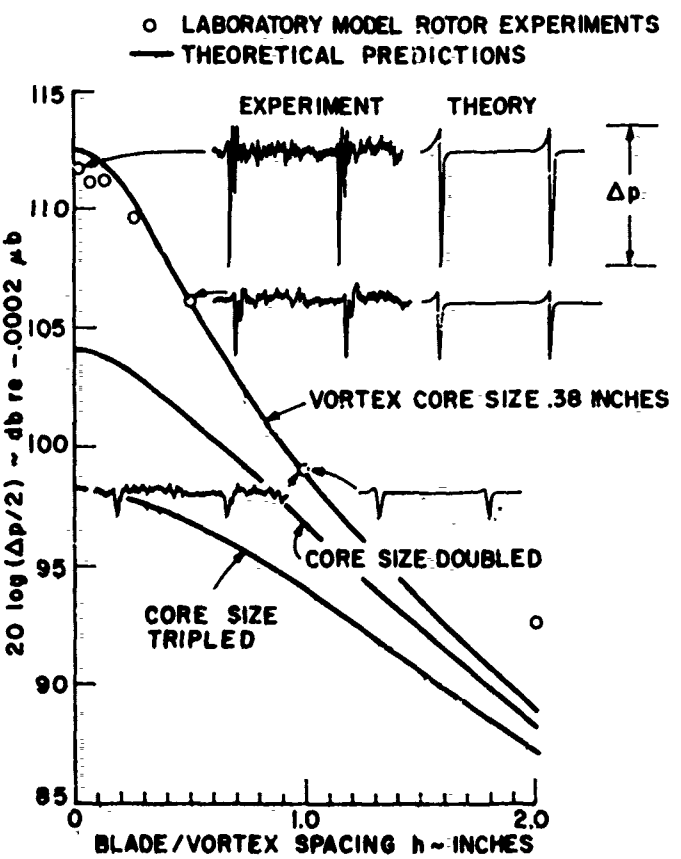

FIG. 6 EFFECT OF TIP VORTEX CORE SIZE ON HELICOPTER NOISE DUE TO BLADE/VORTEX INTERACTION.

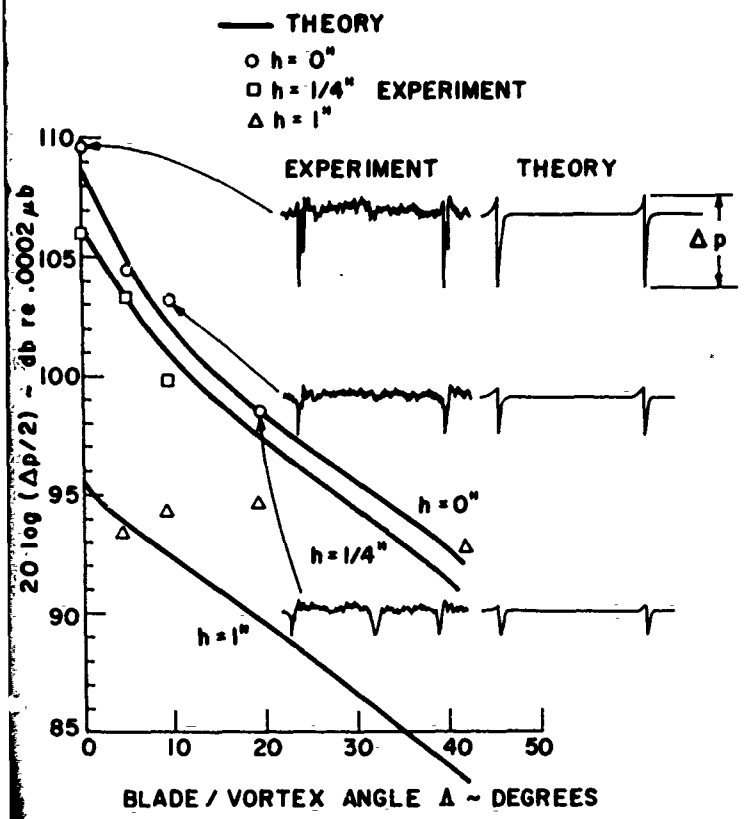

FIG.7 COMPARISON OF THEORY AND EXPERIMENT ON THE EFFECT OF BLADE/VORTEX ANGLE AND SPACING ON THE TRANSIENT SIGNAL h = BLADE/VORTEX SPACING ROTOR RPM = 1500.

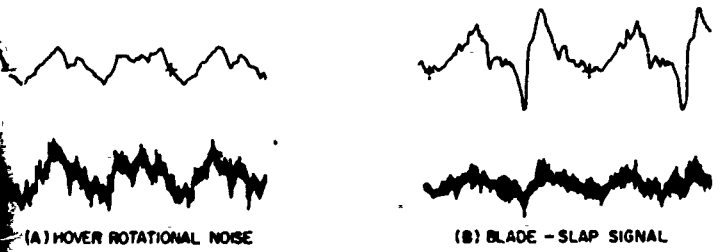

(A) HOVER ROTATIONAL NOISE (B) BLADE - SLAP SIGNAL

UPPER TRACE IS AVERAGED TRANSIENT SIGNAL; LOWER TRACE IS RAW DATA

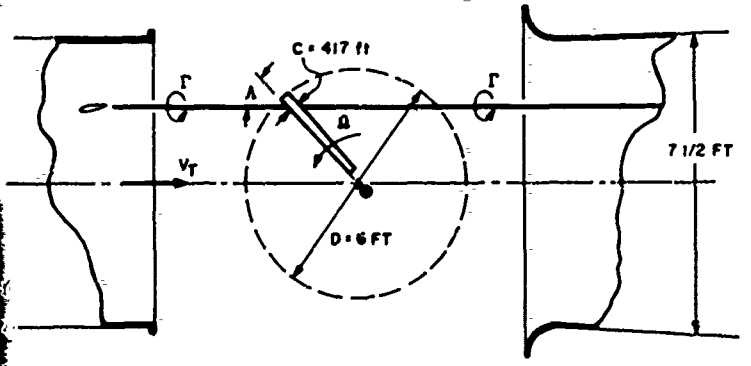

FIG. 8 EXPERIMENT TO MEASURE TRANSIENT ACOUSTIC SIGNAL DUE TO BLADE-VORTEX INTERACTION.

data. The typical shape of the blade-vortex interaction transient is clearly visible in the processed signal. One can also see the reflected pulse from the concrete ceiling (the ceiling will eventually be covered with an anechoic treatment). This reflected pulse is much clearer in some of the acoustic data which will be presented later in this paper.

In order to predict the transient acoustic pulse one must know the tangential velocity distribution in the vortex. This was obtained by measuring the vorticity distribution in the vortex (near the point of intersection) with the vorticity meter developed by McCormick (8). The experimentally determined vorticity distribution and the calculated tangential velocity distributions are shown in Fig. 9. In applying the analytical prediction method for intersection through the vortex core, the vortex is modeled as a potential vortex with the effective distance and circulation chosen so as to match both the location and magnitude of the maximum normal velocity at the blade.

The experimental results for the peak-to-peak pressure in the transient acoustic signal, present in the form 20 log Δp re .0002 μb vs. the blade-vortex separation h in inches, are presented in Figs. 10, 11, 12 and 13 for values of blade-vortex interaction angle Λ of 0°, 11°, 38.5° and 63°. The results indicate a rapid decrease in SPL as Λ and h increase. The agreement between theory and experiment is certainly acceptable considering the simplicity of the model. In replacing a rotating blade interacting with a vortex with a finite length blade translating over a vortex, one does not know precisely how to choose the effective translational velocity and the effective blade interaction length. The agreement between theory and experiment is poor for very large interaction angles, (Λ>45°). This is to be expected since many of the assumptions in the simple model are not valid as the blade-vortex interaction occurs near the tip region. The present analytic model seems to underpredict the radiated noise although we consider the experimental results to be somewhat preliminary

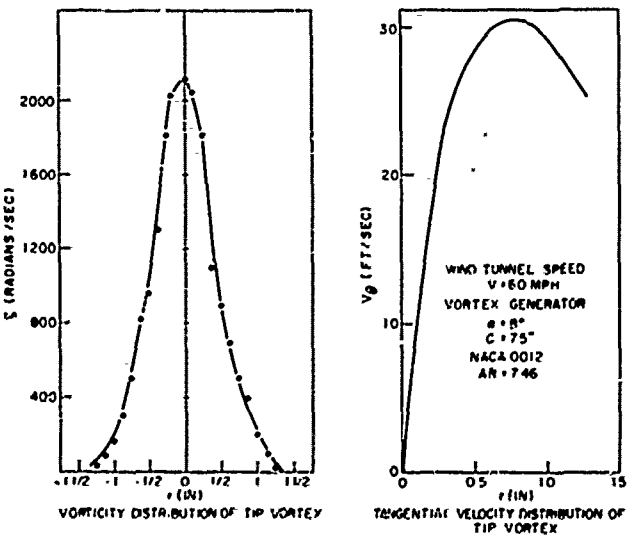

FIG 9 MEASURED VORTICITY DISTRIBUTION AND COMPUTED TANGENTIAL VELOCITY DISTRIBUTION OF THE VORTEX.

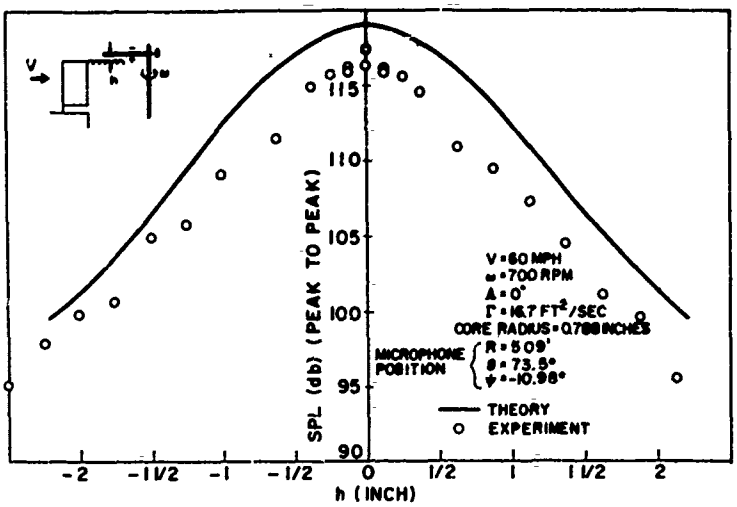

FIG. 10 THE EFFECT OF SPACING BETWEEN TIP VORTEX AND ROTOR ON SPL OF TRANSIENT SIGNAL; A = 0°.

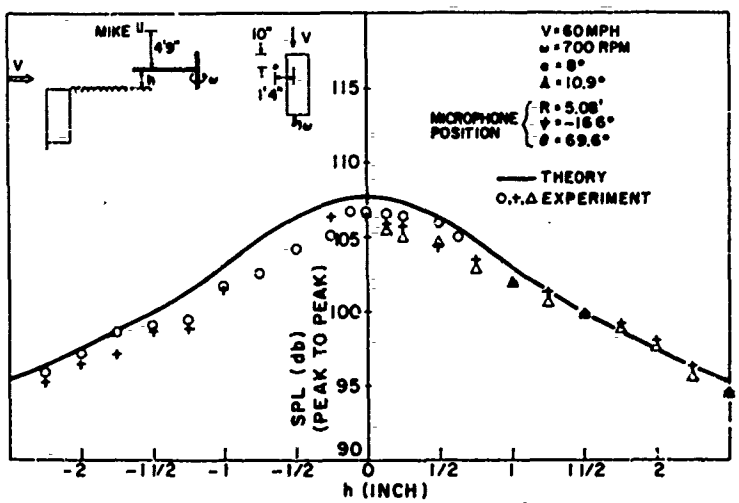

FIG. 11 THE EFFECT OF SPACING BETWEEN VORTEX AND ROTOR ON SPL OF TRANSIENT SIGNAL; A = 11°.

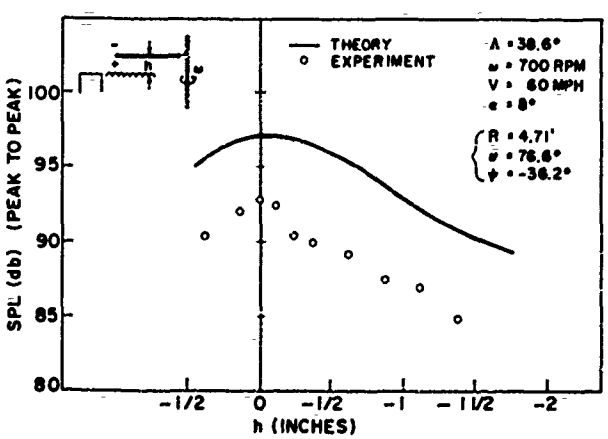

FIG. 12 THE EFFECT OF SPACING BETWEEN VORTEX AND ROTOR ON SPL OF TRANSIENT SIGNAL; A = 38.6°

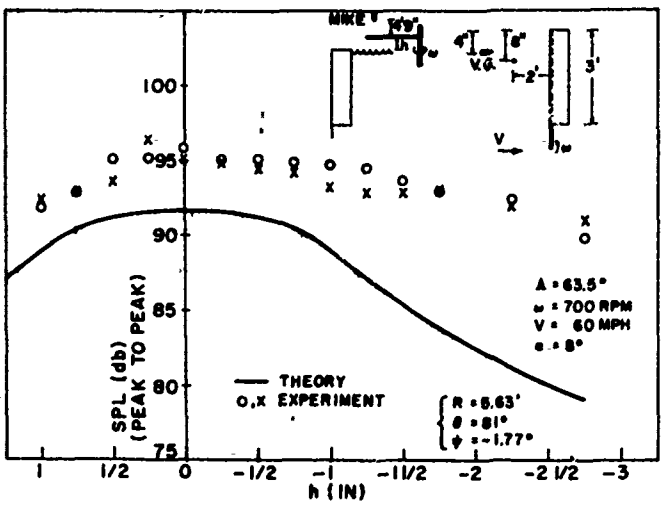

FIG. 13 THE EFFECT OF SPACING BETWEEN VORTEX AN ROTOR ON SPL OF TRANSIENT SIGNAL; A = 63.5°.

since the anechoic treatment has not yet been applied to the walls of the test area.

Figures 14 and 15 show the shape of the transient pulse for A = 11° and A = 63° obtained from the experiment as well as from analytic predictions. The experimental results show many reflections from the walls of the enclosure which make the interpretation of just what constitutes the blade-slap signature a bit difficult. The second pulse has been identified as a reflection from the ceiling with later returns coming from the walls and the floor. The analytic predictions do agree with the shape of the "first arrival" of the transient signal.

The effect of rotor angular velocity on Δp is shown in Fig. 16. In this experiment, the circulation of the vortex was held constant. The theoretical curve predicts an increase in SPL proportional to U^4, the experiment suggests U^5 with some scatter. The U^4 dependence occurs because the induced angle of attack for a given circulation is inversely proportional to velocity.

In an actual helicopter (holding the lift constant) the circulation would be roughly inverse to the velocity so that the blade-slap signature SPL would increase as U^2. This however ignores the effect of this change in operating condition on both the vortex core size and the blade-vortex separation--both very important parameters in determining the blade-slap signature.

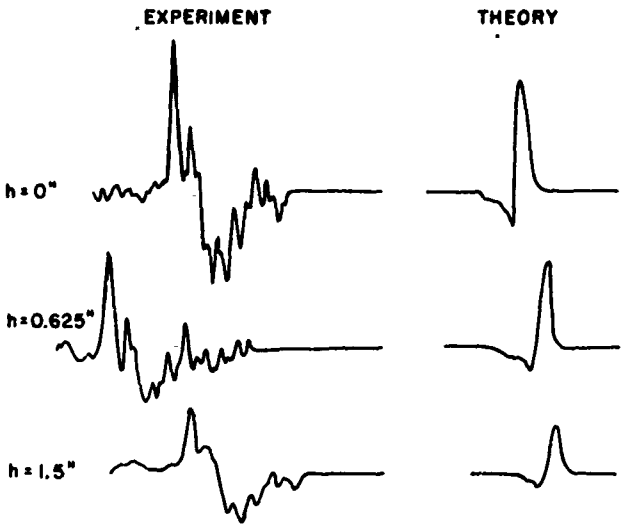

FIG. 14 EXPERIMENTAL RESULTS AND THEORETICAL PREDICTIONS OF THE ACOUSTIC PULSE DUE TO BLADE-VORTEX INTERACTION; $\Delta = 11°$.

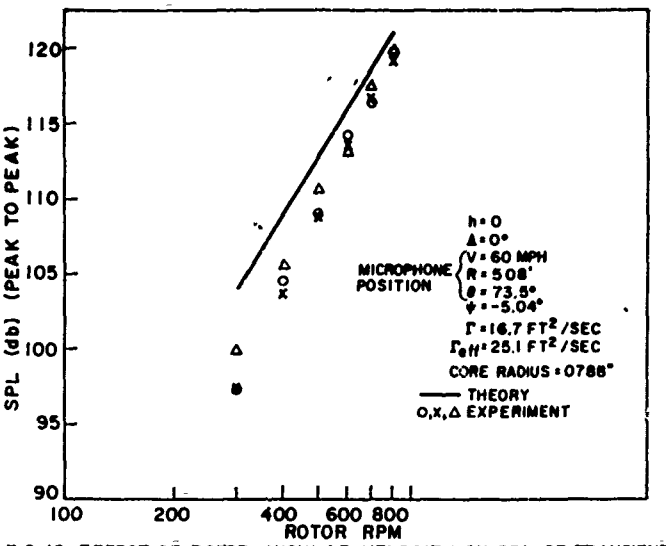

FIG. 16 EFFECT OF ROTOR ANGULAR VELOCITY ON SPL OF TRANSIENT SIGNAL.

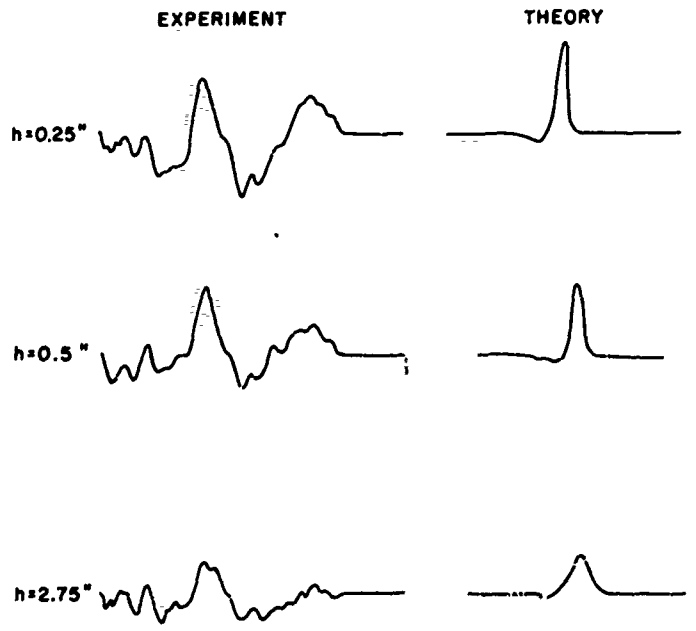

FIG. 15 EXPERIMENTAL RESULTS AND THEORETICAL PREDICTIONS OF THE ACOUSTIC PULSE DUE TO BLADE-VORTEX INTERACTION; $\Delta = 63°$.

IMPULSIVE NOISE DUE TO TIP INTERACTION -- MODEL II

While the analytic model of blade-vortex interaction is very suitable for the tandem rotor interactions, it does not correctly predict the radiated noise due to blade-vortex interaction near the tip on the advancing blade side of a single rotor helicopter. This is because the unsteady aerodynamics assumes an infinite (two-dimensional) blade with no tip. This aerodynamic model is not able to account for the unsteadiness as the tip of the blade rotates and moves over the vortex.

Qualitatively, we expect the force on the blade due to blade-vortex interaction to behave as shown (fig. 17). When the blade is in position (1) the net force due to the presence of the vortex is small, in position (4) it is also small because the positive and negative forces along the span will nearly cancel. However, as the blade moves from (1) to (4) a negative force will be felt as the tip interacts with the negative downwash of the vortex; the net unsteady force, F(t), should behave as sketched. The radiated noise is determined by the rate-of-change of this force $\frac{dF}{dt}(t)$.

We will argue that since the rate of change of angle of attack at the tip due to the presence of the vortex, especially in the situation where the vortex is very close to the surface of the wing the unsteady flow field may be analyzed by applying slender body theory to the tip region. This of course is not valid in from the tip. Although analytic difficulties prevent a rigorous matching to a two-dimensional or lifting-line theory for the rest of the blade, we feel that some insight into possible optimum tip plan form shapes might be gained by applying the simple ideas of slender-body theory rather than attempt a complete numerical treatment of the full three-dimensional unsteady aerodynamics of the tip. Slender-body theory does however have a number of peculiar features even in steady flow which are difficult to accept for helicopter blade tips--as will be seen.

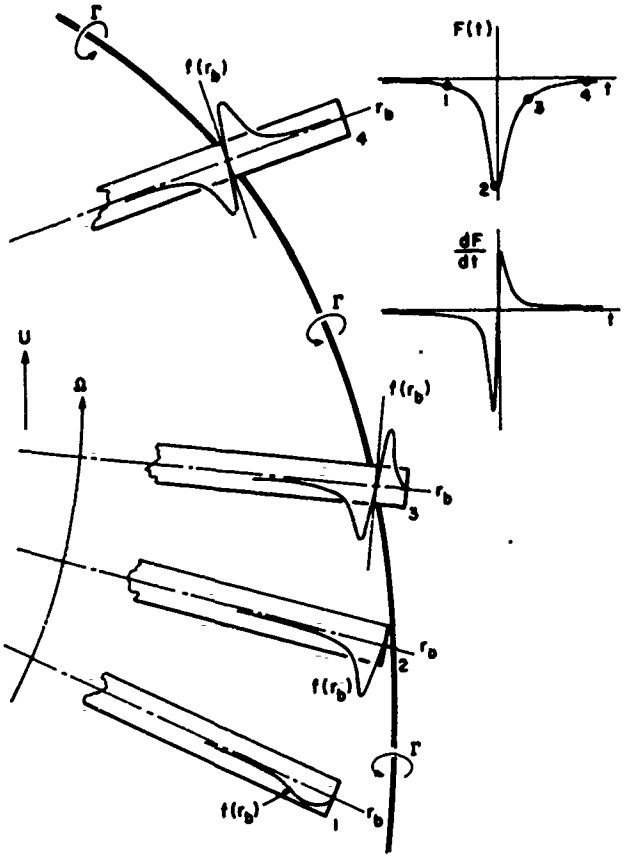

FIG. 17 BLADE-VORTEX INTERACTION IN THE ROTOR TIP REGION.

Figure 18 shows the geometry of blade-vortex interaction at the tip in which the coordinate system is so chosen that ξ and η axes are on the blade with the ξ axis parallel to the vortex while the η axis is normal and passes through the intersection of leading edge and trailing edge (in the case shown in figure 18, the tip edge is also treated as a trailing edge). Since the vortex-filament is static with respect to the fluid (under the rigid wake assumption) in this coordinate system, the free stream velocity V_f is in the ξ axis direction and the blade is moving in η direction with velocity V_c. Both V_f and V_c are functions of flight speed and advance ratio. They are also functions of time but for the short period of interaction, they are assumed to be uniform for simiplicity.

From many experimental works such as Simons, Pacifico and Jones (9) and Piercy (10) it is found that the core diameter of the tip vortices are of the order of one tenth of the blade chord. This fact allows the use of slender-body theory to calculate the unsteady force acted on the blade and thus its time derivative. By using the slender-body theory, three-dimensional unsteady compressible flow problem can be reduced to two-dimensional steady incompressible flows in the cross-flow plane with the third space coordinate and time as parameters so the governing equation is

$$\frac{\partial^2 \phi}{\partial \eta^2} + \frac{\partial^2 \phi}{\partial \zeta^2} = 0 \tag{11}$$

and the pressure is given by

$$p = -\rho\left[\frac{\partial \phi}{\partial t} + V_f \frac{\partial \phi}{\partial \zeta}\right] \tag{12}$$

From Fig 18 the crossflow has a semi-infinite plate and a vortex, the potential of the flow can be found through Schwarz - Christoffel transformation

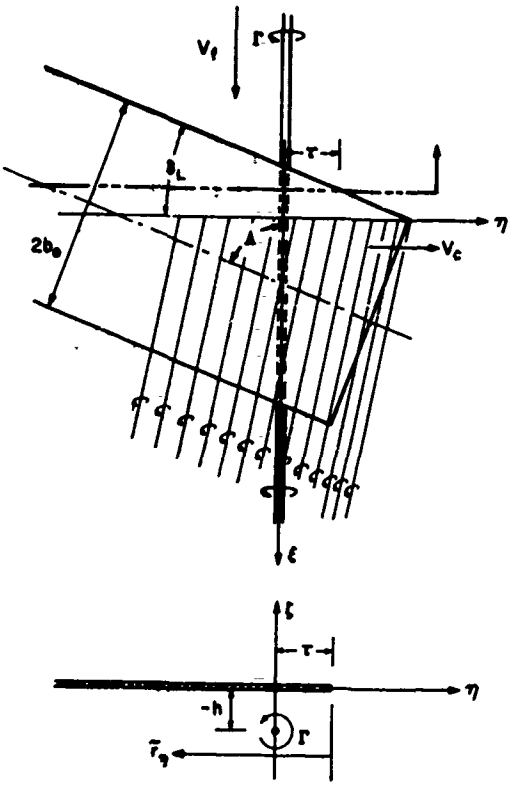

FIG. 18 BLADE-VORTEX INTERACTION NEAR THE TIP AND THE TWO-DIMENSIONAL FLOW IN THE CROSS-FLOW PLANE.

$$\phi = \frac{\Gamma}{2\pi}\left[\tan^{-1}\frac{\sqrt{r}\sin(\tilde{\theta}/2) - \sqrt{A_\Gamma}\sin(\theta_\Gamma/2)}{\sqrt{r}\cos(\tilde{\theta}/2) - \sqrt{A_\Gamma}\cos(\theta_\Gamma/2)}\right. \tag{13}$$

$$\left. - \tan^{-1}\frac{\sqrt{r}\sin(\tilde{\theta}/2) - \sqrt{A_\Gamma}\sin(\theta_\Gamma/2)}{\sqrt{r}\cos(\tilde{\theta}/2) + \sqrt{A_\Gamma}\cos(\theta_\Gamma/2)}\right]$$

where

$$r = [(\eta - \tau)^2 + \zeta^2]^{1/2} \tag{14}$$

$$\tilde{\theta} = \tan^{-1}\left(\frac{\zeta}{\eta - \tau}\right) \tag{15}$$

$$A_\Gamma = [\tau^2 + h^2] \tag{16}$$

$$\theta_\Gamma = \tan^{-1}\left(\frac{h}{-\tau}\right) \tag{17}$$

ζ and t exist as parameters in τ, for straight leading edge

$$\tau(\zeta, t) = V_c t + \zeta \cot \delta_L \tag{18}$$

where δ_L is the interaction angle with leading edge.

So the pressure can be written as

$$p = -\rho\frac{\partial \phi}{\partial \tau}\left(\frac{\partial \tau}{\partial t} + V_f \frac{\partial \tau}{\partial \zeta}\right) = -\rho V_f\left[1 + \frac{\partial \tau/\partial t}{V_f(\partial \tau/\partial \zeta)}\right]\frac{\partial \phi}{\partial \zeta} \tag{19}$$

with $\tau(\zeta,t)$ given by (18)

$$p = -\rho V_f \left(1 + \frac{V_c}{V_f} \tan \delta_L\right) \frac{\partial \phi}{\partial \zeta} \tag{20}$$

In this process, the unsteady part of the pressure is written in terms of the steady part; this will simplify the space integration process to get the force. From the slender-body theory, the portion of the blade after the intersection of leading edge and trailing edge will make no contribution to the lifting force so the force per unit length along the blade is given by

$$f(\bar{r}_\eta; t) = \int_{LE}^{\zeta = 0} \Delta p)_{\zeta = 0\pm} d\zeta \tag{21}$$

$$= \rho V_f \left(1 + \frac{V_c}{V_f} \tan \delta_L\right) \Delta \phi)_{\zeta = 0\pm}^{\zeta = 0}_{LE}$$

where

$$\bar{r}_\eta = \bar{r}(\zeta, t) - r \tag{22}$$

since ϕ is continuous at the leading edge so

$$f(\bar{r}_\eta; t) = \rho V_f \left(1 + \frac{V_c}{V_f} \tan \delta_L\right) \Delta \phi]_{\substack{\zeta = 0 \\ \zeta = 0\pm}} \tag{23}$$

with (13) substitute into (23)

$$f(\bar{r}_\eta; t) = -\frac{\rho \Gamma}{\pi} V_f \left(1 + \frac{V_c}{V_f} \tan \delta_L\right) \left[\tan^{-1} \frac{2\sqrt{\bar{r}_\eta}\sqrt{A_r} \cos(\theta_r/2)}{A_r - \bar{r}_\eta}\right]_{\zeta = 0} \tag{24}$$

The section lift coefficient can be obtained as

$$C_\ell(\bar{r}_\eta; t) = \frac{f(\bar{r}_\eta; t)}{1/2\, \rho V_f^2 (2b_o)} \tag{25}$$

$$= -\frac{1}{\pi} \left(\frac{\Gamma}{b_o V_f}\right) \left(1 + \frac{V_c}{V_f} \tan \delta_L\right) \left[\tan^{-1} \frac{2\sqrt{\bar{r}_\eta}\sqrt{A_r} \cos(\theta_r/2)}{A_r - \bar{r}_\eta}\right]_{\zeta = 0}$$

But it should be noted that this result is applicable only to the tip region of the blade while away from it, two dimensional lifting line theory should be used to calculate the section lift coefficient. This gives

$$C_{\ell 2D}(r; t) = 2\pi \frac{w}{V_f}$$

$$= \left(\frac{\Gamma}{b_o V_f}\right) \frac{b_o (t - \bar{r}_\eta)}{(t - \bar{r}_\eta)^2 + h^2} \tag{26}$$

(To correctly match these two regions, an intermediate three-dimensional region should be used. This may be investigated in the future.)

In Fig. 19 $C_\ell(\bar{r}_\eta; t)$ and $C_{\ell 2D}(\bar{r}_\eta; t)$ for given V_c, δ_L and h are plotted for various times.

There should be a region on the blade, say $(\bar{r}_\eta)_{\zeta = 0} = r_m$, where the theory used to calculate the force should be changed from the tip slender-body theory to the two-dimensional lifting line theory. Then the total force on the blade will be

$$F(t) = [1/2\, \rho V_f^2 (2b_o)] \times \left(\int_o^{r_m} C_\ell(\bar{r}_\eta; t)\, d\bar{r}_\eta + \int_{r_m}^{r_-} C_{\ell 2D}(\bar{r}_\eta; t)\, d\bar{r}_\eta\right)_{\zeta = 0} \tag{27}$$

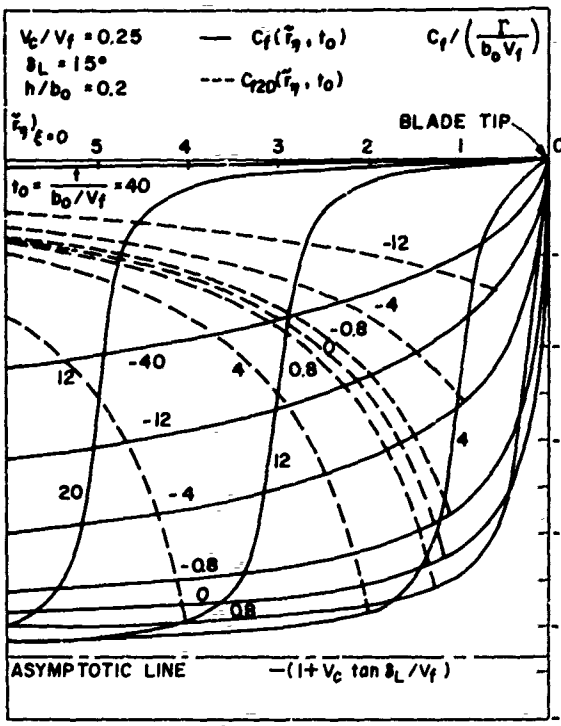

FIG. 19 THE SECTION LIFT COEFFICIENTS FROM SLENDER-BODY THEORY AND LIFTING LINE THEORY AT THE TIP REGION.

Before we evaluate the force and its time derivative, we first examine the characteristic of the "unsteadiness" of the two parts of the force due to the tip region and due to the rest of the blade.

The second part of the force, which can be obtained from two-dimensional theory, has a definite lift distribution which depends only on the angle of attack. Hence, its "unsteadiness" comes just from its uniform translation along the blade. From early consideration for the tip-interaction of single rotor, this translation speed is very low and the acoustic radiation from this translating force is negligible.

So the effective force that contributes to the acoustic radiation is only that due to the tip region

$$F_{eff}(t) = [1/2\, \rho V_f^2 (2b_o)] \left[\int_o^{r_m} C_\ell(\bar{r}_\eta; t)\, d\bar{r}_\eta\right]_{\zeta = 0} \tag{28}$$

With (25) substituted into (28), this becomes

$$F_{eff}(t) = -\frac{\rho \Gamma V_f}{\pi} \left(1 + \frac{V_c}{V_f} \tan \delta_L\right) \times \tag{29}$$

$$\left((r_m - r) \tan^{-1} \frac{2\sqrt{r_m}\sqrt{A_r} \cos(\theta_r/2)}{A_r - r_m} - 2\sqrt{A_r}\sqrt{r_m} \cos(\theta_r/2)\right.$$

$$\left. - \frac{h}{2} \log \left(\frac{r_m + A_r - 2\sqrt{r_m}\sqrt{A_r} \sin(\theta_r/2)}{r_m + A_r + 2\sqrt{r_m}\sqrt{A_r} \sin(\theta_r/2)}\right)\right]_{\zeta = 0}$$

the time derivative of the force is given by

$$\frac{dF_{eff}}{dt}(t) = \frac{\partial F_{eff}}{\partial t} \frac{\partial t}{\partial t} = \frac{\rho \Gamma V_f V_c}{\pi} \left(1 + \frac{V_c}{V_f} \tan \delta_L\right) \times \tag{30}$$

$$\left(\tan^{-1} \left(\frac{2\sqrt{r_m}\sqrt{A_r} \cos(\theta_r/2)}{A_r - r_m}\right) - 2\sqrt{(r_m/A_r)} \cos(\theta_r/2)\right)$$

This is the strength of the acoustic dipole and the acoustic pressure field can easily be calculated.

The value of r_a remains an open question. It may depend on the unsteadiness i.e. V_c. Results from (30) are plotted in Fig. 20 by choosing a cutoff of one chord length; this shows the shape of the impulse qualitatively.

From (30) we can see that the magnitude of the time derivative of force increases with V_c and δ_L. This suggest that it can be reduced by modifying the rotor and blade design.

First consider V_c, for a given flight speed. V_c can be reduced by reducing the advance ratio with the extreme limit $V_c = 0$ at hovering.

The leading edge interaction angle δ_L depends on both the interaction angle Λ and the swept angle of leading edge (Fig. 21). δ_L is decreasing as Λ increases, this can be accomplished by two ways -- reduce the advance ratio and increase the number of blades. To increase the number of blades has another benefit that the loading on each blade is reduced and thus the strength of the tip vortices can be reduced. δ_L can also be reduced by having a swept forward leading edge near the tip; this is described geometrically in Fig. 21.

To summarize, the blade slap noise of a single rotor can be reduced by having a smaller advance ratio, more blades on the rotor and a swept forward leading edge near the tip of the blade. Of course, the noise could be further reduced by reducing the flight speed and gross weight.

CONCLUSIONS

We have presented the results of our ongoing theoretical and experimental studies of signature due to blade-vortex interaction. The experimental and theoretical results obtained to date clearly demonstrate the ability of simple unsteady potential flow models to predict the blade-slap signature. The analysis of the tip region using slender body theory is still in the very preliminary stages. We would hope to obtain some insight into possible optimum tip shapes to reduce blade slap noise and to test these concepts in the wind tunnel.

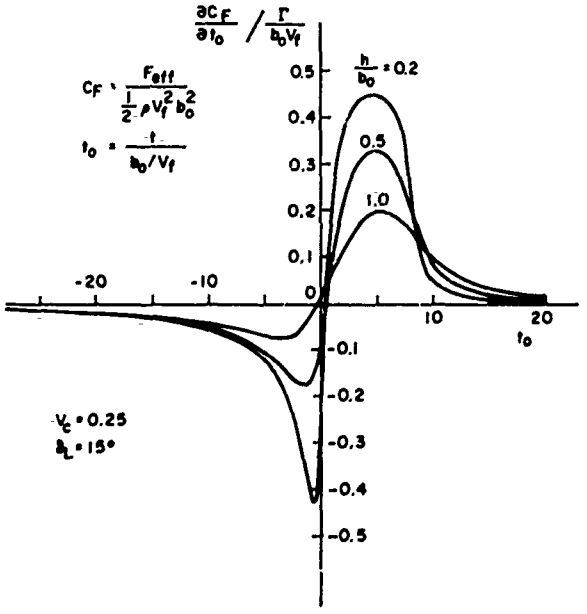

FIG. 20 THE TIME DERIVATIVE OF FORCE DUE TO TIP-VORTEX INTERACTION FROM SLENDER-BODY THEORY.

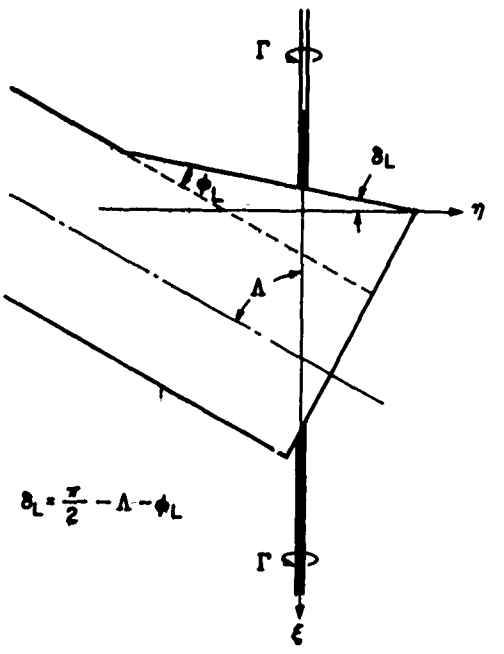

FIG. 21 MODIFIED BLADE TIP WITH SWEPT-FORWARD LEADING EDGE.

REFERENCE

1. R. H. Lyon, "Radiation of Sound by Airfoils that Accelerate near the Speed of Sound," J. Acoust. Soc. Amer. 49, 894-905 (1971).

2. L. T. Filotas, "Theory of Airfoil Response in a Gusty Atmosphere--Part I Aerodynamic Transfer Function," Inst. for Aerospace Studies, Univ. of Toronto, UTIAS Rep. No. 139, AFOSR 69-2150TR (Oct. 1969).

3. W. Johnson, "A Lifting Surface Solution for Vortex Induced Airloads and Its Application to Rotary Wing Airloads Calculations," Aeroelastic and Struct. Res. Lab. MIT, Cambridge, Mass., ASRL TR 153-2 (Apr. 1970).

4. S. E. Widnall, "Helicopter Noise due to Blade-Vortex Interaction," J. Acoust. Soc. Amer. 50, Number 1, (Part 2), (1971).

5. W. R. Sears, "Operational Methods in the Theory of Airfoils in Nonuniform Motion," J. Franklin Inst. 230, 95-111 (1940).

6. S. C. Riedel and J. O. Schairer, "Acoustics Data Obtained from Blade/Vortex Interaction Study," Vertol. Interoffice Mem., The Boeing Co., Vertol Div., Phila., Pa. (June 1970).

7. M. Surendraiah, "An Experimental Study of Rotor Blade/Vortex Interaction," Penn. State Univ., University Park, Pa., NASA CR-1573 (May 1970).

8. D. M. May, "The Development of a Vortex Meter," M.S. Thesis, 1964, Pennsylvania State Univ., University Park, Pa.

9. I. A. Simons, R. E. Pacifico, & J. P. Jones, "The Movement, Structure and Breakdown of Trailing Vortices from a Rotor Blade," CAL/USAAV LABS Symposium Proceedings Vol. 1 (1966).

10. M. A. V. Piercy, "On the Vortex Pair Quickly Formed by Some Airfoil," J. Roy. Aero. Soc. (October 1923).

SYNTHESIS OF HELICOPTER ROTOR TIPS FOR LESS NOISE

Richard H. Lyon*, William D. Mark, and Robert W. Pyle, Jr.

Bolt Beranek and Newman Inc.
Cambridge, Massachusetts 02138

ABSTRACT

Theoretical and computational studies of rotor tip sound radiation have been conducted for the purpose of designing rotor tips that radiate less sound in specified frequency bands. Consideration is given to radiation due to lift and thickness effects. Effects of unsteady vortex shedding on lift radiation are examined. It is shown that lift radiation is generally negligible in comparison with thickness radiation. A computational algorithm is developed for the synthesis of tip shapes that cause minimum thickness radiation in specified frequency bands. Numerical results are obtained for tip shapes that minimize high-frequency radiation, and a substantial reduction of radiation in comparison with existing shapes is shown. The uncertainty principle is used to establish a fundamental relationship between the tip section chord length and the minimum possible cutoff frequency for effective suppression of high-frequency sound. Factors that affect trade-offs between choices of airfoil section and planform are discussed.

I. INTRODUCTION

In this paper, we present the results of theoretical and computational studies of rotor tip sound radiation. The purpose of the research is the design of rotor tips that radiate less sound in particular frequency bands. By design, we mean the selection of a combination of planform and airfoil section shapes based on acoustical and aerodynamic considerations. The sound radiation that we consider is that due to compressibility effects that are important as the Mach number of the advancing rotor tip approaches unity.

The theory of sound radiation from accelerating airfoils has been presented in another paper [1]. Sound radiation is due both to the lift distribution on the tip and to the longitudinal section area. Since a functional relation was developed between the radiated sound spectrum and these functions, it is implicit that we should be able to derive tip shapes that will radiate less sound, at least in some frequency bands.

As we seek other shapes however, it will be necessary to impose constraints on the area and lift distributions. The area function must be positive. We can keep the tip volume constant by fixing the integral of the area function, and the center of gravity is fixed if the first moment of area is fixed. In the case of the lift distribution, we might like to keep the total lift, the pitching moment (first chordwise moment of lift), and the center of pressure fixed. The actual constraints employed are discussed below.

It is not necessary to point out that designing airfoils by acoustical considerations is unusual. To aerodynamicists such an approach may seem naive and presumptive. But we do not minimize the aerodynamic problems. The design suggestions offered here are only partial. Sufficient freedom will be available after the acoustical design is complete to allow for aerodynamic performance optimization, which must include both acoustical and aerodynamic experimentation. We do feel, however, that our approach — the definition of thickness and lift distributions through acoustical considerations — is a viable and desirable procedure.

II. RADIATION BY LIFT AND THICKNESS EFFECTS

In Ref. 1, a particular model is used for the calculation of the sound radiation. The rotor tip is modeled as a "torpedo", an axially symmetric shape with lift and longitudinal section area (LSA) identical to that of the tip section. Further, the lift and area effects are replaced by body force and volume velocity distributions along the axis of the torpedo. Thus, we replace a boundary value problem on an airfoil that has dimensions in feet with an inhomogeneous wave equation problem where the source terms are concentrated along a single line. It is worthwhile discussing the limitations that may result from this approximation.

The area effect alone can be treated as a distribution of simple sources over the tip planform. Generally, these sources produce no normal velocity in the plane in which they are located. Thus, the rigid boundary condition is automatically satisfied for thin airfoils. In addition, as we showed in Ref. 1, the direction of sound radiation from the area effect is very strongly forward. Thus, in the spanwise direction, the trace wavelength for radiating wavenumbers is quite large compared to the tip spanlength. This means that the radiated sound is insensitive to the distribution of volume velocity in this dimension. The volume velocity may therefore be concentrated into a line in the chordwise direction.

The justification for the lift-body force replacement is more difficult. In part it is, as we shall see, that the lift radiation is so much weaker than the area radiation that it doesn't much matter what we assume as long as we get a "ball park" estimate. We can, however, do better than that.

The dipole distribution over the planform representing the lift stress would produce nonzero velocities in the plane of the airfoil; therefore, the rigid surface of the airfoil will affect the radiation from these sources. We need to estimate the size of this effect that we are not accounting for. We can do this by noting that Frowcs Williams has shown that supersonic multipoles radiate independently of each other [2].

*Presently, Professor of Mechanical Engineering, Massachusetts Institute of Technology, Cambridge, Massachusetts 02139.

Thus, at least for the supersonic wavenumbers describing the source distribution, the effect of an infinite rigid plane passed through the plane between the positive and negative monopoles making up the elementary dipoles is to increase the sound radiation by 6 dB (3 dB for each side of the plane). Since the actual rigid plane is the size of the tip planform, the radiation augmentation will be less than 6 dB. With the infinite rigid plane inserted, the justification for collapsing the dipoles into a chordwise line is the same as above, since the radiation from the lift distribution is also very strongly forward [1].

In Ref. 1, the lift force per unit length in the chordwise direction is given by

$$\ell(x) = \rho_\infty V_t^2\, \alpha(t)\, [BC_p(x)] \,. \qquad (1)$$

The product BC_p is proportional to the incremental lift force per radian increase in angle of attack, and is expressed in Ref. 3 by the product

$$\frac{1}{2} BC_p(x) = \frac{v}{V_t} \frac{\Delta v_a}{V_t} \,, \qquad (2)$$

where the two factors on the rhs of Eq. 2 are tabulated for various airfoils.

Applying the formulation of Ref. 1, we have calculated the sound power radiated by an airfoil of the following specifications:

Section Shape	NACA 0012	Rotor Disk Diameter	48 ft
Chord Length	18 in.	RPM	300 (5 Hz)
Number of Blades	2		
Tip Span	46 in.	Forward Speed	333 ft/sec
Average Angle of Attack	8°	Advancing Tip Mach No.	0.96

The radiated sound power is expressed as the m.s. pressure at 50 ft averaged over all directions. The results of the calculations are shown in Fig. 1. The difference in level in nearly all bands is at least 40 dB and in the higher bands it approaches 70 dB. Thus, even with a 6 dB augmentation of lift radiation due to blade baffling effects, our conclusion that lift radiation is unimportant would not be affected.

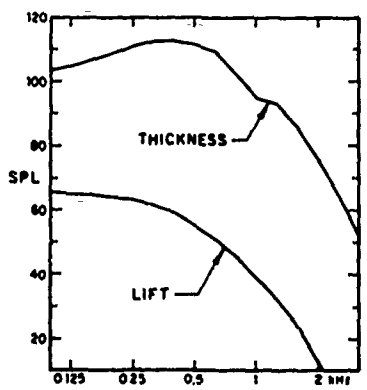

Fig. 1. One-third octave band spectra for thickness and lift radiation. (See text for parameters.)

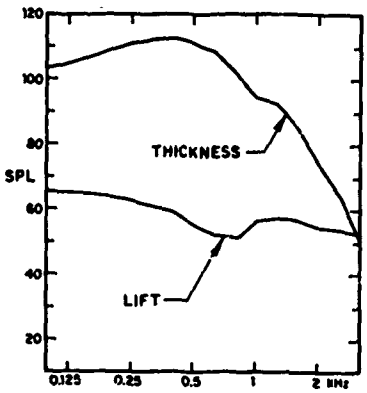

Fig. 2. One-third octave band spectra for thickness and lift radiation including high-frequency vortex shedding. (See text for parameters.)

We can include the effects of unsteady vorticity shedding from the rotor tip by postulating a "high frequency" component in the angle of attack. As an example, we have assumed the same conditions as those for Fig. 1, but have added a fluctuating angle of attack of 1 degree amplitude at the 50th harmonic of the rotor rotation rate (frequency of vortex shedding = 250 Hz). The results of this calculation are shown in Fig. 2. Note that the augmentation in radiation is quite broad band, and does not show up in the 250 Hz band at all. This example does show, however, that excessive fluctuation in the shed vorticity during the forward sweep of the blade may cause lift radiation that could compete with thickness radiation in the higher bands.

The principal lesson from the foregoing, insofar as design is concerned, is that we can concentrate on minimizing thickness radiation. This circumstance is fortunate since the relation between tip shape and thickness radiation is very direct, while the lift distribution depends on shape in a rather complicated fashion [3]. Thus, our approach is to synthesize tip shapes for minimal noise, under certain constraints. We can then look at the pressure distributions on these derived "optimal" shapes from the viewpoint of flow separation and lift radiation. If they appear to be acceptable, they will become candidates for a new tip design, to be studied experimentally.

III. MATHEMATICAL FORMULATION AND NUMERICAL RESULTS

In Ref. 1, the LSA function A(x) was expanded in an exponential Fourier series,

$$A(x) = \ell^{-1} \sum_{m=-\infty}^{\infty} A_m e^{ik_m x} \,, \qquad 0<x<\ell \qquad (3)$$

where $k_m = 2m\pi/\ell$. The period ℓ is the spacing between rotor tips in the rotor model used in Ref. 1; each interval ℓ contains one rotor tip. It was shown in Ref. 1 that, for practical purposes, there is a one-to-one correspondence between the frequency spectrum of thickness radiation and the squared magnitudes $|A_m|^2$ of the expansion coefficients of A(x). The radiated angular frequency corresponding to a spatial wavenumber k_m is ck_m, c being the speed of sound. We can therefore find optimal LSA functions

by minimizing the values of $|A_m|^2$ over chosen wavenumber bands, where the minimization is subject to an appropriate set of constraints applied to the function A(x).

The expansion coefficients in Eq. 3 are

$$A_m = \int_0^L A(x)e^{-ik_m x}\,dx \ , \tag{4}$$

which is also the Fourier transform of A(x) evaluated at wavenumber k_m. We can therefore formulate the optimization problem in terms of the Fourier integrals,

$$A(x) = \frac{1}{2\pi}\int_{-\infty}^{\infty} \tilde{A}(k)e^{ikx}\,dk \ , \qquad -\infty<x<\infty \tag{5}$$

$$\tilde{A}(k) = \int_{-\infty}^{\infty} A(x)e^{-ikx}\,dx \ , \tag{6}$$

instead of Fourier series. The optimization problem is thus reduced to minimizing the integral

$$I \triangleq \int_0^{\infty} V(k)|\tilde{A}(k)|^2\,dk \ , \tag{7}$$

where V(k) is a nonnegative real spectrum weighting function that is chosen to be large over the range of k where we wish to minimize $|\tilde{A}(k)|^2$, and where the admissible A(x) are required to satisfy an appropriate set of constraints.

A. Choice of Constraints

The LSA function A(x) must be constrained in the minimization process so that it will be possible to design an aerodynamically acceptable tip from the minimizing A(x) function by choosing an appropriate tip planform. (Factors affecting this choice are discussed in Sec. IV.) To help insure that the minimizing form of A(x) is "reasonable", we shall constrain the admissible class of A(x) to those functions lying between appropriately specified upper and lower bounds which are functions of x. That is, the admissible A(x) shall be constrained to satisfy

$$a(x)\le A(x)\le b(x) \ , \qquad 0<x<L \tag{8}$$

where a(x) and b(x) are these bounds, and where L is the maximum chord of the tip section under consideration. At the very least, it is clear that A(x) must be constrained to be positive and finite; that is, $a(x)>0$ and $b(x)<\infty$.

If $|\tilde{A}(k)|^2$ were to be minimized over a certain interval of k subject only to the constraint of Eq. 8, it is clear that the minimizing A(x) function would tend to fall on the lower bounding function a(x), since the requirement that $|\tilde{A}(k)|^2$ be small favors small values of A(x). Such behavior unnecessarily restricts the *shape* of A(x) and can be avoided by also constraining the area of A(x) — i.e., by requiring that the admissible A(x) also satisfy

$$\int_0^L A(x)\,dx = M_0 \ , \tag{9}$$

where M_0 is a specified number.

We shall require A(x) to satisfy one additional constraint. It is shown in Appendix A that, insofar as the constraint of Eq. 8 permits, the minimization of $|\tilde{A}(k)|^2$ over given bands, subject only to the constraint of Eq. 9, would lead to minimizing functions A(x) that tend to be symmetric about the midchord point x = L/2. This aerodynamically undesirable result can be controlled by additionally constraining the first moment of A(x):

$$\int_0^L xA(x)dx = M_1 \ , \tag{10}$$

where M_1 is specified. Equations 9 and 10, taken together, are equivalent to constraining the area and center of gravity of A(x). It is clear that intelligent choices for M_0 and M_1 will not be independent of the choices for the bounding functions a(x) and b(x).

B. Formulation of Problem in Terms of Sampled Area Functions

For numerical solution of the minimization problem, the limit constraint described by Eq. 8 is, in large measure, the determining factor in our choice of method of representing the LSA function. This is because it must be possible to conveniently transform this constraint to whatever representation of the LSA function we decide upon. This transformation is most easily carried out if we base our representation of A(x) on an appropriate set of the sample values $A_j = A(x_j)$. It will be convenient to use equally spaced samples; that is, $x_j = j\Delta$, $j = 0,1,\ldots, N$, where Δ is the sampling interval, and where $N = L/\Delta$. For values of $x \neq x_j$, A(x) is *defined* from the set of samples A_j, $j = 0,1,\ldots, N$ by interpolation. Our representation of A(x) can thus be expressed as

$$A(x) = \sum_{j=0}^{N} A_j w_j(x) \ , \qquad A_j = A(j\Delta) \ , \tag{11}$$

where

$$w_j(x) = w(x-j\Delta) \ , \tag{12}$$

where w(ξ) is an appropriate interpolating function with the properties

$$w(0) = 1 \tag{13}$$

$$w(n\Delta) = 0, \quad n = \pm 1, \pm 2,\ldots \ . \tag{14}$$

In most of our numerical work we have used for the interpolating function

$$w(\xi) = \frac{\sin(\pi\xi/\Delta)}{\theta^{-1}\sinh(\theta\pi\xi/\Delta)} \ , \tag{15}$$

which is a generalization of an interpolating function suggested by Lerner [4]. The decay of the tails of Eq. 15 is controlled by the parameter θ. For large θ, the tails have strong decay, whereas, as θ→0, the rhs of Eq. 15 approaches the familiar $[\sin(\pi\xi/\Delta)]/(\pi\xi/\Delta)$. For most of our numerical work, we have used θ = 0.40.

To minimize the integral of Eq. 7 subject to the constraints of Eqs. 8-10, it is first necessary to express $|\tilde{A}(k)|^2$ in terms of A(x) as represented by Eq. 11. After carrying out the integration in Eq. 7, we can then express the integral I as an ex-

plicit function of $A_0, A_1, \ldots, A_N$.

Defining

$$\tilde{w}_j(k) \triangleq \int_{-\infty}^{\infty} w_j(x) e^{-ikx}\, dx \ , \tag{16}$$

we obtain, by substituting Eq. 11 into Eq. 6,

$$\tilde{A}(k) = \sum_{j=0}^{N} A_j \tilde{w}_j(k) \ . \tag{17}$$

Multiplying Eq. 17 by its complex conjugate yields

$$|\tilde{A}(k)|^2 = \sum_{j=0}^{N} \sum_{m=0}^{N} A_j A_m \tilde{w}_j(k) \tilde{w}_m^*(k)$$

$$= \sum_{j=0}^{N} A_j^2 \tilde{w}_j(k) \tilde{w}_j^*(k) + \sum_{j<m} \sum A_j A_m [\tilde{w}_j(k) \tilde{w}_m^*(k) + \tilde{w}_j^*(k) \tilde{w}_m(k)]$$

$$= \sum_{j=0}^{N} A_j^2 |\tilde{w}_j(k)|^2 + 2 \sum_{j<m} \sum A_j A_m \mathrm{Re}[\tilde{w}_j(k) \tilde{w}_m^*(k)] \ , \tag{18}$$

where the asterisk denotes the complex conjugate, and where Re[...] denotes the real part of the quantity within the brackets. We now substitute Eq. 12 into Eq. 16 and then introduce the change of variable $\xi = x - j\Delta$:

$$\tilde{w}_j(k) = \int_{-\infty}^{\infty} w(x - j\Delta) e^{-ikx}\, dx$$

$$= e^{-ikj\Delta} \tilde{w}(k) \ , \tag{19}$$

where we have used the definition

$$\tilde{w}(k) \triangleq \int_{-\infty}^{\infty} w(\xi)\, e^{-ik\xi}\, d\xi \ . \tag{20}$$

Combining Eqs. 18 and 19 yields

$$|\tilde{A}(k)|^2 = |\tilde{w}(k)|^2 \Big(\sum_{j=0}^{N} A_j^2 + 2 \sum_{j<m} \sum A_j A_m \cos[k(m-j)\Delta] \Big)$$

$$= |\tilde{w}(k)|^2 \Big(\sum_{n=0}^{N} A_n^2 + 2 \sum_{n=1}^{N} \Big(\sum_{j=0}^{N-n} A_j A_{j+n} \Big) \cos(kn\Delta) \Big) \ . \tag{21}$$

One can show that as $\Delta \to 0$, Eq. 21 becomes in the limit

$$|\tilde{A}(k)|^2 = 2 \int_{\xi=0}^{L} \Big[\int_{x=0}^{L-\xi} A(x) A(x+\xi)\, dx \Big] \cos(k\xi)\, d\xi \ , \tag{22}$$

which is the Wiener-Khintchine theorem for deterministic waveforms $A(x)$ that are defined over a finite interval $0 < x < L$. We can therefore interpret Eq. 21 as the Wiener-Khintchine theorem for sampled deterministic waveforms.

To express I explicitly in terms of $A_0, A_1, \ldots, A_N$, we must now substitute Eq. 21 into Eq. 7. Defining

$$G_n \triangleq \int_0^{\infty} V(k) |\tilde{w}(k)|^2 \cos(kn\Delta)\, dk \ , \quad n = 0, 1, \ldots, N \ , \tag{23}$$

we obtain

$$I(A_0, A_1, \ldots, A_N) = G_0 \Big(\sum_{n=0}^{N} A_n^2 \Big) + 2 \sum_{n=1}^{N} \Big[G_n \Big(\sum_{j=0}^{N-n} A_j A_{j+n} \Big) \Big] \ . \tag{24}$$

Equation 24 is the desired explicit expression for the weighted integral of Eq. 7 in terms of the samples $A_j = A(j\Delta)$. The coefficients G_n are defined by Eq. 23.

Next, we must express the constraints in Eqs. 8-10 in terms of the LSA function samples $A_1, A_2, \ldots, A_N$. From Eqs. 11-13, we immediately have for the limit constraint

$$a_j \le A_j \le b_j \ , \qquad j = 0, 1, \ldots, N \ , \qquad \textit{Constraint A} \ , \tag{25}$$

where

$$a_j \triangleq a(j\Delta) \ , \qquad j = 0, 1, \ldots, N \ , \tag{26}$$

and

$$b_j \triangleq b(j\Delta) \ , \qquad j = 0, 1, \ldots, N \ , \tag{27}$$

are specified sets of numbers. From Eqs. 6, 17, and 19, we have for the volume constraint

$$\sum_{j=0}^{N} A_j = \frac{M_0}{\tilde{w}(0)} \qquad \textit{Constraint B} \ , \tag{28}$$

where, from Eq. 20, it follows that

$$\tilde{w}(0) = \int_{-\infty}^{\infty} w(\xi)\, d\xi \ , \tag{29}$$

is the area under the interpolating function. Turning to the first moment constraint, we have by differentiating Eqs. 6 and 17, and then combining the results with Eq. 10

$$M_1 = \frac{1}{i} \sum_{j=0}^{N} A_j \tilde{w}_j'(0) \ , \tag{30}$$

where the prime denotes differentiation. Next, we differentiate Eq. 19 and combine the result with Eq. 30 which gives, after some rearrangement,

$$\sum_{j=0}^{N} (j\Delta + \gamma) A_j = \frac{M_1}{\tilde{w}(0)} \ , \qquad \textit{Constraint C} \ , \tag{31}$$

where

$$\gamma \triangleq \frac{1}{i} \frac{\tilde{w}'(0)}{\tilde{w}(0)} = \frac{\int_{-\infty}^{\infty} \xi w(\xi)\, d\xi}{\int_{-\infty}^{\infty} w(\xi)\, d\xi} \ , \tag{32}$$

according to Eq. 20. Notice that γ is the center of gravity of the interpolating function $w(\xi)$; thus γ is zero for symmetric interpolating functions such as Eq. 15. Equation 31 is the desired expression for the first moment constraint in terms of the LSA function samples $A_1, A_2, \ldots, A_N$.

Equations 24, 25, 28, and 31 collectively define the optimization problem under consideration. The problem is to minimize $I(A_0, A_1, \ldots, A_N)$, as given by Eq. 24, where the admissible vectors $(A_0, A_1, \ldots, A_N)$ are subject to the constraints given by Eqs. 25, 28, and 31. Our method of solution, which is based on the Gradient Method, is described in Appendix B.

C. Solutions for Particular Cases

For several combinations of parameters, we have used the technique described in Appendix B to find optimum LSA functions. In all of our numerical work, the initial vector $(A_0^{(0)}, A_1^{(0)}, \ldots, A_N^{(0)})$ was taken to be a sampled version of an NACA 0012 airfoil. The upper and lower bounding vectors that constitute Constraint A were both taken proportional to the initial vector.

In most cases, $(a_0,a_1,\ldots,a_N)$ and $(b_0,b_1,\ldots,b_N)$ were taken to be 0.5 and 1.5 times $(A_0^{(0)},A_1^{(0)},\ldots,A_N^{(0)})$ respectively. The moments M_0 and M_1, used in Constraints B and C, were evaluated from the initial vector using Eqs. 28 and 31. This insured that, at every stage of the iterative procedure described in Appendix B, $(A_0^{(i)},A_1^{(i)},\ldots,A_N^{(i)})$ had the same area and center of gravity as the NACA 0012 starting vector.

Figure 3 shows the optimum LSA functions and their corresponding spectra for chord lengths L ranging, in 0.5-ft increments, from 1.5 ft to 4.0 ft. For all of the results presented in Fig. 3, the spectrum weighting function V(k) was chosen to minimize the sound radiated over the entire frequency band above 700 Hz. This was accomplished by taking V(k), $k = 2\pi f/c$, to be unity in the band from 700 Hz to 11,300 Hz and zero outside this band. However, the value of 11,300 Hz can be regarded as being effectively infinite since the sampled LSA function representation used in computing the results of Fig. 3 has an inherent cutoff frequency of about 5500 Hz as we shall now show.

Using tabulated integrals, we find the Fourier transform, Eq. 20, of the interpolating function, Eq. 15, to be

$$\bar{w}(k) = \frac{\Delta\sinh(\pi/\theta)}{\cosh(\pi/\theta)+\cos(k\Delta/\theta)} . \qquad (33)$$

In all of the cases shown in Fig. 3, we have taken $\theta = 0.40$. For this value of θ, Eq. 33 is very close to a rectangular function with cutoff wavenumber $k_c = (\pi/\Delta)$. Hence, the cutoff frequency f_c, in Hz, is $f_c = [ck_c/(2\pi)] = [c/(2\Delta)]$. For all cases shown in Fig. 3, we have taken $\Delta = (L/N) = 0.10$ ft; hence, $f_c = 5c = 5500$ Hz, the number cited above. The fact that the cutoff wavenumber of w(k) coincides with the inherent cutoff wavenumber of our sampled LSA function representation follows directly from Eq. 21.

The radiated spectra were computed using the formula

$$\int_{k_1}^{k_2} |\bar{A}(k)|^2\, dk = \gamma_0(k_1,k_2)\left[\sum_{n=0}^{N} A_n^2\right] + 2\sum_{n=1}^{N}\gamma_n(k_1,k_2)\left[\sum_{j=0}^{N-n} A_j A_{j+n}\right], \qquad (34)$$

where

$$\gamma_n(k_1,k_2) \triangleq \int_{k_1}^{k_2} |\bar{w}(k)|^2 \cos(kn\Delta)dk, \qquad (35)$$

where k_1 and k_2 are the lower and upper wavenumbers ($k = 2\pi f/c$) corresponding to the standard one-third octave bands. Equation 34 was obtained by integrating Eq. 21 between the limits k_1 and k_2. The spectra of both the initial sampled version of the NACA 0012 airfoil and the final optimized LSA function is shown for each of the cases studied.

Referring now to the spectra shown in Fig. 3, we see that virtually no improvement in the spectrum of the LSA function with a 1.5-ft chord was possible. However, as the chord was increased from 1.5 ft to 3.0 ft, considerable improvement was achieved. Increasing the chord beyond 3.0 ft produced no further significant improvement relative to the NACA 0012 shapes.

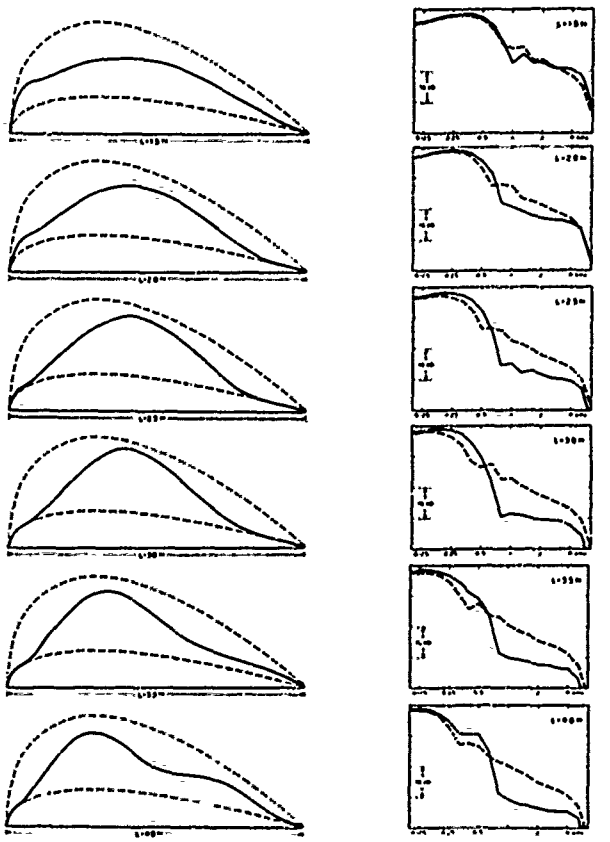

Fig. 3. Optimum LSA functions and their radiated one-third octave band spectra (solid curves) for chord lengths L ranging from 1.5 to 4.0 ft. Radiation is minimized above 700 Hz. Upper and lower bounds (dashed curves) on allowable LSA functions are 0.5 and 1.5 times NACA 0012 airfoil of uniform spanwise thickness. Dashed spectra are those of NACA 0012 airfoils of same chord length, sectional area, and center of gravity as optimum LSA functions.

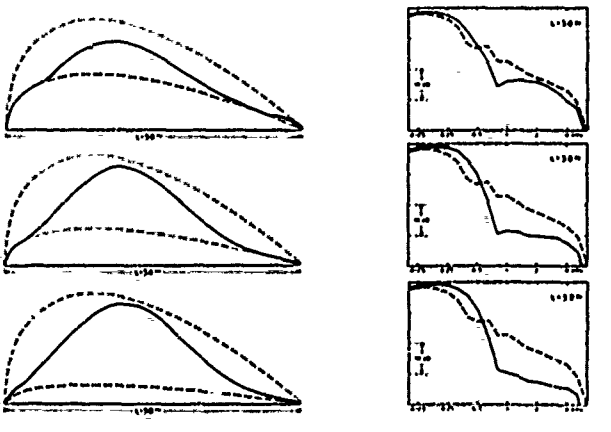

Fig. 4. Optimum LSA functions and their radiated one-third octave band spectra (solid curves) for 3.0 ft chord lengths. Radiation is minimized above 700 Hz. Lower bound on allowable LSA functions is 0.75, 0.5 and 0.25 times NACA 0012 airfoil of uniform spanwise thickness. Upper bound is 1.5 times NACA 0012 airfoil for all cases. Dashed curves have same meaning as in Fig. 3.

Turning now to the optimum LSA functions shown in Fig. 3, we see that the result in the 1.5-ft chord case has a very blunt leading edge. As the chord is increased to 3.0 ft, both the leading and the trailing edges drop onto the lower bound constraint. Then, as the chord is further increased, the trailing edge rises and takes on a more complex shape.

Table 1 lists the ordinates of the optimum LSA functions shown in Fig. 3. Since the termination of the optimization technique was chosen to given answers accurate to one part in one thousand, three significant figures are tabulated in Table 1.

TABLE 1. ORDINATES OF OPTIMUM LSA FUNCTIONS SHOWN IN FIG. 3. ORDINATES ARE GIVEN AS FRACTIONS OF CHORD LENGTH L.

x, ft	L=1.5	L=2.0	L=2.5	L=3.0	L=3.5	L=4.0
0.0	.000	.000	.000	.000	.000	.000
0.1	.094	.056	.038	.030	.028	.026
0.2	.089	.067	.049	.040	.038	.036
0.3	.107	.088	.068	.053	.053	.052
0.4	.114	.102	.085	.069	.068	.067
0.5	.122	.118	.103	.086	.086	.084
0.6	.123	.129	.118	.103	.102	.100
0.7	.120	.136	.132	.119	.118	.115
0.8	.112	.139	.143	.133	.132	.129
0.9	.103	.137	.150	.145	.143	.140
1.0	.084	.131	.152	.153	.151	.147
1.1	.067	.120	.150	.158	.155	.151
1.2	.048	.106	.144	.159	.156	.152
1.3	.030	.090	.134	.157	.154	.150
1.4	.013	.072	.121	.151	.149	.145
1.5	.001	.054	.106	.141	.141	.137
1.6		.037	.089	.130	.131	.129
1.7		.022	.073	.116	.121	.120
1.8		.014	.057	.102	.110	.112
1.9		.008	.042	.088	.099	.104
2.0		.001	.029	.073	.090	.097
2.1			.022	.060	.081	.090
2.2			.017	.048	.073	.083
2.3			.012	.037	.067	.086
2.4			.007	.029	.062	.084
2.5			.001	.022	.057	.083
2.6				.016	.052	.082
2.7				.014	.048	.079
2.8				.010	.044	.077
2.9				.006	.039	.073
3.0				.004	.034	.068
3.1					.028	.061
3.2					.023	.054
3.3					.017	.046
3.4					.012	.037
3.5					.008	.028
3.6						.021
3.7						.014
3.8						.008
3.9						.005
4.0						.001

In Fig. 4 we show the effects of varying the height of the lower bound constraint for the case of a 3.0-ft chord. Going from top to bottom in Fig. 4, the lower bound was taken to be 0.75, 0.50, and 0.25 times the NACA 0012 starting shape. The spectrum weighting function V(k) and interpolating function w(ξ) were the same as those used in obtaining the results of Fig. 3. Thus, the middle result shown in Fig. 4 is a repeat of the 3.0-ft chord result shown in Fig. 3. The general behavior of the spectra shown in Fig. 4 is as expected.

In Fig. 5 we show the LSA function that was obtained by taking V(k), $k = 2\pi f/c$, to be unity in the two octave band from 700 Hz to 2800 Hz and zero outside this band. For the interpolating function, we used Eq. 15 with $\theta = 0.50$. The chord L was taken to be 3.0 ft, and the number of samples N to be 50. This gives $\Delta = (L/N) = 0.06$ ft; hence, $f_c = [c/(2\Delta)] = 9200$ Hz is the inherent cutoff frequency of the sampled LSA function representation.

Fig. 5. Optimum LSA function and its radiated spectrum (solid curves) where radiation was minimized between 700 and 2800 Hz. Chord length is 3.0 ft. Dashed curves have same meaning as in Fig. 3.

It is clear from the spectrum shown in Fig. 5 that the frequencies between 2800 Hz and 9200 Hz were not suppressed in the optimization process. It is this high-frequency content that causes the erratic behavior of the LSA function shown in Fig. 5. However, in comparing the spectrum shown in Fig. 5 with the spectrum for the L = 3.0 ft case shown in Fig. 3, we see that virtually the same reduction of radiated sound in the two octave band from 700 Hz to 2800 Hz was obtained for the two cases.

To test the dependence of the above results on the particular interpolating function chosen, the 3.0 ft chord case shown in Fig. 3 was also run with a triangular interpolating function that decreased linearly from unity at any given sample to zero at its two nearest neighbors. The maximum fractional difference between the two LSA functions obtained was 2.3%. The optimum LSA function obtained with the interpolating function of Eq. 15 would seem to be somewhat preferable, however, since the continuous function defined between the sample points by Eq. 11 is smooth when Eq. 15 is used for interpolation.

The general behavior of the spectra shown in Fig. 3 can be partially explained with the aid of the uncertainty principle for Fourier transforms, which can be expressed [5] as

$$2k_m L_e \geq 2\pi \ , \tag{36}$$

or, in our application, as

$$2f_m L_e \geq c \ , \tag{37}$$

where k_m is the maximum angular wavenumber in the spectrum of the LSA function; hence, $f_m = ck_m/(2\pi)$ is the maximum frequency in the radiated spectrum in Hz, and where L_e is the nominal [5] *effective* LSA function chord, and c is the speed of sound.

Since we are considering rather sharp cutoffs in the frequency domain, we might first take $L_e = L/2$, where L is the actual chord. The "uncertainty principle", Eq. 37 in this case becomes $f_m L \geq c$. Solving the equality in this relation for L, using c = 1100 ft/sec and f_m = 700 Hz, gives L = 1.57 ft. For the situation studied in Fig. 3 we could not, therefore, have expected sharp reductions in the radiated spectrum for chord lengths less than about 1.5-ft. In fact, we saw little reduction for the 1.5 ft chord, but began to see strong reductions for the larger chords. However, we must recall that the center of gravity of the LSA functions of Fig. 3 has also been constrained to be off center. As far as the uncertainty principle is concerned, this has the effect of reducing the effective chord length somewhat further. The sharp reduction in the sound

radiation at frequencies beyond 700 Hz that occurs as the chord is increased from 1.5 ft to 3.0 ft is therefore completely consistent with the "uncertainty principle", as described by Eq. 37. The results of Fig. 3 therefore can be regarded as verification of Eq. 37, which is an expression of the fundamental limitation on the reduction of high-frequency sound radiation due to thickness effects.

IV. IMPLICATIONS FOR ROTOR TIP DESIGN

The synthesis results presented in Sec. III determine an LSA function only. The relation between the LSA function and the airfoil section and planform functions is shown graphically in Fig. 5, which is reproduced from Ref. 1. It is clear that having determined a new LSA function, we have the option of using a standard airfoil section and modifying the planform or the reverse, or modifying both planform and airfoil section. The purpose of this section is to discuss the factors that affect our choices in doing this.

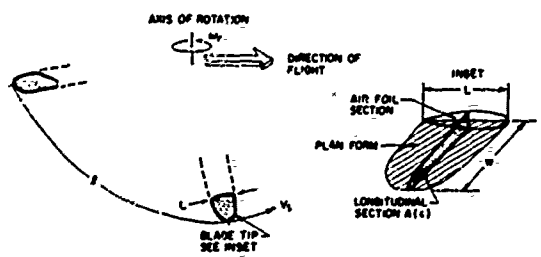

Fig. 6. Diagram of rotor blade tip showing how area function A(x) is derived.

If we vary the airfoil section shape, then two-dimensional airfoil theory can be used to compute the new pressure distribution as a function of chord for both surfaces [3]. Of course we wish the lift to remain constant, but we will also have to examine the pitching moment, and center of pressure. Certain aerodynamic derivatives, such as the changes of pitching moment and lift with angle of attack should also be evaluated so that the aeroelastic stability of the rotor is maintained.

A major difficulty with tip design of current rotors is the rather bluff end of the rotor. This is thought to cause separation of flow when the tip is forward of its maximum relative speed point, so that the inflow vector has a component *inward* along the blade span. When the inflow has this component, then the bluff end of the rotor is heading into the flow, and irregular or separated flow is likely to result. To avoid this problem, a combination of planform and airfoil section that presents an aerodynamic section to the flow as the inflow vector changes would be desirable. From an acoustical viewpoint, this means that the LSA function should also be relatively invariant to the direction of inflow, at least for variations in inflow direction of 20 degrees or so from the normal to the span. The LSA function must now be defined along the direction of the inflow vector, not along the chord (normal to the span).

The forces and moments on the outer regions of the rotor also affect the airfoil section/planform tradeoff. The lift on the rotor increases as one proceeds outward toward the tip, falling off rapidly at the tip. The distribution of lift along the span must be compatible with the spanwise bending rigidity. This would not seem to be a serious factor, however, in choosing the planform or airfoil section shapes.

If the lift varies along the span, vorticity will be shed along the span and the tip vortex will be spread out in a sheet. The amount of this spreading may have some effect on the shape (core size) of the trailing vortex from the tip and on the interaction of this vortex with a trailing rotor blade. Such interaction is known to produce acoustical impulses, termed "blade slap".

Clearly, the research presented in this paper does not allow us to draw detailed designs of rotor tips that not only produce less sound, but are also aerodynamically well behaved, etc. There is still enough flexibility in the choice of an airfoil to allow considerable latitude in designing for proper aerodynamics, since the allowable set of planform-airfoil-section combinations that meet the required LSA shape is still quite large. We believe that more theoretical research should be carried out on the simultaneous optimization for both acoustical and aerodynamic performance. We also believe that supporting experimental studies – both acoustical and aerodynamic – should be carried out to clarify actual benefits of the new designs and how sensitive the gains are to minor modifications in the airfoil and flow parameters.

Quite apart from the improved design of rotor tips for less noise radiation, we believe that the optimization method presented in Sec. III and the Appendices has a much broader application potential to minimizing the noise from rotors and propellors. Since analytical formulations for the sound radiated from rotating airfoils have been developed, it should be possible to minimize the rotational noise from propellors, for example, by procedures very similar to those presented in this paper.

V. ACKNOWLEDGEMENT

The authors are grateful to Dr. Sudhir Kumar who encouraged this research while he was at the U.S. Army Research Office/Durham, and to Mr. James Murray of that office. Dr. Robert Truitt, consultant to ARO/D has also been most helpful during the progress of this research. Discussions with Mr. Herbert Fox of BBN were very helpful in the early stages of the work.

APPENDIX A. MATHEMATICAL MOTIVATION FOR THE FIRST MOMENT CONSTRAINT

We show here that minimization of $|\tilde{A}(k)|^2$ over given bands of k, subject only to the constraint of Eq. 9, would lead to minimizing functions A(x) that are even functions about the mid-

chord point x = L/2. After changing the origin of the abscissa to the midchord point x = L/2 by defining the new coordinate y = x-(L/2), we express the translated longitudinal section area function $A^{\dagger}(y)$ as the sum of its even and odd parts $A_e^{\dagger}(y)$ and $A_o^{\dagger}(y)$ respectively:

$$A^{\dagger}(y) \triangleq A(y+[L/2])$$

$$= A_e^{\dagger}(y) + A_o^{\dagger}(y). \qquad (A.1)$$

For the Fourier transform $\tilde{A}^{\dagger}(k)$ of $A^{\dagger}(y)$ we have

$$\tilde{A}^{\dagger}(k) \triangleq \int_{-\infty}^{\infty} A^{\dagger}(y)e^{-iky}dy \qquad (A.2)$$

$$= \tilde{A}_c^{\dagger}(k) - i\tilde{A}_s^{\dagger}(k) \quad ,$$

where

$$\tilde{A}_c^{\dagger}(k) = \int_{-\infty}^{\infty} A_e^{\dagger}(y)\cos(ky)dy$$

$$\tilde{A}_s^{\dagger}(k) = \int_{-\infty}^{\infty} A_o^{\dagger}(y)\sin(ky)dy \; . \qquad (A.3)$$

From Eqs. A.1 and A.2 it follows that

$$|\tilde{A}(k)|^2 = |\tilde{A}^{\dagger}(k)|^2$$

$$= [\tilde{A}_c^{\dagger}(k)]^2 + [\tilde{A}_s^{\dagger}(k)]^2 \; . \qquad (A.4)$$

Now, since $A_o^{\dagger}(y)$ is an odd function, it contributes nothing to the area of $A^{\dagger}(y)$ which is the same as the area of A(x); however, the contribution of $A_o^{\dagger}(y)$ to $|\tilde{A}(k)|^2$, according to Eqs. A.3 and A.4, is $[\tilde{A}_s^{\dagger}(k)]^2$. It follows that the minimization of $|\tilde{A}(k)|^2$ over given bands, subject only to the area constraint of Eq. 9, would yield minimizing functions $A^{\dagger}(y)$ that have no odd part; that is, minimizing functions A(x) that are symmetric about the midchord point x = L/2.

APPENDIX B. METHOD OF OPTIMIZATION

The problem is to minimize $I(A_0,A_1,\cdots,A_N)$, as given by Eq. 24, where the admissible vectors $(A_0,A_1,\cdots,A_N)$ are subject to the constraints given by Eqs. 25, 28, and 31. Before discussing our approach to this problem, it is instructive to consider the problem with constraint A, Eq. 25 removed. The resulting problem is a classical minimization problem that, in principle, is easily solved using Lagrange multipliers. The solution involves matrix inversion and the solution of *linear* algebraic equations only. We would generally expect the solution to be unique; that is, we would expect only one vector $(A_0,A_1,\cdots,A_N)$ to yield a stationary value of $I(A_0,A_1,\cdots,A_N)$ subject to the constraints of Eqs. 28 and 31. However, we would *not* generally expect this solution vector to satisfy the constraint given by Eq. 25. In fact, some elements of this solution vector may have negative values. A similar situation exists with the *variational* problem that is formulated by finding an extremum of the integral in Eq. 7, where in this case $|\tilde{A}(k)|^2$ is given by Eq. 22, and where the admissible A(x) functions are subject to the constraints of Eqs. 9 and 10. In this case we would not generally expect the minimizing function to satisfy Eq. 8.

Our approach to the minimization problem defined by Eqs. 24, 25, 28 and 31 has been based on an intuitively appealing technique generally called either the method of gradients or the method of steepest descent. In discussing our approach, it is convenient to consider any set $(A_0,A_1,\cdots,A_N)$ of LSA function samples as a *point* in a space of N+1 dimensions. Constraint A defines a rectangular region of this space. The collection of points that satisfies *both* constraint B and constraint C defines a N-1 dimensional hyperplane within this space. Thus, the admissible points are points on this hyperplane that lie within the closed rectangular region defined by constraint A. Associated with each of these admissible points is a value of $I(A_0,A_1,\cdots,A_N)$. The problem is to find the admissible point $(A_0,A_1,\cdots,A_N)$ where $I(A_0,A_1,\cdots,A_N)$ takes on its minimum value.

Our numerical solutions were obtained using an iteration procedure. The procedure we used was chosen instead of one of the rather sophisticated gradient methods such as Davidson's method or the method of conjugate gradients because of the restriction imposed on the admissible domain of $I(A_0,A_1,\cdots,A_N)$ by constraint A. The approach described below is conceptually simple and allows the straightforward imposition of all of the constraints.

Our numerical procedure is begun with an initial choice $(A_0^{(0)},A_1^{(0)},\cdots,A_N^{(0)})$ of LSA function samples that satisfies constraints A, B and C. Hence, this starting point in our N+1 dimensional space lies on the hyperplane defined by constraints B and C, and it lies in the interior of the region defined by constraint A. The computation begins with the evaluation and storing of the N+1 values of G_n defined by Eq. 23. $I^{(0)}(A_0^{(0)}, A_1^{(0)},\cdots,A_N^{(0)})$, the initial value of I, is then evaluated using Eq. 24. An increment δA_j in each of $A_0, A_1, \cdots, A_N$ is then computed such that the new point

$$(A_0^{(1)},A_1^{(1)},\cdots,A_N^{(1)}) = (A_0^{(0)}+\delta A_0,A_1^{(0)}+\delta A_1,\cdots,A_N^{(0)}+\delta A_N) \qquad (B.1)$$

also satisfies constraints A, B and C.

The increments $\delta A_j, j=0,1,\cdots,N$ are chosen to maximize the rate of decrease of $I(A_0,A_1,\cdots,A_N)$ by taking the vector $(\delta A_0,\delta A_1,\cdots,\delta A_N)$ parallel to the negative of the gradient of $I(A_0,A_1,\cdots,A_N)$. Since we want to constrain the argument of $I^{(1)}(A_0^{(1)},A_1^{(1)},\cdots,A_N^{(1)})$, where $I^{(1)}$ is the new value of I, to lie on the hyperplane defined by constraints B and C, $I(A_0,A_1,\cdots,A_N)$ must be regarded as a function of only N-1 *independent* A_j, the two remaining A_j also being regarded as functions of the N-1 independent A_j, where this latter functional dependence is determined by constraints B and C, Eqs. 28 and 31. We must adhere to this rule in forming the gradient of $I(A_0,A_1,\cdots,A_N)$. Let us designate the two dependent A_j by A_m and A_n. Then A_m and A_n can be explicitly expressed as functions of the N-1 independent A_j by solving Eqs. 28 and 31 for A_m and A_n using Cramer's rule. The result is

$$A_m = \frac{1}{(n-m)}\left[\frac{(n\Delta+\gamma)M_0-M_1}{\Delta\tilde{W}(0)} - \sum_{j\neq m,n}(n-j)A_j\right] \tag{B.2}$$

$$A_n = \frac{1}{(m-n)}\left[\frac{(m\Delta+\gamma)M_0-M_1}{\Delta\tilde{W}(0)} - \sum_{j\neq m,n}(m-j)A_j\right] , \tag{B.3}$$

where $j\neq m,n$ designates the set of all integers $0\leq j\leq N$ except $j=m$ and $j=n$. Continuing to consider A_m and A_n as functions of the N-1 independent A_j, we can now find $\partial I/\partial A_k$ by differentiating Eq. 24:

$$\frac{\partial I}{\partial A_k} = 2\,G_0\left(A_k - \frac{n-k}{n-m}A_m - \frac{m-k}{m-n}A_n\right)$$

$$+ 2\sum_{j=1}^{N} G_j\left[\sum_{i=0}^{N-j} A_i\left(\delta_{i+j,k} - \frac{n-k}{n-m}\delta_{i+j,m} - \frac{m-k}{m-n}\delta_{i+j,n}\right)\right. \tag{B.4}$$

$$\left. + A_{i+j}\left(\delta_{i,k} - \frac{n-k}{n-m}\delta_{i,m} - \frac{m-k}{m-n}\delta_{i,n}\right)\right] \quad , \; k\neq m,n$$

where $\delta_{i,j}$ denotes Kronecker's delta, and where in carrying out the above differentiation, we required the partial derivatives

$$\frac{\partial A_m}{\partial A_k} = -\frac{(n-k)}{(n-m)} , \qquad \frac{\partial A_n}{\partial A_k} = -\frac{(m-k)}{(m-n)} \quad , \; k\neq m,n \tag{B.5}$$

which were obtained by differentiating Eqs. B.2 and B.3. From the definition of the gradient, the increments $\delta A_j (j\neq m,n)$ are thus given by

$$\delta A_j = -h\frac{\partial I}{\partial A_j} \quad , \; j\neq m,n \tag{B.6}$$

where h is a constant independent of j that determines the step size, and where $\partial I/\partial A_j$ is determined for all $0\leq j\leq N$ except $j=m,n$ by evaluating the right-hand side of Eq. B.4 using the initial set $\{A_0^{(0)},A_1^{(0)},\cdots,A_N^{(0)}\}$ of A_j's.

From the increments δA_j determined by Eq. .6, the new set of A_j's is then evaluated for all $0\leq j\leq N$ except $j=m,n$:

$$A_j^{(1)} = A_j^{(0)} + \delta A_j, \; j\neq m,n . \tag{B.7}$$

It is possible that one or more of these values of $A_j^{(1)}$ will fall outside the intervals defined by constraint A. Hence, at this juncture, each of these values of $A_j^{(1)}$, $j\neq m,n$ is tested to insure that it satisfies constraint A. Any value that crossed either of the boundaries, a_j or b_j, is set equal to the value of the boundary that was crossed.

Using Eqs. B.2 and B.3, $A_m^{(1)}$ and $A_n^{(1)}$ are then evaluated from the N-1 values of $A_j^{(1)}$ determined by Eq. B.7. These values of $A_m^{(1)}$ and $A_n^{(1)}$ are then tested to insure that they do not violate constraint A. If either violates constraint A, a smaller value of h in Eq. B.6 is chosen, and the procedure from Eq. B.6 on is repeated. The method explained in Appendix C for choosing the values of m and n insures that the computed values of A_m and A_n will seldom violate constraint A when reasonable values of h are used. The above procedure for determining $\{A_0^{(1)},A_1^{(1)},\cdots,A_N^{(1)}\}$ guarantees that this new point will satisfy constraints A, B and C.

At this stage, the value of $I^{(1)}(A_0^{(1)},A_1^{(1)},\cdots,A_N^{(1)})$ is computed using Eq. 24. It is then compared with the value of $I^{(0)}(A_0^{(0)},A_1^{(0)},\cdots,A_N^{(0)})$. Unless h was taken too large, $I^{(1)}$ will be less than $I^{(0)}$. If $I^{(1)}$ is greater than $I^{(0)}$ a smaller value for h is chosen, and the operations beginning with Eq. B.6 are repeated. If $I^{(1)}$ is less than $I^{(0)}$, $\{A_0^{(1)},A_1^{(1)},\cdots,A_N^{(1)}\}$ becomes the new starting point, and the operations beginning with the evaluation of Eq. B.4 are repeated.

Eventually, for some value of i, $I^{(i+1)}(A_0^{(i+1)},A_1^{(i+1)},\cdots,A_N^{(i+1)})$ will be greater than $I^{(i)}(A_0^{(i)},A_1^{(i)},\cdots,A_N^{(i)})$. When this occurs, the admissible point $(A_0,A_1,\cdots,A_N)$, where $I(A_0,A_1,\cdots,A_N)$ takes on its minimum value, has been overshot. Hence, at this stage, h is given a smaller value and the computation is returned to the operations beginning with Eq. B.6. Using this smaller value of h, we again continue to march toward the admissible point where I takes on its minimum value, always going in the most downhill direction on the admissible hyperplane defined by constraints B and C, and always staying within the admissible region defined by constraint A. When it is observed that, for some larger i, $I^{(i+1)}$ again exceeds $I^{(i)}$, then the value for h is further reduced, and computation is again returned to the operations beginning with Eq. B.6. This process is terminated when negligibly small step sizes lead to an increase in $I(A_0,A_1,\cdots,A_N)$. In our numerical calculations, we automatically terminated the above process when changes in A_j, with magnitudes no larger than (1/1000) of the largest value of A_j, led to an increase in the value of $I(A_0,A_1,\cdots,A_N)$.

Because evaluation of the function I and its gradient involves only computation of quadratic forms in the A_j's, each "downhill step" took relatively little computer time. Thus the comparatively slow convergence (typically, on the order of 100 steps were required) was not costly. In fact, more processor time was required for the evaluation of the coefficients G_n through the integrals of Eq. 23 than was needed for the entire gradient descent.

APPENDIX C. METHOD USED FOR DETERMINING m AND n

At any given stage of the iteration procedure described in Appendix B, the use of Eqs. B.2 and B.3 to evaluate $A_m^{(1)}$ and $A_n^{(1)}$ from the remaining $A_j^{(1)}$'s guaranteed that the set of $A_j^{(1)}$'s, $j=0,1,\cdots,N$ would satisfy constraints B and C. At each stage of iteration, m and n were chosen so that the values of A_m and A_n, computed from Eqs. B.2 and B.3, were very unlikely to violate constraint A when reasonably small values for h were used. This was accomplished by choosing m to be the index j of the A_j function sample of the prior iteration that had the largest minimum distance from the bounds a_j and b_j in the first one-third of the interval $0\leq j\leq N$, and by choosing n in a similar fashion from the indices j in the last one-third of the interval $0\leq j\leq N$. That is, to determine m at a given stage of the iteration, we found the maximum over j of the smaller of $(A_j^{(i-1)}-a_j)$ or $(b_j-A_j^{(i-1)})$ as j was varied over the integers $0\leq j\leq[(N-2)/3]$. The resulting value of j was chosen for m. The rule determination over the integers

$[(2N+2)/3] \leq J \leq N$ yielded the value $j = n$. We chose m from the first one-third and n from the last one-third of $0 \leq J \leq N$ to insure that the magnitudes of the denominators n-m and m-n in Eqs. B.2 and B.3 were reasonably large. By choosing m and n in the above manner, it was assured that the magnitudes of the increments $\delta A_m = (A_m^{(i)} - A_m^{(i-1)})$ and $\delta A_n = (A_n^{(i)} - A_n^{(i-1)})$ could be relatively large without the new values $A_m^{(i)}$ and $A_n^{(i)}$ violating constraint A.

REFERENCES

1. R.H. Lyon, "Radiation of Sound by Airfoils that Accelerate Near the Speed of Sound," *J. Acoust. Soc. Am.* 49, pp. 894-905 (1971).

2. J.E. Ffowcs Williams, "The Noise from Turbulence Convected at High Speed," *Phil Trans. Roy. Soc.*, London, A255, pp. 469-503 (1963).

3. I.H. Abbott and A.E. Von Doenhoff, *Theory of Wing Sections* (Dover Publications, Inc., New York 1959).

4. R.M. Lerner, "Representation of Signals," Chapter 10 of *Lectures on Communication System Theory*, E.J. Baghdady Ed., (McGraw-Hill Inc., New York, 1961).

5. L. Brillouin, *Science and Information Theory*, 2nd Ed. (Academic Press, New York, 1962). See p. 87, Eq. 8.30a.

LIST OF FIGURE CAPTIONS

Figure 1. One-third octave band spectra for thickness and lift radiation. (See text for parameters.)

2. One-third octave band spectra for thickness and lift radiation including high-frequency vortex shedding. (See text for parameters.)

3. Optimum LSA functions and their radiated one-third octave band spectra (solid curves) for chord lengths L ranging from 1.5 to 4.0 ft. Radiation is minimized above 700 Hz. Upper and lower bounds (dashed curves) on allowable LSA functions are 0.5 and 1.5 times NACA 0012 airfoil of uniform spanwise thickness. Dashed spectra are those of NACA 0012 airfoils of same chord length, sectional area, and center of gravity as optimum LSA functions.

4. Optimum LSA functions and their radiated one-third octave band spectra (solid curves) for 3.0 ft chord lengths. Radiation is minimized above 700 Hz. Lower bound on allowable LSA functions is 0.75, 0.5 and 0.25 times NACA 0012 airfoil of uniform spanwise thickness. Upper bound is 1.5 times NACA 0012 airfoil for all cases. Dashed curves have same meaning as in Fig. 3.

5. Optimum LSA function and its radiated spectrum (solid curves) where radiation was minimized between 700 and 2800 Hz. Chord length is 3.0 ft. Dashed curves have same meaning as in Fig. 3.

6. Diagram of rotor blade tip showing how area function A(x) is derived.

SOME ASPECTS OF HELICOPTER NOISE THEORY

Part I Acoustic Radiation from a Plane Surface with Application to Rotors*

by Gregory F. Homicz

Abstract

A formalism is developed for predicting acoustic radiation from a plane surface that exerts a fluctuating load upon the surrounding fluid. The development assumes the pressure field on the surface to be random and stochastic; it may be both non-stationary and inhomogeneous. The result is an expression for the acoustic power spectrum in terms of an integral over the disturbance region of the generalized four-dimensional Fourier spectrum of the forces. It is capable of predicting discrete-frequency as well as broad-band spectra. A few illustrative examples pertaining to rotors are presented; the results agree with those cases that have been treated previously. The treatment is being extended to the broad-band noise emanating from a rotor in turbulent air.

I. Introduction

The classic problem in rotor noise theory was analyzed by Gutin[1] in 1936. He modeled the blades as B point forces rotating at constant angular velocity with no variation in their magnitudes and obtained a discrete spectrum at multiples of the blade-passage frequency $B\Omega$. Lowson and Ollerhead[2,3], as well as Wright[4], have extended this to the case where the force varies sinusoidally in the azimuth angle. The spectrum is still discrete, though Lowson et al.[2] briefly discuss the extension to random loads, and hence broad-band acoustic spectra. Sharland[5] gives evidence that free-stream turbulence can be a significant factor in such loadings. He estimates the total radiated acoustic energy from a fan rotor under such circumstances; however, his result leans rather heavily on empirical estimates of the correlation areas and is useful primarily in estimating orders of magnitude or in interpreting data. Ffowcs Williams and Hawkings[6] calculate the radiation from a rotating point force with random loading in terms of the load spectrum as measured moving with the dipole. Morfey and Tanna[7] consider the same problem and obtain the acoustic spectrum as a power series in Ω/f. Both leave open the question of how the load spectrum might be related to the turbulence characteristics. Morfey[8] and Sevik[9] handle this by modeling the blades as an infinite cascade and then using two-dimensional incompressible airfoil theory; this is a better approximation for compressors and fans than for helicopter rotors. Both also assume the blade chords to be acoustically compact, i.e., a blade becomes a line of dipoles. In many practical applications, particularly at higher frequencies, and higher subsonic Mach numbers, the above assumptions are difficult to justify a priori.

It is hoped that the present treatment will point the way toward relaxing some of these approximations. A groundwork is presented for the prediction of broad-band as well as discrete-frequency noise radiated from a surface distribution of dipoles in an otherwise unbounded fluid; it is directly applicable to calculation of the acoustic signatures of rotors encountering atmospheric turbulence. The acoustics equations themselves are linear, and linearized aerodynamic theory will be used to obtain the lift response. Hence the overall problem can be viewed as that of determining the statistical response characteristics of a linear system subjected to a random input.

The system may be conveniently divided into two sub-systems: The first determines the lift response of a fixed point in the rotor to a given pattern of turbulence, and the second determines the radiated sound from the lift response. The lift response is characterized by an impulse-response function, or equivalently by an aerodynamic transfer function. We will neglect the effects of drag and centrifugal forces, as well as those of turbulent velocity components in the rotor plane. Assuming the appropriate transfer functions are known, these could be easily included. The second sub-system, using the above response as input, transforms it into the resultant noise spectrum at the observer's position. This is achieved through the far-field solution of the inhomogeneous acoustic wave equation as formulated by Lighthill[10]. The present discussion concerns primarily the latter analysis, and its results are generally applicable to a much broader class of problems than that of rotating forces; it is easily extended to surface distributions of other acoustic singularities, such as monopoles or quadrupoles. A few elementary examples pertinent to lifting rotors are presented; the results agree with those of other authors in those cases previously investigated. A preliminary discussion of the analysis of the lift response is then given.

II. Solution of Acoustic Wave Equation

The equation describing the generation of traveling waves by a distribution of acoustic dipoles is[10]

$$\frac{1}{a_0^2}\frac{\partial^2 \rho}{\partial t^2} - \nabla^2 \rho = \frac{\partial F_i}{\partial x_i} \qquad (1)$$

where $\vec{F}$ represents force/volume. The far-field solution can be expressed as

$$\rho = \frac{1}{4\pi a_0^2}\frac{x_i}{r^2}\int \left[\frac{\partial F_i}{\partial t}\right] d^3y \qquad (2)$$

Equation (2) is valid under the following conditions:

$$kr \gg 1 \qquad (A)$$

$$r \gg |\vec{y}|_{max} \qquad (B)$$

Assumption (B) is a statement that the disturbance region appears geometrically compact to the observer. Using the isentropic relation, $p = a_0^2 \rho$, and our supposition that $\vec{F} = L\,\hat{n}$, (see Fig. 1), we get

$$p = \frac{1}{4\pi a_0}\frac{x_i}{r^2}\int \left[\frac{\partial L}{\partial t}\right] d^3y \qquad (3)$$

In our case, not only does (B) hold, but to lowest order the forces all lie in the plane $y_3 = 0$. Hence we can substitute $L = l\,\delta(y_3)$, resulting in the surface integral form

$$p = \frac{1}{4\pi a_0}\frac{\sin\phi}{r}\int \left[\frac{\partial l}{\partial t}\right] d^2y \qquad (4)$$

where it is understood that $\vec{y}$ now lies in the horizontal plane.

* This research was supported under contract NIH-CO- 70 C 0057; it was carried out under the supervision of Professor A. R. George, whose invaluable guidance is gratefully acknowledged.

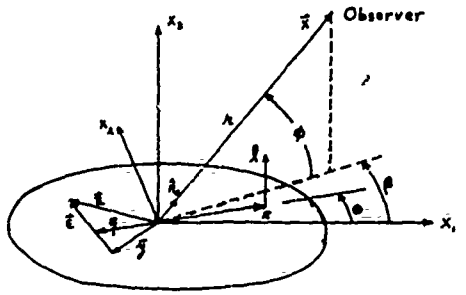

Fig. 1. Rotor geometry and coordinate systems.

Since our problem is random, we cannot get an expression for $p(\vec{x},t)$ as a deterministic function, but we can work with an acoustic intensity averaged over a hypothetical ensemble of realizations. Consider the quantity

$$p(\vec{x},t-\tau/2;j)\,p(\vec{x},t+\tau/2;j)$$

where the argument j is an ensemble parameter whose different integer values 1, 2,... N refer to different realizations of the same experiment. Performing a statistical average over all realizations, we obtain

$$R_{pp}(\vec{x},t,\tau) \equiv \overline{p(\vec{x},t-\tau/2)\,p(\vec{x},t+\tau/2)} \tag{5}$$

and hence the ensemble-averaged instantaneous intensity as

$$\overline{I}(\vec{x},t) = \frac{\overline{p^2(\vec{x},t)}}{\rho_0 a_0} = \frac{R_{pp}(\vec{x},\tau,0)}{\rho_0 a_0} \tag{6}$$

Now consider the Fourier transform of $R_{pp}(\vec{x},t,\tau)/\rho_0 a_0$ with respect to τ, and its inverse:

$$S(\vec{x},t,f) = \int_{-\infty}^{\infty} \frac{R_{pp}(\vec{x},t,\tau)}{\rho_0 a_0} e^{-i2\pi f\tau}\,d\tau \tag{7a}$$

$$\frac{R_{pp}(\vec{x},t,\tau)}{\rho_0 a_0} = \int_{-\infty}^{\infty} S(\vec{x},t,f)\,e^{+i2\pi f\tau}\,df \tag{7b}$$

Substituting from (7b) into (6) we find:

$$\overline{I}(\vec{x},t) = \int_{-\infty}^{\infty} S(\vec{x},t,f)\,df \tag{8}$$

and hence S is the spectral decomposition of $\overline{I}$; it represents the acoustic energy radiated within the frequency interval f to $f+df$.

Substituting for $p(\vec{x},t;j)$ from (4) into (5) yields

$$\frac{R_{pp}(t,\tau)}{\rho_0 a_0} = \frac{\sin^2\phi}{16\pi^2\rho_0 a_0^2 h^2} \times$$

$$\iint_{-\infty}^{\infty} \overline{\frac{\partial f}{\partial t}(\vec{\eta},t-\tau/2-|\vec{x}-\vec{\eta}|/a_0)\;\frac{\partial f}{\partial t}(\vec{\xi},t+\tau/2-|\vec{x}-\vec{\xi}|/a_0)}\;d^2\eta\,d^2\xi \tag{9}$$

It is convenient to denote the geometric coefficient preceding the integral by the symbol G. We also introduce the average and relative position vectors, $\vec{\eta}$ and $\vec{\epsilon}$, defined by (see Fig. 2)

$$\eta = \frac{\vec{\eta}+\vec{\xi}}{2} \qquad \epsilon = \vec{\xi}-\vec{\eta}$$

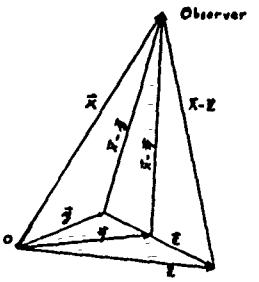

Fig. 2. Coordinate transformations.

It is easily verified that the Jacobian of this transformation is 1, and hence $d^2\eta\,d^2\xi \longrightarrow d^2\eta\,d^2\epsilon$ directly.

Now consider the term $|\vec{x}-\vec{y}|/a_0$ occurring in the first retarded time. From Fig. 2 we see that

$$\vec{x}-\vec{y} = \vec{x}-\vec{\eta}+\vec{\epsilon}/2$$

$$|\vec{x}-\vec{y}| = \left\{|\vec{x}-\vec{\eta}|^2+\vec{\epsilon}\cdot(\vec{x}-\vec{\eta})+|\vec{\epsilon}|^2/4\right\}^{1/2}$$

$$|\vec{x}-\vec{y}| \simeq |\vec{x}-\vec{\eta}|\left\{1+\frac{\vec{\epsilon}\cdot(\vec{x}-\vec{\eta})}{2|\vec{x}-\vec{\eta}|^2}+O\left(\frac{|\vec{\eta}|_{max}}{\lambda}\right)^2\right\}$$

$$|\vec{x}-\vec{y}| = |\vec{x}-\vec{\eta}|+\vec{\epsilon}\cdot\hat{n}/2+O\left(\frac{|\vec{\eta}|^2_{max}}{\lambda}\right) \tag{10a}$$

$\hat{n}$ being the unit vector along $\vec{x}-\vec{\eta}$.

Similarly

$$|\vec{x}-\vec{\xi}| \simeq |\vec{x}-\vec{\eta}|-\vec{\epsilon}\cdot\hat{n}/2+O\left(\frac{|\vec{\eta}|^2_{max}}{\lambda}\right) \tag{10b}$$

Thus (9) becomes

$$\frac{R_{pp}(t,\tau)}{\rho_0 a_0} = G\iint_{-\infty}^{\infty} \overline{\frac{\partial f}{\partial t}\left(\eta-\epsilon/2,\,t-\tau/2-\frac{|\vec{x}-\vec{\eta}|-\vec{\epsilon}\cdot\hat{n}/2}{a_0}\right)}\times$$

$$\overline{\frac{\partial f}{\partial t}\left(\eta+\epsilon/2,\,t+\tau/2-\frac{|\vec{x}-\vec{\eta}|-\vec{\epsilon}\cdot\hat{n}/2}{a_0}\right)}\;d^2\eta\,d^2\epsilon \tag{11}$$

Form the Fourier transform with respect to τ :

$$S(\vec{x},t,f) = G\int_{-\infty}^{\infty} e^{-i2\pi f\tau}\,d\tau \iint \overline{\frac{\partial f}{\partial t}(\cdot\,\cdot)\,\frac{\partial f}{\partial t}(\cdot\,\cdot)}\;d^2\eta\,d^2\epsilon$$

and define

$$t_{ma} \equiv t - |\vec{x}-\vec{\eta}|/a_o$$

$$s = \tau + \vec{\epsilon}\cdot\hat{n}/a_o, \quad d\tau = ds$$

being the average retarded time between $\vec{\eta}$ and $\vec{\epsilon}$. Then

$$S(\vec{x},t,f) = G\int_{-\infty}^{\infty} e^{-i2\pi fs}\,ds \iint_{-\infty}^{\infty} e^{+i2\pi f\frac{\vec{\epsilon}\cdot\hat{n}}{a_o}} \times$$

$$\overline{\frac{\partial f}{\partial t}\left(\vec{\eta}-\frac{\vec{\epsilon}}{2},\, t_{ma}-\frac{s}{2}\right)\frac{\partial f}{\partial t}\left(\vec{\eta}+\frac{\vec{\epsilon}}{2},\, t_{ma}+\frac{s}{2}\right)}\;d^2\eta\,d^2\epsilon \qquad (12)$$

The arguments appearing in the correlation now appear in symmetric form, allowing us to write

$$S(\vec{x},t,f) = G\int_{-\infty}^{\infty} d^2\eta \int_{-\infty}^{\infty} ds\, e^{-i2\pi fs} \int_{-\infty}^{\infty} d^2\epsilon\, e^{+i2\pi f\frac{\vec{\epsilon}}{a_o}\cdot\hat{n}_o\cdot\vec{\epsilon}} \times$$

$$R_{jj}(\vec{\eta},\vec{\epsilon},t_{ma},s) \qquad (13)$$

It is easily shown that replacement of $\hat{n}$ by $\hat{n}_o$ in the exponent requires $|\vec{\eta}|^2_{max}/\lambda \ll a_o/f$, or

$$k\frac{|\eta|^2_{max}}{2} \ll 1 \qquad (c)$$

which is called the Fraunhofer or diffraction parameter. Carrying out the last two integrations,

$$S(\vec{x},t,f) = G\int_{-\infty}^{\infty} d^2\eta\; P_{jj}\left(\vec{\eta},-\frac{f}{a_o}\hat{n}_o,\, t_{ma},\, f\right) \qquad (14)$$

where $P_{jj}(\vec{\eta},\vec{\kappa},t_{ma},f)$ is the generalized four-dimensional Fourier transform of R_{jj} with respect to $\vec{\epsilon}$ and s , but evaluated at $\vec{\kappa} = -\frac{f}{a_o}\hat{n}_o$. Note that the appearance of the spatial transform with this argument is a result of having retained differences in retarded times in (11); the decomposition of the lift distribution into its Fourier components in space would be unnecessary had we assumed an acoustically compact source region. There is a simple physical interpretation of why the two-dimensional spatial load spectrum must be evaluated in terms of a three-dimensional wave vector. It is easily seen that the spatial transform of a single-wavelength two-dimensional sinusoid (see Fig. 3) is simply $\frac{1}{2}[\delta(k_1-k_s)+\delta(k_1+k_s)]\,\delta(k_2)\,\delta(k_3)$. We have singled

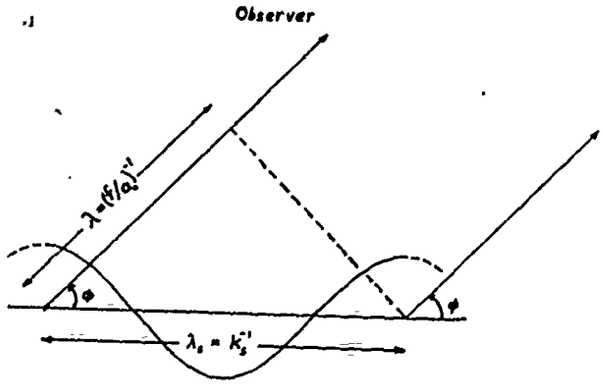

Fig. 3. Constructive interference at frequency f .

out a magnitude, f/a_o , and direction, $\hat{n}_o$, for $\vec{K}$, and hence $k_1 = -\frac{f}{a_o}\cos\phi$. So the above requires that

$$k_s = \pm\frac{f}{a_o}\cos\phi \quad \text{or} \quad \lambda_s = \pm\,\lambda/\cos\phi$$

i.e., just as in a diffraction grating, the intensity at frequency at an elevation angle ϕ depends only on those sources oscillating with frequency f and distributed spatially with the wavelength λ_s given above. Only then do the signals constructively interfere, as is easily seen from the geometry of Fig. 3.

While (14) provides more detailed information than (11), we would like to get the integral in terms of P_{ll} , since l is more commonly available than $\dot{l}$. To this end we quote a useful result from stochastic-process theory, which expresses R_{jj} in terms of $R_{ll}^{(1)}$:

$$R_{jj}(t_1,t_2) = \frac{\partial^2 R_{ll}(t_1,\tau_2)}{\partial t_1\,\partial t_2} \qquad (15)$$

where here t_1 and t_2 are both absolute values of time. In our notation,

$$t = \frac{t_1+t_2}{2} \qquad \tau = t_2 - t_1$$

and the chain rule for differentiation easily transforms the above to

$$R_{jj}(t,\tau) = \frac{1}{4}\frac{\partial^2 R_{ll}}{\partial t^2} - \frac{\partial^2 R_{ll}}{\partial\tau^2} \qquad (16)$$

which we use in

$$P_{jj} = \iint_{-\infty}^{\infty} R_{jj}\, e^{-i2\pi(f\tau+\vec{K}\cdot\vec{\epsilon})}\,d\tau\,d^2\epsilon$$

$$= \iint_{-\infty}^{\infty}\left\{\frac{1}{4}\frac{\partial^2}{\partial t^2} - \frac{\partial^2}{\partial\tau^2}\right\} R_{ll}\, e^{-i2\pi(f\tau+\vec{K}\cdot\vec{\epsilon})}\,d\tau\,d^2\epsilon$$

In the first term, $\frac{\partial^2}{\partial t^2}$ may be brought outside the integrals, and the second term may be integrated by parts twice to yield

$$P_{ii} = \left\{ \frac{1}{a^2} \frac{\partial^2}{\partial t^2} + (2\pi f)^2 \right\} P_{ll} \tag{17}$$

so that (14) becomes

$$S(\vec{x},t,f) = G\left(\frac{1}{a^2} \frac{\partial^2}{\partial t^2} + 4\pi^2 f^2 \right) \times \int_{-\infty}^{\infty} P_{ll}\left(\vec{\eta}, -\frac{f}{a_0}\hat{n}_0, t - |\vec{x}-\vec{\eta}|/a_0, f\right) d^3\eta \tag{18}$$

If the integrand was only weakly non-stationary, the $\frac{\partial^2}{\partial t^2}$ term could be negligible in comparison with the f^2 term in a particular application. In any case, in most acoustical applications and measurements, the physical quantity of interest is the time-averaged power spectral density [12]:

$$\langle S(\vec{x},f)\rangle = \lim_{T\to\infty} \frac{1}{T} \int_{-T/2}^{T/2} S(\vec{x},t,f)\, dt$$

Under such an averaging process, the first term in (18) contributes nothing, as

$$\left\langle \frac{\partial^2 P_{ll}}{\partial t^2} \right\rangle = \lim_{T\to\infty} \frac{1}{T} \int_{-T/2}^{T/2} \frac{\partial^2 P_{ll}}{\partial t^2}\, dt$$

$$\left\langle \frac{\partial^2 P_{ll}}{\partial t^2} \right\rangle = \lim_{T\to\infty} \frac{1}{T} \left. \frac{\partial P_{ll}}{\partial t} \right|_{-T/2}^{T/2} = 0$$

provided only that $\frac{\partial P_{ll}}{\partial t}$ is finite at $\pm\infty$.

Thus the acoustic analysis reduces to its final form in terms of time-averaged quantities:

$$I \equiv \langle \overline{F}(\vec{x}) \rangle = \int_{-\infty}^{\infty} \langle S(\vec{x},f)\rangle\, df \tag{19}$$

where

$$\langle S(\vec{x},f)\rangle = \frac{\sin^2\phi\, f^2}{4\rho_0 a_0^3 R^2} \int_{-\infty}^{\infty} \left\langle P_{ll}\left(\vec{\eta}, -\frac{f}{a_0}\hat{n}_0, f\right)\right\rangle d^3\eta \tag{20}$$

Equation (20) is the main result of this section. It assumes only that the disturbance region is planar and that

$$kR \gg 1 \;;\quad |\vec{y}|_{max}/R \ll 1 \;;\quad k|\vec{y}|^2_{max}/R \ll 1$$

Either broad-band or discrete-frequency spectra can be handled, and no simplification for the case of rotors has yet been made. Since the manipulations involved are concerned primarily with the arguments of the disturbance functions, rather than their physical significance, results analogous to (20) for acoustic monopoles and quadrupoles are easily derived.

We note that the calculations in (20) are all performed in space-fixed coordinates; this can be a big advantage in calculating noise from rotors in turbulence, since it is in such a coordinate frame that turbulent velocity correlations and spectra are most easily specified. Most investigations have assumed that the spectrum of lift fluctuations as seen by the moving blade is known, which is usually true only if such measurements have been made.

Section IV will give a brief introduction as to how $\left\langle P_{ll}\left(\vec{\eta}, -\frac{f}{a_0}\hat{n}_0, f\right)\right\rangle$ can be determined theoretically. The next section gives a few elementary examples in which P_{ll} is prescribed a priori, to demonstrate the application of (20).

III. Examples of Acoustic Analysis

In this section three examples of the application of (20) to lifting rotors are given. The first two involve discrete spectra; the last is broad-band. They all involve a point dipole rotating in a circle and experiencing fluctuations of the forms

Case A: $\cos\gamma\theta$ (cf. Gutin[6], Lowson and Ollerhead[3], Wright[4])

Case B: $\sin\gamma\Omega t$, new

Case C: "white noise" (cf. Ffowcs Williams and Hawkings[6])

In Case C, the result has been extended to any planar motion.

Case A: Consider B point lift forces rotating at angular frequency Ω about the origin, with their magnitude varying as $\cos\gamma\theta$, γ being a positive integer or zero (see Fig. 1). By inspection,

$$l(R,\theta,t) = L_0 \cos\gamma\theta\, \delta(R-R_0) \sum_{j=0}^{B-1} \delta\left(R_0\theta - \frac{2\pi R_0 j}{B} - 2\pi R_0\Omega t\right)$$

$$= \frac{L_0}{R_0} \cos\gamma\theta\, \delta(R-R_0) \sum_{j=0}^{B-1} \delta\left(\theta - \frac{2\pi j}{B} - 2\pi\Omega t\right) \tag{21}$$

where we have used

$$\int f(x)\, \delta\{a(x-x_0)\}\, dx = \int \frac{f(x)}{a}\, \delta(x-x_0)\, dx$$

Even though this is a deterministic problem, it is still valid to speak in terms of correlations and spectra, if one keeps in mind that $\overline{(\;)} \equiv \langle\; \rangle$ and hence all realizations by definition coincide with the mean value. We form

$$R_{ll} = \frac{L_0^2}{R_0^2} \delta(R-R_0)\, \delta(\epsilon_R) \cos\gamma\left(\theta - \epsilon_\theta/2\right) \cos\gamma\left(\theta + \epsilon_\theta/2\right) \times \sum_{j=0}^{B-1} \sum_{m=0}^{B-1} \delta\left(\theta - \epsilon_\theta/2 - \frac{2\pi j}{B} - 2\pi\Omega(t-\tau/2)\right) \delta\left(\theta + \epsilon_\theta/2 - \frac{2\pi m}{B} - 2\pi\Omega(t+\tau/2)\right)$$

$$= \frac{L_0^2}{R_0^2} \delta(R-R_0)\, \delta(\epsilon_R)\, \frac{1}{2}\left(\cos\gamma\epsilon_\theta + \cos 2\gamma\theta\right) \sum_{j=0}^{B-1} \delta\left(\theta - \frac{2\pi j}{B} - 2\pi\Omega t\right) \sum_{m=0}^{B-1} \delta\left(\epsilon_\theta - \frac{4\pi m}{B} - 2\pi\Omega\tau\right) \tag{22}$$

We can perform the time average immediately. Since dependence on t is periodic with a fundamental frequency of $B\Omega$, we average over the interval 0 to $1/B\Omega$, which picks up one "pulse" from the sum over j. The result is

$$\langle R_{ll}\rangle = \frac{B L_0^2}{4\pi R_0^2} \left[\cos\gamma\epsilon_\theta + \cos 2\gamma\theta\right] \delta(R-R_0)\, \delta(\epsilon_R) \times \sum_{m=0}^{B-1} \delta\left(\epsilon_\theta - \frac{2\pi m}{B} - 2\pi\Omega\tau\right) \tag{23}$$

From (20),

$$\langle S\rangle = 4\pi^2 f^2 G \int_0^\infty R\,dR \int_0^{2\pi} d\theta \int_{-\infty}^{\infty} d\tau\, e^{-i2\pi f\tau} \times$$

$$\int R\,d\epsilon_\theta \int_0^\infty d\epsilon_R\, e^{+i2\pi \frac{f}{a_0}\hat{n}_0\cdot\vec{\epsilon}} \langle R_{ll}\rangle \tag{24}$$

The integrations over R and ϵ_R are easily performed due to the presence of the δ functions. Making use of the geometry in Figs. 1 and 4 and a little manipulation in the exponent gives

$$\langle S\rangle = \frac{\beta L_0^2}{4\pi}(4\pi^2 f^2) G \int_{-\infty}^{\infty} d\tau\, e^{-i2\pi f\tau} \int_0^{2\pi} d\theta \int d\epsilon_\theta \left(\cos\gamma\epsilon_\theta + \cos 2\gamma\theta\right) e^{+i4\pi R_0 \frac{f}{a_0}\cos\phi \sin(\beta-\theta)\sin\epsilon_\theta/2} \times$$

$$\sum_{m=0}^{B-1} \delta\left(\epsilon_\theta - \frac{2\pi m}{B} - 2\pi\Omega\tau\right) \tag{25}$$

$$\langle S\rangle = \frac{\beta L_0^2}{4\pi}(4\pi^2 f^2) G \int_{-\infty}^{\infty} d\tau\, e^{-i2\pi f\tau} \int_0^{2\pi} d\theta \sum_{m=0}^{B-1} \left\{\cos\gamma\left(\frac{2\pi m}{B} + 2\pi\Omega\tau\right) + \cos 2\gamma\theta\right\} e^{+i4\pi R_0 \frac{f}{a_0}\cos\phi \sin(\beta-\theta)\sin\left(\pi\Omega\tau + \frac{\pi m}{B}\right)} \tag{26}$$

Integration over θ of the first term yields a zeroth-order Bessel function; the change of variable $\chi = \theta - \beta + \pi/2$ is useful in the second term, which gives, after some manipulation, another Bessel function:

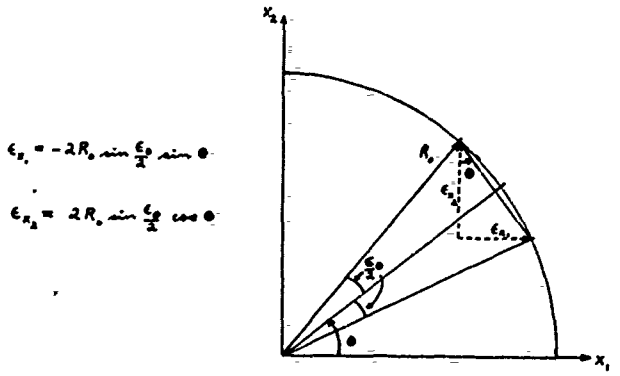

Fig. 4. Polar coordinates for rotating point forces.

$$\langle S\rangle = \frac{\beta L_0^2(4\pi^2 f^2) G}{2} \int_{-\infty}^{\infty} d\tau\, e^{-i2\pi f\tau} \times$$

$$\sum_{m=0}^{B-1} \left\{\cos\gamma\left(\frac{2\pi m}{B} + 2\pi\Omega\tau\right) J_0 + \cos 2\gamma\beta\, J_{2\gamma}\right\} \tag{27}$$

The argument of the Bessel functions is

$$4\pi R_0 \frac{f}{a_0}\cos\phi \sin\left(\pi\Omega\tau + \pi m/B\right)$$

The factor in curly brackets is periodic; hence we expect a discrete spectrum, i.e., δ functions. To this end, after much algebra, we can manipulate both terms into integrals of the form

$$\int_{-\infty}^{\infty} J_{2\mu}(2z\sin t)\, e^{i2\mu t}\, dt = \pi\left\{J_\mu^2(z)\,\delta(\mu) + 2\sum_{l=0}^{\infty}(-1)^l J_{\mu-l}(z)\, J_{\mu+l}(z)\left[\delta(\mu+l) + \delta(\mu-l)\right]\right\} \tag{28}$$

Also needed are

$$J_{-\mu}(z) = (-1)^\mu J_\mu(z) \tag{29}$$

$$\sum_{m=0}^{B-1} e^{i2\pi m\mu} = \begin{cases} B & \text{if } \mu = 0, \pm 1, \pm 2, \ldots \\ 0 & \text{otherwise} \end{cases} \tag{30}$$

The final result is

$$\langle S(\vec{x},f)\rangle = \frac{B^2 L_0^2 \sin^2\phi}{8\rho_0 a_0^3 R^2} \sum_{n=1}^{\infty} f^2\left(J_{nB-\gamma}^2 + J_{nB+\gamma}^2 + 2(-1)^\gamma \cos 2\gamma\beta\, J_{nB-\gamma} J_{nB+\gamma}\right)\delta(f - nB\Omega) \tag{31}$$

The argument of all the Bessel functions is

$$2\pi R_0 \frac{f}{a_0}\cos\phi = 2\pi R_0 k\cos\phi = nBM\cos\phi$$

The above result is in agreement with those obtained by Lowson and Ollerhead[a] and by Wright.[4] The former have defined $\theta = 0$ as the observer's azimuth; hence our results differ by the phase angle β.

For $\gamma = 0$, (31) reduces to

$$\langle S(\vec{x},f)\rangle = \frac{B^2 L_0^2 \sin^2\phi}{2\rho_0 a_0^3 R^2} \sum_{n=1}^{\infty} f^2 J_{nB}^2\,\delta(f - nB\Omega) \tag{32}$$

which agrees with Gutin's analysis[1] of a constant point force rotating in a circle.

A computer program was used to evaluate (31) for rotational Mach numbers of 0.5 and 0.9, for $\gamma = 1$ and 10. The observer's position was taken as $\phi = 30°$ and $\beta = 45°$. Results are presented in Fig. 5a and 5b in the form of the dimensionless power, $\frac{(\rho_0 a_0)^2}{L_0^2}\left(\frac{R_0}{R}\right)^2\langle S\rangle$ versus n, the harmonic of the blade-passage frequency. The spectra

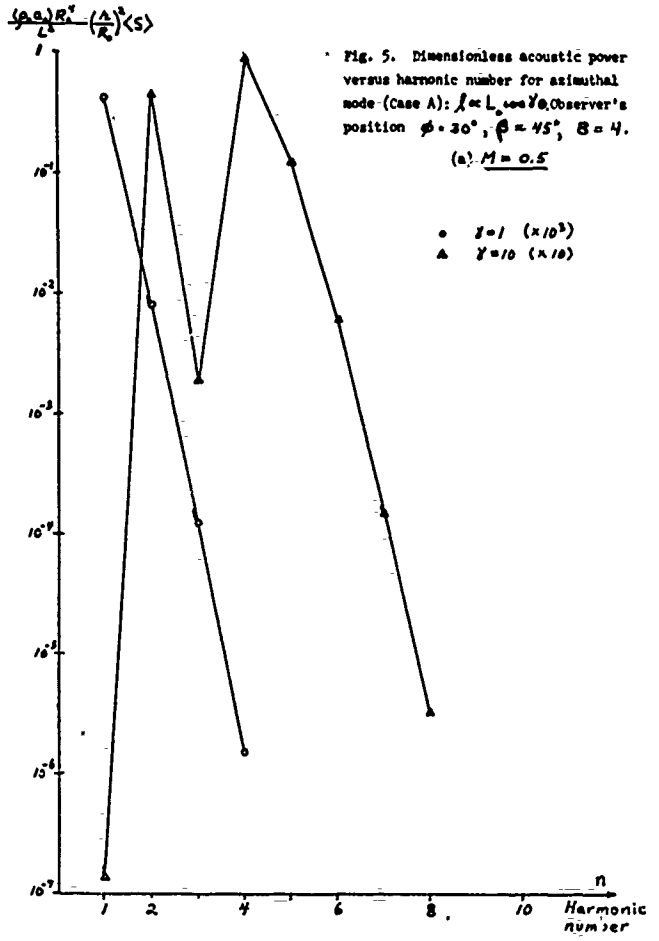

Fig. 5. Dimensionless acoustic power versus harmonic number for azimuthal mode (Case A): $f \propto L_0 \cos\gamma\theta$, Observer's position $\phi = 30°$, $\beta = 45°$, $B = 4$.

(a) $M = 0.5$

● $\gamma = 1$ $(\times 10^3)$

▲ $\gamma = 10$ $(\times 10)$

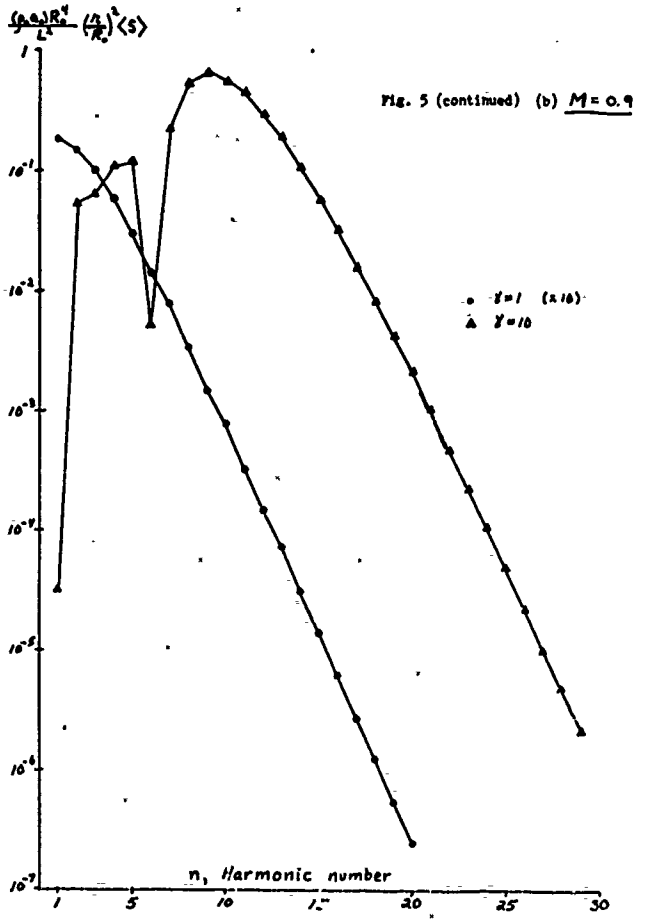

Fig. 5 (continued) (b) $M = 0.9$

● $\gamma = 1$ $(\times 10)$

▲ $\gamma = 10$

tend to peak near the lower harmonics with the peak broadening as M increases. Increasing γ tends to shift the spectrum to the right, as one would expect due to the faster fluctuations of the dipoles.

Case B: Any spatially fixed two-dimensional upwash pattern that is frozen in time can be represented as a Fourier superposition of waves of the form $\sin q\{x_1\}$ and $\cos q\{x_1\}$. In principle, the resultant lift response can then be modeled in the same manner. Thus, the acoustic response to such a fundamental mode would be useful as a building block in situations in which a decomposition into azimuthal modes as discussed in Case A is inconvenient.

Consider B point lift forces rotating at angular frequency Ω about the origin, with their magnitudes varying as $\sin q x_1$, where q is any real number (see Fig. 6). Hence, rather than each dipole oscillating at constant frequency, as in the previous example, at any instant its variation now depends on whether it is moving along or perpendicular to the x_1 direction. By inspection,

$$f(R,\theta,t) = \frac{L_0}{R_0}\sin q x_1\,\delta(R-R_0)\sum_{j=0}^{B-1}\delta\left(\theta - \frac{2\pi j}{B} - \Omega t\right) \tag{33}$$

Forming R_{11}, and setting $x_1 = R_0\cos\theta$ yields

$$R_{ll} = \frac{L_z^2}{R_o^2}\,\delta(R-R_o)\,\delta(\epsilon_\Omega)\sin\left\{qR_o\cos\left(\theta-\tfrac{\epsilon_\theta}{2}\right)\right\}\sin\left\{qR_o\cos\left(\theta+\tfrac{\epsilon_\theta}{2}\right)\right\}\times$$

$$\sum_{l=0}^{B-1}\sum_{m=0}^{B-1}\delta\left(\theta-\tfrac{\epsilon_\theta}{2}-\tfrac{2\pi l}{B}-2\pi\Omega\left(t-\tau_{\tfrac12}\right)\right)\delta\left(\theta+\tfrac{\epsilon_\theta}{2}-\tfrac{2\pi m}{B}-2\pi\Omega\left(t+\tau_{\tfrac12}\right)\right) \tag{34}$$

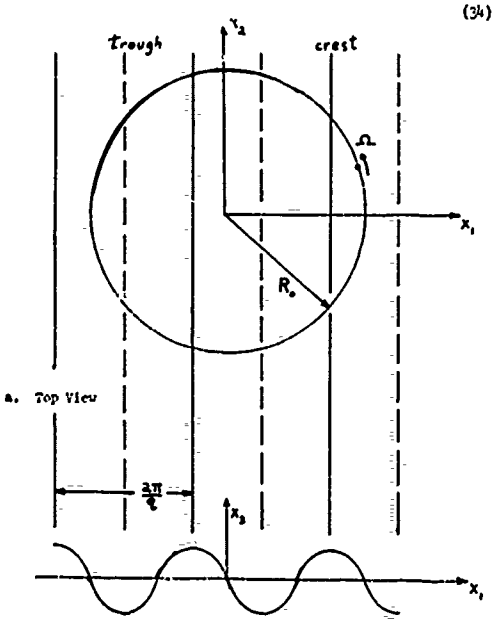

Fig. 6. Rotating point dipole fluctuating sinusoidally in X_1.

The dependence on θ and ϵ_Ω can be separated using standard trigonometric identities, and the time average yields a factor $B/2\pi$ just as in Case A. Hence,

$$\langle R_{ll}\rangle = \frac{BL_z^2}{4\pi R_o^2}\,\delta(R-R_o)\,\delta(\epsilon_\Omega)\left\{\cos\left(2qR_o\sin\theta\sin\tfrac{\epsilon_\theta}{2}\right)\right.$$

$$\left.-\cos\left(2qR_o\cos\theta\cos\tfrac{\epsilon_\theta}{2}\right)\right\}\sum_{m=0}^{B-1}\delta\left(\epsilon_\theta-\tfrac{2\pi m}{B}-2\pi\Omega\tau\right) \tag{35}$$

From (29)

$$\langle S(\bar r,f)\rangle = G(4\pi^2f^2)\int_0^\infty R\,dR\int_0^{2\pi}d\theta\int_{-\infty}^{\infty}d\tau\,e^{-i2\pi f\tau}\times$$

$$\int R\,d\epsilon_\theta\int_0^\infty d\epsilon_R\,e^{+i2\pi\frac{f}{a_o}\hat n_o\cdot\bar\epsilon}\langle R_{ll}\rangle \tag{36}$$

The transformation of $\frac{f}{a_o}\hat n_o\cdot\bar\epsilon$ to polar coordinates is the same as used in Case A, and so the integration over ϵ_θ yields

$$\langle S\rangle = \frac{BL_z^2(4\pi^2f^2)G}{4\pi}\int_{-\infty}^{\infty}d\tau\,e^{-i2\pi f\tau}\int_0^{2\pi}d\theta\sum_{m=0}^{B-1}\times$$

$$\left\{\cos\left(2qR_o\sin\theta\sin\left(\tfrac{2\pi m}{B}+\pi\Omega\tau\right)\right)-\cos\left(2qR_o\cos\theta\cos\left(\tfrac{2\pi m}{B}+\pi\Omega\tau\right)\right)\right\}\times$$

$$e^{\,i4\pi\frac{r_o}{a_o}f\cos\phi\sin(\beta-\theta)}\sin\left(\pi\Omega\tau+\tfrac{\pi m}{B}\right) \tag{37}$$

By writing the cosines as complex exponentials and several changes of variable, one can show that the integral over θ results in four terms; all involve J_o, but each with a different argument. Two of these terms can be integrated with respect to τ using (28). The other two can be manipulated into a form in which the following expansion by Sonine[10] is useful:

$$J_o\left[\sqrt{A^2+C^2-2AC\cos x}\right] =$$

$$J_o(A)\,J_o(C)+2\sum_{l=1}^{\infty}J_l(A)\,J_l(C)\cos lx \tag{38}$$

Identities (27) and (30) are also required, and the final result is

$$\langle S(\bar r,f)\rangle = \frac{B^2L_z^2\sin^2\phi}{8\rho_o a_o^2\lambda^2}\sum_{n=1}^{\infty}f^2\left\{J_{nB}^2(A)+J_{nB}^2(C)\right.$$

$$\left.-2\cos nB\psi\,J_{nB}(A)\,J_{nB}(C)\right\}\delta(f-nB\Omega) \tag{39}$$

where

$$A = R_o\left[q^2+4\pi q\frac{f}{a_o}\cos\phi\cos\beta+4\pi^2\left(\frac{f}{a_o}\right)^2\cos^2\phi\right]^{1/2}$$

$$C = R_o\left[q^2-4\pi q\frac{f}{a_o}\cos\phi\cos\beta+4\pi^2\left(\frac{f}{a_o}\right)^2\cos^2\phi\right]^{1/2}$$

$$\psi = \tan^{-1}\frac{4\pi q\frac{f}{a_o}\cos\phi\sin\beta}{q^2-4\pi^2\left(\frac{f}{a_o}\right)^2\cos^2\phi}$$

The response to $\cos qx_1$ is the above with a (+) sign preceding the last term. It is easily seen that this reduces to Gutin's result for $q=0$. For a $\left\{\begin{matrix}\sin\\ \cos\end{matrix}\right\}qx_2$ variation, the response is that for $\left\{\begin{matrix}\sin\\ \cos\end{matrix}\right\}qx_1$ but with $\sin\beta$ replaced by $\cos\beta$ and vice versa.

The asymptotic behavior of (39) as $q\to 0$ is

$$\langle S(\bar r,f)\rangle \sim \frac{(qR_o)^2B^2L_z^2\sin^2\phi}{8\rho_o a_o^2\lambda^2}\sum_{n=1}^{\infty}f^2\left\{J_{nB-1}^2+J_{nB+1}^2\right.$$

$$\left.-2\cos2\beta\,J_{nB-1}J_{nB+1}\right\}\delta(f-nB\Omega) \tag{40}$$

where the argument of the Bessel functions is $2\pi R_o\frac{f}{a_o}\cos\phi$.

Since

$$\sin qx_1 = \sin(qR_0\cos\theta)$$

$$= 2\sum_{\substack{\gamma=1 \\ \text{odd}}}^{\infty}(-1)^{\frac{\gamma-1}{2}} J_\gamma(qR_0)\cos\gamma\theta$$

$$\sim qR_0\cos\theta + O(qR_0)^3$$

the above should agree with a calculation using (31) with $\gamma = 1$ and multiplied by the factor $(qR_0)^2$. This is easily seen to be the case.

The computer was again used to evaluate (39) for $M = 0.5$ and 0.9 and values of $(qR_0) = 10^{-3}$, 1, and 10 for $\phi = 30°$ and $\beta = 45°$. Results are plotted in Figs. 7a and 7b. Again, raising M broadens the spectrum while increasing (qR_0) shifts it to the right. For all practical purposes, the curves for $\gamma = 1$ of Case A and $qR_0 = 1$ of Case B essentially coincide; however, the difference between the $\gamma = 10$ curve and that for $qR_0 = 10$ is significant, and here the Mach number plays a strong role. Most likely, directionality is also important. The case $qR_0 = 10^{-3}$ was run to verify numerically that the asymptotic behavior of (39) as $qR_0 \to 0$ agreed with (31) for $\gamma = 1$, as discussed above. Accounting for the factor $(qR_0)^2 = 10^{-6}$, they essentially lie atop one another at $M = 0.5$, at $M = 0.9$ the difference is discernible, though still negligible. Figs. 5 and 7 display nearly constant slopes for all the curves at the higher harmonics, evidently independent of γ or qR_0. Apparently M does have a strong effect on this exponential decay rate. Unfortunately, results for very large values of γ or qR_0 are unavailable at this writing due to numerical difficulties with the Bessel functions.

Case C: Consider B point forces rotating at angular speed Ω about the origin, but with their magnitudes varying randomly in such a way that no correlation exists from one instant to the next, or equivalently from one point to another. This is commonly referred to as white noise, and results in a flat load spectrum independent of frequency. The correlation function for such a system is easily seen to be

$$R_{ll} = \frac{\overline{L^2}}{R_0^2}\,\delta(R-R_0)\,\delta(\epsilon_R)\,\delta(\epsilon_\theta)\,\delta(\tau)\sum_{m=0}^{B-1}\delta\left(\theta - \frac{2\pi m}{B} - 2\pi n_1 t\right) \tag{41}$$

where $\overline{L^2}$ is the mean-square lift exerted by one of the dipoles. Even though we know that the acoustic spectrum will be broad-band and hence have no "fundamental" frequency, the non-stationarity in time exhibited by (41) is still periodic. Hence a time average over the interval 0 to $1/2n_1$ is still meaningful and results in a factor $\frac{B}{2\pi}$. From (20)

$$\langle S\rangle = G(4\pi^2 f^2)\int_0^\infty R\,dR\int_0^{2\pi}d\theta\int_{-\infty}^{\infty}d\tau\, e^{-i2\pi f\tau}\int R\,d\epsilon_\theta$$

$$\int_0^\infty d\epsilon_R\, e^{+i2\pi\frac{f}{a_0}\hat{n}_0\cdot\vec{\epsilon}}\,\frac{B\overline{L^2}}{2\pi}\,\delta(R-R_0)\,\delta(\epsilon_R)\,\delta(\epsilon_\theta)\,\delta(\tau) \tag{42}$$

All the integrations involving delta functions are easily carried out, giving

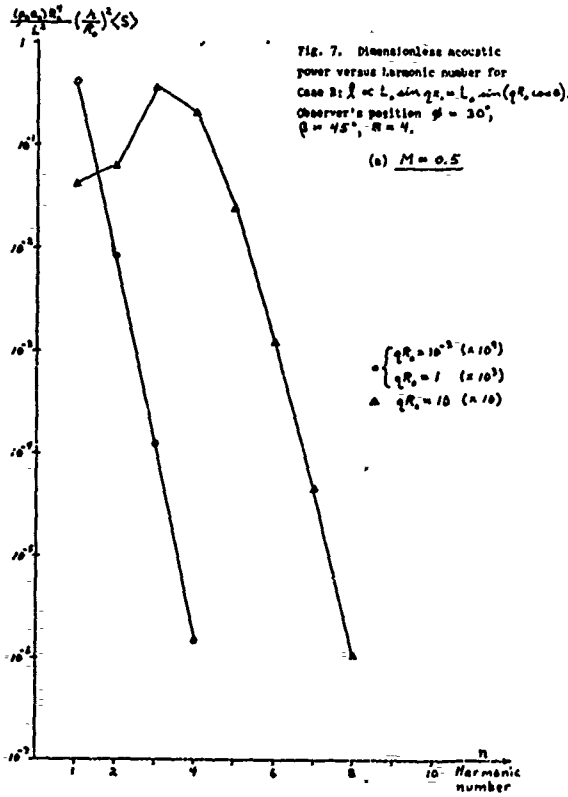

Fig. 7. Dimensionless acoustic power versus harmonic number for Case B: $\ell \propto L_0 \sin qx_1 = L_0 \sin(qR_0\cos\theta)$. Observer's position $\phi = 30°$, $\beta = 45°$, $R = 4$.

(a) $M = 0.5$

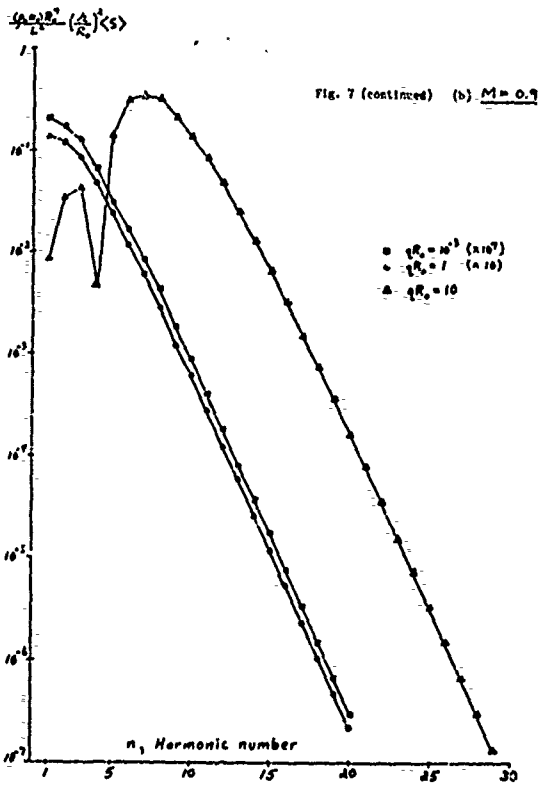

Fig. 7 (continued) (b) $M = 0.9$

$$\langle S(\vec{x},f)\rangle = 4\pi^2 f^2 B\overline{L^2} G = \frac{B\overline{L^2}\sin^2\phi\, f^2}{4\rho_0 a_0^3 R^2} \tag{43}$$

which is independent of the dipoles' motion. This result was noted for the case $B = 1$ by Powers Williams and Hawkings [6]. Note that we only gain a factor of B in power as contrasted to B^2 in Cases A and B. This is because successive dipoles no longer reinforce each other's signals, as their phases are random; hence the intensities add rather than the pressure amplitudes.

The ease with which this result was arrived at due to the delta functions in τ and $\vec{\epsilon}$ suggests that it may hold for any planar motion, not circular or even periodic. A single point force whose path is prescribed as $\vec{y}_0(t)$ and which fluctuates in the above manner is described by

$$R_{ll}(\vec{\eta},\vec{\epsilon},t,\tau) = \overline{L^2}\,\delta(\vec{\eta}-\vec{y}_0(t))\,\delta(\vec{\epsilon})\,\delta(\tau) \tag{44}$$

$$S(\vec{x},t,f) = G\left(\frac{1}{r}\frac{\partial^2}{\partial t^2} + 4\pi^2 f^2\right)\int_{-\infty}^{\infty} d^3\eta \int_{-\infty}^{\infty} d\tau\, e^{-i2\pi f\tau} \times$$

$$\int_{-\infty}^{\infty} d^3\epsilon\, e^{+i2\pi\frac{f}{a_0}\hat{n}_0\cdot\vec{\epsilon}}\,\overline{L^2}\,\delta(\vec{\eta}-\vec{y}_0(t))\,\delta(\vec{\epsilon})\,\delta(\tau)$$

$$= \overline{L^2}\,G\left(\frac{1}{r}\frac{\partial^2}{\partial t^2} + 4\pi^2 f^2\right)\int_{-\infty}^{\infty}\delta(\vec{\eta}-\vec{y}_0(t))\,d^3\eta$$

$$= 4\pi^2 f^2\overline{L^2}\,G = \frac{\overline{L^2}\sin^2\phi\, f^2}{4\rho_0 a_0^3 R^2} \tag{45}$$

Hence, as long as the dipole remains in a plane, its acoustic radiation is the same as if it were immobile. The result for B dipoles is B times the above, by linear superposition, even if each executes a different motion. This is because the assumption that trajectories are geometrically compact precludes amplitude variations in the spectrum, and the Doppler shifts are indiscernible in a flat spectrum.

IV. Lift Response of Rotor to Turbulent Upwash Pattern

As mentioned above, our acoustic analysis requires the space-time load spectrum, P_{ll}, expressed in fixed coordinates as seen by the observer. To obtain this quantity, we begin with the following approximations:

1) linearized aerodynamic theory is applicable - hence, we can superpose solutions,

2) the turbulence is homogeneous in space.

The need for 1) is obvious; 2) is not absolutely necessary, but it considerably simplifies the analysis.

The variations in $w(\vec{y},t;j)$ give rise to fluctuations in the angle of attack $\alpha = w/U$, U being the local mean horizontal velocity, which varies linearly with distance from the hub. We presume that we have $l_y(\vec{y},t,\vec{v})$, the lift loading at a fixed point $\vec{y}$ at time t due to a sinusoidal upwash distribution of wave-vector $\vec{v}$. This function, generally complex, is referred to as the aerodynamic transfer function. Then the response at $\vec{y}$ at time t to a turbulent upwash pattern is, by linear superposition

$$l(\vec{y},t;j) = \int_{-\infty}^{\infty} l_y(\vec{y},t,\vec{v})\,F_w(\vec{v};j)\,d^3v \tag{46}$$

where

$$F_w(\vec{v};j) = \int_{-\infty}^{\infty} w(\vec{\eta};j)\,e^{-i2\pi\vec{v}\cdot\vec{\eta}}\,d^3\eta \tag{47}$$

where w and F_w are taken as generalized random functions. Now we form the correlation of the lift loading,

$$R_{ll}(\vec{y},t_1,\vec{z},t_2) \equiv R_{ll}(\vec{\eta},\vec{\epsilon},t,\tau)$$

$$= \iint_{-\infty}^{\infty} l_y(\vec{\eta}-\vec{\epsilon}/2,t-\tau/2,\vec{v})\,l_y^*(\vec{\eta}+\vec{\epsilon}/2,t+\tau/2,\vec{v}')\,\overline{F_w(\vec{v})F_w(\vec{v}')}\,d^3v'\,d^3v \tag{48}$$

Homogeneous turbulence has the property that oscillations of any given wavelength must be uncorrelated with those of any other; i.e.,

$$F_w(\vec{v})F_w(\vec{v}') \equiv P_{ww}(\vec{v})\,\delta(\vec{v}'-\vec{v}) \tag{49}$$

P_{ww} being the power spectral density of the turbulence. Performing the integration over $\vec{v}'$ gives

$$R_{ll}(\vec{\eta},\vec{\epsilon},t,\tau) = \int_{-\infty}^{\infty} l_y(\vec{\eta}-\vec{\epsilon}/2,t-\tau/2,\vec{v})\,l_y^*(\vec{\eta}+\vec{\epsilon}/2,t+\tau/2,\vec{v})\times P_{ww}(\vec{v})\,d^3v \tag{50}$$

Consequently,

$$P_{ll}(\vec{\eta},-\tfrac{f}{a_0}\hat{n}_0,t,f) = \int_{-\infty}^{\infty} d^3\epsilon\, e^{+i2\pi\frac{f}{a_0}\hat{n}_0\cdot\vec{\epsilon}}\int_{-\infty}^{\infty} d\tau\, e^{-i2\pi f\tau}\times$$

$$\int_{-\infty}^{\infty} d^3v\, l_y(\vec{\eta}-\vec{\epsilon}/2,t-\tau/2,v)\,l_y^*(\vec{\eta}+\vec{\epsilon}/2,t+\tau/2,\vec{v})\,P_{ww}(\vec{v}) \tag{51}$$

Unfortunately, (51) in conjunction with (20) implies a total of eight scalar integrations, well beyond the capability of even the fastest computers. It is hoped that some may be done analytically; but even with the simplest forms for P_{ww}, l_y is usually complicated enough to prohibit this.

One simplification would be to neglect retarded-time differences across turbulent eddies; i.e., to assume that they are much smaller than the acoustic wavelength. Unfortunately, integral scales in the atmosphere typically run to several feet, so such an approximation breaks down at high frequencies. A more reasonable approach is to consider the chord as acoustically compact:

$$kc \propto \frac{U}{c a_0}c = M << 1$$

where we have taken U/c as typical of the highest frequency. Hence this effectively limits the results to incompressible flow. Another approach

would be to model the chordwise loading as rectangular. However, this and the previous assumption both imply that $\partial l/\partial t$, as seen by a fixed point in the disk, is zero except at the discontinuities. The form of (13) suggests that this would tend to overemphasize the higher frequency components; indeed, this may explain why Gutin's calculation overestimates the higher harmonics as the transonic regime is approached.

We plan to apply the present analysis to a point dipole rotating at constant angular velocity in a homogeneous and isotropic turbulent field, with an ad hoc application of quasi-steady aerodynamics or the Sears function to obtain l_j. We then plan to consider the effects of finite chord and span including the different orientations of the spatial Fourier components of turbulence relative to the blades.

V. Summary and Conclusions

An acoustic analysis of a surface distribution of dipoles has been made with a minimum of assumptions; both discrete and broad-band spectra can be accomodated, and extension to acoustic monopoles and quadrupoles is straight-forward. The formulation has been applied here to several examples and shown to agree with previous approaches where applicable.

In particular, it is expected to be of value in treating the problem of a lifting rotor in atmospheric turbulence, as it assumes knowledge of the space-time loading spectrum in fixed coordinates, P_{ll}. This is a frame in which the turbulence characteristics are most easily specified. However, a number of integrations are involved in the determination of P_{ll}, and further approximations will probably be required before practical results will be obtained.

VI. Nomenclature

$\vec{x}$	position vector of observer
$\vec{y}, \vec{z}$	position vectors of disturbances within the rotor
$\vec{\eta}$	average position vector of disturbances
$\vec{\epsilon}$	relative displacement vector between disturbances
x	$= \lvert\vec{x}\rvert$
$\hat{n}_o$	unit vector along $\vec{x}$
R, Θ	polar coordinates in plane
θ	azimuth angle of observer
ϕ	angular elevation of observer
t	time
t_{ret}	mean retarded time
τ	separation in time
p	pressure
ρ	density
a_o	speed of sound
Ω	angular rotation frequency, Hz.
c	blade chord
f	acoustic frequency, Hz.
λ	acoustic wavelength, a_o/f
$\vec{K}$	acoustic wave vector, $\hat{n}_o/\lambda$
γ, q	wave number of lift fluctuations
w	upwash component of turbulence
$\vec{\nu}$	turbulence wave vector
J	instantaneous acoustic intensity
I	time averaged acoustic intensity
S	acoustic spectrum
R_{--}	correlation function
P_{--}	power spectral density
M	Mach number
l	lift loading (force/area)
L	lift force
j	ensemble parameter
i	$\sqrt{-1}$
G	geometrical factor, defined in Eq. (9)
δ	delta function
B	blade number
n	harmonic number
$(\ )_o$	undisturbed value
$(\ )$	deviation from $(\ )_o$
$[\ ]$	to be evaluated at retarded time
$\lvert\ \rvert$	absolute value
$\overline{(\ )}$	ensemble averaged quantity
$\langle\ \rangle$	time averaged quantity
$(\ )^*$	complex conjugate

VII. References

1. Gutin, L., On the Sound Field of a Rotating Propeller, NACA TM 1195, 1948.
2. Lowson, M.V. and Ollerhead, J.B., Studies of Helicopter Rotor Noise, USAAVLABS Tech. Rep. 68-60, Jan. 1969. Wyle Lab. Research Staff Rep. WR 68-9.
3. Lowson, M.V., and Ollerhead, J.B., Theoretical Study of Helicopter Rotor Noise, J. of Sound and Vib., 9, 2, March, 1969.
4. Wright, S.E., Sound Radiation from a Lifting Rotor Generated by Asymmetric Disk Loading, J. Sound and Vib., 9, 2, March, 1969.
5. Sharland, I.J., Sources of Noise in Axial Flow Fans, J. Sound and Vib., 1, 3, 1964.
6. Ffowcs Williams, J.E. and Hawkings, D.L., Theory Relating to the Noise of Rotating Machinery, J. Sound and Vib., 10, 1, p. 10, 1969.
7. Morfey, C.L. and Tanna, H. K., Sound Radiation from a Point Force in Circular Motion, J. Sound and Vib., 15, 3, p. 325, 1971.
8. Morfey, C.L., Broadband Sound Radiated from Subsonic Rotors, International Symposium on the Fluid Mechanics and Design of Turbomachinery, Penn State University, August 31-Sept. 3, 1970.
9. Sevik, M., Sound Radiation from a Subsonic Rotor Subjected to Turbulence, International Symposium on the Fluid Mechanics and Design of Turbomachinery, Penn State University, August 31-Sept. 3, 1970.
10. Lighthill, M. J., On Sound Generated Aerodynamically - I, Proc. Roy. Soc. Lond., 211A, 1952, pp. 564-587.
11. Sveshnikov, A. A., Applied Methods of the Theory of Random Functions, 1st ed., Pergamon Press, New York, 1966.
12. Bendat, J. S. and Piersol, A. G., Measurement and Analysis of Random Data, John Wiley and Sons, New York, 1966.
13. Sonine, N.J., Recherches sur les fonctions cylindriques et le développement des fonctions continues en séries, Mathematische Annalen, 16, p. 23, 1880.

SOME ASPECTS OF HELICOPTER NOISE THEORY

Part II Recent Results Relating to Engine Noise*

by W. R. Sears

Cornell University

Abstract

An investigation of blade forces arising from rotor-stator interactions in subsonic flow is reported. One conclusion is that the Kemp-Sears type of approximation can be extended to include compressibility effects by means of the technique suggested recently by Amiet and Sears.

In the course of this investigation, some apparent discrepancies in the results of Johnson on gust loads in subsonic two-dimensional flow were encountered. These are reported here, without explanation, especially in view of the importance of Johnson's three-dimensional results in helicopter-noise research.

I. Aerodynamic Interference between Moving Blade Rows

Under contract with the Mechanics Branch of AFOSR we have continued our studies, begun in the 1950's, of unsteady effects in axial-flow fans and compressors. Although there exist, in principle, methods for solution of these problems, within the two-dimensional and small-perturbation approximations but without further simplifications, the practical situation is that these are generally not in forms suitable for practical use. It is, therefore, still of interest to investigate possibilities of extending the Kemp-Sears type of approximations to subsonic compressible flows. Mr. C. Osborne has carried out such an investigation.

The Kemp-Sears theory[1] treats inter-row interference as a perturbation of steady flow through a stage consisting of an upstream stationary row of blades and a downstream moving row - stator and rotor, say. It is clear, first of all, how to account for compressibility in the steady flow fields attached to the respective rows; namely, by the Prandtl-Glauert rule. A possible approximation ($\#1$) is to make only this correction for compressibility and to use, as Kemp and Sears did, incompressible unsteady-airfoil results to estimate the unsteady forces that result from the motion of the up- or downstream blades through this periodic flow field. Proposal $\#2$ might be to invoke Prandtl-Glauert theory again, in a straightforward quasi-steady fashion, to estimate the unsteady forces; i.e., to transform the flow field encountered by the moving blade by Prandtl-Glauert stretching with respect to its relative flow direction, before employing incompressible unsteady-airfoil results, and so forth.

But in a recent paper[2] Amiet and Sears pointed out that a consistent first-order theory for unsteady flow, analogous to the Prandtl-Glauert, involves an additional effect: there is the Prandtl-Glauert stretching, but there is also a first-order distortion of any time-varying boundary condition. (For want of a better name, I suggest calling this the "GASP" approximation, although unfortunately this acronym puts Prandtl last!) This yields a related incompressible unsteady flow if terms of order ϵ^2 are neglected compared to 1 and terms of order ϵ are retained, where ϵ denotes the ratio of body length b to wave length of sound:

$$\epsilon \equiv bf/a \qquad (1)$$

where f is the frequency and a the speed of sound. Thus ϵ is also equal to $1/2\pi$ times the product of the Mach number and the conventional "reduced frequency" of unsteady-airfoil theory based on the half-chord.

It is only when terms of order ϵ are also neglected that the approximation of $\#2$ above - "straightforward quasi-steady Prandtl-Glauert" - is obtained. Thus, our third proposition ($\#3$, say) is to proceed, once again, as in $\#1$ and $\#2$, but to transform the flow field (which is unsteady in the frame of reference involved here) as per the GASP approximation.

Of course, one would employ, instead, compressible-flow unsteady-airfoil results to estimate fluctuating forces if such were available. To a limited extent they are available: some years ago Drischler et al.[3] of NACA obtained the gust-response functions for three Mach numbers, by a series of ingenious numerical approximations.* Two parts of the inter-row interaction are gust-like, viz. viscous-wake and vortex-wake interference, i.e., the passage of downstream blades through these two kinds of wakes. (Incidentally, viscous-wake interference is said to be the most important part of inter-row interaction in present-day engines.) Consequently we have calculated these two phenomena by use of Drischler's results, especially for comparison with approximations $\#1$, $\#2$, and $\#3$, above; we call this $\#4$.

Our numerical results are admittedly limited. They all pertain to the 45°-45° stage treated by Kemp and Sears, with varying Mach number, gap/chord, and axial row-spacing. Two different assumptions were made regarding the unperturbed rotor-blade-loading distribution. More cases could easily be calculated, since the results appear in closed-form formulas for direct evaluation for all four approximations. The conclusions are simple: Taking $\#4$ as our standard of comparison,

1. Approximation $\#1$ (incompressible unsteady-airfoil theory) shows the right trends with Mach number, but seems to underestimate the effects of compressibility.

2. Approximation $\#2$ (quasi-steady Prandtl-Glauert) is completely without merit, predicting compressibility effects that even have the wrong trends with varying Mach number.

3. Approximation $\#3$ ("GASP") is relatively satisfactory, even up to $M \approx 0.7$, and even for relatively large ϵ.

4. The principal effect of compressibility, in general, is to reduce the magnitude of inter-row interaction (lift fluctuations). This is recognized as a general phenomenon in unsteady-airfoil flows, and can be explained easily in the framework of the GASP transformation. It also becomes clear, in this framework, why the predictions of our $\#2$ are so wrong.

Having thus succinctly stated our conclusions, we shall not present any of Osborne's graphs here. They appear in his thesis[6], which we propose to abstract in the form of one or more published papers as soon as possible.

II. The Response of Thin Airfoils to Sinusoidal Gusts at Subsonic Flow Speeds

Calculations of the pressures and forces on airfoils of infinite span in convected sinusoidal gust fields have been carried out, for compressible flow, in References 4 and 5.

Both investigations involve solving integral equations for the singularity distributions in the presence of vortex wakes. Johnson[4] transforms to a coordinate system in which the flow becomes steady (three-dimensional) - an ingenious device which, of course, cannot be used to produce the two-dimensional case. Nevertheless, both authors do present

* This work was partially supported by the U.S. Air Force Office of Scientific research under contract #AF49(620)-69-C-0063.

data for the two-dimensional case; Johnson's are in the form of exponential formulas obtained from his numerical solutions by curve-fitting, while Graham's[6] are presented (to date) only in a single vector diagram whose scale is not adequate to provide accurate values for computations. It is, therefore, impossible to make meaningful comparisons of Johnson's and Graham's results at this meeting.

On the other hand, it is possible to compare Johnson's values (a) with the corresponding incompressible-flow function[7], (b) with the results of applying the GASP transformation to this function, and (c) with Drischler's approximate results[3]. These comparisons are presented in Figs. 1-3, where the absolute value of the ratio of lift to quasi-steady lift is plotted against reduced frequency ω and Mach number of flight M. It should be recalled that the validity of the GASP approximation is limited by M and the frequency parameter ϵ; viz.,

$$\beta^2 \equiv 1 - M^2 \ll 1$$

and

$$\epsilon^2 = \left(\frac{M\omega}{2\pi}\right)^4 \ll 1$$

The curves of Figs. 1-3 therefore leave us with some concern for the accuracy of Johnson's results for the two-dimensional case. It is hard to believe that the effect of compressibility is so large at very small M. As indicated, the value of ϵ^2 for $M = 0.3$ and $\omega = 4$ is only .04, so that we expect the accuracy of the GASP approximation to be very good.

We have, therefore, foregone the application of Johnson's results. What is more important, especially to those interested in broad-band noise prediction, is whether Johnson's results for other angles of inclination of the sinusoidal gusts to the wing are dependable. Pending the publication of detailed results by Graham, or the equivalent, it seems impossible to answer this important question.

References

1. Kemp, N.H. and Sears, W. R., "Aerodynamic Interference Between Moving Blade Rows," J. Aero. Sci. 20, 585 (1953); also "The Unsteady Forces due to Viscous Wakes in Turbomachines," J. Aero.Sci. 22, 478 (1955).
2. Ariel, R. and Sears, W. R., "The Aerodynamic Noise of Small-Perturbation Subsonic Flows," J. Fluid Mech., 44, 787 (1970).
3. Mazelsky, B., Numerical Determination of Indicial Lift of a Two-Dimensional Sinking Airfoil at Subsonic Mach Numbers from Oscillatory Lift Coefficients with Calculations for Mach Number 0.7., NACA TN 2562, (1951); Mazelsky, B. and Drischler, J.A., Numerical Determination of Indicial Lift and Moment Functions for a Two-Dimensional Sinking and Pitching Airfoil at Mach Numbers 0.5 and 0.6, NACA TN 2739 (1952); Drischler, J.A., Calculation and Compilation of the Unsteady-Lift Functions for a Rigid Wing Subjected to Sinusoidal Gusts and to Sinusoidal Sinking Oscillations, NACA TN 3748 (1956).
4. Johnson, W., "A Lifting Surface Solution for Vortex Induced Airloads and Its Application to Rotary Wing Airloads Calculation," TR 153-2, Aeroelastics and Structures Research Lab., M.I.T. (1970).
5. Graham, J.M.R., "Similarity Rules for Thin Airfoils in Non-Stationary Subsonic Flows," J. Fluid Mech. 43, 753 (1970).
6. Osborne, Colin, Compressibility Effects in the Unsteady Interactions Between Blade Rows, Cornell University Ph.D. Thesis, 1971. Available from University Microfilms, Inc., Ann Arbor, Michigan.
7. Sears, W. R., "Some Aspects of Non-Stationary Airfoil Theory and its Practical Applications," J. Aero. Sci. 8,104 (1941).

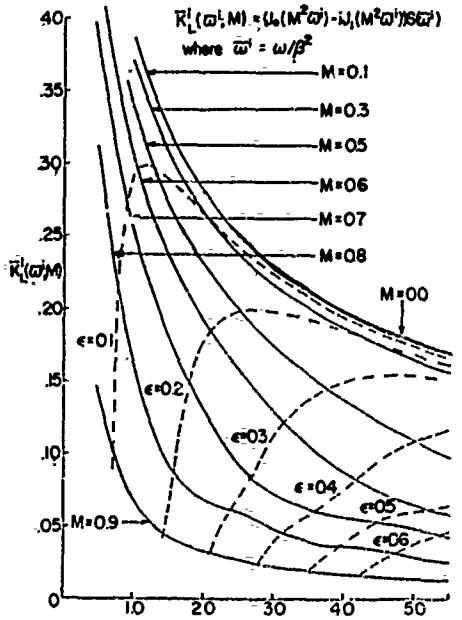

Figure 1. Ratio of lift magnitude to quasi-steady lift as function of reduced frequency, for sinusoidal gust at various Mach numbers of flight, according to "GASP" approximation[2]. Cross-plotted curves show values of $\epsilon = M\omega/2\pi$. (From Reference 6)

* More recently, papers by Graham[5] and Johnson[4] have appeared, which also include the compressible-flow gust-response function in principle. Our reasons for using Drischler's approximation instead of these will be mentioned below.

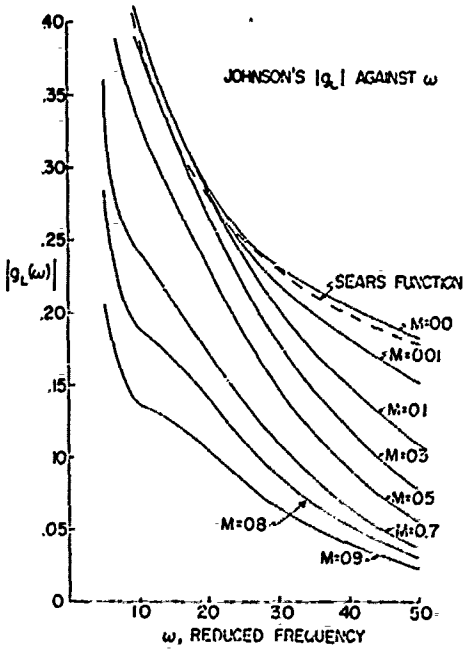

Figure 2. Ratio of lift magnitude to quasi-steady lift as function of reduced frequency, for sinusoidal gust at various Mach numbers of flight, according to Johnson [4]. (From Reference 6)

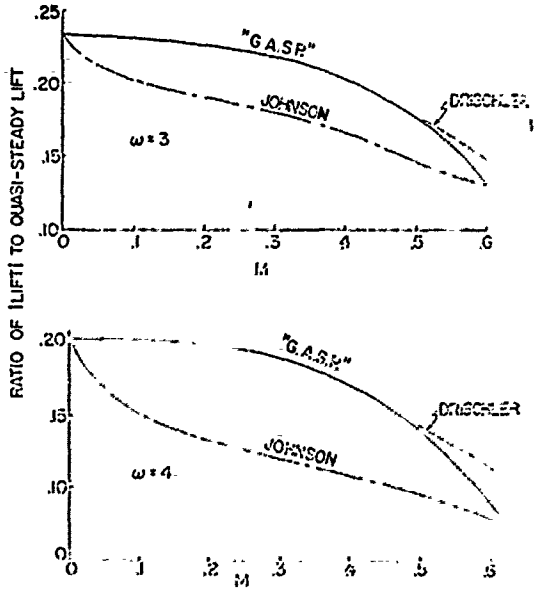

Figure 3. Ratio of lift magnitude to quasi-steady lift, for sinusoidal gusts, according to "GASP" [2], Johnson [4], and Drischler et al. [3], as functions of Mach number M for two values of reduced frequency ω. (From Reference 6)

DETERMINATION OF THE AERODYNAMIC CHARACTERISTICS OF VORTEX SHEDDING FROM LIFTING AIRFOILS FOR APPLICATION TO THE ANALYSIS OF HELICOPTER NOISE*

By

S. G. Sadler

ROCHESTER APPLIED SCIENCE ASSOCIATES, INC.
140 Allens Creek Road
Rochester, New York

ABSTRACT

The purpose of this project is to determine whether or not vortex shedding noise from helicopter rotors exists, and if it exists, to determine the associated aerodynamic characteristics. The first year's effort was directed toward an evaluation of the feasibility of an experiment to attempt to measure vortex shedding noise on an airfoil. It was determined that the state-of-the-art experimental techniques and equipment would be adequate to measure vortex shedding if it had certain assumed frequency characteristics and if some specific model, instrumentation, and wind tunnel requirements were met. The second year's effort was directed toward coordinating design of the airfoil model and instrumentation and conducting experiments on two-dimensional and three-dimensional airfoil models. Surface pressure measurements on the airfoil, hot-wire measurements in the wake, sound measurements, and accelerometer measurements were made. Those measurements indicate that vortex shedding at a discrete frequency exists but that its frequency may be higher than has been used in helicopter noise prediction techniques. Details of this and other noise characteristics as observed from the experimental data will be presented and discussed. A brief discussion of the upcoming year's effort will be presented.

Introduction

Helicopter rotors are an important helicopter noise source. Reductions in helicopter rotor noise are desirable from various considerations, including detection, annoyance, and hearing damage. An improved understanding of the mechanisms involved in helicopter noise generation are important in the obtainment of reduced helicopter rotor noise. Vortex shedding noise has been suggested as one source of high frequency noise, and under some flight conditions it has been suggested as a source of high amplitude high frequency noise.

The primary purpose of this work is to establish whether or not vortex street shedding from helicopter rotors is a significant noise source. The bulk of studies of vortex shedding have involved blunt bodies. Considerable work in the area of vortex shedding from airfoils has been done recently, and is presently being conducted. Of particular interest is work done at UARL by Patterson, et al.[1] Hanson[2] has done extensive experimental work on notched and bluff airfoils. An extensive survey of literature concerned with the singing propeller problem (primarily for hydrodynamic application) by Ross[3] contains interesting papers which are pertinent to the current work on airfoils.

The first year's efforts were directed toward determining, insofar as was available from existing literature and simple theory, important vortex shedding characteristics, orders of magnitude of frequencies and amplitudes which might be expected, and important aerodynamic parameters and their effects on vortex shedding characteristics. The feasibility of an experimental investigation to attempt to determine vortex shedding characteristics of an airfoil was evaluated. It was determined that such an experiment was feasible, subject to certain restrictions and requirements on experimental facilities and instrumentation. The second year's effort was to perform the experiment and to analyze the experimental data. The third year's effort is to be directed toward the use of the experimental results in modeling helicopter noise.

The effort has been completed through the obtainment of experimental data. Data analysis has not been completed, so the results presented here are of a preliminary nature. The experimental effort was delayed approximately nine months from the schedule originally planned, and completion of the data analysis had been delayed accordingly. The delay in the experimental phase of the effort was due to problems associated with experimental facility construction, instrumentation, and shakedown.

Summary of Expected Vortex Characteristics and Test Feasibility Studies

Expected vortex shedding characteristics which were determined early in the investigation included the following:

1. The oscillatory lift force, $L(t)$, due to vortex shedding at frequency, ω, from an airfoil with chord, c, length, ℓ, and lift curve slope, a_0, in a fluid with density, ρ, and relative velocity, V, with angle of attack magnitude due to vortex shedding of α_v, is given by

$$L(t) = (\tfrac{1}{2}\rho V^2 c \ell a_0)\,\alpha_v e^{i\omega t}.$$

2. Similarly, the first harmonic drag force, $D(t)$, is given by

$$D(t) = (\tfrac{1}{2}\rho V^2 c \ell a_0)\,\alpha_0 \alpha_v e^{i\omega t}$$

where α_0 is the steady airfoil angle of attack.

3. The vortex shedding angle of attack magnitude, α_v, is expected to have a range as given by

$$\alpha_v \leq 1.5\, c_d/a_0$$

where c_d is the airfoil drag coefficient, and is a

*This study is supported by the Department of the Army, U.S. Army Research Office-Durham, Durham, North Carolina, under Contract DAHC04-69-C-0030.

Preceding page blank

function of airfoil shape and surface condition, angle of attack, and Mach number.

4. The second harmonic drag force is negligible with respect to the first harmonic drag force except at very small angles of attack, is of the order of α_o times the first harmonic lift, and is expected to be negligible for essentially all practical flight conditions for helicopter rotors.

The feasibility study for the experimental tests indicated that tests were desirable if certain test facility, model, and instrumentation requirements could be achieved.

Test facility requirements included the following:

1. Wind tunnel turbulence, $\sqrt{\overline{u^2}}/U_\infty \leq .0004$
2. Known wind tunnel speed and angularity distributions; speed range to 600 ft/sec.
3. Sound field measurements outside the open jet test section, with tunnel empty and with a known sound source in the test section (both with tunnel running).
4. Capability to achieve full-scale helicopter Reynolds number range.

Model and instrumentation requirements included the following:

1. Size large enough to achieve full-scale helicopter Reynolds number range.
2. Standard airfoil shape, preferably NACA 0012.
3. Two- and three-dimensional models.
4. Models and mounts as rigid as possible to reduce model motion.
5. Known model natural frequencies in flap and torsion.
6. Accelerometer measurements to determine model motion.
7. Surface pressure measurements to determine pressure magnitudes, correlation lengths, and frequencies.

Tests were performed at the United Aircraft Research Acoustic wind tunnel, which was designed for a turbulence level ($\sqrt{\overline{u^2}}/U_\infty$) of 0.0004. An SPL of the turbulence has not yet been made by RASA, but the overall level was reported to be approximately 0.001, somewhat higher than the design level. The tunnel test section can be operated as an open jet, in an acechoic chamber. The chamber is anechoic above 270 Hz. Microphones were positioned within the anechoic chamber so as to be in the far field of the sound radiated from the model in the test section. The test section used during these tests had an open top and bottom with approximate dimensions of 21 inches (spanwise) by 30 inches (streamwise). Steel side walls provided model and instrumentation support, and some flow containment. Various arrangements of flow control devices were used to reduce noise levels associated with the open jet nozzle and collector. Alternate downstream open jet lengths were available, and offered advantages and disadvantages. The 30 inch length was chosen because it represented, in our view, the most "well known" and reliable operating configuration of a new tunnel facility. The general arrangement of the test section is shown in Figure 1. The tunnel fan underwent some modifications between the times that the 2-D and 3-D model tests were conducted. Detailed analyses of tunnel noise have not been made for the two fan configurations, but preliminary investigations indicate that changes in the test section conditions were small. (A more detailed analysis may be available by the date this paper is presented).

Two wing models were used in these tests. Plan views are shown in Figure 2. Both were NACA 0012 airfoils, made of steel, with spanwise internal holes for surface pressure microphone and accelerometer cables, and with a surface pressure microphone mounted in a spanwise slider mechanism to permit the 30% surface pressure microphone to be traversed along the airfoil span. The two-dimensional model (21 inch span) was clamped at each end, and the slider microphone could be moved to any desired spanwise position. The slider mechanism was observed to have a slight gap along its leading edge and to be a few thousandths of an inch above the airfoil surface. The three-dimensional model (= 11 inch span) was clamped at one end, and the slider microphone could be moved incremental amounts, depending upon available inserts to fill the slider gap. The slider mechanism fit was better on the three-dimensional model than on the two-dimensional model. A chordwise array of surface microphones was located seven inches from one end, for both wing models, with microphones at 15%, 30% (slider), 38%, 50% and 70% chord. An accelerometer was located at midchord; at midspan of the 2-D model, and near the tip of the 3-D model. The accelerometers were internal to the surface. The surface pressure microphones were mounted so as to have a very small gap around the exposed diaphragm, and with the diaphragm mounted as nearly flush with the airfoil surface as possible. During some of the 3-D tests, not all of the surface pressure microphones were operational, and in any event only five of the surface pressure microphones, the accelerometer, and the two sound pressure microphones could be recorded at one time due to the limited number of power supply units which were available for various amplifiers.

Two hot-wire anemometers were mounted downstream of the wire, as shown in Figure 3. One was on a traverse mechanism which permitted spanwise and vertical (normal to airfoil middle surface) motions, and is referred to as the "movable" hot-wire. The other could be adjusted manually only, and is referred to as the "fixed" hot-wire. It could be located at any spanwise position and at one inch vertical increments. The movable hot-wire required a vertical slot in one side wall to allow vertical motions. Holes were drilled in the side to permit vertical adjustment of the fixed hot-wire. Only positions below the 0° angle of attack plane were attainable. Originally, it had been intended to make wake surveys at approximately 0.5 and 3.0 chord lengths downstream of the trailing edge of the airfoil. The use of a 30 inch test section opening together with rather severe buffeting near the collector precluded making surveys at 3.0 chord lengths downstream, and the surveys at 0.5 were shifted to 1.0 due to interference with other instrumentation.

Two sound pressure microphones were located in the anechoic chamber, as shown in Figure 4. One was located directly above the

model centerline, midway between the tunnel walls, had an easily adjusted height, and is referred to as the overhead microphone. Another was located at a lower, more downstream location, but not so as to be in the direct "shadow" of the collector nozzle, was normally kept at a somewhat smaller radius from the model centerline as the overhead microphone, and is referred to as the "downstream" microphone.

Appropriate amplification of transducer signals was provided when necessary. An oscilloscope was available for some on-line monitoring and investigation, and an oscillograph and a magnetic tape recorder were used to record transducer output. The oscillograph had 7 mirror-type galvanometers which were flat within $\pm$ 5% to about 1K Hz and had a gradual drop off above that. (The response is down about 25% at 2K Hz, and about 75% at 3K Hz.) The tape recorder was a one inch, 14 channel, FM recorder with a 27K Hz carrier signal, and had a flat frequency response up to 5K Hz.

Test Procedures and Results

Instrumentation was tested and calibrated before each set of tests. Individual components were monitored with the oscilloscope and replaced, repaired, or removed when found to be defective. System check-out included runs made with the tunnel empty and with a one inch diameter steel cylinder placed at the airfoil midchord position. Some of these tests indicated significant characteristics of the system. They provide a base of reference for other measurements, as well.

It was noted during calibration of other instrumentation that the accelerometer seemd to have a residual output of 0.05g at about 60 Hz and 0.02g at about 180 Hz. This was probably line noise, and could be a significant part of some of the accelerometer time histories. The overhead microphone also had a residual signal with 30 Hz and higher frequency noise contained in it.

The oscillograph records are the source of most of the results presented in this paper. The primary function of the oscillograph was to serve as an on-line multi-channel monitoring device. Thus, all channels were used for primary transducer output, and for most runs no reference signal for frequency (or paper speed) was recorded on the oscillograph. The maximum nominal paper speed was 80 ips, and there were occasionally variations by as much as a factor of two or more. Frequency values based on an assumed paper speed of the oscillograph are known to be inaccurate.

Tunnel-empty tests and cylinder tests indicated that noise from objects within the tunnel should be of sufficient amplitude to be measurable, and not be masked by tunnel background noise. A beating pattern, which was observed during the cylinder tests in the overhead and downstream sound microphone records, could be from slight spanwise nonuniformities in the tunnel velocity or angularity. (Regular shedding from the cylinder was observed at all velocities through peak velocities of about 670 ft/sec, or Reynolds numbers of about 2.4×10^5.)

Spanwise correlation lengths in the wake and on the airfoil surface were investigated. Preliminary estimates of the length over which wake velocities were in phase were made by observing whether or not Lissajous figures were generated on the oscilloscope when one hot-wire anemometer was used as the horizontal input and the other was used as the vertical input. In-phase velocity variations for the two-dimensional model were indicated for only a 4° angle of attack, at low velocities. At 4° and 100 ft/sec this length was approximately 1.5 inches; at 200 ft/sec the length fell to approximately 1 inch. The correlation was not found, however, except on the vertical "edge" of the most turbulent region as indicated in Figure 5, and at the spanwise coordinate position of the chordwise array of surface pressure microphones. This indicates that either (1) the surface pressure microphones caused the correlation in the wake, or (2) the wake was warped vertically and surveys at other spanwise locations missed the region of correlation. It was observed that the maximum amplitude disturbance for 4° and 100 ft/sec occurred from approximately 0.2 inch to 0.4 inch below the 0° plane. The observed dominant frequencies, together with this size of peak amplitude region indicates that the wake thickness is approximately one-tenth the airfoil's projected dimension on the free stream. It is possible that helicopter rotors have lower frequencies and larger wake thicknesses than those observed during these tests. Different turbulent levels, airfoil surface conditions, and other differences in operating conditions could result in different frequencies, and it is expected that most of these differences would tend to lower the shedding frequency.

For those configurations where pure tones were observed, the surface pressure microphone measurements indicate that the surface pressures were correlated over the entire length of the airfoil. As shown in Figure 6, at 4° and 100 ft/sec the 15% surface pressure microphone, the overhead and downstream sound pressure microphones, the accelerometer, and to a degree, the 70% surface pressure microphone and the hot-wire anemometers all appeared to be correlated and have a dominant frequency of about 1160 Hz. A traverse with the 30% surface pressure microphone indicated no variation of magnitude, phase, or frequency with span, and appeared to have the same amplitude as the 15% microphone.

One result of the spanwise surface pressure microphone traverse was the observation that the 15% microphone (and probably all "upstream" microphones) had a significant effect on the 30% microphone (and probably other downstream microphones), as shown in Figure 7. A high frequency disturbance of significant magnitude was introduced by placement of the 30% microphone downstream of the 15% microphone (see Figure 7.a) and was eliminated when the 30% microphone was removed from the downstream position by approximately 0.5 inch (see Figure 7.b). The 30% microphone output shown on Figure 7.a is as free from this high frequency disturbance as any downstream microphone signal recorded during most of the runs. Other conditions of angle of attack and velocity showed similar effects of moving the

30% microphone out of the "downstream" position. All downstream surface microphones had output containing significant amounts of high frequency output as compared with the 15% microphone output for cases where it had a relatively clean signal. (That is, output was similar to the 30% microphone when it was downstream of the 15% microphone). Thus, it must be assumed that most, if not all, of such output is due to the upstream surface microphone. The oscillograph records of the chordwise surface pressure microphones are of doubtful value, but analysis of the magnetic tape records may yeild more information.

Wake correlation was also investigated during the three-dimensional model tests. Correlation lengths of approximately 0.5 inch were observed for the wing at 4° angle of attack and at tunnel velocities of 100 ft/sec and 200 ft/sec, downstream of the surface pressure microphone array during the three-dimensional model tests. Again, a wake region of peak disturbances and observed frequencies indicated a wake thickness on the order of one tenth the airfoil's projected dimension on the free stream. There did not appear to be increased spanwise correlation lengths in the wake near the tip of the three-dimensional model. Surface pressure microphone traverses indicated that the 15% and 30% (movable) microphones had the same amplitude, frequency, and phase along the entire span, for those cases investigated.

The models could be expected to respond most readily near their natural frequencies. An attempt was made to determine natural frequencies of the three-dimensional model by tapping the model near the tip. Resulting accelerometer output indicated that the two lowest bending natural frequencies of the three-dimensional model were at approximately 135 Hz and 527 Hz. Higher frequency modes exist, but mode types and frequencies were not clearly indicated by these simple tests. Model physical properties and support conditions are not felt to be known sufficiently well to permit a theoretical estimate of the model natural frequencies.

The accelerometer output indicated that there was model motion at the same frequency as surface and far field microphone pressure variations for many angle of attack and flow conditions. At other conditions the accelerometer either had no significant output with the same frequency as the microphones, or that frequency component was not clearly distinguishable from the oscillograph record. The possibility of model motion exists, and either torsional or flat-wise motions would have a corresponding angle of attack, lift variations, and possibly wake velocity and sound pressure variations. Model motion, as measured by the accelerometer, was calculated for the two-dimensional model for $\alpha = 4°$ and $v = 100$ ft/sec. This condition resulted in very nearly pure tone (single frequency) output from all instrumentation. It also had one of the largest ratios of model velocity to sound pressure ratios, indicating that if model motion were ever important, it should be for this condition. Calculations for this case indicate that (1) the airfoil motion as a flat plate would not be large enough to cause the observed sound pressures at the overhead microphone, and (2) lift variations due to the angle of attack caused by flapping velocities would not be large enough to cause the observed sound pressures at the overhead microphone. The measured surface pressures, however, would be sufficient to cause the observed sound pressure. Therefore, model motion does not appear to be the primary source of sound even when it is at a relatively large level compared to the sound. It is entirely possible that model motion, though small, does contribute to the mechanism(s) involved in vortex shedding and turbulence, and thus plays an important roll in sound generation for some model configurations. The observed surface pressures for these conditions was approximately 1/2 the maximum pressure predicted in the preliminary study mentioned earlier, so is the correct order of magnitude for vortex shedding pressure disturbances. Analysis of other test conditions is dependent upon frequency analysis of the magnetic tape records, which was not completed at the time of the printing of this paper. It is expected that further analysis of the experimental data will be done, including spectral analysis of some of the recorded pressure time histories. The results of this and other available work will be used to develop methods for predicting vortex shedding parameters as a function of airfoil and operating characteristics. These methods will be used in conjunction with existing rotor blade loads programs and rotor noise prediction programs to predict helicopter main rotor vortex noise for helicopters in various flight regimes.

Conclusions

The expected magnitude of surface pressures was observed for cases where "pure tone" signals were observed, but frequencies were an order of magnitude higher than predicted on the basis of airfoil dimension perpendicular to the free stream. Model motion did not appear to be of sufficient magnitude to account for the observed sound levels, but may be an important part of the mechanism(s) involved in vortex shedding noise, particularly where pure tones are emitted. Shedding frequencies may be different on operational helicopter rotors than those observed during these controlled tests.

Most angle of attack and velocity conditions did not result in pure tone emission, but was characterized by sound emission over a range of frequencies. None of the observed frequencies were in the range which would be predicted using a Strouhal number of approximately 0.2 and the airfoil's dimension perpendicular to the free stream; the observed frequencies were approximately an order of magnitude higher than those predicted on that basis.

For conditions where pure tones were observed the surface pressure variations were in phase over the entire airfoil, wake velocities were in phase for lengths on the order of the airfoil thickness, and accelerometer, surface and sound pressure microphones, and hot-wire anemometers all had the same dominant frequency.

No increase was observed in the spanwise length within which wake velocities were correlated in the tip region of the three-

dimensional model, as compared with two-dimensional model results. Three-dimensional effects do not appear to have a significant effect on surface pressure or sound pressure frequencies or magnitudes.

Further analysis of the data is anticipated, and may modify these conclusions and indicate other important facts related to the generation of sound by airfoils.

References

1. Patterson, Robert; Amiet, Roy; Voitt, Paul, and Fink, Martin R.: Broadband Noise from an Isolated Airfoil. Presented at the Helicopter Noise Symposium; Durham, North Carolina; September 1971.

2. Hanson, Carl E.: An Investigation of the Near-wake Properties Associated with Periodic Vortex Shedding from Airfoils. MIT, Acoustics and Vibration Lab Report No. 76234-5, September 1970.

3. Ross, D.; Vortex Shedding Sound of Propellers. Bolt Beranek and Newman Inc. Rep. 1115, 1964.

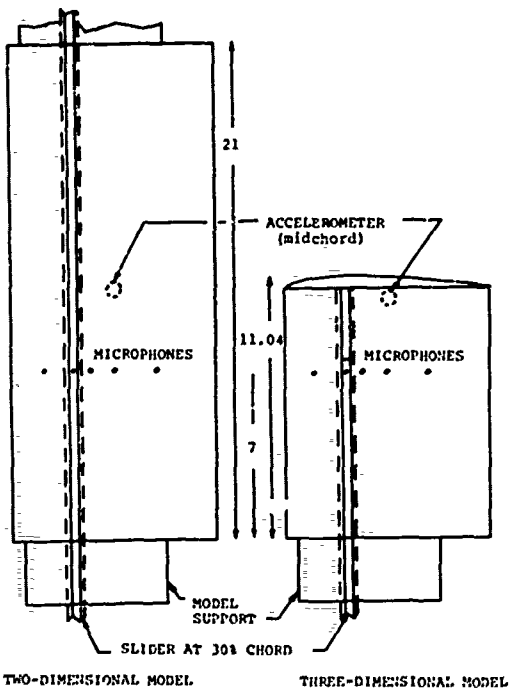

Figure 2. Plan view of NACA 0012 airfoil models. 9 inch chord, 1.08 inch maximum thickness.

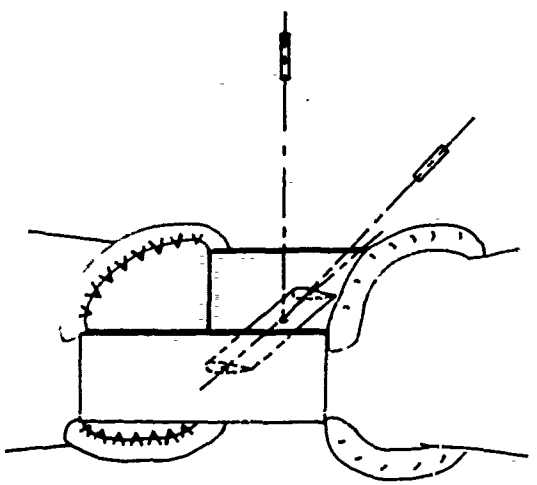

Figure 1. Test section arrangement

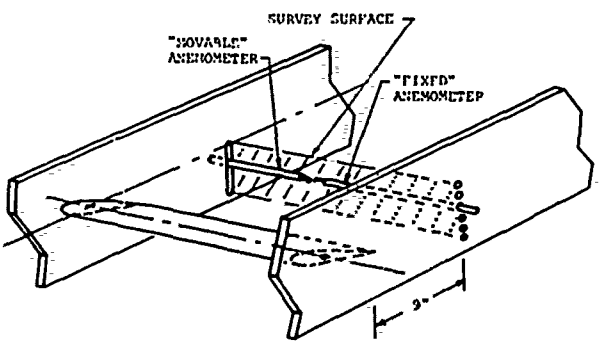

Figure 3. Hot-wire anemometer arrangement

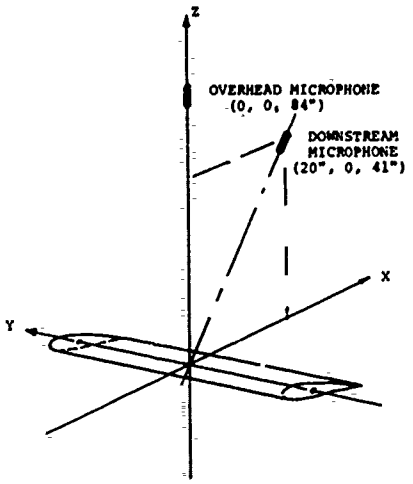

Figure 4. Typical sound pressure microphone arrangement

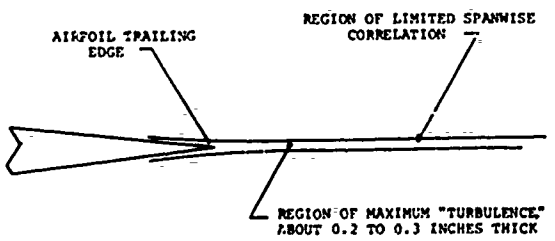

Figure 5. Wake correlation region

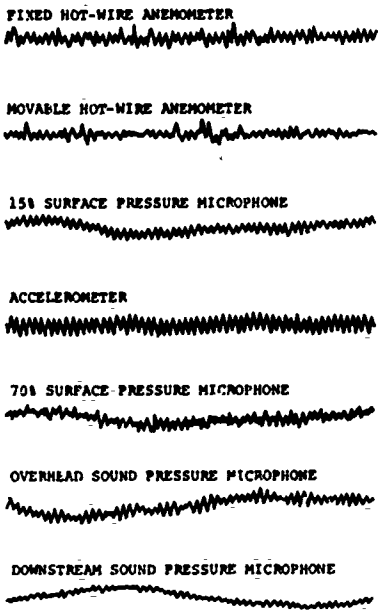

Figure 6. Typical transducer signals for "pure tone" conditions

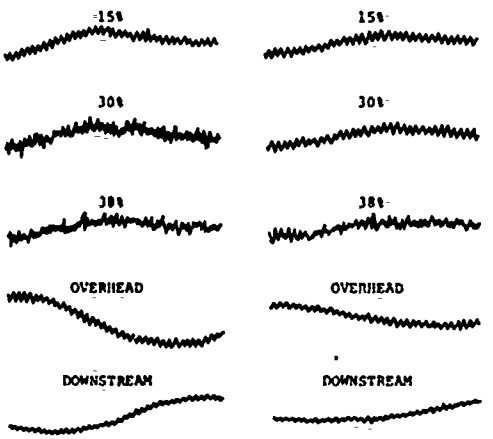

A. 30% downstream of 15%

B. 30% not downstream of 15%

Figure 7. Effect of upstream surface pressure microphone on downstream surface pressure microphone

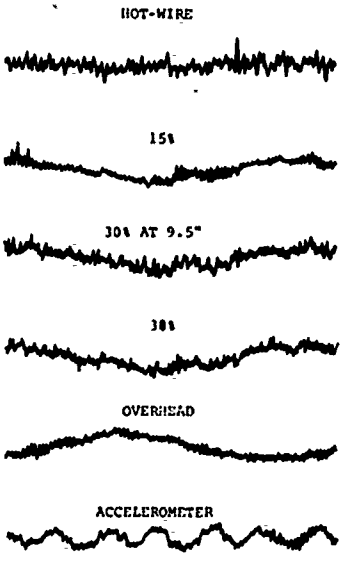

Figure 8. Model motion - sound pressure comparison

ROTATING BLADE VORTEX NOISE WITH AND WITHOUT AXIAL VELOCITY

James Scheiman and David A. Hilton

NASA Langley Research Center
Hampton, Virginia

SUMMARY

An experimental investigation has been made in the Langley full-scale tunnel and outdoors to investigate some of the characteristics of vortex noise generated on a rotating blade system. Acoustic measurements were made for two different blade sections with several tip shapes when the blades were rotating in their own shed wake and when the shed wake was blown downstream. The blades were operated only at zero lift at each radial section. The results indicate that the tip shape changes had very little effect on the overall sound pressure level. Introducing axial velocity to blow away the blade shed wake for the rotating circular blade section resulted in an increase in the noise level, while, for the airfoil section, the overall noise level decreased.

INTRODUCTION

Rotor noise is a major operating problem of helicopter and propeller driven aircraft. The development of satisfactory methods for predicting so-called "vortex noise" has been an objective of the helicopter and propeller industry, but a lack of experimental data has retarded this goal. For example, in reference 1, Yudin encountered difficulties in the experimental separation of rotational and vortex noise. Also, Deming, reference 2, states that gusts of wind may cause the sound pressure to vary considerably.

The origin of "vortex noise" is controversial. In reference 3, Stowell and Deming designed special rods in an attempt to isolate peaks in the spectrum corresponding to the Strouhal frequency; however, they found that such attempts were unsuccessful. More recently, the origin of vortex noise has been attributed by some to Von Kármán vortex shedding and by others to turbulence ahead of the blade. For example, reference 4 assumes that the oscillating blade surface pressures are associated with the shedding of eddies resulting from vortex street effects; whereas reference 5 indicates that the vortex noise is associated with the random turbulence ahead of the blade, which in turn causes surface-pressure oscillations.

A shortage of experimental information on vortex noise had seemed the major impediment to devising and correlating theory with test results. To help overcome this obstacle, the NASA Langley Research Center has recently completed a test program within the Langley full-scale tunnel and outdoors. The test program consisted of noise measurements for a rotor operating at zero lift for two airfoil sections. The tests included rotor operation with the blades rotating in their own shed wake and with the blade wake blown downstream. The two blade sections were a circular pipe and an NACA 0012 airfoil section. Both blades had the same radius, diameter and blade thickness, namely, 7.05 m and 5.08 cm, respectively. For the wind-on conditions, the NACA 0012 section blade was provided with a helical twist so the airfoil operated at zero lift all along its span. Various blade-tip configurations were tested.

SYMBOLS

D rotor diameter, m

f frequency, Hz

N rotor rotational speed, rpm

R rotor radius, m

r hall radius (see text for definition), m

V velocity along the axis of rotor rotation, m/sec

Ω rotor angular speed, rad/sec

TESTS

Test Setup

The indoor tests were conducted in the Langley 9.15 × 18.3 m full-scale wind tunnel. A schematic sketch of the test setup drawn to scale is shown in figure 1 and a photograph of the setup is shown in figure 2. The rotor rotational axis was in the center of the tunnel and approximately 3.96 m above the ground board. The pertinent microphone locations are indicated by the solid dots in figure 1. The microphones shown are alined with or at 45° to the rotor rotational axis. The zero-wind indoor tests were duplicated in the outdoors. For the outdoor tests the rotor axis was alined parallel to and approximately 2.44 m above the ground level. The recording microphones were located at every 22.5° azimuth angle and at a 2-diameter distance. The outdoor tests were conducted to obtain a reverberation evaluation of the full-scale tunnel.

Full-Scale Tunnel Reverberation Effects

The question of the reverberation effects arises whenever acoustic measurements are made in a closed chamber. Two separate test programs were conducted in order to answer this question. The first program consisted of identical tests conducted with the rotors inside the tunnel and outdoors under zero-wind conditions. The second program was conducted inside the test chamber only and was directed specifically toward obtaining directivity and reverberation times within the test chamber.

Comparisons of indoor and outdoor noise-frequency spectra for two different models are shown in figure 3. One of the models is the blade with the circular cross section and the other is the blade with the NACA 0012 airfoil section. The comparison is for zero axial velocity and for one microphone position, namely, at a distance of two rotor diameters and alined along the rotor rotational axis. The comparison of the amplitude and spectrum distribution for the circular blade section is quite good. For the NACA 0012 blade section the comparison is also quite good, but not so good as for the circular blade section.

With indoor data only, an evaluation was made on the basis of noise decay rate with distance (inverse-square law). The measured data indicated a 5- to 6-dB difference as compared with a theoretical free-field value of 9.6 dB. This difference of about 3 dB is the magnitude of the reverberation effect.

In addition to the indoor-outdoor noise comparison, reverberation tests were conducted in the test chamber. The results of this program are presented in reference 6. These results, for zero-wind velocity, have been extrapolated for the models tested herein, and samples of the conclusions are presented in figures 4 and 5 for the two different rotor blade sections. The 0° azimuth position on these figures is alined with the rotor rotational axis vector (using the right-hand rule). These plots are in terms of the hall radius divided by the rotor diameter. The hall radius is defined as the distance from the source where the sound pressure from the direct field equals the space average sound pressure of the reverberant field. In other words, acoustic measurements at one hall radius will be 3 dB above the corresponding

free-field measurements. Further, at a distance of one-half the hall radius, this difference would be 1 dB. In general, the original test-chamber acoustical evaluation (ref. 6) indicated that a 1000-Hz frequency band resulted in the smallest hall radius. Further, for octave-band center frequencies outside of the range plotted, the hall radius is greater than that for a frequency of 250 Hz. Figures 4 and 5 indicate that microphone positions alined with and at 45° to the rotor rotational axis at the 2D distance are inside of or near a distance of one hall radius, with the exception of the 1000-Hz frequency band. Therefore, except for the 1000-Hz band the indoor data presented herein should be between 1 and 3 dB too high. Comparison of the two methods of evaluating the test-chamber reverberation effects shows that use of the hall-radius concept indicates less reverberation than the comparison of the indoor and outdoor measurements.

RESULTS AND DISCUSSIONS

A plot of the radiation pattern is presented in figure 6 for the two rotor blade sections. This is based on outdoor measurements and presents the overall sound pressure level at a two-rotor-diameter distance with zero axial velocity and for variations in rotor rotational speeds. The zero angle is alined with the rotor rotational axis (using the right-hand rule). The data indicate that the radiation is nearly symmetrical about the 90° azimuth angle, as would be expected for zero-wind conditions.

For the circular bladed rotor, figure 6(a), the radiation pattern indicates almost equal radiation in all directions. Since rotor torque will produce dipole radiation in the plane of the rotor whereas vortex shedding will produce dipole radiation along the axis of the rotor, figure 6(a) indicates that the radiation pattern of both noise sources are nearly equal. Further, it appears that the radiation pattern increases equally in all directions as the rotor rotational speed is increased.

The radiation pattern for the airfoil bladed rotor is shown in figure 6(b). At low rotational speeds the vortex shedding seems to be the predominant noise source, whereas at the high speed the torque radiation is dominant. This behavior is certainly different for the two blade sections. The reason for this difference will be explored further in figures 7 and 8.

Figure 7 is a plot of the 1/3 octave frequency spectra for the airfoil bladed rotor. One plot is for a microphone alined with the rotor rotational axis (fig. 7(a)) and the other plot is for a microphone in the blade rotational plane (fig. 7(b)). From figure 7(b), it is seen that for the higher rotational speeds, the high-amplitude noise levels originate in the low-frequency spectrum, namely, 50 to 125 Hz center-band frequencies. This result is indicative of rotor torque or blade thickness noise radiation.

These same data are shown scaled in figure 8. The amplitudes were scaled according to the sixth power of the rotational tip speed and the frequencies are shown divided by the tip speed. This figure shows that the data alined with the rotor rotational axis (fig. 8(a)) scale well, whereas the data in the blade rotational plane (fig. 8(b)) do not. This observation is another manifestation of the results from figure 6(b). Figure 8(b) shows not only that amplitude does not scale but also that the scaled frequencies are mixed. A search of the literature shows no explanation; therefore, it is concluded that this strong phenomenon is not understood.

Effect of Tip Shapes

Vortex noise radiation has been shown to be proportional to the velocity to the 5.5 power (e.g., ref. 3). By far the largest portion of the noise level, therefore, originates from the extreme outer part of the blade. Thus, it might be reasoned that changes in the blade-tip fluid flow conditions might produce large changes in the noise level. Further wind-tunnel tests of loads on stationary circular cylinders (refs. 7 and 8) with various tips had shown a significant effect of tip shape. In order to confirm this influence on rotating blades, various geometric tip shapes were tested. The results of a portion of these tests are shown in figure 9 for a microphone position alined with the rotor rotational axis and at a distance of two rotor diameters from the source. From figure 9 it is evident that the various blade tip shapes tested did not produce any significant difference in the overall sound pressure level. Similar results were obtained for other microphone positions.

For the NACA 0012 bladed rotor a squared-off blade tip and a blade tip body of revolution were tested. The body of revolution blade tip had a radius equal to one-half the blade thickness at that chord station. A comparison of the noise radiation for these two blade tips (fig. 9) shows the same result as tests with the circular bladed rotor, that is, no noticeable difference in the overall noise level.

On the basis of the results of references 7 and 8 the blade-tip flow conditions are certainly changing. However, the results herein indicate that sound pressure radiated from the remainder of the blade dominates, and therefore the effects of tip changes are unnoticed.

Effect of Blade Airfoil Section

Figure 10 presents a comparison of the sound pressure level for the two different blade cross sections (circular and NACA 0012) with and without axial velocity. The results indicate that the blade with the circular section makes a significantly larger noise level both with and without axial fluid flow when the blade frontal areas are equal. This conclusion is in agreement with the conclusions in reference 1, where it is stated that the intensity of vortex sound increases in proportion to the form drag. However, Yudin in reference 1 encountered difficulties seperating "rotational" and "vortex" noise with the commencement of axial flow. This difficulty is not believed present in this investigation because the blades did not produce lift. Acoustically, it is concluded that the same frontal area, rod, and airfoil blade sections behave differently and this difference exists when the rotor operates with or without axial velocity.

Effect of Turbulence

An attempt was made to determine more explicitly the origin of vortex noise. Figure 11 depicts the effect, for two different microphone positions, of imposing a small axial velocity on the rotating blades to blow their shed wake away before the passage of the following blade. One microphone is alined with the rotor rotational axis and the other is at 45° to the rotor rotational axis. Both microphones are at a distance of two rotor diameters. Recall that the rotor with the airfoil section had a helical twist and that keeping zero lift on the entire blade span requires precise combinations of rotational and axial velocity. Therefore, the axial velocity for this model varied continuously with each change in rotational speed. The results in figure 11 indicate that the introduction of axial velocity on the circular blade section

increases the overall sound pressure level by about 3 dB; whereas, the introduction of axial velocity on the NACA 0012 bladed rotor resulted in a decrease of about 6 dB in the overall sound pressure level.

Part of the reason for the foregoing results might be explained as follows: The airfoil rotating in its own wake contains some "rotational noise" due to lift which is caused by velocity fluctuations in the shed wake. These fluctuations in lift do not occur when the shed wake is blown downstream, thus resulting in a decreased noise level. Small axial-velocity fluctuations (present when the blade rotates in its own shed wake) will produce relatively large lift fluctuations on the airfoil section because of its high lift-curve slope but would produce zero lift on the symmetrical circular blade section.

On the other hand, the fact that the circular airfoil section produced more noise when its shed wake was blown away by axial velocity cannot be explained. This section is a poor aerodynamic section, so that blowing the wake away would not seem to affect the section either aerodynamically or acoustically. Introducing axial velocity certainly increases the dynamic pressure on the blade; however, the vectorial addition of the axial velocity and tangential velocity vectors will not produce a sufficient increase in total head to explain the 2 to 3 dB increase in sound level.

CONCLUDING REMARKS

An experimental investigation was conducted to define further the characteristics of vortex noise generated from a rotating blade system. The analysis of the data indicates the following results:

1. A comparison of the amplitude and spectrum distribution for two models tested in the wind tunnel and outdoors is good. Evaluation of the wind-tunnel reverberation from the inverse-square law of the overall sound pressure levels is also relatively good. Further, the test chamber "hall radius" has been determined for the two different blade sections operating in the wind-off condition.

2. The sound-pressure radiation pattern indicates that for the circular bladed rotor, the noise level increases equally in all directions with increase in rotor rotational speed, whereas the radiation pattern for the airfoil-bladed rotor increases more rapidly in the plane of the rotor than along the axis of the rotor with increasing rotor rotational speed. The reason for this is presently not understood.

3. The blade tip shapes tested did not show any appreciable effect on overall sound pressure level.

4. The circular section is much the noisier of the two sections even though the frontal areas of both blades were the same. This result confirms previously found results indicating a direct relationship between increased noise level and increased form drag.

5. The introduction of axial velocity to blow away the turbulent shed wake of one blade before the passing of the following blade caused a decrease of approximately 6 dB in the noise level of the airfoil section as compared to the case for zero axial velocity. Part of the explanation of this result would seem to be that small axial-velocity fluctuations (present when the blade rotates in its shed wake) would produce relatively large lift fluctuations on the airfoil section because of its high lift-curve slope, but would produce zero lift on the symmetrical circular blade section.

REFERENCES

1. Yudin, E. Y.: On the Vortex Sound From Rotating Rods. NACA TM 1136, 1947.

2. Deming, A. F.: Noise From Propellers With Symmetrical Sections at Zero Blade Angles. NACA TN 679, 1938.

3. Stowell, E. Z., and Deming, A. F.: Vortex Noise From Rotating Cylindrical Rods. NACA TN 519, 1935.

4. Sadler, G. S., and Loery, R. G.: A Theory for Predicting the Rotational and Vortex Noise of Lifting Rotors in Hover and Forward Flight. NASA Report 68-11. (Available as NASA CR-1333.)

5. Lowson, M. V., and Ollerhead, J. B.: A Theoretical Study of Helicopter Rotor Noise. Journal of Sound Vib., 1969.

6. Ver, Istvan L., Malme, C. I., and Meyer, E. B.: Acoustical Evaluation of the NASA Langley Full-Scale Wind Tunnel. NASA CR-111868, Jan. 1971.

7. Keefe, R. T.: An Investigation of the Fluctuating Forces Acting on a Stationary Circular Cylinder in a Subsonic Stream and of the Associated Sound Field. University of Toronto Institute of Aero-physics, Rept. 76, Sept. 1961.

8. Gerrard, J. H.: Measurements of the Fluctuating Pressure on the Surface of a Circular Cylinder. Part I – Cylinder of 1-Inch Diameter. Aeronautical Research Council Rept. 19, 844, Jan. 1958.

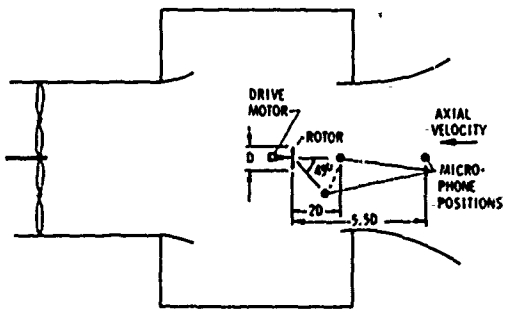

Figure 1.- Test setup.

Figure 2.- Test setup.

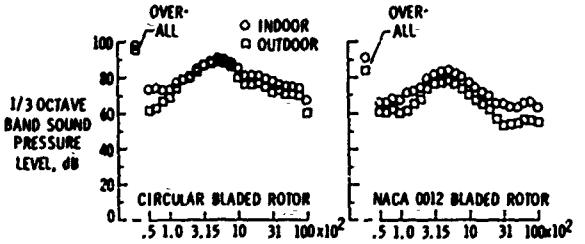

Figure 3.- Reverberation evaluation at N = 850 rpm.

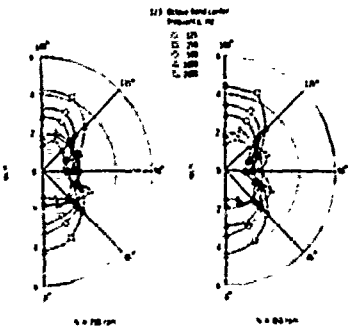

Figure 4.- Hall radius for circular bladed rotor.

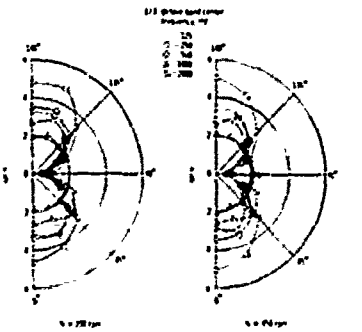

Figure 5.- Hall radius for NACA 0012 bladed rotor.

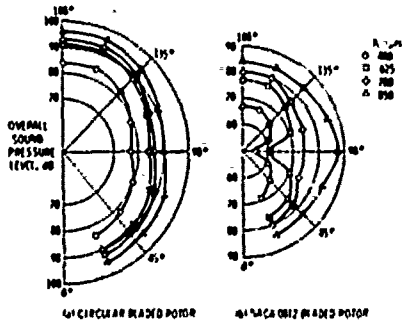

(a) Circular bladed rotor. (b) NACA 0012 bladed rotor.

Figure 6.- Radiation pattern.

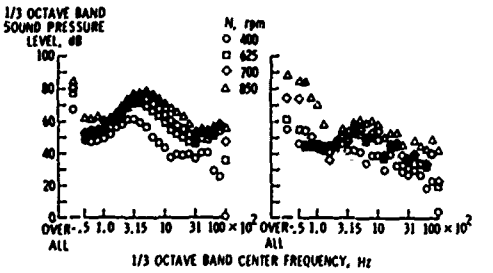

(a) Microphone alined with rotor rotational axis.

(b) Microphone in the rotor rotational plane.

Figure 7.- Noise spectrum for NACA 0012 bladed rotor.

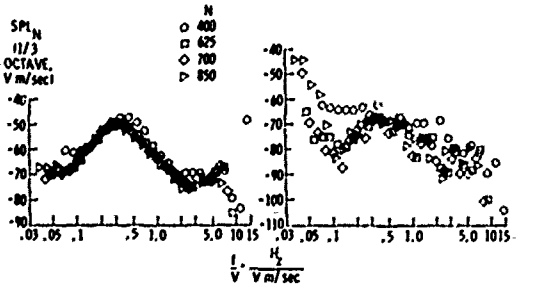

(a) Microphone alined with the rotor rotational axis.

(b) Microphone in the rotor rotational plane.

Figure 8.- Noise spectrum for NACA 0012 bladed rotor.

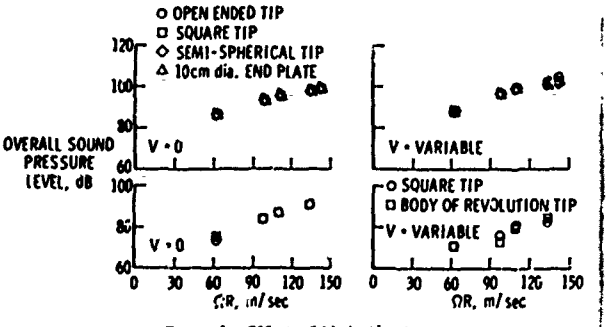

Figure 9.- Effect of blade tip shape.

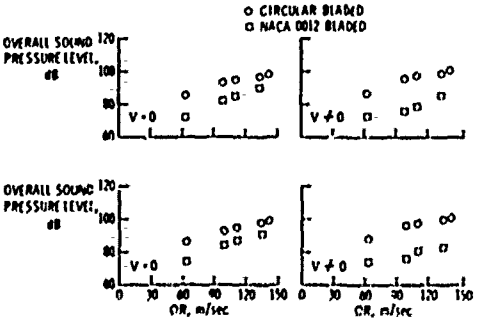

Figure 10.- Noise level versus rotational tip speed.

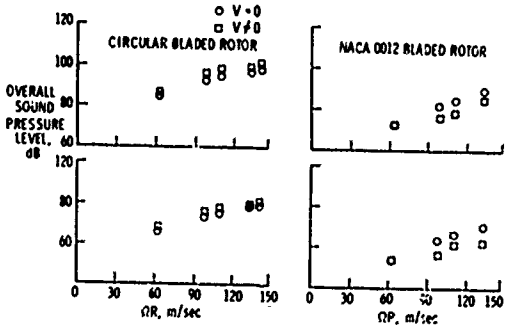

Figure 11.- Noise level versus rotational tip speed.

Vortex Shedding Noise of an Isolated Airfoil

Robert W. Paterson, Paul G. Vogt, Roy K. Amiet, and Martin R. Fink
United Aircraft Corporation Research Laboratories
East Hartford, Connecticut 06108

ABSTRACT

Vortex noise produced by an isolated nonrotating airfoil in low-turbulence flow is being investigated analytically and experimentally. This paper serves as a progress report on the not yet completed investigation. Surface and far-field acoustic spectra and cross-correlations were obtained with full-span and semispan NACA 0012 airfoil models of 9-in. (23 cm) chord. These were tested in a semi-open jet with solid sidewalls 21 in. (53 cm) apart and open jet boundaries above and below the test section. Airspeeds ranged from about 100 to 670 fps (30 to 200 m/sec), providing a range of Reynolds number from 0.5×10^6 to 2.7×10^6.

At low Reynolds numbers, the observed far-field spectra were dominated by a discrete tone. The intensity of this tone increases to a maximum and then decreases with increasing velocity. The airfoil noise could not be detected above the far-field background noise for high Reynolds numbers and low angles of attack. The measured surface pressure spectra then were typical of those expected for turbulent boundary layer pressure fluctuations.

An approximate analytical method for describing and predicting the surface and far-field tone noise phenomena is being developed.

INTRODUCTION

A helicopter rotor generates three major types of noise: periodic, interference, and vortex. The periodic noise is caused by the pressure pattern of the rotor blade's thickness and lift distribution. That pattern varies once per revolution relative to the blade as it moves past an observer as the blade rotates. Interference noise is caused by relative motion between the blade and an adjacent physical or aerodynamic obstruction (a fuselage or another blade's tip vortex). The remaining type of noise, vortex noise, is caused by interaction of a blade with its own boundary layer and near wake. Vortex noise imposes a floor on the noise generated when rotor loading and interactions have been minimized. Thus the study of vortex noise is important since it represents a practical minimum limit on helicopter rotor noise and forms an interesting problem in basic fluid dynamics.

Prior to studying the vortex noise of rotating blades, it would be useful to understand the simpler problem of the vortex noise produced by a nonrotating airfoil. This vortex noise will be accompanied by broadband noise from lift fluctuations induced by upstream turbulence and from pressure fluctuations within the airfoil's turbulent boundary layer. The only analytical description of vortex noise is that of Sharland (Ref. 1), which does not permit calculation of surface pressure fluctuations. Few experimental studies are available. Most of these were conducted with low aspect ratio models supported through the shear layer and tested at relatively low Reynolds numbers and might not be representative of high aspect ratio blades at full-scale conditions. Also, the contribution of free stream turbulence to previously measured vortex noise characteristics is not known. Finally, in vortex noise experiments only far-field sound pressure measurements have been made with no determination of surface pressure fluctuations and correlation areas. Availability of such data would be useful for separate evaluation of different assumptions within various portions of analytical methods for calculating vortex noise.

Recently, an acoustic wind tunnel was constructed at United Aircraft Research Laboratories. This tunnel is capable of testing airfoil models at full-scale Reynolds numbers and Mach numbers for the rotor blades of small helicopters. Such models are large enough to contain commercially available microphone instrumentation for measurement of very weak surface pressure fluctuations. Provisions have also been made to ensure a very low turbulence level in the airflow in an attempt to minimize its effect on vortex noise. The objectives of the investigation described herein were (1) to obtain airfoil surface and far-field acoustic data in that wind tunnel for variations of velocity and incidence, (2) to utilize these data in evaluating analytical assumptions concerning details of the process that generates vortex noise, and (3) to combine the validated assumptions into a new analytical method for predicting airfoil-vortex noise.

The experimental effort is being funded by Army Research Office - Durham under Contract No. DAHC04-69-C-0089. The analytical effort is being conducted as part of the United Aircraft Research Laboratories Corporate-funded research program. Both portions of this investigation are in progress as of the date of this report; completion and preparation of a final report are scheduled for the end of this year. This paper therefore should be regarded as a progress report rather than a description of completed effort.

DESCRIPTION OF EXPERIMENTAL EQUIPMENT

Acoustic Research Tunnel

The Acoustic Research Tunnel, shown schematically in Fig. 1, is a controlled turbulence level, open circuit, open jet wind tunnel designed specifically for aerodynamic noise research. Insensitivity of test section flow to external wind conditions is achieved by the use of a high length to diameter ratio (72) honeycomb at the tunnel inlet. For the present experiment, five 28 mesh turbulence suppression screens were provided in the inlet. Use of the screens in conjunction with a contraction ratio of 14 produced both a low turbulence level and a spatial mean velocity distribution in the test section measured to be uniform to within ±0.25 percent. The ratio of the rms vertical turbulent velocity fluctuation to mean velocity was measured to be less than 0.4 percent for frequencies above 200 Hz. The open jet is contained within a 16 ft high, 18 ft long (axial direction), and 20 ft wide sealed reinforced concrete chamber lined with one foot fiberglass wedges. Measurements of the chamber acoustic properties have demonstrated that the chamber is anechoic (6 dB decrease in SPL per doubling of distance from source) for frequencies at and above 250 Hz.

Figure 2 shows the test section arrangement employed in the present study. A rectangular test section 21 in. high by 21 in. wide with 5 in. rounded corners was chosen to provide two-dimensional flow. To provide a uniform spanwise variation of loading on full-span airfoil models, the vertical sides of the jet were closed with sideplates extending from the contraction outlet into the jet collector inlet. The use of sideplates also eliminates the need to extend the airfoil or airfoil support through the thick, highly turbulent jet shear region which would normally exist in

Preceding page blank

their absence. With sideplates installed, variations in spanwise velocity distribution occur only in the sideplate boundary layers. The sideplates were constructed of aluminum with a smooth finish and were not acoustically treated.

To isolate the airfoil models from vibrations of the tunnel structure, the airfoils were directly supported from the anechoic chamber floor. A 1/2-in. annular clearance, filled with sponge rubber, provided isolation between the sideplates and the airfoil's circular end supports.

The semi-open jet was collected at the diffuser entrance by a jet collector. The interior edge of the collector was located on the constant mass flux streamline which divides the mean jet flow from the chamber recirculation pattern. This positioning helped to minimize streamline distortion in the test section. Based upon model tests, a 4-in. radius collector lip was provided which minimized the background noise due to shear layer -- collector lip interaction. In addition to this broadband noise, an acoustic coupling between the contraction outlet and the collector lip produced strong discrete-frequency background noise (edge tones) at certain tunnel speeds. To suppress this noise source mechanism, an array of 20 small triangular tabs projecting 1/2 in. into the jet were installed at the contraction outlet. Based on the measured variation of tunnel background noise with open jet length, a test section length of 30 in. was chosen for the present experiments.

The three-stage diffuser located downstream of the jet collector operates unstalled and is therefore not a major source of background noise. To attenuate tunnel fan noise, an absorptive Z-shaped muffling section consisting of parallel fiberglass baffles and lined bends is located between the diffuser and fan inlet. For frequencies above which the chamber is anechoic (250 Hz), the fan muffling is sufficiently high that the background noise level in the chamber is set by noise radiated from the jet shear layer and from the shear layer -- collector interaction. Radial vanes located at the inlet of the 1800 rpm centrifugal fan provide continuously variable test section velocities from 60 to 670 ft/sec. Tunnel speed is determined from total pressure at the contraction inlet and static pressure from a ring of taps at the contraction outlet. Fluctuations in tunnel speed with time were measured to be less than ± 0.5 percent.

Models and Instrumentation

Three airfoil models of 9-in. chord were fabricated for this program. Two have NACA 0012 sections and the third has an NACA 0018 section. One of the NACA 0012 airfoil models and the NACA 0018 airfoil model completely span the 21-in. wide UARL Acoustic Research Tunnel test section. The other model spans only half of the test section and has a tip fairing to simulate a wing tip. The models were fabricated from stainless steel with a surface finish of approximately 32 micro-inches. A tolerance of ± 0.010 in. was obtained with 0.005 to 0.015 in. discontinuity on the instrumented side and less than 0.005 in. on the other side. Drawings of the three airfoil models are presented in Figs. 3 and 4. The airfoils were mounted as shown in Fig. 2 with the leading edge 9.5 in. downstream of the inlet contraction lip. The mounting was designed to permit variations in airfoil angle of attack.

The microphone installation sketched in Fig. 4 required a minimum of 0.75-in. airfoil thickness. In order to obtain microphone positions between 15 and 50 percent chord of an NACA 0012 airfoil, a 9-in. airfoil chord was required. Bruel & Kjaer (B&K) condenser microphones were used because of their high sensitivity to pressure fluctuation and low sensitivity to vibration and temperature changes. From the results of small-scale tests conducted with microphones flush and cavity-mounted, it was decided to flush-mount the microphones to avoid cavity resonance. It was also decided to test without the microphone grid to avoid high-frequency noise caused by the grid. The microphones in the airfoil were optically aligned to within 0.004 in. of the airfoil surface. An annular gap of 0.008 in. existed around the installed microphones. The microphones were installed in a manner similar to that described in Ref. 2. In order for the microphones to be flush mounted in the airfoil surface, B&K right-angle adapters had to be used. The 1/4-in. microphones were the smallest for which such adapters are made. As shown in Fig. 3, five 1/4-in. B&K microphones were located on the NACA 0012 airfoil models. Four were fixed at one-third span and 15, 38, 50, and 70 percent chord. The right-angle adapter was rebuilt in order to fit within the airfoil section at 70 percent chord. The fifth microphone was mounted at 30 percent chord in a slider which allowed spanwise travel (Fig. 3). For the half-span model, inserts were used to close the gap caused by movement of the slider. To obtain far-field pressure measurements, a 1/2-in. microphone was mounted on a boom 7 ft above the tunnel centerline.

Data were acquired on line with swept one-third octave and 10 Hz filters and real-time correlations. A B&K Audio Frequency Spectrometer (Type 2113) coupled with a B&K Level Recorder (Type 2305) produced the one-third octave spectra. All sound pressure levels in decibels were determined for 2×10^{-4} dynes/cm^2 reference pressure. A Quan-Tech Wave Analyzer (Model 305-R) produced the 10 Hz spectra and a Saicor Correlation and Probability Analyzer (SAI-42) the correlograms.

The microphones were calibrated with a B&K Pistonphone at 250 Hz and with a General Radio Calibrator at 125, 250, 500, 1000, and 2000 Hz. An acoustic coupler fabricated at UARL was used during calibration of the surface microphones. The signals were filtered (with UISA type 55D 25 filters) when using the correlator in order to remove low-frequency noise associated with the tunnel drive fan.

A B&K Accelerometer (Type 4336) was installed in the airfoils as shown in Figs. 3 and 4. This accelerometer operated in conjunction with a B&K Vibration Pick-Up Preamplifier (Type 1606) and Microphone Amplifier (Type 2603). The accelerometer was calibrated at 60 Hz with the Vibration Pick-Up Preamplifier.

DESCRIPTION OF ANALYTICAL METHOD

A general framework for studying the acoustic radiation caused by vortex noise is provided by the relationship between surface pressure and the far-field radiated sound field. Within this framework, measured or analytically predicted surface pressure fluctuations can be used to predict the radiated acoustic field of an airfoil undergoing vortex shedding. In addition, such a framework can be used to help interpret aerodynamic and acoustic data and to evaluate assumptions within various analyses of vortex noise.

The theoretical foundations for relating surface pressures on a body in a fluid to the sound produced by this body were originally developed in Ref. 3 and later generalized in Refs. 4 and 5. These analyses permit the sound produced by the body to be expressed in terms of a distribution of monopoles and dipoles on the surface of

the body. Since the monopole distribution is proportional to the normal velocity of the surface, and since the airfoil for the present experiment is stationary relative to the free stream velocity, the monopole term is zero. Thus, only the dipole distribution over the surface contributes to the noise. If the surface loading (or pressure) at each point on the airfoil is known as a function of time, the far-field sound pressure produced by the airfoil can be calculated by integration of Eq. (2.18) of Ref. 4 over the airfoil surface, i.e., by

$$p = \frac{x\omega z}{4\pi a x^2} e^{i\omega(t - x/a)} \int_A Q(\omega, \underline{x}_s) e^{\frac{i\omega}{a}\left(\frac{xx_s}{x} + \frac{yy_s}{x}\right)} d\underline{x}_s \qquad (1)$$

where the x axis is in the flow direction, the y axis is in the span direction, and z normal to the span. In general, however, for a random or nondeterministic process, the detailed distribution of airfoil loading as a function of time and position required for evaluation of Eq. (1) is not known. This equation must then be cast in terms of functions characteristic of random processes such as the loading power spectrum and correlation length.

The Power Spectral Density (PSD) in the far field is obtained by multiplying the Fourier transfer of Eq. (1) by its complex conjugate. When this is done, Eq. (2) is obtained.

$$\frac{p^2}{\rho^2} = S_{pp}(\omega, \underline{x}) = \frac{\omega^2 z^2}{16\pi^2 a^2 x^2} \int_A \int_A S_{qq}(\omega, \underline{x}_s, \underline{x}_s') e^{\frac{i\omega}{a}\left[\frac{x(x_s - x_s')}{x} + \frac{y(y_s - y_s')}{x}\right]} d\underline{x}_s d\underline{x}_s' \qquad (2)$$

This equation relates the PSD in the far field to the cross-correlation of surface pressure fluctuations on the airfoil and is valid for any loading distribution. Significant simplification of this equation is possible for random processes whose dominant wavelengths are much larger than the linear dimensions of the regions on the airfoil over which pressure fluctuations are correlated or in phase. These regions are considered correlation areas. It is important to note that the phasing between correlation areas is random for a random process. This permits the airfoil PSD to be computed by summing up the separate PSD contributions of each area. If the process is deterministic (i.e., not random) then even though regions on the airfoil can be found over which pressure fluctuations are in phase, the contributions from each area cannot be added separately since the phasing between areas is not random. In this case, the contibution of all the "areas" to the pressure must be computed first and then the PSD obtained. Thus, for deterministic processes, the concept of correlation area loses some of its physical appeal.

The assumption that the wavelength is large compared to a correlation area is equivalent to a compact source assumption. This assumption allows the exponential phase in the integral of Eq. (2) to be neglected, significantly simplifying the integral. Use of the compactness assumption is valid if the difference in distance from the observer to any two points within a correlated area is small compared to an acoustic wavelength. This assumption will be met if, as discussed above, the correlation length is small compared to a wavelength. The assumption can also be met if the far field observer is directly above the airfoil since all points of the airfoil will then be equidistant from the observer (for an airfoil with small camber and angle of attack). This is an important point since the z axis is also where most of the far field acoustic measurements are being made.

The neglect of the exponential factor in Eq. (2) for either of these two reasons then allows a correlation area to be introduced as

$$S_c(\underline{x}_s, \omega) = \frac{1}{S_{qq}(\omega, \underline{x}_s)} \int_A S_{q,q_s}(\omega, \underline{x}_s, \underline{x}_s') d\underline{x}_s' \qquad (3)$$

For a random process, this area takes on the physical significance discussed earlier. The far field PSD can now be written as:

$$S_{pp}(\omega, \underline{x}) = \frac{\omega^2 z^2}{16\pi^2 a^2 x^2} \int_A S_c(\underline{x}_s, \omega) S_{qq}(\omega, \underline{x}_s) d\underline{x}_s \qquad (4)$$

Equation (4) is now in a form which can be easily interpreted and in which S_c and S_{qq} can be obtained from surface pressure measurements and correlations. As can be seen, Eq. (4) essentially sums the contributions of each correlation area over the whole airfoil as discussed above. It is generally valid for all field point locations if the wavelength is large compared to the correlation length and, in particular, is exact, independent of wavelength for field point locations directly above the airfoil.

If airfoil vortex noise is assumed to be a broadband random process, as in Ref. 1, the far field PSD given by Eq. (4) can be integrated over all frequencies and over a spherical area surrounding the airfoil to obtain the total radiated energy. This procedure yields Eq. (3) of Ref. 1. It was assumed in that analysis that broadband noise was caused by fluctuating loadings generated by fluctuations of near-wake flow direction. The center frequency of this broadband noise was taken as that for a Strouhal number of 0.2 referenced to airfoil maximum thickness. The correlation area was taken equal to the maximum eddy size, which was assumed to have a linear dimension equal to the airfoil half-thickness.

An alternate approach is obtained by assuming that vortex noise occurs as a discrete tone, as was observed in this experimental program. The aerodynamic behavior of the near-wake fluctuations and surface pressure fluctuations that radiate noise to the far field could then be examined.

An approach to calculation of near-wake fluctuations has been developed by Krzywoblocki (Ref. 6) to predict the buffeting of aircraft tail surfaces caused by the wing wake. In that analysis, it was recognized that the wing produces a steady boundary layer that becomes unstable as it flows into the wake. For sufficiently low Reynolds numbers, the near wake then develops into a periodic Karman vortex street. Some fraction of the vorticity generated by the boundary layer during one period of the vortex street then would be concentrated to comprise each vortex. The wing pressure distribution must fluctuate in response to formation and downstream movement of vortices in the near wake. The change in airfoil lift force, and hence the radiated acoustic energy, could then be calculated from the circulation of each vortex. This circulation would depend on the frequency, which should be that for a constant Strouhal number referenced to the near-wake thickness. It was incorrectly assumed in Ref. 6 that the relevant thickness was the projected maximum thickness of the airfoil. For thin airfoils having smooth pressure distributions, it is assumed herein that the thickness of a laminar boundary layer at the airfoil trailing edge should be used. The lift force would be caused by vortices in the near wake rather than by airfoil incidence. As can be seen from Fig. 3 of Ref. 7, the chordwise distribution of loading due to a vortex in the

near wake would be relatively constant along most of the chord and peaked near the leading and trailing edges. In contrast, the loading caused by fluctuating incidence was shown in Ref. 7 to resemble that for steady incidence (sharply peaked near the leading edge and decaying smoothly to zero at the trailing edge).

If the pressure fluctuations on the airfoil are caused by vortices located in the near wake, relatively little variation of Δp_{rms} along the chord would be expected except near the leading and trailing edges. Also, the surface pressure fluctuations measured at low Reynolds numbers and described in a following portion of this report had relatively little variation along the instrumented chordwise region. The dominant portion of the measured PSD's was a discrete tone. Therefore the power spectral density of the surface pressure fluctuation at each spanwise position was assumed to occur at only one frequency $f = \omega/(2\pi)$ and to be independent of chordwise position. Then, with

$$\Phi_{pp} = \Delta p_{rms}^2 \, \delta(\omega - \omega_0) \tag{5}$$

for a discrete tone and Z equal to r, Eq. (4) becomes

$$\overline{p^2} = \frac{1}{\pi} \int_0^\infty \int_0^\infty \Delta p_{rms}^2 \cos(\omega_0 \tau) \, d\omega \, d\tau \tag{6}$$

For a two-dimensional airfoil of span b, the correlation area and the surface pressure fluctuation (and its frequency) should be independent of spanwise position. Then

$$\overline{p^2} = \frac{\pi}{2} \left(\frac{b}{2}\right)^2 \left(\frac{c}{2}\right)^2 \Delta p_{rms}^2 \tag{7}$$

so the ratio of correlation area to planform area could be determined experimentally from the measured frequency and the measured pressure fluctuations on the surface and in the far field. Also, the correlation area for each surface microphone location could be measured by cross-correlation with the other surface microphones.

As shown in the next section, it is observed that vortex tone noise occurs when a laminar boundary layer is expected along most of one or both surfaces of an airfoil. The thickness of a laminar boundary layer at the trailing edge would be approximately

$$\delta \propto c \, R^{-1/2} \tag{8}$$

where R is the Reynolds number based on airfoil chord. If the Strouhal number $f\delta/U$ is assumed constant when referenced to the laminar boundary layer thickness at the trailing edge,

$$f = K_1 U \delta^{-1} = K_1 U^{3/2} c^{-1/2} \nu^{-1/2} \tag{9}$$

where K_1 would be 1/60 if the Strouhal number were equal to 0.2 referenced to twice that thickness. The tone frequency therefore is predicted to vary with velocity to the 3/2 power and to be inversely proportional to the square root of airfoil chord.

The rate at which vorticity is convected within an attached boundary layer was shown in Vol. I, Section 22 of Ref. 8 to be $(1/2)U^2$. It has been found for bluff bodies that approximately half of the vorticity (Ref. 8, Vol. II, Section 244) is transported into the individual eddies that comprise the vortex street and the remainder cancels itself or breaks down into turbulence. This rate at which vorticity is transformed into vortex-street circulation, multiplied by the period of the fluctuation, must equal the circulation of each vortex.

$$\Gamma = \left(\frac{\partial \Gamma}{\partial t}\right)\left(\frac{1}{f}\right) = \frac{K_2 U^2}{f} \tag{10}$$

The fluctuation of airfoil lift force would be proportional to the circulation and also to the product of airfoil chord and the chordwise-average surface pressure fluctuation. Therefore,

$$L \propto \Delta p_{rms} = K_3 \rho U \Gamma \tag{11}$$

Combining Eqs. (9), (10), and (11),

$$\Delta p_{rms} = 2 K_2 K_3 \left(\tfrac{1}{2}\rho U^2\right)\left(fc/U\right)^{-1} \tag{12}$$

or, in terms of Reynolds number,

$$\Delta p_{rms} = \left(2 K_2 K_3 / K_1\right)\left(\tfrac{1}{2}\rho U^2\right) R^{-1/2} \tag{13}$$

The product of the two constants K_2 and K_3 can then be evaluated experimentally from measured surface pressure fluctuations and tone frequency. From Eq. (13), the ratio of average surface pressure fluctuation to free-stream dynamic pressure is expected to vary inversely with the square root of Reynolds number. In contrast, the surface pressure fluctuations caused by velocity fluctuations within a turbulent boundary layer, divided by dynamic pressure, are approximately constant (Ref. 1). The root mean square pressure fluctuation at the surface is predicted to vary with velocity to the 1.5 power, while the method of Ref. 1 predicts a variation with velocity to the 1.8 power. A variation with velocity squared would be expected for a bluff-body dipole process.

This prediction of surface pressure fluctuation from Eq. (12) can then be combined with Eq. (7) to determine the functional dependence of the far-field acoustic pressure fluctuation above a two-dimensional airfoil.

$$\overline{p^2} = \left[\left(2 K_2 K_3 / K_1\right)\left(\tfrac{1}{2}\rho U^2\right)\left(U/a\right)^{-5/2}\right]^2 \left(\frac{\pi}{2}\frac{b}{2}\right) \tag{14}$$

Thus the far-field mean square of the acoustic pressure is predicted to vary with velocity to the sixth power multiplied by the as yet unknown velocity dependence of the correlation area.

In summary, the numerical constants for predicting the tone frequency and the surface pressure fluctuation can be determined from narrow-band surface pressure measurements. These can then be used for predicting surface spectra for other airfoils. Ratios of correlation area to planform area can be determined from the measured surface and far-field pressure coefficients. These ratios, whose values are difficult to anticipate for a deterministic process, should be approximately equal to those determined by the lengthier technique of cross-correlating the surface microphones. If the experimentally evaluated ratios can be generalized in terms of the ratio of near-wake laminar boundary layer thickness to airfoil chord, the far-field sound pressure level generated by an arbitrary airfoil could then be predicted. The oversimplified analysis would be verified if the assumed constants as determined from the data actually prove to be approximately independent of the experimental variables. A simple method for

predicting surface and far-field spectra of arbitrary airfoils and three-dimensional rotating blades would then exist.

DISCUSSION OF EXPERIMENTAL RESULTS

General Regimes of Noise Generation

One major result of this investigation was the finding that airfoil vortex noise reaches a maximum intensity and then decreases with increasing velocity. As judged from acoustic spectra measured in the far field at different velocities and angle of attack, three different regimes of noise behavior occurred. Approximate boundaries of these regimes are shown in Fig. 5 for the full-span NACA 0012 airfoil. At sufficiently low velocities and moderate angles of attack, the far-field acoustic spectra were dominated by a strong discrete tone. Vortex tone noise also was reported in Ref. 4 for small airfoil models at Reynolds numbers up to 0.75×10^6. Broadband vortex noise with an intensity and center frequency predicted by the method of Ref. 1 was not observed.

At sufficiently large velocities and all but large angles of attack, the airfoil did not raise the far-field noise spectrum above its background level. For this region, designated in Fig. 5 as "no tone", airfoil vortex noise appears to have decreased below that produced by the pressure fluctuations within the airfoil turbulent boundary layer. In the intermediate regime, the intensity of the vortex tone noise decreased with increasing velocity at constant incidence.

The boundary between the regime of increasing tone strength and that for tone decay resembles another type of aerodynamic boundary. Judging from the data shown in Fig. 8 of Ref. 9, this curve also gives the minimum angle of attack for which the pressure-surface boundary layer on an NACA 0012 airfoil remains laminar over the entire blade chord. Agreement between these aerodynamic and acoustic boundaries tends to confirm the physical mechanism described earlier for vortex tone noise. Decay of tone intensity with increasing velocity could then be associated with a rapid decrease in the chordwise extent of laminar flow.

The measured range of these three regions was not symmetrical about zero angle of attack for this nominally symmetrical NACA 0012 airfoil model. Tones were observed for a considerably smaller range of Reynolds number when the model was tested at negative angles of attack. The model contained a slider that produced surface discontinuities at approximately 28 and 32 percent chord across the model span on one surface. At negative angles of attack relative to the wind tunnel, these discontinuities caused premature transition of the pressure-surface boundary layer. The model then was inverted in the wind tunnel so that the slider was on the suction surface at negative angles of attack. For those tests, the boundaries shown in Fig. 5 for positive angles of attack were approximately reproduced at negative angles of attack. This result helps to demonstrate that the measured vortex tone noise was caused by the airfoil itself rather than by some unusual interaction between the airfoil, the wind tunnel, and the anechoic chamber.

The semispan NACA 0012 airfoil model had a smaller regime in which the tone increased with increasing velocity. The boundaries between the three regimes resembled those shown in Fig. 5 but were located at Reynolds numbers roughly 0.5×10^6 smaller at constant angle of attack. The presence of the wing tip vortex may cause earlier transition of the boundary layer. Only a small fraction of this model's span would have been unaffected by either the tip vortex or the sidewall turbulent boundary layer.

High Reynolds Number

The test conditions that had seemed of greatest applicability to noise generation by helicopter rotor blades were those corresponding to outboard portions of full-scale blades. A convenient reference condition for calculation of rotor performance has been the 75 percent radius location. For typical light observation helicopters, the corresponding Reynolds numbers are near 2×10^6 and the relative Mach numbers near 0.40. Therefore, tests were conducted at a velocity of 450 fps which produced a Reynolds number of about 2.0×10^6 and a Mach number of 0.41. At these conditions and small angles of attack, neither the full-span nor the semispan NACA 0012 model produced far-field noise greater than the tunnel background noise. They did produce measurable high-frequency broadband noise in the far field at large angles of attack. For the full-span model, this increased noise was observed at 8-deg angle of attack which is well below the 11-deg angle of attack expected for stall at this Mach number and Reynolds number.

Surface pressure spectra at different chordwise locations on the suction surface of the full-span model are shown in Fig. 6 for 0 and 8 deg angles of attack at 450 fps velocity. The spectra were essentially identical up to 1030 Hz. A broad peak, not shown in Fig. 6, was produced by tunnel edge tones between 200 and 400 Hz. The surface pressure spectra shown in Fig. 6 have the general appearance expected for static pressure fluctuations associated with the velocity fluctuations of a turbulent boundary layer. This is most noticeable in the spectra measured at 50 and 70 percent chord. Center frequencies of the measured broad peaks decreased with increasing streamwise distance (increasing boundary layer thickness), but the maximum amplitudes were approximately constant. Spectra measured further forward on the airfoil would be expected to have their peaks at frequencies larger than the 20,000 Hz limit of the one-third-octave recorder.

The overall sound pressure level of the high-frequency portions of the spectra for zero angle of attack at 50 and 70 percent chord corresponded to a root mean square pressure fluctuation about 0.005 times the free-stream dynamic pressure. As can be shown from Refs. 1, 3, 10, and 11, this value is close to but slightly below that expected for turbulent boundary layers in mild pressure gradients. The measurements have not been corrected for the effect of a nonzero microphone diameter relative to the expected correlation length of turbulent eddies in the boundary layer. This effect would probably raise the measurements to the expected level. As would be expected from Ref. 11, the chordwise correlation between prefiltered signals from the two closest surface microphones (30 and 38 percent chord) was small. A 1000-Hz high-pass filter was utilized to remove the highly correlated signals at the tunnel fan and edge tone frequencies. Increasing the angle of attack increased the pressure fluctuations on the airfoil suction surface (Fig. 6). This result would be expected because of the increasing adverse pressure gradient. Surface pressure spectra measured on the semispan model at small angles of attack were essentially identical to those for the full-span model. Their amplitude increased less rapidly with increasing geometric angle of attack, probably because the effective angle of attack at the instrumented spanwise position would be about half the geometric angle of attack. Apparently the

acoustic radiation from airfoils with extensive turbulent boundary layers on both surfaces is approximately that caused by velocity fluctuations within the turbulent boundary layer. This radiation can be calculated by the method of Ref. 10. Its far-field intensity is small, not because the surface pressure fluctuations are small but because the correlation lengths are of the order of the boundary layer thickness, which is very small relative to the airfoil chord and span. This result that the surface pressure fluctuation spectra for an airfoil at full-scale Reynolds numbers are those for a turbulent boundary layer and therefore produce very small far-field acoustic radiation was also determined in the sailplane flight tests reported in Ref. 12.

Low Reynolds Numbers

One-third-octave spectra taken in the far field generally contained one band that was much stronger than the background along with the first harmonic of that band at 10 to 15 dB smaller amplitude. When analyzed at 10 Hz bandwidth, the apparent fundamental tone usually appeared as one strong sharp tone and one or more weak nonharmonic tones at nearby frequencies. The amount by which the weak tone protruded above the broadband noise usually was at least 5 dB below that of the strong tone. Typical 10 Hz spectra are shown in Fig. 7 for the full-span NACA 0012 airfoil over a small range of velocity of 6 deg angle of attack. The measured variation of far-field tone frequency with velocity for the full-span NACA 0012 airfoil at 6 deg angle of attack is shown in Fig. 8. For small changes of velocity, the frequency of the strong tone and usually those of the very weak tones shown in the upper portion of Fig. 7 varied approximately with velocity to the 0.8 power. With sufficient increase of velocity, one of the very weak tones at a larger frequency than the strongest tone became considerably stronger than the others. As is shown in Figs. 7 and 8, this tone then became dominant, and the formerly strongest tone became weaker. The resulting sequence of points, with quantum jumps of frequency in narrow ranges of velocity, qualitatively resembles the behavior of edge tones. However, there was no hysteresis of frequency with velocity for these tones. The same relative strength of tones was found whether a test condition was approached by increasing or decreasing the velocity. Because of these jumps of frequency, the general trend, as shown in Fig. 8, was that of a variation with velocity to the 3/2 power. The numerical values of frequency at each velocity are predicted reasonably well by use of Eq. (9) with K_1 arbitrarily taken equal to 1/90, as would occur if the trailing-edge boundary layer was 50 percent thicker than that for a flat plate. These frequencies are in order of magnitude larger than those calculated for a Strouhal number of 0.2 referenced to the airfoil maximum thickness (Fig. 8).

The jumps of frequency seemed to occur when an integer number of acoustic wavelengths was approximately equal to the chord. Below about 130 fps, the wavelength was greater than the airfoil chord. Data for this model at other angles of attack had roughly the same behavior. Tests of these closely spaced velocities were not conducted with the semispan NACA 0012 airfoil model, but its narrow-band tone frequencies generally matched those for the full-span model.

At the time this written paper was prepared, only limited surface pressure data had been obtained. A typical comparison of one-third-octave spectra in the far field and on the suction and pressure surfaces of the semispan model is given in Fig. 9. On the pressure surface, where the boundary layer was laminar despite the presence of the slider as a surface discontinuity, the one-third-octave bands that contained the tone and its first harmonic were prominent. On the suction surface, the tone band was only a weak disturbance as compared with the broadband level of the transitional boundary layer at 30 and 50 percent chord. At 15 percent chord, upstream of the slider, the spectrum resembled that for the pressure surface. Sound pressure levels at the tone frequency, as determined from narrow-band spectra or these one-third-octave spectra, were approximately equal on both surfaces. They were approximately independent of chordwise position from 15 to 50 percent chord and generally were largest at 70 percent chord. In contrast, loadings caused by fluctuations of incidence angle would have caused the sound pressure level at 15 percent chord to be about 8.5 dB stronger than that for 50 percent chord. Surface pressure fluctuations at velocities near 100 fps were about half as large for the semispan as for the full-span NACA 0012 airfoil. If the far-field tone was strong, these levels were roughly independent of angle of attack. The effect of velocity on surface pressure fluctuations at the strong tone frequency for the full-span NACA 0012 airfoil is shown in Fig. 10. The general level of these data is given by Eq. (12) with K_2 and K_3 taken equal to 0.02 and K_1 taken as 1/90. It is possible that improved agreement could be obtained at higher velocities if either K_2 or K_3 were not actually constant but varied with Reynolds number.

Cross-correlations at these low velocities led to the interesting result that the disturbance on the airfoil appears to be propagating from the trailing edge toward the leading edge. A sample plot of the cross-correlation and auto-correlations of the 30 and 70 percent chord microphones is shown in Fig. 11. The cross-correlation function and the two auto-correlations are seen to vary nearly sinusoidally with the delay time because of the discrete, deterministic character of the tone. The normalized cross-correlation coefficient for this particular case had a magnitude of 0.4 showing that there is significant correlation between the 30 and 70 percent microphone pressure measurements.

The indication that a wave was moving from the trailing edge toward the leading edge becomes evident on examining the phase of the cross-correlation. It is observed that its first peak occurred at a time delay of about 0.07 milliseconds. The distance between the centers of the two microphones was 3.6 in. so that the predicted value of time delay based on the assumption of a sound wave moving toward the leading edge and a sound speed of 1130 fps is 0.3 milliseconds. The cross-correlation between the 30 and 50 percent chord microphones, not shown, had a measured time delay of 0.10 milliseconds compared to a calculated value of 0.14 milliseconds. Similar agreement between measured and calculated values of time delay was obtained from cross-correlations between the other microphones on the airfoil surface.

The time delay between arrival of a signal at an aft microphone and at the slider microphone varied with spanwise position of the slider. The corresponding spanwise correlation lengths have not yet been determined. Correlation areas also can be formally computed from the measured narrow-band frequencies and the surface and far-field sound pressure levels by use of Eq. (12). When this was done, the calculated correlation areas were a significant fraction of the planform area. It is possible that the pressure fluctuations actually are not relatively constant along the chord but are highly peaked near the uninstrumented trailing edge. If this were the case,

the correlation areas determined in this manner for those larger surface pressure areas would be much smaller. Tests with NACA 0018 full-span airfoil model (Fig. 4), which has surface microphones from 5 to 80 percent chord, should be useful in determining the actual chordwise variation of fluctuating loading. They may also provide a better indication of whether the concept of correlation area is meaningful for this apparently deterministic acoustic process.

COMPARISON WITH OTHER DATA

Hot-wire investigations of the vortex shedding frequency of flat plates at low Reynolds numbers were reported in Ref. 13. For thin plates relative to the boundary layer, the Strouhal number referenced to the effective displacement thickness of the near wake was constant. The Strouhal number for an NACA 0012 airfoil at zero angle of attack, referenced to the airfoil maximum thickness, also is given in Fig. 1 of Ref. 13. This quantity was found to be proportional to the square root of Reynolds number, as is predicted by use of Eq. (6) herein. The frequencies reported for those hot-wire data measured on the wake centerline should be twice the acoustic frequency. As expected, those frequencies were closely predicted by Eq. (9) with a numerical constant K_1 taken equal to twice the value of 1/90 used in calculating the solid line shown in Fig. 8.

Far-field acoustic spectra were given in Ref. 14 for an uncambered and a cambered NACA 65 series airfoil of 10 percent thickness ratio and 2-in. chord. Frequencies at which the peak intensities occurred were plotted in Figs. 14 and 15 of Ref. 14 for velocities from 200 to 500 fps (Reynolds numbers from roughly 0.2×10^6 to 0.5×10^6) and several angles of attack. These values are compared in Fig. 12 herein with the frequencies calculated from Eq. (9) with K_1 taken equal to 1/90. The predicted variation with velocity to the 3/2 power is in good agreement with the data. It is more easily justified than the linear variations taken from Ref. 14 and shown as solid lines in Fig. 12, which would pass through zero frequency at about 100 fps velocity.

Far-field acoustic spectra and overall sound pressure levels for high aspect ratio wings of larger chord and span are given in Ref. 15. These data were obtained from low-altitude flyby's of several sailplanes. A one-third-octave spectrum for the Libelle sailplane, taken from Fig. 66 of Ref. 15, is reproduced in Fig. 13. The spectrum contains a broad tone centered in the 1000 Hz band caused by the sailplane wing and a tone in the 5000 Hz band described as background noise caused by crickets. It should be noted that the presence of a wing-generated tone at these large Reynolds numbers (up to 3×10^6) is attributed to the airfoil sections used on the sailplanes. They are of types that achieve low drag at their design conditions by maintaining a long chordwise extent of laminar flow on the pressure surface. Tone frequencies calculated for the root and tip chords of this tapered wing planform also were shown in this figure. The observed dominant frequency is about half a one-third-octave band higher than that calculated for the wing tip chord. In contrast, the frequency that corresponds to a Strouhal number of 0.2 referenced to wing maximum thickness is below 100 Hz, an order of magnitude smaller. By use of Eq. (9), the observed frequency of 1000 Hz for 104 fps velocity and 75 in. mean chord would scale to roughly 9000 Hz for 195 fps velocity and 2 in. chord. This scaled frequency is in good agreement with the data of Ref. 14 for airfoils with 2 in. chord as shown in Fig. 12 herein. Thus the predicted variation of frequency with the inverse square root of chord is verified for an order of magnitude change in chord.

DESCRIPTION OF REMAINING EFFORT

During the remainder of this investigation, we plan to (1) conduct additional measurements of surface pressure spectra and cross-correlations for the full-span NACA 0012 airfoil to determine the acoustic phenomena at wavelengths less than the chord length, (2) conduct limited tests with the full-span NACA 0018 airfoil to determine the qualitative effect of airfoil thickness ratio and obtain surface pressure data over a larger percentage of the chord, and (3) compare sound pressure levels calculated by any prediction method developed from these tests with data for small-scale (Ref. 14) and full-scale (Ref. 15) configurations.

REFERENCES

1. Sharland, I. J.: Sources of Noise in Axial Flow Fans. Journal of Sound and Vibration, Vol. I, No. 3, 1964, pp. 302-322.
2. Murphy, J. S., D. A. Bies, W. W. Speaker, and P. A. Franken: Wind Tunnel Investigations of Turbulent Boundary Layer Noise as Related to Design Criteria for High Performance Vehicles. NASA TN D-2247, April 1964.
3. Lamb, Sir H.: "Hydrodynamics". Cambridge Press, 1932, 6th ed., paragraph 290.
4. Curle, N.: The Influence of Solid Boundaries Upon Aerodynamic Sound. Proc. Royal Society, Series A, No. 231, 1955, pp. 505-514.
5. Ffowcs Williams, J. E. and D. L. Hawkings: Sound Generation by Turbulence and Surface in Arbitrary Motion. Phil. Trans. Royal Society, Series A, No. 264, 1969, pp. 321-342.
6. Krzywoblocki, M. Z.: Investigation of the Wing-Wake Frequency with Application of the Strouhal Number. Journal of the Aeronautical Sciences, Vol. 12, No. 1, January 1945, pp. 51-62.
7. von Karman, T. and W. R. Sears: Airfoil Theory for Non-Uniform Motion. Journal of the Aerospace Sciences, Vol. 5, No. 10, August 1938, pp. 379-390.
8. Goldstein, S.: Modern Developments in Fluid Dynamics. Vols. I and II, Clarendon Press, Oxford, 1938.
9. McCroskey, W. J.: Measurements of Boundary Layer Transition, Separation and Streamline Direction on Rotating Blades. NASA TN D-6321, April 1971.
10. Magridge, B. D.: Acoustic Radiation from Aerofoils with Turbulent Boundary Layers. Journal of Sound and Vibration, Vol. 16, No. 4, June 1971, pp. 593-614.
11. Bull, M. K.: Properties of the Fluctuating Wall-Pressure Field of a Turbulent Boundary Layer. AGARD Report 455, April 1963.
12. Mofgson, T. H.: On the Dipole Radiation from a Rigid, Plane Surface. Paper presented at the Noise Control Conference, Purdue University, Lafayette, Indiana, July 14-16, 1971.
13. Bauer, A. B.: Vortex Shedding from Thin Flat Plates Parallel to the Free Stream. Journal of the Aerospace Sciences, Vol. 28, No. 4, April 1961, pp. 340-341.
14. Clark, L. T.: The Radiation of Sound from an Airfoil Immersed in a Laminar Flow. ASME Paper No. 71-GT-4, ASME 6th Annual Gas Turbine Conference and Products Show, Houston Texas, March 1971. (Also, to be published in Transactions of the ASME,

Journal of Engineering for Power.)

15. Smith, D. L., R. P. Paxson, R. D. Talmadge, and E. R. Hotzo: Measurements of the Radiated Noise from Sailplanes. U. S. Air Force Flight Dynamics Laboratory Report TM-70-3-FDAA, July 1970.

LIST OF SYMBOLS

a	Speed of sound, ft/sec
b	Span, ft
c	Chord, ft
f	Frequency, Hz
K_1, K_2, K_3	Empirical constants
P	Acoustic pressure in far field above airfoil, lb/ft^2
Q	Pressure jump across airfoil surface, lb/ft^2
r	Distance above airfoil in far field, ft
$\underline{r}_0, \underline{r}_1$	Position on airfoil surface A, ft
R	Reynolds number, equal to Uc/ν
S_c	Correlation area, ft^2
S_{pp}	Power spectral density of far-field pressure fluctuation, $lb^2/ft^4 sec$
S_{QQ}	Power spectral density of surface loading fluctuation, $lb^2/ft^4 sec$
$S_{Q_0 Q_1}$	Cross power spectral density of loading fluctuations at two points on the airfoil surface, $lb^2/ft^4 sec$
t	Time, sec
U	Free stream velocity, ft/sec
x,y,z	Cartesian coordinates in the streamwise, spanwise, and normal directions, ft
Γ'	Circulation of an individual vortex, ft^2/sec
δ	Boundary layer thickness of trailing edge, ft
Δp_{RMS}	Root mean square pressure fluctuation on airfoil surface, lb/ft^2
ν	Kinematic viscosity, ft^2/sec
ρ	Density, $slugs/ft^3$
ω	Frequency, rad/sec

Subscripts

0,1	Coordinate on airfoil surface
—	Vector quantity

Superscripts

—	Mean value
*	Complex conjugate

ACOUSTIC RESEARCH TUNNEL FIG. 1

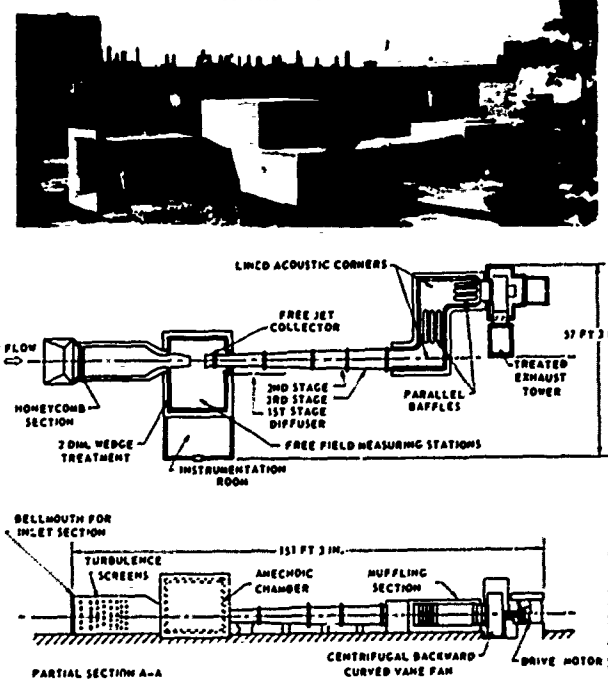

ACOUSTIC TUNNEL TEST SECTION FIG. 2

ALL DIMENSION IN INCHES

TOP VIEW WITH NACA 0012 FULL SPAN AIRFOIL INSTALLED

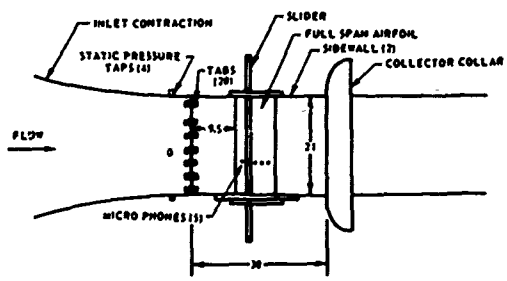

SIDE VIEW

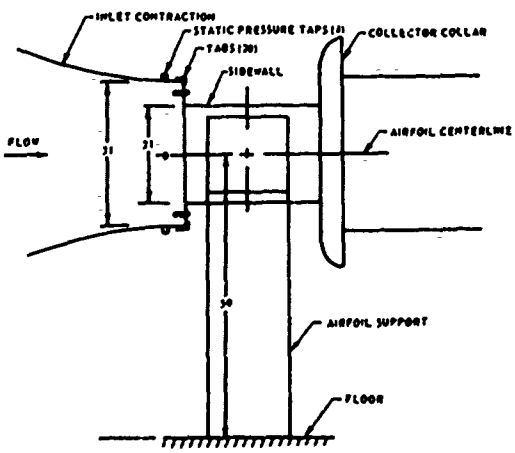

FIG. 3

NACA 0012 AIRFOIL MODELS

ONE-QUARTER SCALE, ALL DIMENSIONS IN INCHES

MICROPHONE LOCATIONS AT 15, 20, 30, 50, AND 70% CHORD

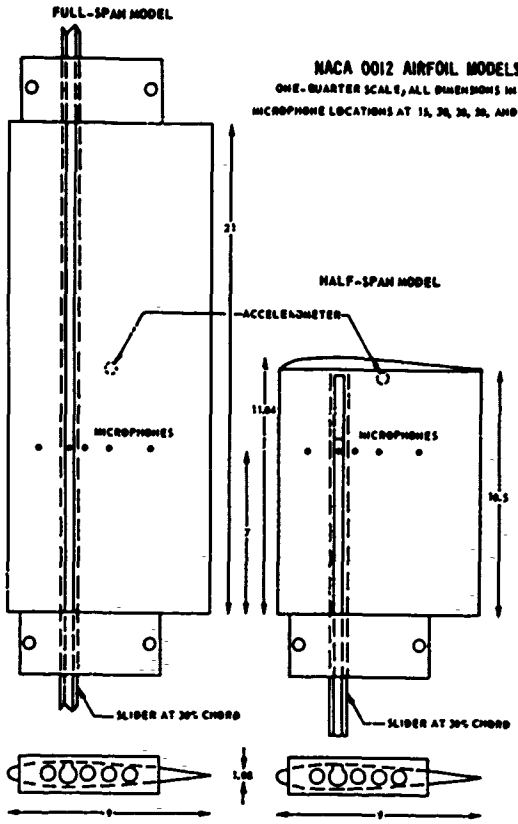

FIG. 4

NACA 0018 FULL-SPAN AIRFOIL MODEL

ONE-QUARTER SCALE, ALL DIMENSIONS IN INCHES

MICROPHONE LOCATIONS AT 5, 15, 3[illegible],

30, 50, 62, 70, AND 80% CHORD

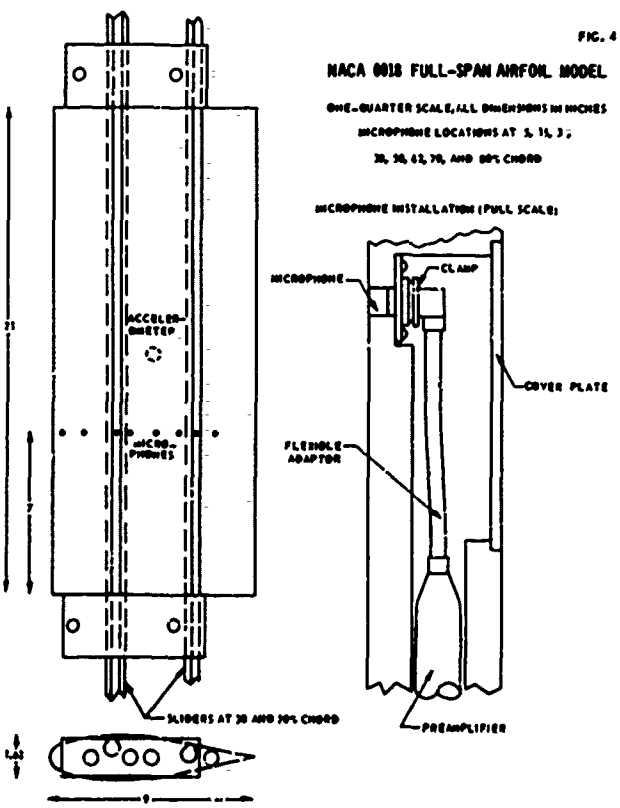

FIG. 5

REGIMES IN WHICH DISCRETE TONE VORTEX NOISE OCCURS

FULL-SPAN NACA 0012 AIRFOIL

SLIDER ON SUCTION SURFACE

SYMBOLS REPRESENT TEST POINTS

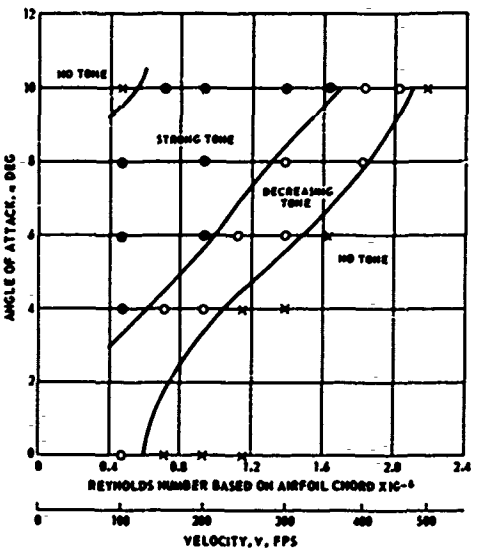

FIG. 6

SURFACE PRESSURE SPECTRA AT REYNOLDS NUMBER = $2X10^6$

NACA 0012 FULL-SPAN AIRFOIL SUCTION SURFACE

VELOCITY = 450 FPS

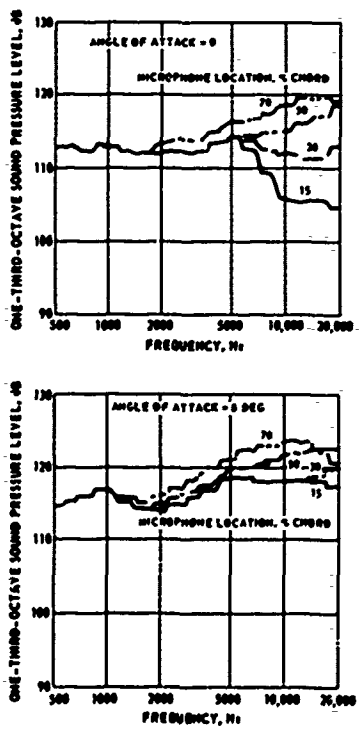

FIG. 7

TYPICAL FAR-FIELD SPECTRA AT 10 Hz. BANDWIDTH

NACA 0012 FULL-SPAN AIRFOIL, 6 DEG ANGLE OF ATTACK

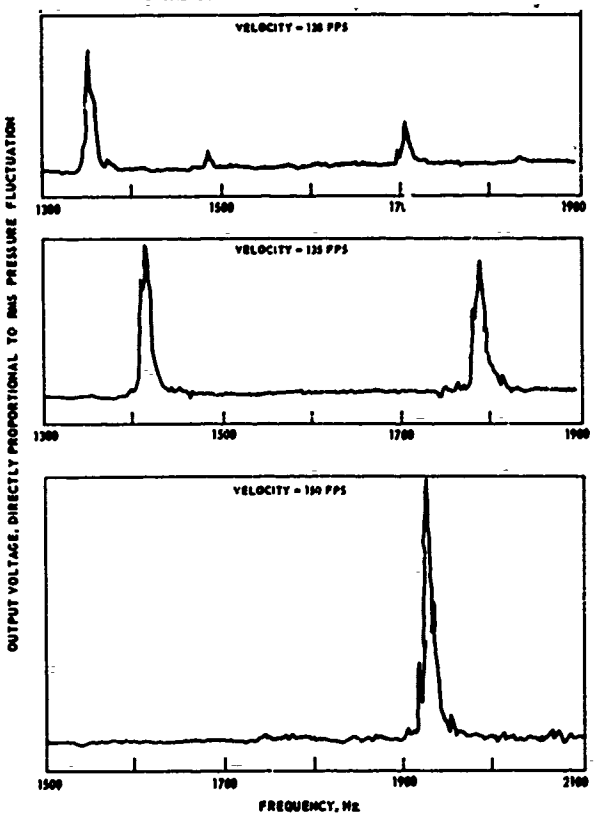

FIG. 8

VARIATION OF FAR-FIELD TONE FREQUENCY WITH VELOCITY

FULL-SPAN NACA 0012 AIRFOIL, 6 DEG ANGLE OF ATTACK

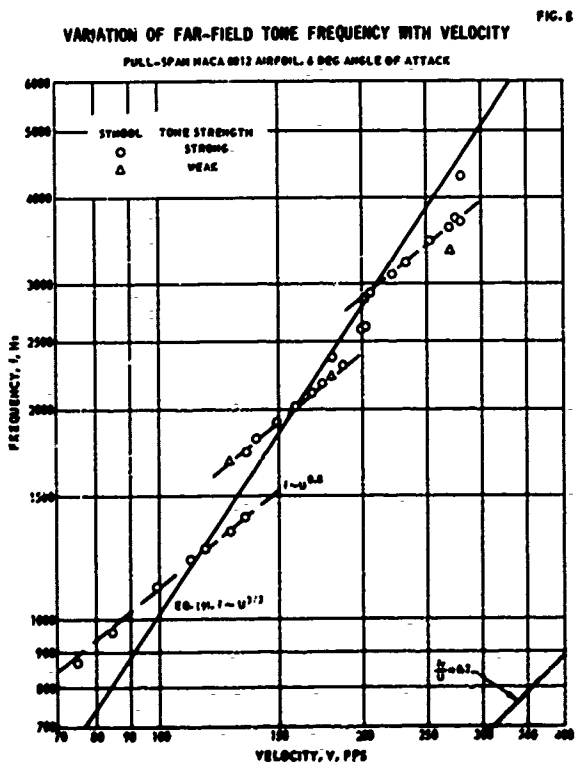

FIG. 10

EFFECT OF VELOCITY ON SURFACE PRESSURE FLUCTUATION

NACA 0012 FULL-SPAN MODEL, 6 DEG ANGLE OF ATTACK

SYMBOLS DENOTE AVERAGE ALONG THE CHORD

BARS DENOTE MEASURED CHORDWISE VARIATION

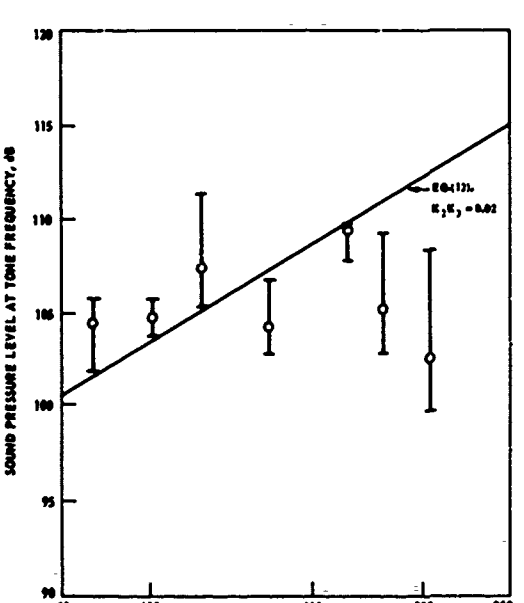

FIG. 9

FAR-FIELD AND SURFACE ONE-THIRD-OCTAVE SPECTRA IN STRONG TONE REGIME

NACA 0012 SEMISPAN MODEL, 100 FPS VELOCITY, 6 DEG ANGLE OF ATTACK

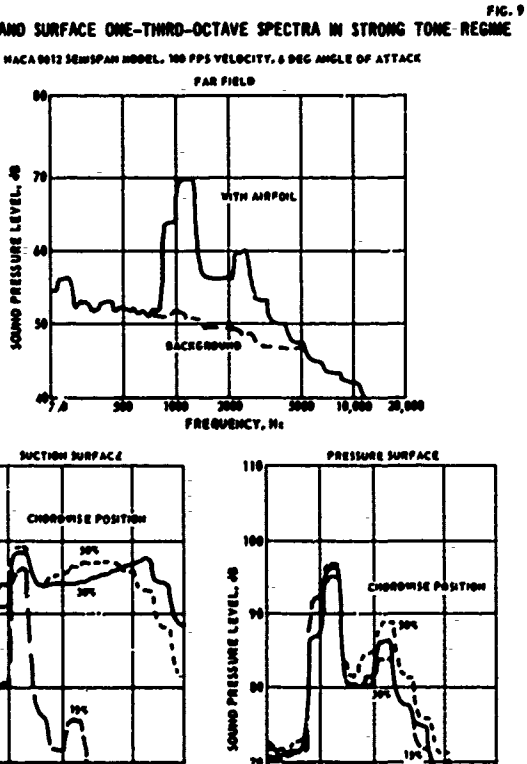

FIG. 11

TYPICAL CROSSCORRELATION AND AUTOCORRELATIONS IN STRONG TONE REGIME

MICROPHONES AT 30% AND 78% CHORD OF NACA 0012 FULL-SPAN MODEL

96 FPS VELOCITY AT 6 DEG ANGLE OF ATTACK

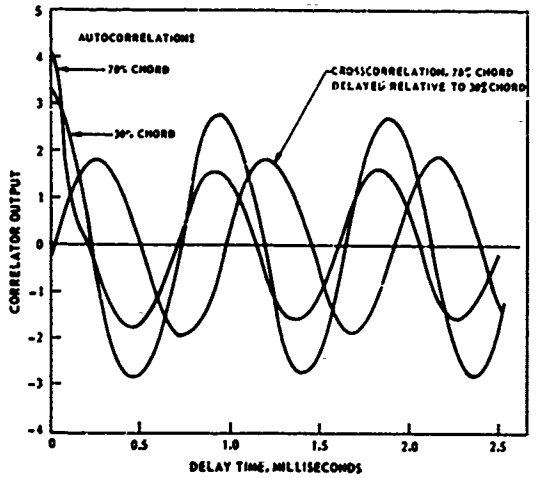

FIG. 12

COMPARISON OF MEASURED AND CALCULATED FREQUENCIES FOR AIRFOILS WITH 2-IN. CHORD

DATA AND SOLID LINE FAIRINGS FROM REF. 14

NACA 65 SERIES UNCAMBERED AIRFOIL

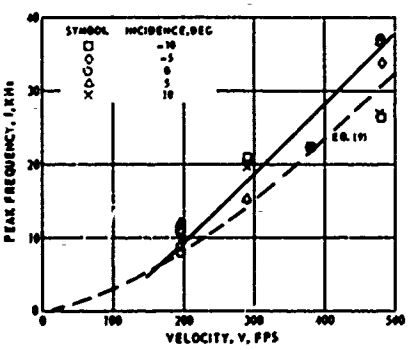

NACA 65 SERIES CAMBERED AIRFOIL

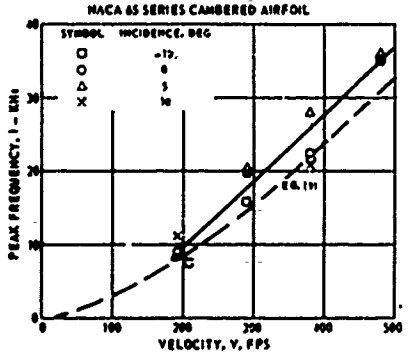

FIG. 13

ONE-THIRD-OCTAVE SPECTRUM OF LIBELLE SAILPLANE FLYBY

90 FT ALTITUDE AT 104 FT/SEC VELOCITY

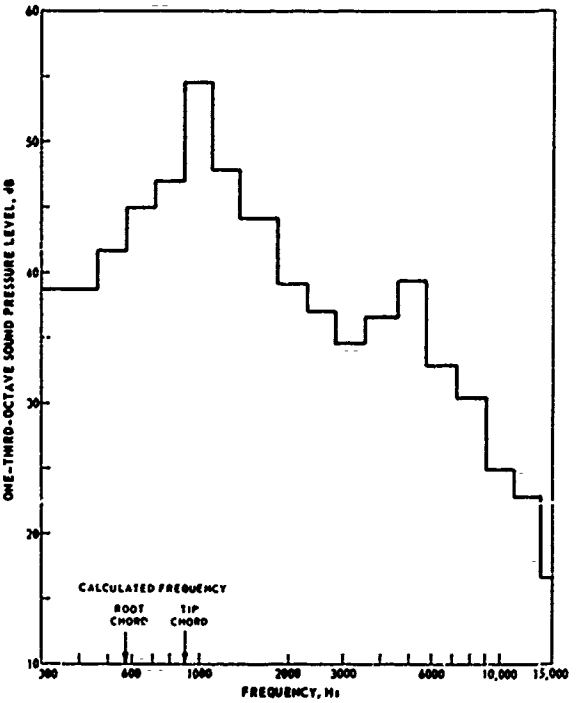

ANALYSIS OF KÁRMÁN-STREET VORTEX SHEDDING USING MEASURED HELICOPTER SOUND PRESSURE DATA*

By

H. Kevin Johnson and Walter M. Katz

ROCHESTER APPLIED SCIENCE ASSOCIATES, INC.
140 Allens Creek Road
Rochester, New York

ABSTRACT

Kármán-street type vortex shedding from a lifting surface was analyzed as a source of noise from a helicopter rotor in hover. The theoretical program that was conducted used acoustic pressure-time histories measured by NASA at the Wallops Island Test Station for a UH-1B helicopter in hover and forward flight.

The experimental pressure-time histories were analyzed and high resolution spectra were developed over a frequency range of 0 to 5000 Hz using a 0.7 Hz filter. On the basis of these spectra the main and tail rotor rotational noise as well as discrete noise sources were identified and then removed from the measured pressure-time histories leaving pressure-time histories representing only the broadband noise radiated from the rotor system. This broadband noise was then related to the noise induced by Kármán-vortex street shedding on the rotor blade.

The theoretical analysis that was developed related the acoustic radiation of the vortex shedding forces on the blade to the pressure-time histories measured by the microphones located in the far field. This analysis was then used to solve for the oscillatory forces on the blade that would duplicate the broadband noise characteristics of measured pressure-time histories of the helicopter in various flight regimes.

The results of the investigation indicated that "vortex noise" is the major source of acoustic radiation from a helicopter rotor in hover or low-speed flight and that it is concentrated in the frequency range of 200 to 500 Hz. Because of the excellent correlation obtained between measured and predicted acoustic signatures using the averaged nondimensional force constants for vortex shedding extracted from the data analysis, it is believed that the basis of a realistic method of predicting the total acoustic signature of any helicopter rotor in various flight regimes has been developed and demonstrated.

INTRODUCTION

The primary contributor to the external sound of modern gas-turbine powered helicopters is the aerodynamically induced noise from the rotor system. Noise measurements have shown that the acoustic pressure time-history at an observer's location is due almost entirely to the noise output of main and tail rotor systems. This means that the helicopter's detectability and to a large extent its effectiveness as a weapons system is determined by the noise signature of its rotor system. In addition, because of the strong emphasis today in noise pollution control there has been interest in rotor noise with regard to commercial helicopter operations. For these reasons, aerodynamically induced sound from rotor systems has been extensively investigated, particularly in the last five years. (See References 1, 2, 3, 4, and 5.)

Rotor noise consists of two basic types of sound signatures: one is repetitive in frequency, the other is broadband or non-repetitive. The repetitive noise is typically called "rotational" noise in which the frequencies are integral multiples of the rotor-blade passage frequency. The broadband or non-repetitive-type noise can be generally classified as "vortex" noise. In addition, there are other helicopter noise classifications such as "blade slap", and sources such as engine and transmission noise. These other noises and sources are not treated explicitly in this report. (See Reference 5 for a discussion of rotor noise sources.)

Rotational noise is typically regarded as a dominant rotor noise source (see Lowson, Reference 5). For this reason it is not surprising that many investigators have concentrated in this area of acoustic research. Results have shown that whereas rotational noise is dominant in all cases for frequencies below 100 Hz, above 100 Hz, rotational noise may dominate but in most cases broadband noise will mask out the rotational noise. It has been found, however, that the noise source that is predominant is dependent upon the location of the noise source relative to the observer.

Since in general broadband noise will be nonperiodic with respect to blade passage frequency, such noise is often classified as nonrotational. The broadband noise that is associated with helicopter rotor blades is usually related to vortex shedding that occurs along the blade. Since vortex-generated noise is believed to occur in the frequency range closer to that of maximum human ear sensitivity, the subjective loudness of such noise can be greater than that of low frequency rotor rotational noise, even though the latter may be of higher absolute magnitude.

Little is known about vortex street shedding from lifting surfaces. Vortex shedding noise from rotating cylindrical bodies was first measured by Stowell and Deming (6). Later Yudin (7) and Blokhintsev (8) developed theories predicting such noise. Hubbard (9) has reported overall noise levels due to all sources on propeller blades, and has given an estimate of noise due to vortex shedding. He found for propellers that the rotational and vortex components can be of the same order of magnitude. He noted that the vortex component has a higher frequency content than the rotational component and increases in intensity with increasing tip speed. Schlegel, et al (3) have made further refinements in Hubbard's vortex noise magnitude formula. Krzywoblocki (10) has measured the vortex shedding frequency for airfoils at low Reynolds numbers; however, the data for angles of attack below stall had wide scatter. Roshko (11) measured the frequency of shedding from circular cylinders in high Reynolds number flow,

*This study was supported by the Eustis Directorate, U. S. Army Air Mobility Research & Development Laboratory, Fort Eustis, Virginia, under Contract DAAJ02-70-C-0023.

but not for airfoil-type sections.

To summarize the experimental work to date, it is noted that measurements have been made of the frequency of vortex shedding, but not within the range of flow conditions encountered by helicopter rotor blades. However, to date no measurements have been made within any range of flow conditions of the magnitude of the oscillating lift and drag forces due to vortex shedding. It is, therefore, necessary that the basic characteristics of vortex shedding from airfoils should be documented in order to develop a better understanding of their effects on rotor noise. Empirical or semi-empirical constants will, therefore, have to be used to investigate the relative importance of vortex shedding on the noise characteristics of helicopter rotors until the time that suitable measurements are obtained.

Sadler and Loewy (2) have determined, by semi-empirical means, overall constants for the lift and drag forces associated with discrete vortex shedding. In this case the constants were assumed to be independent of Mach number, angle of attack, blade radius, and azimuth. It is, however, believed that these force constants are not entirely independent of the aforementioned parameters.

The program reported on herein was set up so that the lift and drag force constants might be developed from experimental data. For the mathematical model the helicopter rotor blade was represented acoustically by a series of dipoles whose strength and frequency varied radially in the case of hover, or both radially and azimuthally in the case of forward flight. If the local angle of attack and Mach number are known at a blade element, then based upon Strouhal number the frequency of vortex shedding could be precalculated. Since there is a known relationship between dipole strength at a given point in space and acoustic pressure at another point, it was possible in this program to use experimental pressure-time histories measured at a fixed observer's location to determine the vortex constants that produced the non-harmonic (broadband) characteristics of the measured signature.

The purpose of the program discussed herein was, therefore, to determine the characteristics of the vortex shedding forces on a helicopter rotor blade in hover and forward flight. A more complete presentation is contained in Reference 12.

ANALYSIS OF EXPERIMENTAL DATA

TEST PROGRAM

The data used in the analysis was generated during controlled acoustic tests of an UH-1B helicopter conducted during November 1969 at Wallops Island, Virginia (13). This data has been discussed by Evans and Nettles (13).

The noise tests were conducted by the Army at the Wallops Island Air Station with cooperation of the Dynamic Loads Division of the NASA/Langley Research Center. The test area consisted of an array of microphones in the form of a cross. This is shown in Figure 1. As shown, the positive X-axis is in the direction of flight and microphones 1, 2, 3 are at X = 200, 500 and 700 feet; microphones 7, 8, and 9 are at X = - 200, - 500, and - 700 feet; microphones 4, 5, 6 are to the right of the flight path at Y = - 200, - 500, - 700 feet; microphones 10, 11, 12 are to the left of the flight path at Y = 200, 500, 700 feet; and microphone 13 is at X = Y = 0. A local coordinate system centered at the main rotor hub moves with the helicopter and is shown in Figure 2. A variety of test conditions were covered during the test program including low, medium and high-speed forward flight and two hover flight conditions (6 feet and 100 feet).

GROUND REFLECTION EFFECT

The importance of ground reflection in the data is revealed by comparing spectra for different microphone-helicopter orientations, see Figures 8 and 3, which represent extended spectra at positions 4 and 6 for the 100 ft hover condition. Observe that the general characteristic of each spectrum in the broadband region reveals a series of maxima and minima separated throughout the record by equal frequency intervals. However, it is seen that this frequency interval is not the same for both recording positions. The frequency interval between successive maxima or minima on the records is seen to change as the orientation between source and observer changes. It should be noted that for a given microphone height above the ground, the microphone receives one signal directly from the sound source and another that is reflected from the ground and then received. It can be shown that the frequency interval referred to between successive peaks or valleys on the SPL records is related to this time separation between original and reflected signal. Thus the frequency spectrum received by an observer is distorted from that of the source, some frequencies will be amplified by reflection while others are suppressed.

The reflected signal time lag at position 6 is less than that of position 4 because the increase in distance travelled by a reflected wave received at position 6 is less than the increase in distance travelled by a reflected wave received at position 4. That is, the increase in distance travelled by a reflected wave at position 6 is 1.48 ft while the increase in distance travelled by a reflected wave at position 4 is 4.65 ft. Therefore, the time lag for a sound wave at position 6 is 1.34×10^{-3} sec (745 Hz) while the time lag for position 4 is 4.22×10^{-3} sec (237 Hz). The maxima or reinforced frequencies would, therefore, correspond to integral multiples of this frequency and the minima or cancelled frequencies correspond to $(n + 1/2)f$. The first minimum frequency at position 6 is 373 Hz and the first and second minima at position 4 is 118 Hz and 350 Hz, respectively (see Figures 8, 3). These frequencies are consistent with the predicted minima (372.5 Hz for position 6 and 118.5 Hz and 355.5 Hz for position 4).

DIGITIZATION

In order to perform computer analysis of the acoustic data the pressure-time history had to be converted into digital form so as to be compatible with computer input format. This process is called digitization. The original FM recordings were digitized using a high-resolution electronic conversion technique specially developed by NASA for carrying out this work. By coupling a mini-computer with special circuitry, a 1.45-second record could be digitized at an 11.3 KHz rate providing approximately 16000 data points. The resulting frequency response of the digitized

data extended from about 0.7 Hz to 5650 Hz, which exceeded the range of the recording system of 20 Hz to 5000 Hz. The signal-to-noise ratio of the developed system was noted to be excellent, at better than 45 db.

To demonstrate the accuracy of this digitization the digitized data was plotted and compared with the corresponding oscillograph records, see Figure 4. The digitized data is seen to be in excellent agreement with the oscillograph trace. In fact, if differences do exist, the electronically digitized results should be considered the more reliable for two reasons. First, the conversion was done directly off the FM carrier of the recorded signal. This technique bypasses the FM demodulator unit, which in itself introduces some distortion to the output. In addition, the electronically digitized data bypasses the frequency response of the oscillograph galvanometers, which were flat to only about 3KC.

EVALUATION OF VORTEX GENERATED NOISE

GENERAL DISCUSSION

Since the shedding of Kármán-type vortices off an airfoil causes variation of lift and drag on the airfoil surfaces, the resulting oscillatory force on the airfoil will create noise. A variety of empirical techniques exist for estimating the magnitude of noise caused by shed vortices from rotating wings. (See References 2, 3 and 9.) The analysis carried out under this program determined the magnitude of these oscillatory forces from the measured pressure-time history of the recorded sound.

The RASA electronically digitized pressure-time histories were separated into broadband and discrete components using spectral analysis techniques. The broadband pressure-time history was then used in a computer program which determined the oscillatory force on the airfoil that created the measured signal. Because of the importance of the value of the Strouhal number used in the calculations and because the Strouhal number has not been accurately measured, particularly for airfoil sections, the fitting technique used to determine the oscillatory forces was also used to determine the "best" Strouhal number.

The data used in this program was only sufficient to determine the contribution of each airfoil section to the pressure-time history. The data was not sufficient to evaluate the relative contribution of both lift and drag. Since it has been estimated that the oscillatory drag forces are very small compared to the oscillatory lift forces as regards the acoustic signal, the contribution from each station was assumed to result only from the oscillatory lift.

THE VORTEX SHEDDING MODEL

The vortex-street phenomenon requires a separated wake caused by the viscous effects in the boundary layer. While airfoil design minimized this separation effect, it did not eliminate it. On a physical basis, the wake formed from a separated boundary layer will be influenced by its width at the separation point and the flow conditions. The Strouhal number correlates the frequency of shedding for various bodies. For cylinders, the Strouhal number changes with Reynolds number and is not known for airfoils or cylinders at large Reynolds number. The Strouhal number is not a universal constant but is dependent on body geometry as well as Reynolds number. The results of References 3, 10, 14, 15 are consistent with a Strouhal number in the range of 0.11 to 0.2 for streamlined bodies. This range is only approximate, but will be used as a guide until tests can determine the existence of Strouhal-type shedding from airfoils and the proper range and dependencies of the Strouhal number on the controlling parameters.

In the present analysis, the Strouhal number for airfoil vortex shedding will be allowed to vary within the range $0.1 \leq S_t \leq 0.3$, which exceeds the limits defined previously. The Strouhal number will be considered constant, however, along the blade for each calculation, that is, the Strouhal number will not be allowed to vary with blade velocity and/or angle of attack. It is anticipated that the Strouhal number is dependent on these parameters, but in lieu of this knowledge, the approach used is believed to be reasonable. Thus, the vortex street shedding frequency is assumed to be:

$$\omega = \frac{S_t U}{d} \qquad (1)$$

where ω = vortex shedding frequency (Hz)

U = resultant velocity (ft/sec)

d = projected dimension of the body perpendicular to the resultant velocity (ft)

and S_t = Strouhal number: $0.1 \leq S_t \leq 0.3$

Effects of vortex shedding on the two-dimensional lift and drag forces acting on the airfoil can be investigated by considering the circulation around the appropriate airfoil section. Assuming regular shedding of vortices of alternating sign, an oscillatory circulation may be considered to be superimposed upon the steady circulation. The corresponding lift and drag forces acting on the airfoil section will then oscillate about a mean value of lift and drag. The oscillatory lift and drag due to vortex shedding can, therefore, be formulated as

$$(L_v)_{ij}(t) = (K_{Lv})_{ij}\left\{\left[1/2\rho U_{ij}^2\right]C_i \Delta r_i\right\} \sin(\omega_{ij}t + \varphi_{ij})$$
$$(D_v)_{ij}(t) = (K_{Dv})_{ij}\left\{\left[1/2\rho U_{ij}^2\right]C_i \Delta r_i\right\} \sin(\omega_{ij}t + \varphi_{ij}) \qquad (2)$$

where $(K_{Lv})_{ij}$ = nondimensional force constant associated with oscillatory lift

$(K_{Dv})_{ij}$ = nondimensional force constant associated with oscillatory drag

ρ = density of air

U_{ij} = relative velocity of the airfoil

C_i = chordlength

Δr_i = station width

ω_{ij} = frequency of vortex shedding

φ_{ij} = phase of the vortex forces

The noise source treated are those generated aerodynamically from helicopter rotors. It is assumed that helicopter rotor noise is produced by variable forces on the rotor blades, not fluid mass displacement by the blades nor flow turbulence. It is, therefore, reasonable to use dipoles to represent these blade forces (see References 5 and 16). The pressure received at an

observer's location from an array of moving dipoles can be cast in the following form (see Reference 5):

$$P(\vec{X}_0,t) = \sum_{i,j}\left[\frac{1}{4\pi c R_{ij}^2\left(1-M_{R_{ij}}\right)^2}\left\{\dot{\vec{F}}_{ij}\cdot\vec{U}_{ij} - (\vec{X}_0 - \vec{X}_{ij})\cdot\left(\dot{\vec{F}}_{ij} + \frac{\vec{F}_{ij}}{\left(1-M_{R_{ij}}\right)}\left(\dot{M}_{R_{ij}} + \frac{c}{R_{ij}}\left(1 - M_{ij}^2\right)\right)\right)\right\}\right]_{t'} \tag{3}$$

where $[\ ]_{t'}$ = evaluation of those quantities inside the brackets are at a "retarded time" t' corresponding to a real time t

c = speed of sound

$\vec{X}_0$ = location of the observer

$R_{ij} = \left[(\vec{X}_0 - \vec{X}_{ij})\cdot(\vec{X}_0 - \vec{X}_{ij})\right]^{1/2}$

$M_{R_{ij}} = \dfrac{(\vec{X}_0-\vec{X}_{ij})\cdot\vec{M}_{ij}}{R_{ij}}$

$\dot{M}_{R_{ij}} = \dfrac{(\vec{X}_0-\vec{X}_{ij})\cdot\dot{\vec{M}}_{ij}}{R_{ij}}$

$\dot{\vec{M}}_{ij} = \dfrac{\dot{\vec{V}}_{ij}}{c}$

$\dot{\vec{F}}_{ij}$ = force on the blade at blade element

With terms comprising Equation (3) formulated, the pressure at an observer's location may be specified once the appropriate sources have been located in retarded time. The acoustic signature of the rotor is assumed to emanate from a series of dipoles located at blade stations. The sound reaching a microphone at some instant in time, t, originates from each of these stations at some earlier time, t'. The time that the sound originated from each station (retarded time) is a function of the position of each station and its motion and is in general different for each station. A retarded time calculation procedure has been programmed for computer use. The program developed locates for an observer's location at time t, the contributing retarded time position of each radial blade station. The results of a typical retarded time calculation is shown in graphical form in Figure 5. As can be seen, the rotor disk has been broken up into 40 azimuthal sections and 10 radial sections and that the azimuthal spacing in retarded time is not equal as it would be in true time. The difference in the spacing between the advancing blade (observer on the negative y-axis) and the retreating blade is very obvious in this graphical presentation.

HOVER ANALYSIS

For this analysis, the UH-1B helicopter was in the hover configuration 100 ft over the microphone data cross with helicopter orientation along the flight path. The data received was recorded at microphone 4 which was 200 ft to the right of the flight path.

DETERMINATION OF ANGLES OF ATTACK, RESULTANT VELOCITIES, SHEDDING FREQUENCIES

The Strouhal shedding frequency of the UH-1B airfoil (NACA 0012) was assumed to be proportional to the flow velocity and inversely proportioned to the separation thickness of the flow. This flow separation has been assumed to be equal to the projected dimension, d, of the airfoil perpendicular to the resultant velocity U. The dependence of the projected dimension as function of angle of attack for the NACA 0012 blade is shown in Figure 6.

NUMERICAL TECHNIQUE

Measured pressures can now be related to the oscillatory force constants. The objective is to solve for the unknown oscillatory force constants in terms of the measured pressure-time history. For the hover configuration, the values of the oscillatory forces are assumed constant about the rotor disk, since angle of attack and velocity are similarly assumed to be constant. The geometric parameters, however, change considerably with respect to an observer so it is desirable to segment the time for each blade passage into smaller time intervals. If the time intervals are small enough, the geometric parameters are essentially constant during the interval.

If the geometric parameters can be assumed constant in a small interval of time then the predictive equations can be linearized. When possible such a linearization of a set of equations greatly reduces the numerical difficulties of their solution. The time interval chosen constrains the frequency range and number of oscillatory stations much in the same way that length of record is related to bandwidth. The largest time interval that was felt consistent with constant geometric parameters was 1/200 sec. For example, if the time for one blade passage is divided into 20 equal time intervals (the blade passage frequency is 10.8 Hz), each time interval is approximately 1/200 sec. Thus, phenomena which change with frequency less than 200 Hz cannot be considered. This cutoff is a judicious compromise between frequency range and blade element station size. That is, if a smaller time interval were chosen, the area swept by the blade (the station size) would be smaller but the lower frequency cutoff would increase. Conversely, if a larger time interval were chosen the lower frequency cutoff would decrease, but the area swept by the blade would increase tending to invalidate this discrete element analysis.

The time intervals when one blade advances toward the observer while the other blade retreats is particularly advantageous.

The Strouhal frequency formulation is such that the shedding frequency increases with radius. Because of the Doppler effect the observed frequencies are increased further on the advancing blade while decreased on the retreating blade. This is coupled to the Mach number effect in Equation (3) which increases the pressure amplitude of the advancing blade stations through the terms $1/1-M_R$ and decreases the pressure amplitude of the retreating blade stations (M_R is negative for a retreating blade, positive for an advancing blade).

The larger frequency spread on the advancing blade allows a larger number of blade elements with observer frequency separations above 200 Hz. On the retreating blade the Doppler effect works in reverse and decreases the observed frequencies. The net result is that for the observer frequencies above 500 Hz the section of the airfoil from midspan to the tip of the advancing UH-1B blade contributes while below 500 Hz the inboard half of

the advancing blade and the whole retreating blade contribute.

SOLUTION TECHNIQUE

In order to solve for the magnitude of the oscillatory forces on the helicopter blade several assumptions have been made. The following list is a review of the assumptions used in this analysis.

1. The oscillatory forces on an airfoil occur at the frequencies associated with Strouhal shedding.
2. The Strouhal number is assumed to be independent of Reynolds number.
3. The oscillatory forces are sinusoidal and have components only in the lift and drag direction.
4. The oscillatory forces on the blade can be represented by oscillatory dipoles acting at the center of ten spanwise stations.
5. For each small increment of time (≈0.005 seconds) the aerodynamic and geometric parameters at each of the ten spanwise regions remains essentially constant.
6. In the time intervals when one blade advances toward the observer while the opposite blade retreats the noise at the observer for frequencies above 500 Hz is assumed to originate from the advancing blade above.

Using these assumptions the pressure-time history at an observer for a blade in the advancing region is:

$$P(t) = \sum_{i=1}^{10}\left\{(K_{Lv})_i[(A_L)_i \sin(\omega_i\tau_i + \phi_i) + (B_L)_i \cos(\omega_i\tau_i + \phi_i)] + (K_{Dv})_i[(A_D)_i \sin(\omega_i\tau_i + \phi_i) + (B_D)_i \cos(\omega_i\tau_i + \phi_i)]\right\} \quad (4)$$

where τ_i is the retarded time

ω_i is the Strouhal shedding frequency

ϕ_i is the phase of the shedding

$(A_L)_i$, $(B_L)_i$, $(A_D)_i$ and $(B_D)_i$ are the geometric coefficients predicted by the moving, oscillatory dipole theory.

The assumption that the aerodynamic and geometric parameters remain constant in a 0.005 second time slice is now applied. The term $\omega_i\tau_i$ is replaced by $\omega' t$ where ω'_i is the Doppler shifted frequency at the observer's location. Equation (4) then becomes for each blade

$$P(t) = \sum_{i=1}^{10}(K_s)_i \sin(\omega'_i t + \phi_i) + (K_c)_i \cos(\omega'_i t + \phi_i) \quad (5)$$

where $(K_s)_i = (K_L)_i (A_L)_i + (K_D)_i (A_D)_i$

$(K_c)_i = (K_L)_i (B_L)_i + (K_D)_i (B_D)_i$

The exact time-interval chosen to solve for the oscillatory forces was 0.0046 seconds. The rate at which the data was electronically digitized was 11.3 KHz. Therefore, there are 52 measured values of the recorded pressure in each 0.0046-second time interval. Linearizing Equation (5) by removing the arbitrary phase gives

$$P(t_t) = \sum_{i=1}^{10}\left[(K'_s)_i \sin(\omega'_i t_t) + (K'_c)_i \cos(\omega'_i t_t)\right] \quad (6)$$

$$t = 1,\ldots,52$$

where $\sqrt{(K'_s)_i^2 + (K'_c)_i^2} = \sqrt{(K_s^2)_i + (K_c)_i^2} = K_i$

and K_i is the total magnitude of the oscillatory force constants. Since there are 20 unknowns in Equation (6) ten $(K_s)_i$ and ten $(K_c)_i$ and 52 equations the problem is overdetermined. The solution was determined using the standard least squares techniques for a set o linear equations.

OBTAINING EXPERIMENTAL MAIN ROTOR VORTEX NOISE

The acoustical pressure-time history recorded at the microphone position is assumed to be a linear supposition of many sources of noise. Among these sources are:

1. engine noise
2. engine exhaust noise
3. main and tail rotor gear box noise
4. tail rotor rotational noise
5. main rotor rotational noise
6. main rotor vortex noise
7. tail rotor vortex noise

Since the analyses that were performed herein are associated with only main rotor vortex noise, item (6), all the other sources of noise in the measured pressure-time histories had to be removed in order to obtain the desired pressure-time history.

In the model developed in this contract, the noise associated with rotor blade vortex shedding is assumed to be generated at discrete frequencies defined by a Strouhal formulation. These shedding frequencies are determined by the airfoils chord, thickness, angle of attack and velocity. Shedding frequencies, while in part determined by rotor rotational speed are not integral harmonics of the rotor rotational frequency. In addition, since the blade is moving and continually changing direction, the Doppler shift on these frequencies also continually changes. This differs from items 1, 2, 3, 4, and 5 of the listed sources of noise which are observed at discrete frequencies. This is clearly illustrated in Figure 8, the spectrum of measured helicopter rotor noise for the hover flight condition. It can be seen that the rotor rotational noise appears at discrete multiples of the blade passage frequency (10.8 Hz) and the tail rotational noise occurs at multiples of its blade passage frequency (55.1 Hz). The peaks at 1922 Hz and 2133 Hz are identified with the tail-rotor gear slash frequencies of the 42-degree and 90-degree (second harmonic) gears.

In the data shown in Figure 8 the rotational and discrete noise peaks are sufficiently narrow so that they can be removed without significantly changing the content of the underlying broadband noise. Once the discrete noise peaks are identified their corresponding Fourier coefficients as determined from the Fast Fourier Transform of the digitized data, are set equal to zero. The broadband pressure-time history is then generated by using the inverse Fourier transform.

In order to correlate the measured pressure-time history with the theory, the azimuthal blade position must be known. The Wallops Island test did not record this important piece of information. The azimuthal location of the rotor was determined

by matching the measured rotation noise signature with a theoretically predicted rotational noise pressure-time history.

RESULTS OF THE THEORETICAL ANALYSIS

A total of four hover cases were analyzed. Three of these cases were from position 4 (200 feet to the right of the helicopter) and one from position 6 (700 feet to the right of the helicopter). The radial stations selected were:

r_i = 7, 9, 11, 13, 15, 17, 18.5, 19.5. 20.5 and 21.5 ft. for i=1 to 10 respectively. The electronically digitized records are ~1.5 seconds long. Therefore, 15 blade passages were analyzed for each of the cases.

The set of equations solved had more equations (52) than unknowns (20). By using the method of least squares the resulting deviation is a measure of the equality of the solution. Since the Strouhal number is not accurately known for airfoils at these Reynolds numbers, a search was performed to determine the Strouhal number which gave the most satisfactory solutions. The optional Strouhal number was determined to be 0.235±.02 which is within the range for which results have been obtained by previous investigations.

One of the recordings obtained 200 ft to the right was used to evaluate the method of removing discrete rotational noise sources. The portion of the recording used was 35 seconds into the recorded signal. For the first of the four cases (to be referred to as Case A) all noise below 140 Hz, the tail rotor peaks at 165 Hz and 220 Hz, and all noise above 1860 Hz was removed. In Case B all noise above 2820 Hz was removed (instead of above 1860 Hz as in Case A) together with the gear clash spikes at around 1930 Hz and 2140 Hz. In order to determine how much the results were dependent on when in time the data was analyzed, another portion of the data taken 200 ft to the right and 26 seconds into the recording was analyzed. This condition is referred to as Case C. The electronically digitized pressure-time history and spectrum for this case are shown in Figures 7 and 8 respectively. The rotational and discrete noise was removed by setting the following coefficients of the Fourier representation of the digitized record equal to zero: <140 Hz, 165 Hz, 220 Hz, 1930 Hz, 2140 Hz, and >2820 Hz. Figure 9 presents the spectrum of the noise that was removed and Figure 10 presents the spectrum of the vortex noise that was analyzed for this case. The pressure-time history of the rotational noise is shown in Figure 11 and of the vortex noise in Figure 12. The fourth case that was analyzed (Case D) was data measured 700 feet to the right of the helicopter. A portion of the recording 26 seconds into the record was analyzed. In this position the gear clash frequencies occur at 1930 Hz and 1990 Hz. The frequency components removed were <140 Hz, 165 Hz, 220 Hz, 276 Hz, 330 Hz, 385 Hz, 1930 Hz, 1990 Hz, and >2820 Hz.

The analyses that were carried out used 15 blade passages of digitized data. Because of the previously noted inability to separate the lift and drag components and because it has been shown elsewhere that the drag contribution is insignificant compared to the lift distribution, the $(K_D)_i$'s were assumed zero in all of the analyses that were conducted. Therefore, only $(K_L)_i$'s were calculated for the 15 blade passages in each case. For each radial station, the distribution of these $(K_L)_i$ values multiplied by that station's dynamic pressure is shown in Figure 13. The $(K_L)_i(1/2\rho U_i^2)$ for the ten radial stations for each of the four cases are tabulated (Table I) and plotted in Figure 14. Although there is some scatter in each of the distributions the mean results are remarkably similar for all four cases. The comparison of Case A and Case B shows that the results are fairly insensitive to variations in the high frequency cutoff in the data, although the magnitudes of station 10 for Case A are somewhat suppressed from Case B. Going to a different position of the record also does not significantly alter the distributions (see distributions for Case C). Some of the distributions for position 6, (Case D) however, do differ from the first three cases. This is due, in part, to the differences in ground reflection. The magnitudes of the oscillatory pressures are ~1 to 2 lb/ft^2 for the tip 1/3 of the blade (14-22 ft). On the inboard stations (6-14 ft) the magnitude of the oscillatory pressure ranges from 4 to 30 lb/ft^2. It must be remembered, however, that these stations include significant contributions from the retreating blade whereas the outboard blade sections do not. For each of the four cases that were analyzed, the calculated oscillatory forces were used in a theoretical program to determine if the essential noise characteristics had been retained. For each of the cases, therefore, a pressure-time history and a corresponding spectral analysis were predicted for comparison with the experimental data. The predicted pressure-time history and the corresponding spectrum for Case C are shown in Figures 15 and 16 respectively. When these predicted results are compared with the measured results in Figures 12 and 10, it is seen that the calculated oscillatory forces have retained all of the essential characteristics of the measured pressure-time history. Similar comparisons were made for Cases A, B, and D.

TABLE I. MAGNITUDES OF THE OSCILLATORY LIFT FORCES AS A FUNCTION OF RADIAL POSITION FOR EACH OF THE FOUR CASES

Station Radius (ft)	Angle of Attack (deg)	Mach Number	Shedding Frequency (Hz)	Oscillatory Pressure (lb/ft^2) Case A	Case B	Case C	Case D
7.0	5.9	0.22	217	20.20	19.26	20.53	20.60
9.0	5.6	0.28	284	22.02	23.02	22.02	23.10
11.0	5.2	0.34	351	8.25	8.95	13.92	10.55
13.0	4.7	0.40	42.	4.83	4.45	4.45	11.33
15.0	4.2	0.46	512	2.15	2.10	2.10	2.25
17.0	3.6	0.52	591	1.33	1.05	1.05	1.07
18.5	3.1	0.57	658	1.20	0.78	1.40	1.56
19.5	2.8	0.60	702	0.83	0.91	0.87	2.55
20.5	2.5	0.63	745	0.61	0.58	0.63	1.66
21.5	2.2	0.66	787	0.39	0.55	0.48	0.81

GENERAL DISCUSSION OF RESULTS

The technique that was developed in this contract effort, of electronically digitizing and analyzing measured sound pressure-time histories to create high resolution spectra, such as shown in Figure 8, has permitted the detailed analysis of various rotor sources. For example, the fine frequency resolution that can be obtained by these techniques, allows separation of the

individual peaks associated with main rotor and tail rotor rotational noise and discrete sources such as oil pumps, gear boxes, etc., from the broadband noise. Since these types of noise sources can now be adequately separated, the characteristics of the various noise sources can be studied independently. The study that was reported on herein stressed the analysis of the broadband noise rather than the rotational noise although the rotational and discrete noise sources were separated from the total noise signature and studied as regards the characteristics of their pressure-time history.

The vortex pressure-time histories (Figure 12, for example) that were generated from the total experimental pressure-time histories by removing the rotational and other discrete noise have the same general characteristics. The signals are essentially random with a modulation in amplitude occurring every blade passage. The high amplitude region has higher frequency than the low amplitude regions. This feature is consistent with the Doppler effect discussed previously, i.e. the advancing blade towards the observer raises the frequency and magnitude of any oscillatory pressure amplitudes recorded at an observer's location. It is noted that each blade passage, however, is distinctly different in its structure. In order to evaluate the effect of this difference on the sound signature of vortex noise each blade passage of the digitized vortex signal was converted to an analog signal and then repeated so that a 5-second analog record of each particular blade passage could be constructed on tape. When a series of each of these 5-second records were played on a tape recorder, it was obvious that each blade passage sounds distinctly different. Qualitatively, this difference from blade passage to blade passage may be described as a modulated signal of varying frequency or "tone". That is, when listening to a series of blade passage recordings a different frequency content may be discerned in each of the blade passages.

The vortex shedding model allowed a finite frequency range to be "fit" to the experimental pressure-time history. The relative magnitudes of each of the radial station's oscillatory forces reflected the frequency content of the signal received at the observer for that blade passage. Thus, since the signal varies from blade passage to blade passage both in frequency and magnitude, the oscillatory pressures calculated at the helicopter blade had a corresponding variation. Since each blade passage is different, each calculation performed results in slightly different radial array of oscillatory forces. This effect is shown in the histograms (see Figure 13), which illustrates how these oscillatory pressures varied at each radial station over the 15 blade passages for each of the four cases that were analyzed. Histograms plot the frequency of occurrences of a given event. In this case, the histograms record the frequency of occurrence of the calculated oscillatory lift forces in a given range. Reference to Figure 13 shows that the scatter of results increases as the radial station decreases which relates to the previous discussion of the gradual degeneracy of the solution technique as the frequency of shedding on the blade decreases. The amount of scatter of a station corresponds to the variability of the frequency appropriate to that station contained in the experimental record. Thus, for Case C, the frequency appropriate to station 2 was changing significantly from blade passage to blade passage while the frequency appropriate to station 6 changed little from blade passage to blade passage.

The mean values for each of these distributions were determined. The mean values are listed in Table I and plotted in Figure 14. The shedding frequencies appropriate to the helicopter rotor reference system are listed as well as the Mach number and angle of attack.

The advancing blade, as previously noted, has its shedding frequencies raised and spread apart while the retreating blade has its shedding frequencies lowered and pushed together. The Doppler shifted frequencies on the advancing blade range from about 275 Hz at 7 ft radius to 2100 Hz at 21.5 ft radius. The exact amount of the shift depends on the observer's location relative to the velocity of that blade station. The Doppler shifted frequencies on the retreating blade range from 180 Hz at 7 ft radius to about 500 Hz at 21.5 ft radius. Hence the outboard section of the advancing blade is associated with high frequency noise and the inboard section of the advancing blade together with the retreating blade are associated with low frequency noise. For the observer, the radial stations at 7 ft and 9 ft on the advancing blade are in the same frequency range as the retreating blade because of the Doppler effect and hence these stations also reflect the noise energy of the retreating blade. This contribution partially leads to higher values of oscillatory pressure calculated at these radial stations. The noise energy of the entire retreating blade has been lumped into these two stations.

As shown in Figure 14, the decreasing oscillatory pressure magnitudes at larger blade radius reflect the gradual fall off with frequency of the noise energy shown in the spectra (see Figure 9 for example). The spectra generated in this analysis compare well with the findings of Cox and Lynn, Reference 17, in that the major source of audible vortex noise is concentrated in the frequency range of 200 Hz to 500 Hz. The maxima and minima in these spectra caused by ground reflection also affect the calculated oscillatory pressures as the model does not include this reflection effect.

The mean oscillatory pressures have been used to create a pressure-time history at an observer's station. As discussed previously, these created pressure-time histories and these spectra compare very well with the experimental pressure-time histories and spectra. See Figures 15, 16, 12 and 10 for example. Audio tapes created from the calculated pressure-time history sound like the experimental tapes except for the frequency variation from blade passage to blade passage eliminated by using the mean values.

Since the essential characteristics of the experimental acoustic signal can be duplicated with these mean oscillatory forces in a rotating blade frame of reference, it is possible with proper parameterization of the force constants to effectively

simulate the noise produced by helicopter rotors for a variety of operating conditions. Because of the advanced data analysis procedures that have been developed, the rotational and broadband vortex noise can be separated and studied independently. It is, therefore, possible to parameterize the vortex noise and the rotational noise as functions of the rotor geometric and operating conditions such as number of blades, rotational speed, thrust, chord, twist, etc. The parameterization of the vortex noise and rotational noise can be carried out by analyzing various rotor data from whirl tower tests, as was done in this program for a hovering helicopter. Once the parameterization has been accomplished, for a number of different rotor systems, it should be possible to predict the acoustic signature of any rotor system given only the geometric and operating conditions of the helicopter.

CONCLUSIONS

On the basis of the analyses carried out in this investigation, it was shown that random or "vortex" noise is a major source of noise from a helicopter in the hover condition. For the cases analyzed, main rotor rotational noise was not significant above 100 Hz and the major audible sources of vortex noise were concentrated in the frequency range of 200 to 500 Hz. In their respective frequency ranges the main rotor rotational noise was about 30 db above the threshold of hearing while the vortex noise was about 45 db above a normal background noise.

In addition to the above general conclusions the following specific conclusions were drawn:

1. Ground reflection effects can significantly distort the radiated acoustic pressure-time history.
2. The broadband noise created by a helicopter rotor can be represented by Kármán-street vortex induced noise.
3. The "vortex" noise correlated for a Strouhal number of 0.235.
4. The vortex noise can be simulated by an array of moving, oscillating dipoles with frequencies corresponding to the Kármán-vortex street phenomena.
5. The basis of a technique by which the acoustic signature of any rotor system can be predicted in hover or forward flight has been developed and demonstrated.
6. A new technique has been developed whereby significantly improved high resolution acoustic spectra can be generated.

REFERENCES

1. Loewy, R.G., Sutton, L.R., A THEORY FOR PREDICTING THE ROTATIONAL NOISE OF LIFTING ROTORS IN FORWARD FLIGHT, INCLUDING A COMPARISON WITH EXPERIMENT, USAAVLABS Technical Report 65-82, U. S. Army Aviation Materiel Laboratories, Fort Eustis, Virginia, January 1966.
2. Loewy, R.G., Sadler, S.G., A THEORY FOR PREDICTING THE ROTATIONAL AND VORTEX NOISE OF LIFTING ROTORS IN HOVER AND FORWARD FLIGHT, NASA CR-1333, May 1969.
3. Schlegel, R., King, R., Hull, H., HELICOPTER ROTOR NOISE GENERATION AND PROPAGATION, USAAVLABS Technical Report 6604, U. S. Army Aviation Materiel Laboratories, Fort Eustis, Virginia, 1966.
4. Lowson, M.V., THE SOUND FIELD FOR SINGULARITIES IN MOTION, Proceedings of the Royal Society, A. Vol. 286, pp. 559-572, 1965.
5. Lowson, M.V., Ollerhead, J.B., STUDIES OF HELICOPTER ROTOR NOISE, USAAVLABS Technical Report 68-60, U. S. Army Aviation Materiel Laboratories, Fort Eustis, Virginia, January 1969.
6. Stowell, E.Z., Deming, A.F., VORTEX NOISE FROM ROTATING CYLINDRICAL RODS, NACA TN 519, 1935.
7. Yudin, E.Y., ON THE VORTEX SOUNDS FROM ROTATING RODS, NACA TN 1136, 1947.
8. Blokhintsev, D., ACOUSTICS OF A NONHOMOGENEOUS MOVING MEDIUM, NACA TN 1399, 1959.
9. Hubbard, H.H., PROPELLER-NOISE CHARTS FOR TRANSPORT AIRPLANES, NACA TN 2968, 1953.
10. Krzywoblocki, M.Z., INVESTIGATION OF THE WING-WAKE FREQUENCY WITH APPLICATION OF THE STROUHAL NUMBER, J. Aeron. Sci., Vol. 12, No. 1, Jan. 1945, pp. 51-67.
11. Roshko, A., EXPERIMENTS ON THE FLOW PAST A CIRCULAR CYLINDER AT VERY HIGH REYNOLDS NUMBER, J. Fluid Mech., Vol. 10, Part 3, May 1961.
12. Johnson, H. Kevin, Katz, Walter M., INVESTIGATION OF THE VORTEX NOISE PRODUCED BY A HELICOPTER ROTOR, Rochester Applied Science Associates, Inc., NASA Report 71-10, USAAMRDL Contract DAAJ02-70-C-0023, Report to be published, 1971.
13. Evans, T.D., Nettles, W.E., FLIGHT TEST NOISE MEASUREMENTS OF A UH-1B HELICOPTER, paper presented at the AHS/UTA Joint Symposium on Environmental Effects on VTOL Designs at Arlington, Texas, November 1970.
14. Roshko, A., ON THE DRAG AND SHEDDING FREQUENCIES OF TWO-DIMENSIONAL BLUFF BODIES, NACA TN 3169, 1954.
15. von Doenhoff, A.E., Tetervin, N., DETERMINATION OF GENERAL RELATIONS FOR THE BEHAVIOR OF TURBULENT BOUNDARY LAYERS, NACA Rept. 772, 1943.
16. Lighthill, M.J., SOUND GENERATED AERODYNAMICALLY, Royal Aircraft Establishment (Farnborough) Technical Memorandum No.: Dir. 8, November, 1961, AD 275 075.
17. Cox, C.R., Lynn, R.R., A STUDY OF THE ORIGIN AND MEANS OF REDUCING HELICOPTER NOISE, TCREC Technical Report 62-73, November 1962.

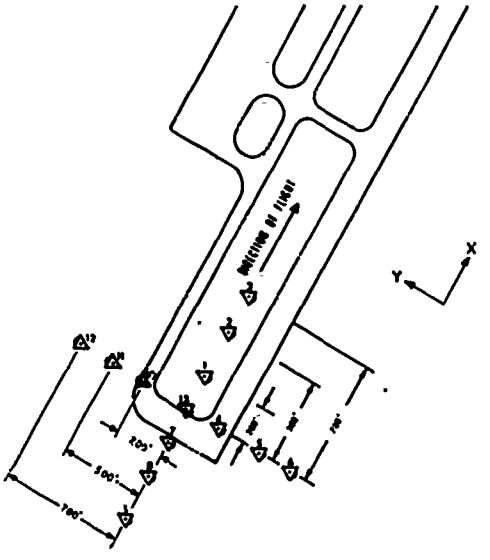

Figure 1. Relative Positions of Microphones at Wallops Island Air Station.

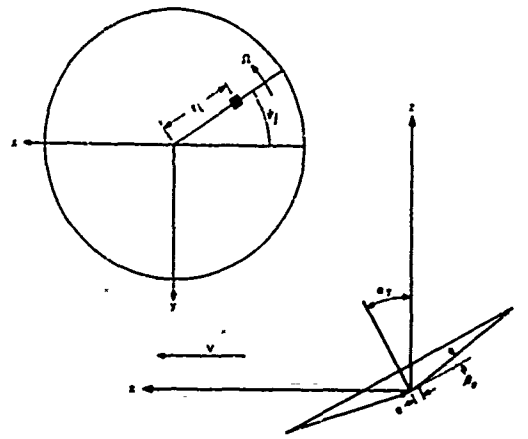

Figure 3. Tip-Path Plane Coordinates.

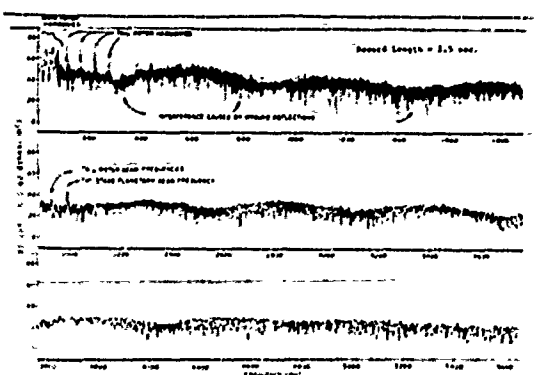

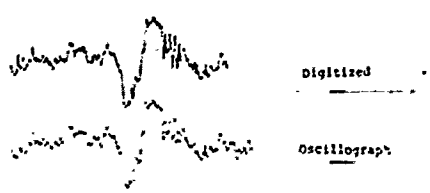

Figure 4. Comparison of Oscillograph and Electronically Digitized Pressure-Time Histories for UH-1B in 115-Knot Flyby. Recorded at 200 ft to the Right.

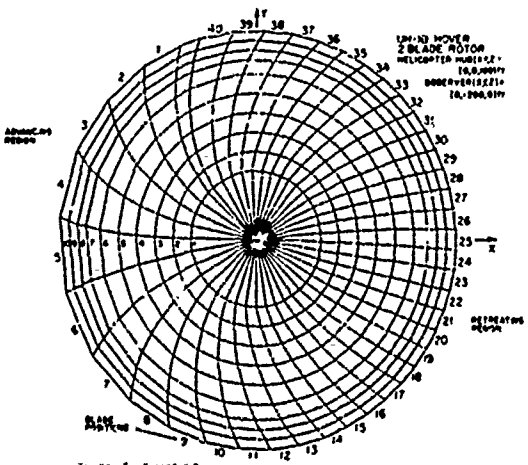

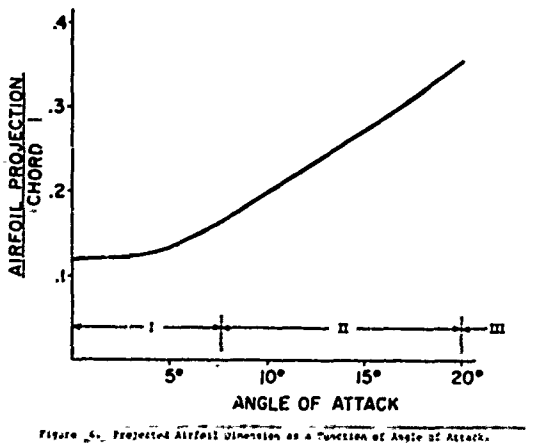

Figure 6. Projected Airfoil Dimension as a Function of Angle of Attack.

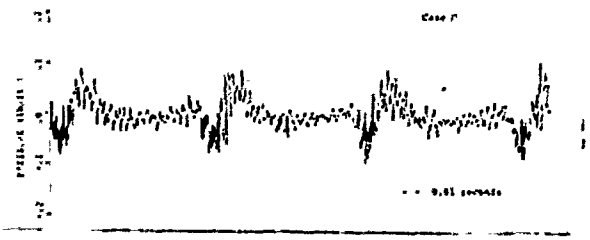

Figure 7. NASA Electronically Digitized Representative Plotter of Total Recorded Signal at Position 7 for UH-1B in Power

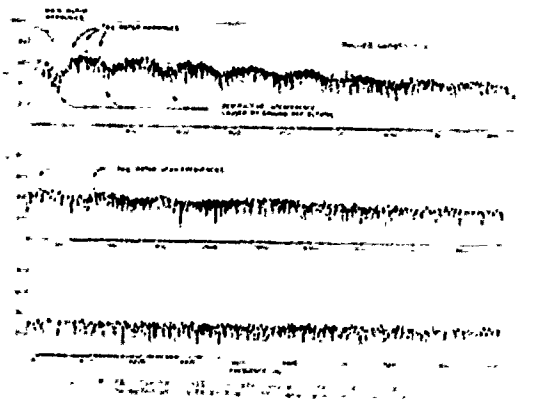

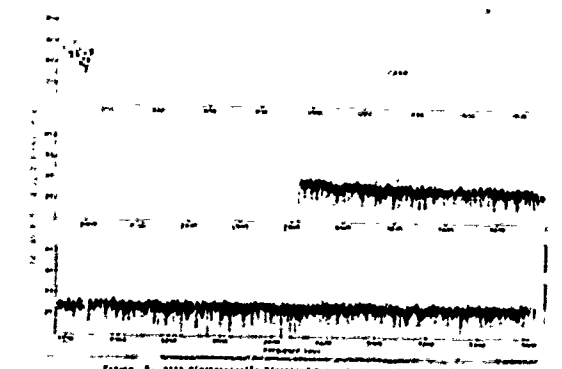

Figure 9. NASA Electronically Digitized Noise Spectrum of Detailed Recognition and High Frequency Broadband Noise at Position 6 for UH-1B in Power

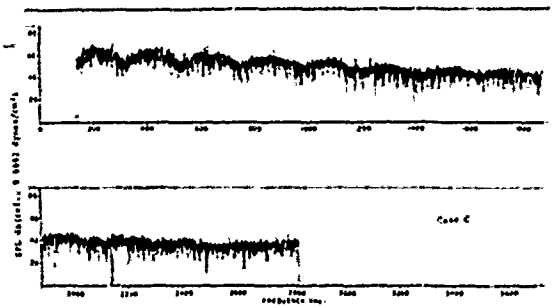

Figure 10. NASA Electronically Digitized Noise Spectrum of "Vortex" Noise at Position 4 for CH-46 in Hover.

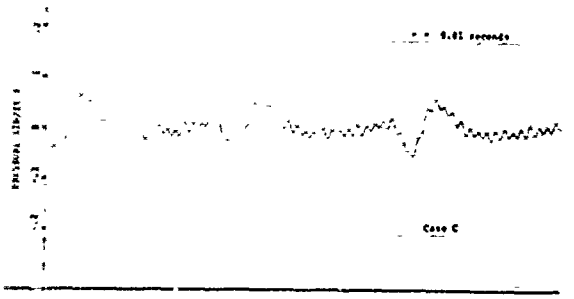

Figure 11. NASA Electronically Digitized Pressure-Time History of Total Sound and Discrete Noise at Position 4 for CH-46 in Hover.

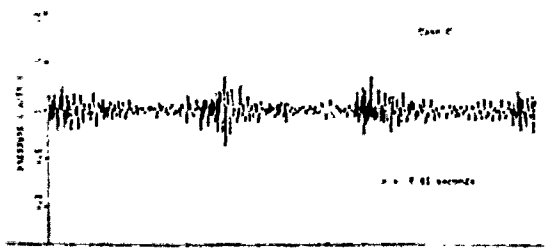

Figure 12. NASA Electronically Digitized Pressure-Time History of Vortex Noise at Position 4 for CH-46 in Hover.

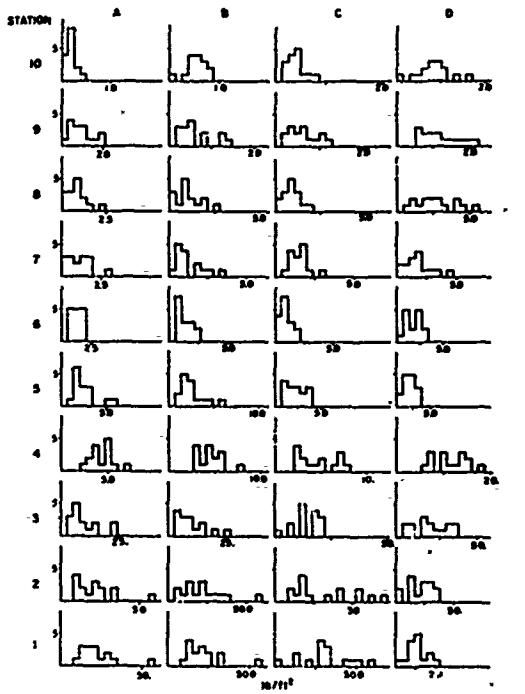

Figure 13. Distribution of the Magnitude of Oscillatory Lift Over Ten Radial Stations for four Cases.

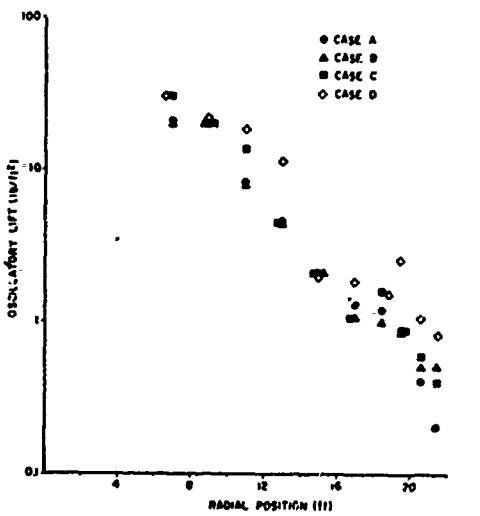

Figure 14. Magnitudes of the Oscillatory Lift Forces as a Function of Radial Position for Each of the Four Cases.

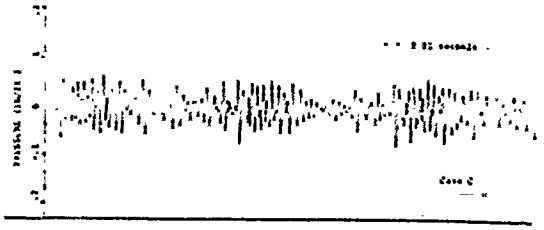

Figure 35. Predicted Vortex Pressure-Time History at Position 6 for 200-kt Dive.

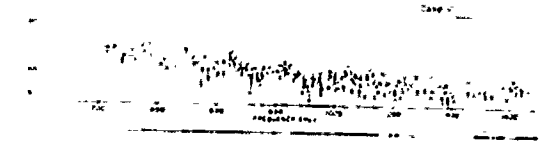

DISCRETE NOISE FROM HIGH AND LOW SOLIDITY ROTORS

S. E. Wright

Institute of Sound and Vibration Research,
University of Southampton, Southampton, SO9 5 NH, England

Introduction

A single unified theory is described to account for the discrete radiation generally from the whole family of heavily run axial flow rotors, including helicopter rotors, propellers and gas turbine compressors.

The approach used, is to Fourier analyse the periodic blade loading variation (aximuth profile) into blade loading harmonics, and then sum the total radiation from each BLH. In this way, the radiation from any arbitrary blade loading variation, and thus the rotor noise can be determined. To indicate trends, the effect of blade loading profile, load excursion width and number of excursions is considered. The blade of course can sweep out some very complicated source distributions, and again to be in a position to assess the radiation, approximations have to be made.

With this in mind, the basic differences between high and low solidity rotor spectrums are considered, emphasizing the difference between subsonic and supersonic rotor noise. The special effect of helicopter blade slap and compressor rotor-stator interaction is discussed, and measured rotor spectrums have been included to help illustrate the theory. The paper is an extract (Section 6) from the publication Discrete radiation from periodic sources in circular motion (1) and is a continuation of the work reported earlier in reference (2).

1. Blade loading spectra

Consider the aerodynamic load on a blade: if the total arithmetic loading varies as the blade rotates, so that is is reproducible for each blade revolution, then the azimuth blade loading profile, see Fig. 1, can be Fourier analysed into blade loading harmonics, such that

$$L(\psi) = L_o + \sum_{s=1}^{\infty} (A_s \cos s\psi + B_s \sin s\psi) \qquad (1)$$

$$L(\psi) = L_o + \sum_{s=1}^{\infty} L_s \cos (s\psi - \theta_s) \qquad (2)$$

$$L_s = (A_s^2 + B_s^2)^{\frac{1}{2}} \qquad \theta_s = \tan^{-1}\left(\frac{B_s}{A_s}\right) \qquad (3)$$

Any arbitrary periodic azimuth B.L. function can be analysed in this way, and again for convenience the B.L. harmonic amplitude can be represented by a constant times a spectrum function, viz.

$$L_s = 2 \text{ Avg. } \chi_s \qquad (4)$$

Here the blade loading spectrum level is given by the average value term, Avg, which is equal to the pulse or excursion area divided by the excursion period. The blade loading spectrum shape is determined by the blade loading spectrum function χ_s, which is a function of the load excursion profile, width and number per blade revolution.

Some simple pulses with their spectra are shown in Fig. 14 ,(1). The representative rectangular pulse is an even function and has cosine terms only, ΔL is the pulse height or load change from the mean value.

$$\chi_s = \frac{\sin \pi f t_o}{\pi f t_o} \quad , \text{ Avg} = \Delta L \frac{t_o}{T} \qquad (5)$$

The smoothly varying half cosine pulse is also an even function and has cosine terms only,

$$\chi_s = \frac{\cos \pi f t_o}{1-(2ft_o)^2} \quad , \quad \text{Avg} = \frac{2\Delta L}{\pi} \cdot \frac{t_o}{T} \qquad (6)$$

and the zero lift full sine pulse is an odd function having only sine terms

$$\chi_s = \frac{\sin\pi (ft_o - 1)}{4(ft_o - 1)} \cdot \frac{\sin\pi (ft_o + 1)}{4(ft_o + 1)} \quad , \text{ Avg} = \frac{2\Delta L}{\pi} \cdot \frac{t_o}{T} \qquad (7)$$

In terms of rotor parameters, if W is the pulse or azimuth excursion width and E is the number of excursions per blade revolution, then the excursion time t_o and periodic time T between excursions is

$$f = \frac{s}{T} \quad , \quad t_o = \frac{W}{V_e} = \frac{W}{2\pi N r_e} \quad , \quad T = \frac{1}{EN} \qquad (8)$$

giving

$$\frac{t_o}{T} = E \rho_w \text{ and } ft_o = sE\rho_w \qquad (9)$$

Where ρ_w is the load solidity, which is the fraction of the effective annulus that the loading region occupies. viz.

$$\rho_w = \frac{W}{2\pi r_e} \qquad (10)$$

The first sE zero is given by

$$(sE)_z = \frac{(ft_o)_z}{\rho_w} \qquad (11)$$

where $(ft_o)_z$ for simple pulses can be read from figure 14 ,(1) e.g. rectangular $(ft_o)_z = 1$, half cosine $(ft_o)_z = 1.5$, triangular $(ft_o)_z = 2$ etc.

As an example, let the blade experience a short stall or an impulsive load change of height ΔL from the mean load L_o. If we represent the load excursion by a rectangular distribution then the blade loading spectrum is

$$L_s = 2 \text{ Avg } \chi_s$$

where

$$\text{Avg} = \Delta L.E.\rho_w. \text{ and } \chi_s = \frac{\sin \pi s E \rho_w}{\pi s E \rho_w} \qquad (12)$$

This and other χ_s for more realistic load excursions are shown in Fig. 2, the average value term for the half cosine and sine excursion is

$$\text{Avg}_{\frac{1}{2}\cos} = \text{Avg}_{\text{sine}} = \frac{2}{\pi} \Delta L.E.\rho_w. \qquad (13)$$

It is shown that the blade loading spectrum level when expressed in dB, is little different for a variety of simple loading functions, providing the pulse height, width and number per blade revolution is the same. Further, for a given function, the spectrum level is independent of how the average value is arrived at, i.e. it does not matter how high, how wide or how many pulses there are per blade revolution, providing the multiple value is the same.

The spectrum shape is similar for simple all positive or all-negatively going pulses. Pulses with equal positive and negative areas (zero lift functions) similar to the full sine function, have zero value blade loading harmonics at zero order. Blade loading functions that have more than one excursion per blade revolution have blade loading harmonics only at multiples of the excursion number E. The parameter that has the largest effect on the B.L. spectrum is the pulse width or load solidity ρ. Figure 3 shows that the spectrum level falls off rapidly with increasing ρ_w or excursion width W.

2. Blade loading radiation

Having considered the blade loading spectrum generated by representative blade loadings, we are now in a position to predict the resulting radiation. From equation 70,(1) the sound pressure from a single blade loading harmonic, s is

$$(\hat{SP}_{mB})_{\text{single } s} = \frac{\alpha_s}{2}.K.Y_q.X_a.X_b.X_I \qquad (14)$$

The distributive functions X_a, X_b, X_I account for the linear interference along the chord and span, and between source and image (ground reflection) respectively. For free-field radiation and point loading or at low frequencies, the three functions are unity. The directivity function Y_q accounts for the circular interference around the rotor disk, and the blade loading spectrum amplitude α_s together with the operating constant K determines the acoustic spectrum level. If the rotor disk is uniformly loaded, then the disk radiates as a whole and s=0 in equation 14 gives the discrete radiation.

If there is a complete spectrum of blade loading harmonics contributing to the sound pressure, then equation 83, (1) together with the relative phase information has to be summed for all values of s, equation 103, (1) will now give the acoustic radiation thus

$$(\hat{SP}_{mB})_{\text{cont. } s} = \frac{\alpha_s}{2}.K_T.mB.X_a.X_b.X_I \qquad (15)$$

Here all the passbands radiated from each B.L.H. sum to a smooth radiation spectrum, and each mode radiation at a particular mB number constructs a smooth polar directivity. For a flat B.L.H. spectrum (α_s is constant for all s values), equation 15 is an exact result. Here there is no circular interference operating as in the case of a uniformly radiating disk and therefore Y_q collapses exactly to mB and K to K_T.

Physically the B.L. spectrum assembles to a B.L. impulse and therefore the acoustic spectrum is dominated by radiation from a local loading region within the rotor disk. It is not suprising then, that the polar directivity term K_T is now that of a dipole inclined at the blade force angle. For general B.L. spectrums including random phasing between blade loading harmonics, equation 15 will basically hold, except K_q increasingly contributes to the radiation normal to the dipole axis for progressively less impulsive loadings.

The blade loading spectrum amplitude α_s can either be measured directly from the blade, or if the blade loading variations can be roughly estimated in terms of the maximum load change ΔL and width of load excursion W, then from section 1, where impulsive blade loadings are our main interest

$$\alpha_s = \frac{L_s}{L_o} \quad , L_s = 2 \text{ Avg } \chi_s \qquad (16)$$

and for the simple load excursion considered

$$\text{Avg} = \Delta L.E\rho_w \text{ and } \rho_w = \frac{W}{2\pi r_e} \qquad (17)$$

giving

$$\frac{\alpha_s}{2} = \frac{\Delta L.E.\rho_w}{L_o} \cdot \chi_s \qquad (18)$$

Three pertinent blade loading spectrums and their resulting radiation are illustrated in figure 4, s has now been replaced by sE to accommodate for multiple blade loading excursions. For a single blade loading harmonic, a passband of discrete frequencies is radiated, (figure 4(a)) whose radiation magnitude in terms of load solidity ρ_w, number of load excursions E, and excursion height ΔL. is from equation 14 and 18

$$\hat{SP}_{mB} = \frac{\Delta L E \rho_w}{L_o} .K.Y_q.X_{sE}.X_a.X_b.X_I \qquad (19)$$

The first two terms are basically constants for a particular blade loading function, and therefore set the spectrum level. The directivity function Y_q determines the width of the radiation passband, and the four distributive functions $X_{sE}X_aX_bX_I$ are unity for point disk, chord and span loading radiating in free field.

Figure 4(b) shows the effect of multiple blade loading excursions per blade revolution. Here blade loading harmonics only exist at multiples of E. (the concept is analaguous to sound pressure harmonics existing at multiples of B in the mB

spectrum.) Each B.L.H. radiates a passband of discrete frequencies situated about sE where s = 1,2,3 etc.

Here the sound pressure spectrum is given by equation 19. For low E numbers or high M_e, the passbands will overlap and simple B.L.H. radiation addition discussed in section 5.1,(1) will have to be considered. Physically multiple blade loading excursions correspond to E equispaced fixed radiated regions within the rotor disk. Therefore the overlapping passbands now reconstruct new interference patterns, which correspond to the interference between an array of E equispaced inclined dipoles.

Figure 4(c) typifies the radiation from a single load excursion per blade revolution (E=1). A single excursion gives rise to a continuous blade loading spectrum, continuous in the sense that the blade loading harmonics exist at every sE number. Therefore equations 15 and 18 now give the acoustic radiation as

$$(\hat{SP}_{mB})_{cont.s} = \frac{\Delta L.E.\rho_w}{L_o} .K_T.mB.X_{sE}.X_a.X_b.X_I \qquad (20)$$

The sound pressure harmonic falloff is now the resultant of the four distributive spectrum functions $X_{sE}X_aX_bX_I$, whose onset of effectiveness (departure from unity) is measured by the reciprocal of their individual solidities ρ. For free field radiation X_I=1 and point chord and span loading (ρ_a=ρ_b=o, X_a=X_b=1), the relation between the acoustic spectrum and the blade loading spectrum is 6dB per octave within the limitations of equation 103,(1)

$$X_{ac} = X_s.mB \qquad (21)$$

The fact that a relationship between the blade loading spectrum and its acoustic spectrum has been established has fascinating possibilities. It means that aerodynamic data can now be accessed from the acoustic spectrum. To obtain the blade loading coefficient for a single load excursion, we combine equations 15 and 14

$$\frac{(SP)_{cont.s}}{(SP)_{s=o}} = \frac{\alpha_s K_T mB X_a Y_b X_I}{2\ K\hat{Y}_{mB} X_a X_b X_I} \qquad (22)$$

then

$$\alpha_{s=mB} = \frac{(SP)_{cont.s}}{(SP)_{s=o}}_{mB} \cdot \frac{K}{K_T} \cdot \frac{2Y_{mB}}{mB} \qquad (23)$$

The blade loading coefficient at the crossover point, i.e. the point where the fluctuating load radiation starts to dominate the steady load radiation is

$$\alpha_{s=mB} = \frac{K}{K_T} \cdot \frac{2Y_{mB}}{mB} = \frac{2K}{K_T} \cdot J_{mB}(x) \qquad (24)$$

Assuming K_T>K_q, $\beta_{s=o}$=$\beta_{s\neq o}$ and for the observer situated along the maximum directivity K_T=K (Note $\beta_{s=o}$ is not necessarily equal to $\beta_{s\neq o}$). The blade loading coefficient in dB is then

$$20 \log \alpha_s = 20 \log (SP)_{cont.s} - 20 \log (SP)_{s=o} + 20 \log \frac{2Y_{mB}}{mB} \qquad (25)$$

where from equation 12,(1)

$$20 \log \frac{2Y_{mB}}{mB} = - (20 \log \frac{mB}{2} + 7 + mB\ 20 \log \frac{0.7}{M_e}) \qquad (26)$$

The fractional change in load $\frac{\Delta L}{L_o}$ can then be calculated from equation 18 thus

$$\frac{\Delta L}{L_o} = \frac{\alpha_s}{2\ E\ \rho_w X_s} \qquad (27)$$

Similarly, to obtain the blade loading coefficient for a large multiple excursion spectrum we can write down equation 14 twice for s = sE and s = o thus

$$\frac{(SP)_{sE}}{(SP)_{s=o}} = \frac{sE K\hat{Y}_q X_a X_b X_I}{2K\hat{Y}_{mB} X_a X_b X_I} \qquad (28)$$

then

$$\alpha_{sE} = \frac{(SP)_{sE}}{(SP)_{s=o}}_{mB} \cdot \frac{2Y_{mB}}{Y_q} \qquad (29)$$

where q=mB-sE, or simply at low frequencies

$$\alpha_{sE} = \frac{2(SP)_{sE}}{K Y_q}_{mB} \quad \text{and} \quad \frac{\Delta L}{L_o} = \frac{(SP)_{sE}}{K Y_q \rho_w X_{sE}}_{mB} \qquad (30)$$

$\hat{Y}$ is preferred to Y_q, as its zeroes in practice are never clearly resolved. From equation 63,(1)

$$\hat{Y}_q = mB J_q(x) = (\tfrac{2}{\pi})^{\frac{1}{2}} \cdot \{\frac{mB}{M_c \cos\alpha}\}^{\frac{1}{2}} \qquad (31)$$

i.e. $\hat{Y}$ rises at the rate of 3 dB per octave in mB.

The load solidity ρ_w, the blade loading spectrum X_s and the static and dynamic loads on the blade can therefore be estimated from a knowledge of the acoustic spectrum. In general for subsonic rotors, if there are large discretes high in the acoustic spectrum, then ρ_w is low and the blade is experiencing impulsive loading. If the discretes fall off quickly, then ρ_w is high and the loading is varying slowly. If the harmonics fall off very rapidly according to equation , (1) then ρ_w = 100% and the blades are sustaining static loading only. For supersonic rotors, the steady lift dominates the acoustic spectrum.

3. General rotor spectrums

From a noise point of view, rotors can be conveniently divided into two classes: high and low solidity rotors. Low solidity rotors are those with a few narrow blades such as helicopter and propeller rotors. As a result of having few concentrated rotating forces (B small), the steady lift or thrust (s=o) on this type of rotor in clean flow, dominates the low frequency rotor spectrum in accordance with equation 11 ,(1). In the case of

higher revving rotor (propeller), the steady lift radiates well into the audible part of the acoustic spectrum and therefore gives a reasonably indication of the rotor noise. However for the lower r.p.m. rotor (helicopter rotor), the steady lift radiation from the higher order B.L.H. is all that is heard. In order to predict propeller noise accurately and account for the subjective noise from helicopter rotors, fluctuating lift radiation (s≠o) must be taken into account.

Fluctuating lift is generated by varying persistence in the rotors disc loading asymmetry. The causes are numerous, some obvious effects are fuselage, wings and forward speed, examples of transient effects are crosswind, atmospheric turbulence and aircraft maneuvers. Some readers may remember the abrupt change in pitch of the Spitfire's maneuver in the last war. To produce strong periodic tones well into the rotor spectrum, the loading asymmetries must be "spike like", produced by impulsive type blade loading functions. Such a source of current interest, is the banging noise heard in certain situations on helicopter rotors, sometimes referred to as blade slap. Here rotor blades are thought to cut or pass near to tip vortices shed by proceeding blade producing a sudden load excursion. It can be argued that strong blade-tip vortex interaction can occur particularly in high forward speed, and in hover in the case of a tandem rotor machine. In either case the radiated spectrum from the impulsive loading will be given by equation 20, and the polar directivity will be dipole like, inclined in the direction of the effective blade force angle. If more than one blade-tip vortex interaction occurs per blade revolution, the multiple load excursion theory has to be considered.

For moderate tip speeds, high solidity rotors such as fans and gas turbine compressors (B large), produce negligible steady lift radiation. This is immediately evident from equations 11 ,(1) and 12,(1). For high values of B, Y_{mB} is very small even for the first harmonic (m=1) and therefore no matter how big K and α_s are within reason, the sound pressure will be very small. However for tip speeds approaching Mach one, the mB fall-off is negligible and the steady lift dominates the acoustic spectrum. For tip speeds greater than Mach one, the harmonics actually increase with order for point loading as shock waves propagate from the blades, and a loud objectionable noise known in the fan industry as buzz saw noise is heard. It is clear than, that to remove steady lift radiation, a rotor must have a large number of blades and operate at low tip speeds.

Unfortunately, fluctuating lift radiation is not reduced by increasing a rotors solidity, and any disc loading asymmetry produced in high solidity rotors again produces large discrete radiation. Further examples of asymmetry are motor support struts on high speed fans and stator blades on gas turbine compressors. Hence the blades experience impulsive blade loading fluctuations as the blades pass over the obstructions in the flow. Essentially there is little difference between rotor-stator interaction and blade-tip vortex interaction previously mentioned. Basically only the number of load excursions and rotor frequency are different, the blade-tip vortex radiation is therefore heard as a banging noise and rotor-stator radiation, because of the more frequent load excursions, is heard as a high pitch whine.

Large number of load excursions produce fascinating rotor spectrums. Figure 5 is an example of such a spectrum. Here the emphasis is on the radiation addition of a few B.L.H. passbands situated at multiples of E, rather than the summation of a complete spectrum of blade loading harmonics s for E=1. In the figure, the passbands are represented by flat plateaus of length given by equation 9,(1) situated about q=o where s=sE for E>1, their level of course would be given by the blade loading function χ_s. The sound pressure harmonics are represented by the dotted lines and occur at multiples of B. Any rotor spectrum can be constructed in this way. In the illustration, the rotor spectrum represents a free field compressor with 23 rotor blades and 36 stator blades. It can be seen that the first sound pressure harmonic does not radiate, it is below cut off, only the first B.L.H. contributes to the second sound pressure harmonic and s=1 and 2 to the third, the radiation addition here is discussed in Section 5.1,(1). By rearranging equation 9,(1) for the lower cut off mB number

$$\left(\frac{sE}{mB}\right)_c = 1 + M_e \cos\sigma \qquad (32)$$

it can be seen that for particular combinations of sE and mB, certain sound pressure harmonics do not radiate. For example it can be said that for the fundamental blade loading harmonic (s=1), the fundamental blade passage frequency (m=1) will not radiate if

$$\frac{E}{B} < 1 + M_e \cos\sigma \qquad (33)$$

Also, by choosing a convenient blade number B and excursion number E combination, the q=o mode radiation can be seen to be avoided. In terms of frequency f=mBN, our compressor example running at say N=100Hz, the spectrum above mB=140 (f=14,000Hz) is of no further interest.

4. Measured rotor spectrums

To help illustrate the theory, several measured rotor spectrums from rotors of widely different solidity and operating conditions are analyzed. Figure 6(a) is one of many acoustic spectrums of a OH4 Bell helicopter measured by Pegg reference 3. Here the main rotor has B=2 blades, a tip radius r_t=16.65 ft. and a shaft frequency of N=6.6 Hz, giving a tip Mach number of M_t=0.62. The rotor was lifting L_T=2750 lbs. at a forward speed of 61 knots, its altitude was 500 ft. and 1200 ft. head of the microphone, making an elevation angle of σ=23°. The microphone height was 5 ft. above a grass coverud terrain and the analysis made on a 2Hz constant bandwidth analyser.

In the figure, the steady lift radiation is seen dominating the low frequencies in accordance with equation 1,(1) for s=o

(assuming $\beta=6^\circ$). The first harmonic m=1 is muted through the low frequency response of the recorder (20 Hz), but the harmonic falloff is 1.5db per mB, and is given by equation 11,(1) using a value of $r_e=0.9r_t$. The remainder of the spectrum is contributed by fluctuating lift, here discrete frequencies stretch well into the acoustic spectrum at multiple of the blade passage frequency. The rotor is therefore experiencing impulsive loading, the radiation from which is given by equation 20. It is difficult to assess the exact contributions of each of the functions in equation 20 without blade loading information, but by making a few first order assumptions progress can be made. Firstly, the spectrum is noticeably modulated by the image spectrum function χ_1, caused through ground reflection (equations 67,(1) and 68,(1)). In this particular measuring set up, the helicopter height is less than its range and therefore the first and second spectrum zeroes f_z are 130Hz and 390Hz and are adequately given by equation 69(b),(1) where n=1 and 3. Other simultaneous acoustic spectrums taken at different observation positions, show that the f_z move around in the spectrum according to the above equations.

Taking account of χ_I and neglecting the harmonics of the tail rotor particularly $m_T=1$ and $m_T=4$, the spectrum falloff will be given by K_T, mB, $\chi_s\chi_a\chi_b$. In all probability the spectrum is generated from a single load excursion per blade revolution E=1, and therefore the polar directivity will be highly directional (that of a dipole inclined at the effective blade force angle). The directivity information is contained in the K_T term and is defined for the observer at 0° azimuth. If the observer lies along the axis of the dipole then cos sin is effectively unity in K_T and the impulsive spectrum will have its maximum value. If the load excursion occurs on the starboard side of the helicopter rotor, then the lower lobe of the dipole will be tilted towards the ground in the direction of forward motion. Listening to the sound pressure time histories of advancing 'blade slapping' helicopters supports this description, i.e. the banging is heard when approaching and then stops overhead.

Before we can estimate the blade loading spectrum function χ_s, we must assess the effectiveness of the chord and span distributive functions. The chord solidity and first $(mB)_z$ would be σ_a=1% and $(mB)_z$=100 assuming a rectangular chord distribution of a=1 ft. If a tip vortex-blade interaction is the cause of the impulsive loading, it is unlikely that the whole span length would be affected. Therefore assuming an effective span length of say b=2 ft. and a rectangular distribution, the corresponding span solidity and first $(mB)_z$ is 1% and 100 respectively. For more realistic distributions, say the half cosine function, a solidity of 1% would give $(mB)_z$=150. In either case the departure from unity of χ_a and χ_b functions, would not be appreciable at mB=30.

With the above assumptions, the spectrum hump situated around mB=30 must be that of the blade loading spectrum function χ_s alone. Referring to figure 2, something similar to the full sine χ_s function with a load solidity σ_w=3% would best account for the acoustic spectrum. This is most encouraging as the full sine type blade loading function is consistent with what is thought to occur when a blade cuts or passes near to a tip vortex, reference 4. Also in-flight blade loading measurements reference 5 on a XH-51A compound helicopter show blade loading functions similar to the zero lift full sine function but with load solidities of the order of 50%. In this case the spectrum hump would occur at mB=2, giving little high order discrete radiation. Assuming a χ_s function of the full sine type (of σ_w=3% and E=1), then from equations 25 and 26, the maximum blade loading coefficient $\hat{\alpha}_s$=30 is -50dB or 1/300th, and corresponds to a fractional load change (equation 27) of $\frac{\Delta L}{L_o}$ = 5%.

Figure 6(b) is an acoustic spectrum from a low solidity high roving rotor (OV10 propeller). The salient operating conditions are B=3, r_t=4.25 ft, N=26.6 Hz, M_t = 0.64 torque 1000 ft. lbs. (T_T=1200 lbs.) a=0.6 ft., σ=0° R=50 ft., analyser bandwidth=2Hz. Because of few blades, the steady lift radiation can be seen dominating the low frequency spectrum according to equation 1,(1) and the harmonic falloff (2.7dB per mB) is given by equation 11,(1) using a value of $r_e=0.8r_t$. The spectrum is typical of many spectrums investigated by Crigler reference 6, and shows the so called vortex shedding hump resolved into an almost flat spectrum of discretes. Subharmonics can also be seen in between the main harmonics, and occur because the blade forces are unequal, i.e. each blade force is unique and therefore generate harmonics at multiples of mB where B=1.

The spectrum is probably generated by a single load excursion E=1 and the harmonic falloff will therefore be given by $mB\chi_s\chi_a\chi_b\chi_I$. Again it is difficult to access the effectiveness of each of the spectrum functions without blade loading data. However χ_I appears ineffective, and assuming a chord and span solidity of less than 1%, $\chi_a\chi_b$ will have little effect on the spectrum shown. The spectrum envelope will then be $mB\chi_s$, i.e. χ_s is falling off at 6dB per octave in mB. Referring to fig. 14,(1) a triangular type blade loading function would then best fit this blade loading spectrum. The same result could be obtained using say a half cosine type function together with lower chord or span solidities. The truth is probably a combination of both. In either case the rotor is experiencing impulsive loading, and the blade loading coefficient α_s at the crossover point (mB=12) from equation 24 and 26 (assuming the observer is along the maximum directivity) is -60dB or $\frac{1}{1000}$. Nothing can be said about the fractional change in load without a knowledge of the load solidity.

Figure 6(c) is a spectrum from a high speed high solidity rotor (3 stage axial flow compressor) investigated by Chestnutt and Clark reference 7. The operating parameters are B=23, E=36, r_t=0.5 ft. N=290Hz, M_t=0.8, horsepower=800 (T_T=200 lbs. first stage) α=60° R=100 ft. from bellmouth. Measurements were made in the anechoic chamber and the analysis performed on a 50Hz analyser. Due to a large blade number, the steady loading also is not contributing to the rotor noise at this particular operating speed (M_T=0.8) and observation angle (α=60°). If for

example the rotor had only one blade (all other things being equal) then the steady load radiation would have been 140dB at the first harmonic. Or at supersonic speeds the steady load line s=0 would become horizontal at $\sigma=0^{\circ}$ (see fig. 10,(1)) and the steady load radiation then dominates the spectrum irrespective of blade number.

However in this particular situation the steady load contribution to the first harmonic is only 28dB and the harmonic falloff given by Y_q is 4.6dB per mB. The spectrum is therefore generated by impulsive loading caused through rotor-stator interaction. Here because of the large number of load excursions E, the acoustic spectrum will be given by equation 19. The first and second sound pressure harmonics $m_1=1$, $m_1=2$ of the first stage compressor can be seen dominating the spectrum at mB=23 and 46. The first harmonic $m_2=1$ of the second stage is at mB=31 and the first harmonic $m_3=1$ of the third stage is at mB=46. The subharmonics at multiples of mB where B=1, is caused through unequal blade forces as explained previously.

Because of the high shaft speed and large blade number, the separation between the first and second sound pressure harmonic of the first stage is almost 7 KHz and practically the entire audible acoustic spectrum 0-14KHz is covered by these first two harmonics. (It is interesting to compare this spectrum with the equivalent first two harmonics of the helicopter rotor spectrum which covers only 24Hz). The passbands for the first and second blade loading harmonic s=1, s=2 for the first stage are shown in dotted outline. It can be seen that only the s=1 blade loading harmonic contributes to the first sound pressure harmonic and s=1 and s=2 to the second. The first harmonic is right at the end of its passband and by reducing the rotor tip speed a little, the passbands will shrink accordingly thus cutting off the first harmonic. From equation 30 the blade loading coefficient at the first harmonic mB=23 is $a_{23} = -47$dB or $\frac{1}{300}$th approximately.

References

(1) S.E. Wright 1971 J. Sound Vib. Vol 17(4), Discrete Radiation from Rotating Sources.

(2) S.E. Wright 1969 J. Sound Vib. Vol 9(2), Sound Radiation From a Lifting Rotor.

(3) R. J. Pegg 1970 Symposium on Environmental Effects on VTOL Design, Arlington, Texas.

(4) J.W. Leverton and F.W. Taylor 1966 J. Sound Vib. 4(345) Helicopter Blade Slap

(5) E.A. Bartsch 1968 USAAVLABS Tech Rept 68-22A,In-Flight Measurements on XH51A.

(6) J. Crigler 1971 NASA Tech Rept shortly to be published.

(7) D. Chestnutt and L.R. Clark 1970 NASA TN D-5507, Effects Of Inlet Guide Vane Configuration on Noise From Compressors.

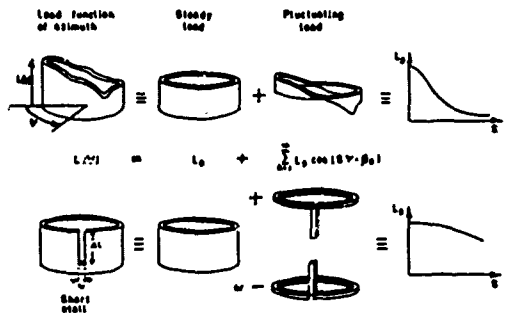

Fig. 1 Azimuth blade loading analysis

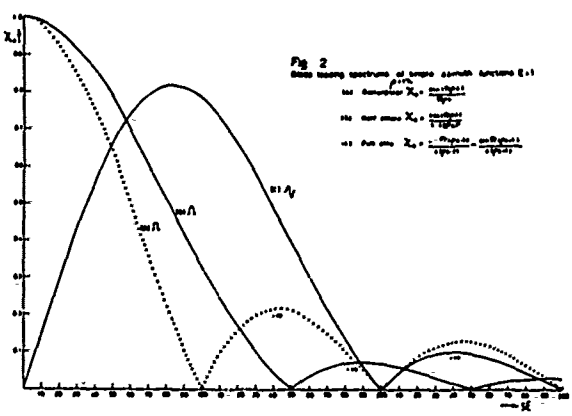

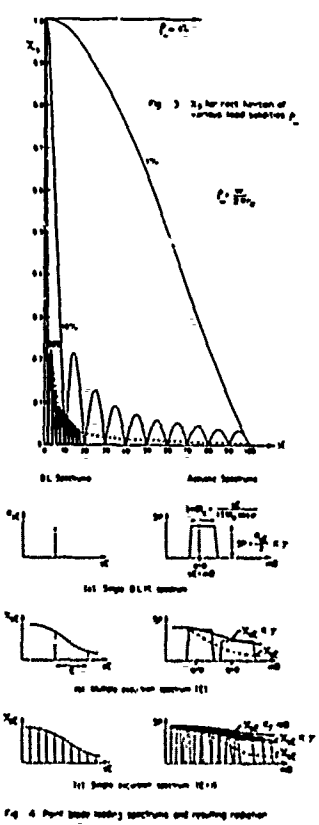

Fig 4

25

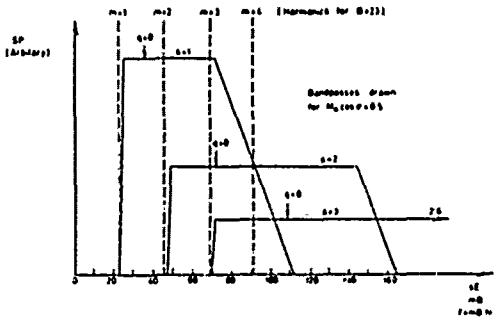

Fig 5 Multiple excursion rotor spectrum E=36

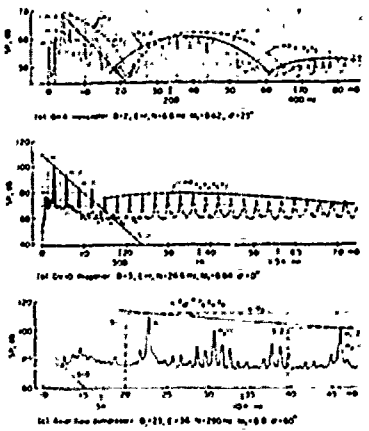

Fig 6 Measured rotor spectrums

An Investigation of Noise Generation on a Hovering Rotor

H. Sternfeld

and

R. H. Spencer

with a discussion of the

Deductive Development of Aerodynamic Criteria for Hovering Single Rotor Impulsive Noise Generation

C. J. Bobo

and

R. F. Child

The Boeing Company

Vertol Division

INTRODUCTION

This paper presents the results of a program of helicopter rotor noise measurement. The program was carried out using a 3 bladed 60-foot-diameter CH-47B rotor on the Boeing-Vertol engineering rotor whirl tower. The primary objectives of the program were:

1. To obtain acoustical data over a frequency range wide enough to define all elements of rotor noise under well-documented ambient conditions.
2. To measure the tip vortex position with respect to a trailing blade using high-speed cameras and smoke to visualize the tip vortex, and to relate blade-vortex separation distance to noise level.
3. To determine the propagation characteristics of rotor noise.
4. To evaluate two current analytical procedures for predicting rotor noise (Ref. 1, 2) against the measured data.

The testing on the 60-foot-diameter rotor encompassed a range of tipspeeds from 600 to 900 fps and thrusts from 6,300 lb to 32,000 lb (disk loadings of 2.2 to 11.3 psf). There have been several programs aimed at measurement of pressures on the surface of a rotor blade, [3, 4, 5] but these studies have been concerned with rotor performance and have not recorded data with sufficient frequency response to be useful in noise research. For the most part this was due to the general unavailability of adequate instrumentation. Several programs have also been performed [6, 7] to collect noise data in the near and far field of the rotor and at several positions of rotor azimuth. Much of this data has been obtained on flight aircraft and therefore includes all other noise sources inherent in such a vehicle. In at least one other program, smoke has been released at the tip of a blade to study the blade wake in terms of the position of the tip vortex.[10] However, no data in terms of a complete noise measurement program has been published for adequate study of the generation and propagation of the noise of helicopter lifting rotors.

The concept of the program described in this paper was (a) to clarify the situation (at least in part) by dealing with the simplest case, namely a single hovering rotor, (b) providing instrumentation adequate to the task of defining the complete acoustical signature, (c) devising a test technique which would, insofar as possible, permit separate identification of the noise sources, and then to (d) compare these results with current "state-of-the-art" analytical predictions in order to more accurately assess current capabilities and to identify the more serious shortcomings.

The rotor system, tested in this program is that designed for the Army CH-47B "Chinook" helicopter and is a three-bladed, fully articulated rotor of 30 feet radius and 25.25 inch chord.

The individual rotor blades are fabricated from a steel "D" spar with fiberglass laminate covered trailing edge boxes. The airfoil is a 23010-1.58 section as shown in Figure 1 and the blade is untapered in either planform or thickness. The tip of the blade terminates in a simple plate closing the outboard box, a "square tip". For the purpose of this investigation the blade was modified by the addition of smoke generators. The smoke generator canisters had been developed previously for a flight test program on a CH-46A helicopter [10].

The subject program was conducted on the Boeing-Vertol Engineering Rotor Test Facility (Figure 2). The rotor on this tower is 50 ft. above the ground and is powered by a 10,000 hp electric motor which drives through a water-cooled clutch. The electric drive, along with suitable gear reduction system, is housed in the concrete base of the structure. This base serves to minimize the drive system noise radiated outside to a level which is negligible when making

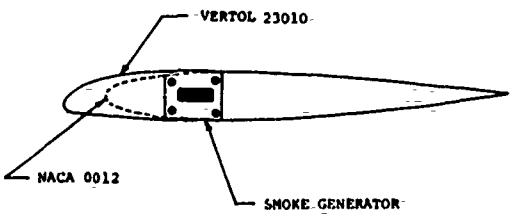

Figure 1 Test Airfoil

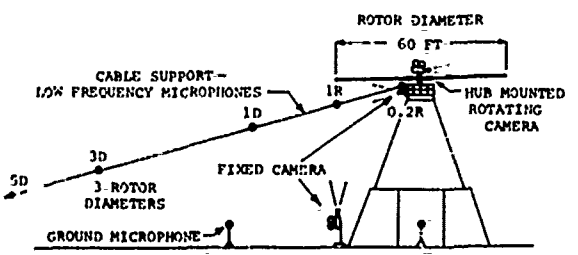

Figure 2 Rotor Test Tower

rotor noise measurements. The fundamental control modes available are rotor speed, and thrust which is achieved through collective pitch. No cyclic pitch, or shaft angle variation was utilized. Rotor rpm readout is available to the tower operator and rotor speed can be maintained to an accuracy limited by variations in ambient wind, generally to within 1 rpm.

The microphones used were of the condenser type and were located as illustrated in Figure 2. The microphones designated 0.2R, 1R, 1D, 3D, 5D were used to acquire the primary data. As shown, they were

supported by cables and arranged along a single path from a point just below the blade hub to the ground. The direction chosen permitted a large radial distance without proximity to other buildings or structures. In general, the microphone array was upwind of the rotor. These microphones were selected for this program because of their high sensitivity at low frequencies as well as flat frequency response characteristics. This is especially important for the study of rotational noise, where fundamental blade passage frequencies may be below 10 Hz. In specific, the microphones employed were Photocon 747 transducers with Dynagage DG-605D signal conditioners.

Ideally, it would have been desirable to have several radial arrays of these low frequency microphones, each along a different azimuth direction. Since program limitations and equipment availability precluded such an extensive system, it was decided to provide four monitor microphones located around the tower base as noted in Figure 2. These were Bruel and Kjaer Type 4131 condenser microphones of more conventional frequency range. In this program it was not intended that this information be made available, but rather that if the primary data should appear inconsistent, they would permit the possibility of determining whether a change in directivity of the radiated sound might be responsible for the inconsistencies.

The acoustical and atmospheric information was recorded on an Ampex FR-1300 wide band FM system operating at a tape speed of 30 ips. The acoustical inputs were continuously monitored on individual oscilloscopes to determine the required attenuation, or amplification in order to ensure optimum quality data with a high signal to noise ratio. The use of monitoring oscilloscopes also permitted the engineer to observe noteworthy changes in noise characteristics as the test progresses. The Boeing-Vertol Mobile Acoustical Laboratory was used as a test control center for data acquisition. Figure 3 shows several views of the instrumentation employed. Prior to the test program each complete data system was calibrated. A system was defined as a combination of microphone transducer, cathode follower, cables, signal conditioner, and recording track. Once calibrated, the elements remained as a non-interchangeable system for the remainder of the program.

Since the program was essentially a hover program, small changes in ambient wind conditions could become important. To monitor ambient conditions, an anemometer and wind vane were erected on a 50 foot high mast approximately 150 ft. from the rotor tower. This tower located the instrumentation at the same height above the ground as the rotor, but kept it far enough away to be relatively unaffected by the rotor downwash. The output of the velocity indicator was recorded directly on the magnetic tape along with the sound pressure level data. Ambient temperature and barometric pressure were measured at ground level but not recorded on tape. These data were used both for correlation with the acoustical information and for the tower torque/thrust calibration. Prior to the test program, an evaluation was made to determine the influence, if any, of the tower structure, nearby buildings, and the terrain itself on the acoustical signals sensed by the microphones by

MOBILE LABORATORY AND TAPE VAN

WEATHER INSTRUMENTS IN MOBILE LAB

SMOKE INSTRUMENTATION

WHIRL TOWER INSTRUMENTATION

Figure 3 Test Instrumentation.

reverberations tests conducted with 38 caliber blank revolver cartridges. The results of this are discussed later.

Smoke generators were ignited in the blade tips to mark the vortex. High speed motion pictures were taken of the smoke utilizing two cameras which were placed on the tower, one aimed toward the blade tip from just under the rotor at about 0.2R, and one aimed upward from the ground at the tower base. These two cameras provided vortex position measurements at one azimuth. Two additional cameras were mounted in the rotating system to measure the separation between a trailed vortex, and the blade which followed the vortex generating blade. In order to measure the films for vortex position, two cable grids with ping-pong balls securely attached for targets were used. Measuring the images of the targets and combining those measurements with knowledge of the camera positions and the target positions produced the desired blade and vortex positions.

DATA REDUCTION

The primary analysis used for the reduction of the acoustical data employed techniques and equipment referred to as Real Time Digital Analysis. Application of this relatively new technique to the study of rotor noise is one of the major innovations of this program.

Before discussing the detailed application of the processing to rotor noise data, it will be helpful to characterize some aspects of rotor noise and to agree on convenient terminology. First of all, it is important to recognize that any real data, even low wind hover, will display many transient changes due to uncontrollab

variables. These may be minor in nature, or may be so large that they completely dominate the acoustical signature. For many purposes, especially when comparing data with analytical predictions, it is important to know whether the data under discussion is invarient with time or contains the aforementioned transients. In this paper, all data will be defined either as "steady state", implying that it is valid at any time, or as "transient", implying that it is only valid at a particular instant in time.

A second set of definitions which apply to the frequency (rather than the time) domain are the terms 'discrete' and 'broadband' which describe the amplitude-frequency distribution. There is no rigorous definition of discrete but it can be easily understood that it implies a concentration of acoustical energy in a rather narrow range such that the levels at adjacent higher and lower frequencies are significantly less. It should be kept in mind that these discrete frequencies may be harmonically related to the rotor passage, (and to each other) or may be independent if produced by a non-harmonic source.

In this program, steady state harmonic analyses were used for comparison with analytical predictions, while transient analysis was used to study tip vortex noise phenomena. In order to compare the broadband vortex noise with analytical prediction, conventional octave band analyses were performed using analog equipment (B&K 2112 Spectrum Analyzer and B&K 2305 Level Recorder). This method was used because the prediction method is essentially a statistical matching of data with blade operating parameters.

RUN 54
TIP SPEED 750 FT/SEC
THRUST 19000 LB

.2 RAD.

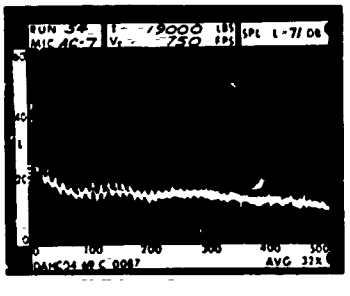

1 RAD.

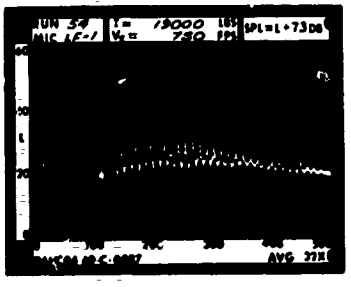

Figure 4

1 DIA.

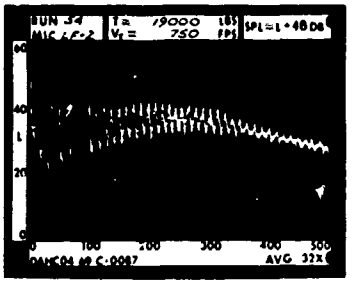

3 DIA.

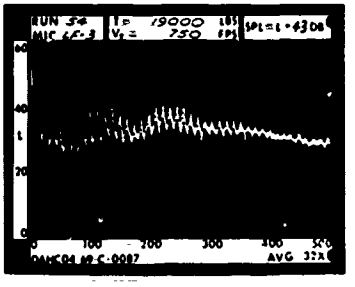

5 DIA.

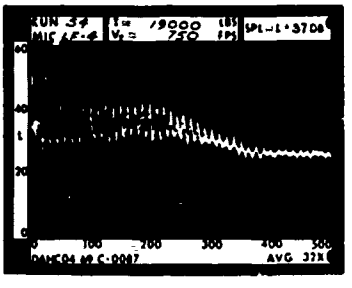

Figure 4

DISCUSSION OF RESULTS

A fundamental purpose of the program was to document the noise of a rotor over a broad range of test variables and under conditions which were closely monitored. This was accomplished with a recording system which, as previously described, had a frequency response which had no sensitivity variation over a frequency range of 2 - 5000 Hz and was within 2 db of the nominal value over the range 5000-10,000 Hz.

The basic data was analyzed for the range 0-500 Hz and averaged over 32 rotor cycles to preserve definition of individual harmonics of blade passage for a broad frequency range. A representative matrix of data was also analyzed over the frequency range 0-10,000.

Figure 4 presents a typical set of data.

REVERBERATION

The influence of reflective surfaces, including the ground plane, was investigated and it was shown that data from microphones at 0.2R, 1R and 1b were not generally degraded from acoustical reflection. However, data observed at the 1b and 3b locations were not free field. Agreement between the prediction and

measurement is evidence that only the ground reflected wave was the major source of interference. Destructive interference of the ground reflected ray with the unreflected incident wave occurs in the range of signal frequencies which correspond to one-half the wavelength of the period associated with the time delay between incident and reflected wavefronts. The pressure amplitude at a microphone resulting from the incident and time delayed reflected wave is,

$$P_{3D} = P_o \sin \omega t + aP_o \sin \{\omega(t + \Delta t)\}$$

P_o = Pressure amplitude of original wave

a = attenuation coefficient

Δt = time delay of reflected wave (sec)

ω = sound frequency (rad/sec)

expanding,

$$P_{3D} = P_o \sin \omega t + aP_o \sin \omega t \cos \omega\Delta t + \cos \omega t \sin \omega\Delta t$$

$$= P_o \sin \omega t (1 + a \cos \omega\Delta t) + (aP_o \sin \omega\Delta t)(\cos \omega t)$$

$$= P_o a' \sin (\omega t + \gamma)$$

where $a' = \{(1 + a \cos \omega\Delta t)^2 + a^2 \sin^2 (\omega\Delta t)\}^{1/2}$

and $\gamma = \tan^{-1}\left[\frac{a \sin (\omega\Delta t)}{1 + a \cos \omega\Delta t}\right]$

In the form of the identity,

$$a' = [1 + 2a \cos \omega\Delta t + a^2 \cos^2 \omega\Delta t + a^2 \sin^2 \omega\Delta t]^{1/2}$$

or $$a' = [1 + 2a \cos \omega\Delta t + a^2]^{1/2}$$

The measured sound level at 3 diameters is

$$SPL_{3D} = SPL_o + 20 \log a'$$

where SPL_o is the level from the incident wave only.

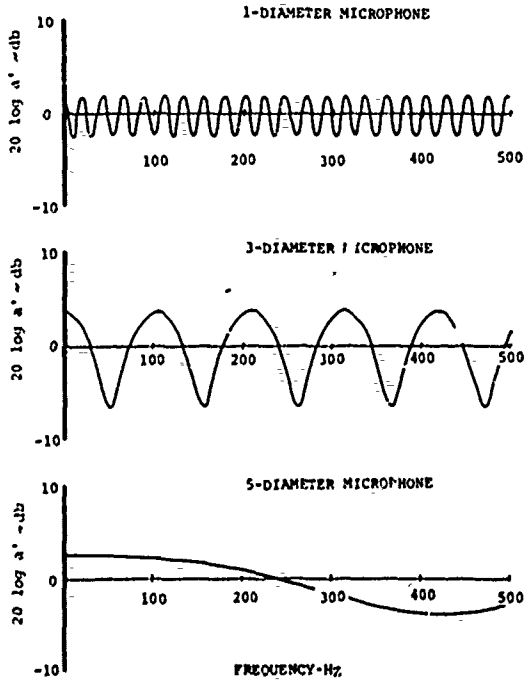

Figure 5 Signal Amplification Due to Reflection.

Evaluation of the attenuation coefficient, a', then permits a correction to be made to obtain free field data. 20 log a' is plotted as a function of frequency in Figure 5.

HARMONIC

Predicted levels for the test rotor have been compared with measurements (e.g. Figure 6) for those frequencies which are identifiable as harmonics of blade passage. The theory of Reference 1 has been corrected for the specific test site conditions for reflection, by the method developed, and the reflected wave amplitude has been corrected for source directivity. The underprediction, as noted by Lowson, is thought to result from the lack of adequate high harmonic sensitivity of the instrumentation which measured airloads utilized by him in developing the theory. This difference between predicted and measured levels is also illustrated in Figure 7, the zero reference being the data value.

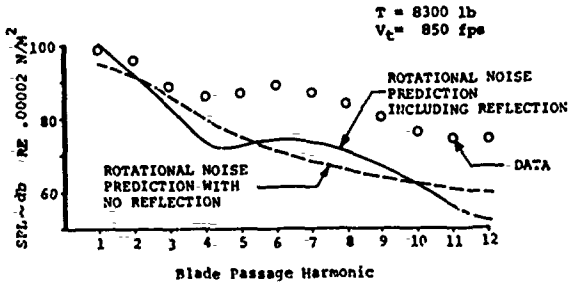

Figure 6 Comparison of Harmonic Data with Theory of Ref. 1

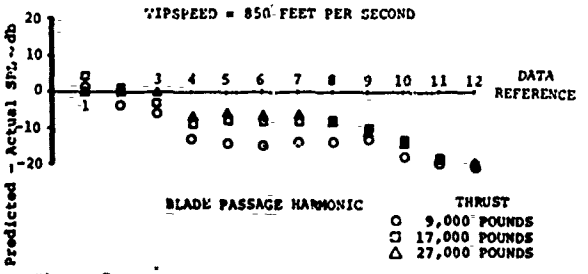

Figure 7 Normalized Comparison of Harmonic Data With Theory.

Comparisons of the data with predictions in terms of tip Mach number and thrust coefficient were also made. Good agreement was also displayed at harmonic numbers of blade passage below five. Because of this agreement, at low harmonic numbers, the fundamental blade passage frequency was used in investigating data trends with tip speed, illustrated in Figure 8. The data shown for the lowest thrust, displays a 5.3 power law trend. This slope decreases with increasing thrust to n = 3.4. Straight lines were fit to the data by the method of least squares. Power law trends at the low thrust values are in conformance with other published data.

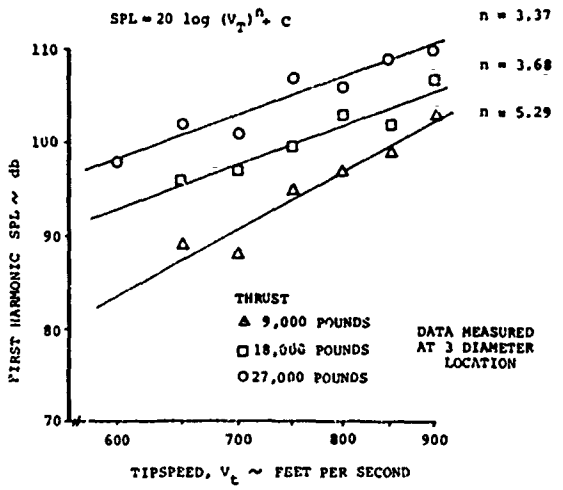

Figure 8 Tipspeed Trends.

It can be generally concluded that the low harmonics of blade passage are predictable in that they can be estimated to within 5 db of the measurement value, at least over the range of operating conditions investigated in this program. Further, it is not surprising that the best agreement between theory and data is in the same range of tip speeds and thrusts as the airload data which Scheiman reported and which Lowson utilized for development of his Reference 1 theory. Airloading data with improved high harmonic content appears to be the solution to increased accuracy of noise prediction of lifting rotors.

BROADBAND NOISE

Table I presents a comparison of methods for broadband noise prediction developed by other researchers working in helicopter noise. The constants in the expressions presented account for the field point where comparison data was obtained. Predictions have been made for only one data point.

TRANSIENT IMPULSIVE NOISE

In previous investigations of the noise generated from a hovering rotor as reported in Reference 9, a transient, impulsive noise was observed above the relatively constant rotational noise. This noise dominates the signature and becomes greater in magnitude with increasing tip speed and thrust. It had been previously

TABLE III
COMPARISON OF VORTEX NOISE PREDICTION METHODS WITH MEASURED DATA

AUTHOR	FORM	f MAX	PREDICTION dB	DATA dB
MUSPARD	$SPL_{180} = 10 \log \left(\frac{KSV_{87}^6}{10^{16}}\right) + 4.6$			EQUIVALENT TO OVERALL VORTEX NOISE LEVEL
SCHLEGEL KING & MULL	$SPL_{180} = 20 \log V_{0.7} + 20 \log T - 10 \log A_b - 31.3$	$\frac{0.28\ V_{0.7}}{n}$	86.1	102
DAVIDSON & HARGEST	$SPL_{180} = 23 \log V_t + 20 \log T - 10 \log S - 16.5$		104.0	102
STUCKEY & GODDARD	$SPL_{180} = 26.8 \log V_t + 16.6 \log T - 20 \log \sec \phi - 49.2$	$\frac{0.18\ V_t}{0.4r}$	98.6	102
LEVERTON	$SPL_{180} = 40 \log V_t + 10 \log S - 91$		104.1	102

V = BLADE VELOCITY 750 FT/SEC
T = ROTOR THRUST 19,000 LB.
S = A_b = BLADE AREA 182.5 FT^2
r = DISTANCE TO MICROPHONE 180 FT
ϕ = ANGLE BETWEEN TIP LOCATED DIPOLE AXIS AND MICROPHONE

hypothesized that this impulsive signature was due to blade-vortex intersections and, therefore, smoke visualization of the vortex was used to measure vortex position in order to correlate blade-vortex separation with recorded noise level. Figure 9 illustrates typical results from the vortex position analysis. These measurements and extrapolations indicate that intersections occur for all the conditions observed. Of special interest is the fact that intersections were observed for a low thrust condition (Figure 9b) for which no transient impulsive noise was observed, and for a higher thrust condition, Figure 9a, which did display a transient impulsive noise in its signature. Thus any correlation between separation and the occurrence of this impulsive noise is not meaningful.

Since the existence or absence of transient impulses in an acoustical signature cannot be determined by the existence or absence of blade-vortex intersections alone, one of the following conclusions can be drawn: (a) the vortex does not enter into the requirement for impulsive noise generation, or (b) the presence of the vortex is not the total determinant of impulsive noise generation. Discussion of this is continued in the following section along with a possible mechanism of generation of single rotor transient noise.

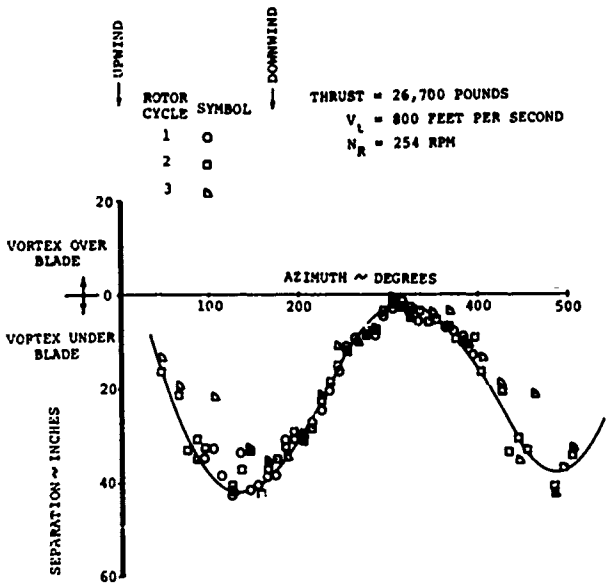

Figure 9a Blade Vortex Separation Measurements With Rotating Camera

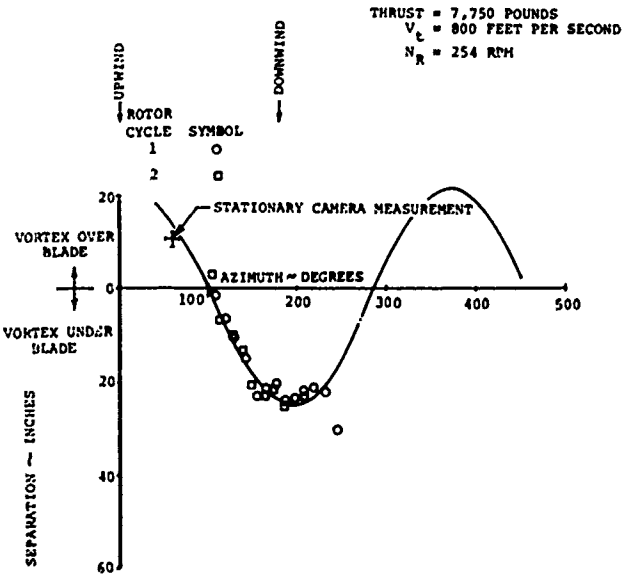

Figure 9b Blade Vortex Separation Measurements With Rotating Camera.

LITERATURE CITED

1. Lowson, M. V., and Ollerhead, J. B., Studies of Helicopter Noise, U.S. Army Aviation Materiel Laboratories Technical Report TR 68-60, January 1969.
2. Schlegel, R. G.; King, R. J.; and Mull, H. R., Helicopter Rotor Noise Generation and Propagation, U.S.Army Materiel Laboratories Technical Report TR 66-4, October 1966.
3. Pruyn, R. R., In-Flight Measurement of Rotor Blade Airloads, Bending Moments, and Motions, Together With Rotor Shaft Loads and Fuselage Vibration on a Tandem Rotor Helicopter, U.S. Army Aviation Materiel Laboratories Technical Report TR 67-9, May 1967.
4. Scheiman, J., A Tabulation of Helicopter Rotor-Blade Differential Pressures, Stresses, and Motions, as Measured in Flight, National Aeronautics and Space Administration, NASA TM-X-952, Washington, D.C., March 1964.
5. Burpo, F. B., and Lynn, R. R., Measurement of Dynamic Airloads on a Full Scale Semi-Rigid Rotor, U.S. Army Transportation Research Command Technical Report TR 62-42, December 1962.
6. Spencer, R. H., and Sternfeld, H., Measurement of Rotor Noise Levels and Evaluation of Porous Blade Tips on a CH-47A Helicopter, U.S. Army Aviation Materiel Laboratories Technical Report TR 69-18, September 1969.
7. Stuckey, T. J., and Goddard, J. O., Investigation and Prediction of Helicopter Rotor Noise: 1 - Wessex Whirl Tower Results, Journal of Sound and Vibration, Volume 5, Number 1, pp. 50-80, January 1967.
8. Hubbard, H. H., and Regier, A. A., Propeller Loudness Charts for Light Airplanes, NASA TN 1353, Washington, D.C., July 1947.
9. Sternfeld, H., and Spencer R. H., Recent Research in Rotor Noise Reduction, Paper Presented at National Aeronautic and Space Engineering and Manufacturing Meeting, Los Angeles, California, October 6-10, 1969.
10. Sternfeld, H., and Schairer, J. O., Study of Rotor Blade Tip Vortex Geometry for Noise and Airfoil Applications, Naval Air Systems Command Contract N00019-68-C-0608, Boeing-Vertol Document D8-2464-1A, December 1969.

STUDIES RELATING TO STEADY AND UNSTEADY AERODYNAMICS OF HELICOPTER ROTORS

by

Barnes W. McCormick
Department of Aerospace Engineering
The Pennsylvania State University

Abstract

This paper describes the results of research projects which are presently being undertaken by the Department of Aerospace Engineering, The Pennsylvania State University, relating to the steady and unsteady aerodynamics of helicopter rotors. Emphasis is placed in particular on the ARO-D sponsored project which is concerned primarily with blade motion and air loads for large helicopters. In addition, however, results of a rotor-vortex interaction study, including a short sound movie are presented. In the ARO-D project means are being explored for reducing the excessive flapping to be expected with large rotors. Using a Lagrangian approach, equations of motion have been developed for coupled flapping, lead-lag and torsional motion. A modified Bernoulli-Euler (slender beam) theory considers the effects of rotary inertia and shear deformation. The numerical solution is designed to handle an arbitrary elastic restraint at the hub as well as a general spanwise and chordwise distribution of mass and structural stiffness. Instantaneous airloads are calculated, knowing the blade's motion, by starting the rotor at rest and calculating the position of the free wake which is generated as the steady operating condition is approached.

The analytical problem of the aerodynamic forces caused by a partial span, oscillating jet flap on a helicopter rotor blade is being investigated as a means of reducing the flapping. An asymptotic expansion technique used to solve the steady-state problem of a full-span jet on a three-dimensional wing, is being applied to the unsteady problem of a jet-flapped wing. The boundary conditions for the wing and jet have been altered to include the unsteady effects and the expansions for velocity potential are being written with the reciprocal of aspect ratio as the small parameter.

A study is underway to design a device capable of controlling the jet flap position. The device would in some manner sense the rotor blade displacement and accelerations to control the jet flap to a position related to the motion. Of particular interest are fluidic control devices because of their mechanical simplicity and available power from the jet flap pressure chamber. A two-dimensional model of the device will be built and investigated in a wind tunnel.

(1) Sponsored by NASA Langley under contract NGR-39-009-111

(2) Sponsored by ARO-Durham under contract DA-ARO-D-31-124-71-G13

Introduction

The Department of Aerospace Engineering at The Pennsylvania State University has been undertaking studies[1] relating to helicopter noise for approximately three years. More recently studies have begun[2] on unsteady aerodynamic problems specifically related to very large helicopters. This paper, in a sense, is a progress report on all of these studies and presents future plans as well as some of the results obtained to date.

The NASA supported studies have been concerned with the rotor-blade, vortex-interaction problem. Both experimental and analytical studies are being conducted. Presently, a modification to our subsonic wind tunnel is being completed which will allow more meaningful noise measurements to be made. A some sacrifice in velocity, the test section has been increased in size from 3' x 3' to 4' x 5'. In addition an anechoic chamber has been purchased which will surround the open-jet configuration of the new test section. Once back in operation, the interior of the tunnel will be treated acoustically in incremental steps to study the effects of such treatment on the ambient noise and test section flow.

The results which have been obtained to date include unsteady pressure measurements on a single-bladed rotor which sweeps through a vortex trailing from a wing mounted in the tunnel ahead of the rotor. Most of these results have already been recorded in references 1 and 2. Some analytical results, which have not received wide dissimination, are to be found in reference 3. Here, numerical calculations of the unsteady flow about a two-dimensional airfoil are presented. A free, point vortex placed in the flow far ahead of the airfoil is carried past the airfoil generating an unsteady pressure distribution on the airfoil. The predicted form of the time-dependent pressure distribution is shown to be similar to the experimental measurements obtained with the rotor in the wind tunnel. Related to the vortex-interaction problem are the results of a brief analysis which the author performed while a consultant to the U.S. Army Aeronautical Research Laboratory at NASA Ames. A recent extension of this work has shown that a simple two-dimensional approximation to the rotor blade slap problem predicts reasonably well the noise spectrum for such a rotor.

The ARO-D studies are concerned primarily with the dynamics of large helicopter rotors and possible means of reducing excessive flapping associated with such rotors. Using a Lagrangian approach, equations of motion are being formulated for coupled flap, lead-lag, and torsional motion of an arbitrarily restrained elastic blade. Hopefully it is planned to calculate the instantaneous air loads for the rotor blade using a free wake analysis beginning with the rotor blade at rest. Initially, however, the usual strip method will be used for determining the air loads in order to proof the numerical problem for calculating the rotor dynamics.

The possibility of reducing the blade flapping by means of an oscillating jet flap is being investigated. The position of this flap will be controlled by sensing in some manner the rotor

blade displacement and acceleration. The analytical formulation of the problem is presently underway and an asymptotic expansion technique, which has been applied to the steady-state problem, is being extended to the unsteady jet-flapped wing. Presently a fluidic control system is being considered for control of the position of the jet flap. It is planned to construct and test a two-dimensional model of such a device.

Vortex Interaction Studies

The experimental apparatus pictured in figure 1 is described in detail in reference 1. This single-bladed, counter-balanced rotor blade as a 1 foot radius, 2 inch chord, a 0015 airfoil section and is equipped with 5 miniature absolute-pressure transducers. Measurements have been made to date of the unsteady chord-wise pressure distributions at the .75, .85, .9 and .95 radius stations for various vortex strengths, rotor advance ratios and rotor positions relative to the vortex center. Typical results are presented in figures 2, 3, and 4.* These measurements were obtained by recording photographically the outputs from the pressure transducer on an oscilloscope. The photographs were then transferred to IBM cards using a trace reader and the results measured on one side of the blade matched with the corresponding results from the other side and processed through a digital computer. From measurements such as these the following tentative conclusions have been drawn.

1. The maximum lift coefficient difference, ΔC_l, and their time variations, as defined in figure 2, are a maximum when the rotor intersects the center of the vortex.

2. Values of ΔC_l at high as 1.15 at 0.75R and 0.75 x 10^3/sec for $\frac{\Delta C_l}{\Delta t}$ at 0.9R were measured in the present experiments.

3. ΔC_l and $\frac{\Delta C_l}{\Delta t}$ increase approximately linearly with vortex strength with the slopes being different for different rotor plane

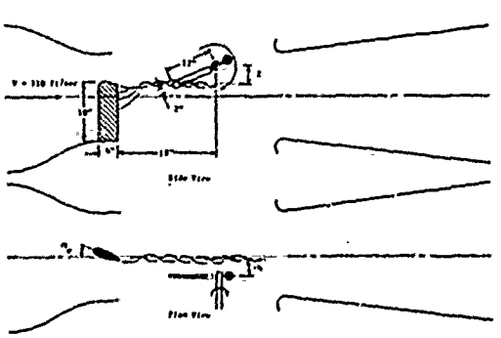

Fig. 3 Schematic Layout of the Test Rig in the Wind-Tunnel

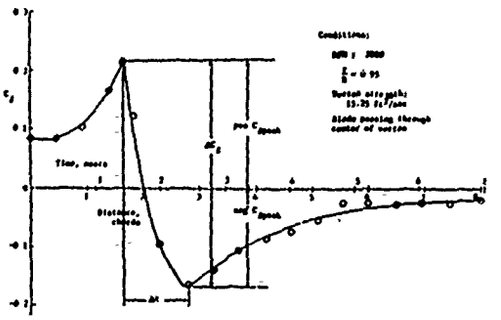

Fig. 2 Typical Section Lift Coefficient Variation on Rotor Blade

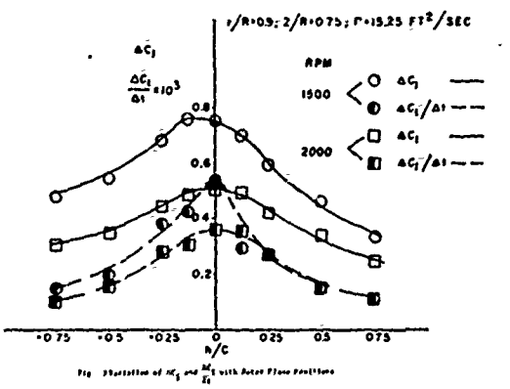

Fig. 4 Variation of ΔC_l and $\frac{\Delta C_l}{\Delta t}$ with Rotor Plane Position

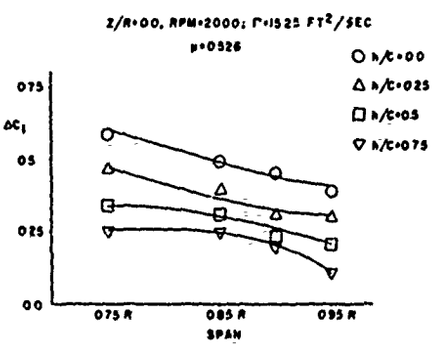

Fig. 5 Variation of ΔC_l with Span

4. ΔC_l at each span station increases as the shaft axis is moved away from the vortex axis (i.e. as the intersection angle decreases).

5. At a particular Z/R, ΔC_l at the inboard span stations are higher than those at the outboard span stations. However, no definite trend exists in the case of the time variation of maximum lift difference; i.e., $\frac{\Delta C_l}{\Delta t}$.

A two-dimensional formulation of this problem was performed in reference 3. The procedure is illustrated in figure 5. Here a thin airfoil is divided into increments with a discrete vortex placed at the "quarter-chord" point of each segment with the boundary condition being satisfied at the "three quarter-chord" point of each segment. The vortex, at zero time, is placed in the flow far ahead of the airfoil. The ensuing unsteady problem is then calculated as the vortex is allowed to move with the flow past the airfoil. At each succeeding time increment induced velocities are calculated at the position of the free vortex and each control point along the airfoil. The strength of the discrete vortices are then found which will satisfy the boundary conditions.

Having determined these the unsteady pressure distribution on the airfoil is then predicted using the unsteady Bernoulli equation which leads to the following expression for the instantaneous lift.

$$L = \rho \int_0^c V_\infty \gamma(x)\, dx + \rho \int_0^c \left[\frac{\partial}{\partial t} \int_0^x \gamma(x)\, dx\right] dx$$

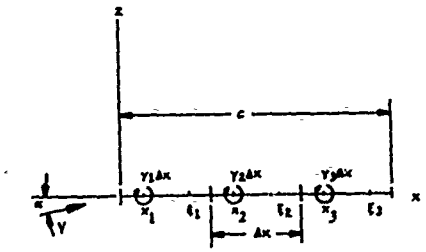

Figure 5

Simulation of Two-Dimensional Airfoil by Point Vortices

A typical result from reference 3 is presented in figure 6. In this instance the experimental results have been normalized in terms of the maximum peak lift coefficient to illustrate that the prediction of the form of the time-wise variation of the sectional lift coefficient agrees with the experimental result. The magnitude of the experimental results were considerably below those predicted by the two-dimensional analysis but as pointed out in reference 3 this discrepancy could easily be attributed to tip losses associated with the three-dimensional flow of the rotor. A typical comparison, corrected for such losses is presented in figure 7. For h/c values of .25 and .5 the predicted ΔC_l agrees fairly well with the measured results. However for h/c of 0.1 the two-dimensional predictions are high, probably due to the reduction in the tangential velocity in the vortex core which is neglected in the calculations.

More recently Johnson, as reported in reference 4, has developed a lifting-surface theory which is applicable to the rotor blade-vortex interaction problem. Although not shown on figures 2, 3 and 4, his results agree closely with the experimental measurements presented in those figures.

A sound movie accompanys this paper. This movie was taken as the plane of rotation of the rotor was gradually moved through the vortex generated by the wing ahead of the rotor. As this is done one can observe on an oscilloscope the output of a pressure transducer on the blade as it develops a sharp spike. Simultaneously the noise produced by the vortex interaction is distinctly heard.

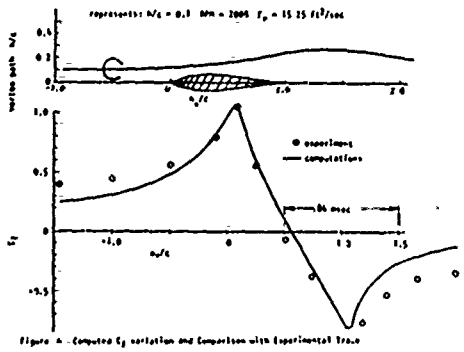

Figure 6 - Computed c_l variation and Comparison with Experimental Trace

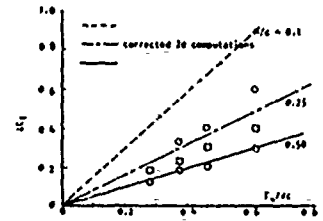

Figure 7a Computed ΔC_l Corrected for Tip Losses at 75% Station

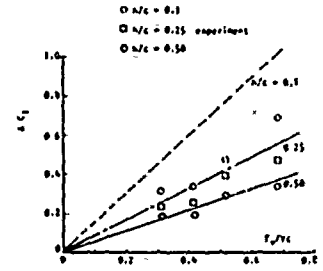

Figure 7b Computed ΔC_l Corrected for Tip Losses at 63% Station

An Approximate Relationship Between Blade Loading and Far-Field Noise for the Condition of Blade Slap

By comparison with the noise spectrum for a rotor without blade slap, the noise levels for the slapping rotor exhibits much higher harmonics than the ordinary rotor. If the assumption is made that the noise produced by blade slap predominates the rotor noise and is generated by a discrete dipole source resulting from a time-varying concentrated force, F(t), then it is possible to relate

F(t) to the noise spectrum. The time, through the rotor angular velocity, can be related to the azimuth angle ψ, hence $F(\psi)$ can be obtained from F(t).

The nonhomogeneous wave equation governing the radiation from a stationary dipole source is

$$\nabla^2 p - \frac{1}{c^2}\frac{\partial^2 p}{\partial t^2} = \nabla\cdot\bar{F} \qquad (1)$$

$\bar{F}$ being the external force per unit volume acting on the fluid. c is the acoustic velocity and p the pressure. The solution to this equation for a concentrated force F(t) can be found in several references and is given by

$$p(x,y,z,t) = -\frac{1}{4\pi}\,\mathrm{div}\left[\frac{\bar{F}(t-\frac{S}{c})}{S}\right] \qquad (2)$$

$\bar{F}(t-\frac{S}{c})$ means that $\bar{F}(t)$ is to be evaluated at the "retarded time," $(t-\frac{S}{c})$ with S being the distance from the source to the observer. To simplify the algebra, let us place the origin of the coordinate system at the concentrated force with the observer located in the x-z plane. The distance S then can be written as

$$S = \sqrt{x^2+z^2}$$

Also, to further simplify matters, let the direction of $\bar{F}$ be along the z-axis. Equation (2) then becomes

$$p(x,z,t) = \frac{1}{4\pi}\left[\frac{Fz}{S^3} + \frac{z}{S^2 c}F'(t-\frac{S}{c})\right] \qquad (4)$$

F' is the derivative of $\bar{F}$ with respect to time and, again, is evaluated at the retarded time. For the far field, the first term on the right side of Equation (4) will be small and is neglected leading to

$$p(x,z,t) = \frac{z}{4\pi S^2 c}F'(t-\frac{S}{c}) \qquad (5)$$

The above equation suggests the interesting possibility of integrating the output from a pressure microphone to obtain F(t) directly.

The curve labelled "with slap" in Figure (8), taken from reference (5), is a 10 cycle band width noise spectrum for a two-bladed rotor operating at 314 rpm and a tip Mach number of 0.9 on the advancing blade. The rotor diameter is 48' and the chord is 1.72'. The fundamental blade passage frequency is 10.5 hz.

Consider now the following closed-form solution which is a two-dimensional equivalent of the solution to the rotor obtained in reference (6).

Consider a row of blades spaced a distance D apart having a uniform chordwise loading as pictured in figure 9. The loading on each blade is zero except as a blade passes through a pulse F(x). Then the total chordwise load is F(x). The problem is to calculate

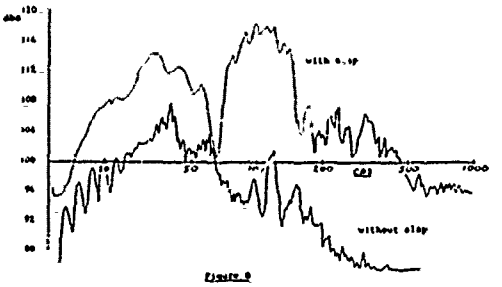

Figure 8

10-cps Bandwidth Helicopter Rotor Noise

the noise level at a point x_1, z_1 as a function of the chord, a; spacing, D; velocity, V; and F(x).

Assuming a concentrated force F(t) at x which radiates only when covered by the blade, F(t) will appear as shown in figure (10). F(t) is periodic with a period of D/V. Let

$$\theta = 2\pi\frac{t}{T} = 2\pi\frac{x}{D}$$

Then F(t) can be expressed as

$$F(t) = F_o + \sum_1^\infty F_n e^{in\theta} \qquad (6)$$

If we arbitrarily let $\theta = 0$ in the center of the pulse, then

$$F_n = \frac{F(x)\,dx}{n\pi a}\sin\frac{n\pi a}{D} \qquad (7)$$

and

$$F_o = \frac{F(x)\,dx}{2\pi a}\int_{-\frac{\pi a}{D}}^{\frac{\pi a}{D}} d\theta = \frac{F(x)}{D}\,dx \qquad (8)$$

Hence F(t) becomes

$$F(t) = \left[\frac{F(x)}{D} + \sum_{n=1}^{\infty}\frac{F(x)}{\pi a}\sin\frac{n\pi a}{D}\cos n\theta\right]dx \qquad (9)$$

Now θ was chosen to be zero for a time $t = (x + a/2)/V$. Hence,

$$\theta = \frac{2\pi}{T}\left[t - \frac{2x+a}{2V}\right] \qquad (10)$$

F(t) then becomes

$$F(t) = \left[\frac{F(x)}{D} + \sum_{n=1}^{\infty}\frac{F(x)}{\pi a}\sin\frac{n\pi a}{D}\cos\left(\frac{2\pi nVt}{D} - \frac{2\pi nx}{D} - \frac{n\pi a}{D}\right)\right]dx \qquad (11)$$

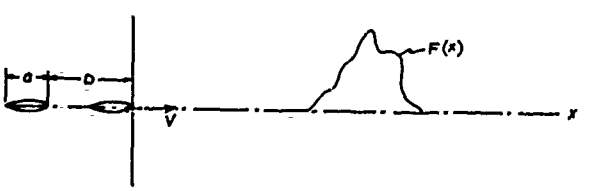

Figure 9

Spatial Variation of Force on Blade Row

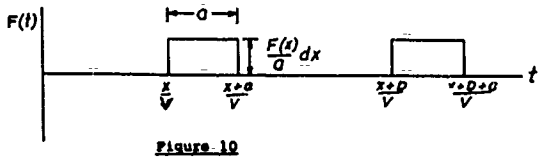

Figure 10

Time Variation of Force at X

In order to calculate the acoustic pressure p(x,z,t), from equation (5), the above is differentiated with respect to time. Hence for the far field,

$$p = \frac{Vz}{2\pi a D s^2 c} \sum_{n=1}^{\infty} \sin \frac{n\pi a}{D} F(x) \sin \left(\frac{2\pi n V T}{D} - \frac{2\pi n x}{D} - \frac{n\pi a}{D}\right) dx \qquad (12)$$

Now let us expand F(x) as follows

$$F(x) = A_0 + \sum_{k=1}^{\infty} A_k \cos \frac{2\pi k x}{\lambda} \qquad (13)$$

Substituting the above into the expression for p, the n^{th} harmonic of the mean pressure over one cycle becomes,

$$\bar{p}_n = \frac{Vz}{2\pi a D s^2 c} \frac{\lambda}{\pi\sqrt{2}} \sin \frac{n\pi a}{D} \sin \frac{n\pi\lambda}{D} \left[\frac{2A_0}{\frac{n\lambda}{D}} + \sum_{k=1}^{\infty} \frac{(-1)^k \frac{n\lambda}{D} \frac{2}{\pi} A_k}{\left(\frac{n\lambda}{D}\right)^2 - k^2} \right] \qquad (14)$$

To examine the behavior of the above consider the case where $A_k = 0$, i.e., F(x) is a pulse. In this case

$$\bar{p}_n = \left[\frac{Vz A_0}{\pi^2\sqrt{2}\, a s^2 c}\right] \frac{1}{n} \sin \frac{n\pi a}{D} \sin \frac{n\pi\lambda}{D} \qquad (15)$$

The above shows that $\bar{p}_n$ decreases as $\frac{1}{n}$ and further, if $\frac{na}{D}$ or $\frac{n\lambda}{D}$ should be close to an integer, $\bar{p}_n$ for these particular n values will be low.

The predicted noise spectrum, in db, will be given by 20 log $\bar{p}_n$, or

$$db = C_n + 20 \log \frac{1}{n} + 20 \log \sin \frac{n\pi a}{D} + 20 \log \sin \frac{n\pi\lambda}{D} \qquad (16)$$

In the above C_n is a constant of proportionality corresponding to the constant terms in the square brackets of equation (15).

Referring to figure 8 it appears likely that, for the slapping case, the sharp decrease in the levels at about 60 and 150 hz result from the width of the region of impulsive loading. A d/λ of 6.7 appears to fit the shape of the spectrum best corresponding to a ψ of 27°. D/a for this rotor is approximately 40, hence this term would not be expected to have much affect except near a frequency of approximately 400 hz.

Figure (11) presents again the spectra with blade slap of figure (8), together with equation (16) with and without the sin terms. The simple two-dimensional approximation to the slapping rotor appears to characterize the spectrum surprisingly well. The decrease of the maximum envolope above 10 hz. is predicted fairly closely as well as the shapes of the valleys and peaks.

Formulation of the Structural Dynamics of Elastic Rotor Blades

Presently rather complete equations defining the response of fully articulated elastic rotors to arbitrary aerodynamic forces are being formulated. Three degrees of freedom are being considered; flapping, lead-lag, and torsional. Generally these three motions are coupled, not only because of the structural properties of the blade, but also because of the nature of the aerodynamic forcing functions. The three unknown displacements which are functions of time and spanwise position will be obtained from three simultaneous equations derived using a Lagrangian approach. For a non-conservative system the Lagrangian form of the equations of motion are well known and can be written as

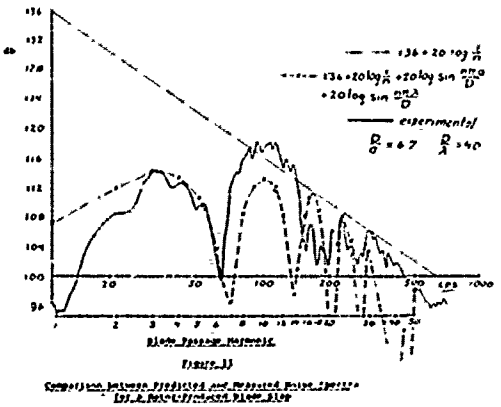

Figure 11

Comparison between Predicted and Measured Noise Spectra for a Rotor-Generated Blade Slap

$$\frac{d}{dt}\left(\frac{\partial L}{\partial \dot{q}_i}\right) - \left(\frac{\partial L}{\partial q_i}\right) = Q_i \qquad (i = 1, 2, 3) \qquad (17)$$

where L, the Lagrangian, is the difference between the total kinetic energy, T, of the blade and its potential energy, V. Q_i is a non-conservative force and q_i a generalized coordinate. The contribution to the total kinetic energy of the blade results from its linear and angular motions due to flapping, its in-plane linear and angular motions and the torsional deflections of the blade about its elastic axis. In writing the kinetic energy terms due to angular displacements of a modified Bernoulli-Euler beam theory is being used where both the angle of rotation of the beam cross section and the angle of shear deformation are considered. Hence the following two relationships are obtained by considering the flapping and lead-lag motions:

$$\frac{\partial}{\partial x}\left[w(x,t)\right] = \xi(x,t) + \gamma(x,t) = \beta$$

$$\frac{\partial}{\partial x}\left[h(x,t)\right] = \eta(x,t) + \tau(x,t) = \zeta \qquad (18)$$

where:

w = linear displacement of section in flapping from reference (Fig. 1))

h = linear displacement of section in lead-lag from reference (Fig. 1))

β = flapping angle of elastic blade

ζ = lead-lag angle of elastic blade

ξ = cross-section angle-of-rotation in flapping

η = cross section angle-of-rotation in lead-lag

γ = angle of shear deformation in flapping

τ = angle of shear deformation in lead-lag

The total potential energy of the blade is the sum of that due to gravity and the strain energy due to blade deflections. This latter energy must include the strains due to flapping, lead-lag, and torsional deflections as well as the strain due to stresses resulting from centrifugal forces. The gravity potential energy is written relative to the initial vertical displacement of the blade in its drooped position. With the Lagrangian being calculated as just described, the next step in deriving the three dynamical equations for a blade is to examine the dynamic equilibrium of a differential element of a blade. Such an element with the forces acting on it is shown in Figure 13. Here for simplicity only, flapping motion is considered. Notice that the rotary inertia term, $J_x \ddot{\beta}\, dx$, is considered in the equilibrium of the element and is an additional modification to the classical Bernoulli-Euler beam theory. If we take as a generalized coordinate, w, the displacement of the blade from a reference position of a pseudo-rigid rotor we then obtain,

$$\frac{d}{dt}\left(\frac{\partial L}{\partial \dot{w}}\right) - \frac{\partial L}{\partial w} = F_w \qquad (19)$$

where F_w is the sum of the non-conservative forces acting on the element. Summing moments about the center of mass results in

$$-\rho_1 I_z \frac{\partial^2}{\partial t^2}(\delta_e + \beta) = -\frac{\partial M_w}{\partial x} + S_w + F_c \sin(\delta_e + \beta) \qquad (20)$$

where ρ_1 is the blade mass per unit length and I_z is the moment of inertia about the z axis. These equations, (19) and (20), are related by the following equations

$$EI_z \frac{\partial^2 w}{\partial x^2} = -M_w(x)$$

$$\frac{\partial}{\partial x}\left[EI_z \frac{\partial^2 w}{\partial x^2}\right] = -\frac{\partial M_w}{\partial x} \qquad (21)$$

$$\frac{\partial^2}{\partial x^2}\left[EI_z \frac{\partial^2 w}{\partial x^2}\right] = -\frac{\partial^2 M_w}{\partial x^2}$$

After considering algebraic reduction the preceding equations reduce to the following equation governing the flapping motion of the blade.

$$\frac{\partial}{\partial x}\left[\rho_1 I_z \frac{\partial^2}{\partial t^2}(\delta_e + \beta)\right] = \left\{-\frac{1}{\cos\beta\, dx}\left[\frac{\partial}{\partial t}\left(\frac{\partial L}{\partial \dot{w}}\right) - \frac{\partial L}{\partial w}\right]\right. \qquad (22)$$

$$\left. + q_L - \frac{\partial F_c}{\partial x}\frac{\sin\delta_e}{\cos\beta}\right\} + \frac{\partial^2}{\partial x^2}\left[EI_z \frac{\partial^2 v}{\partial x^2}\right] + \frac{\partial}{\partial x}\left[F_c \sin(\delta_e + \beta)\right]$$

Similarly for the lead-lag motion,

$$\frac{\partial}{\partial x}\left[\rho_1 I_y \frac{\partial^2}{\partial t^2}(\delta_d + \eta)\right] = \left\{\frac{1}{\cos\eta\, dx}\left[\frac{d}{dt}\left(\frac{\partial L}{\partial \dot{\eta}}\right) - \frac{\partial L}{\partial \eta}\right]\right. \qquad (23)$$

$$\left. - q_D + \frac{\partial F_c}{\partial x}\frac{\sin\Gamma}{\cos\zeta}\right\} - \frac{\partial^2}{\partial x^2}\left[EI\frac{\partial^2 \eta}{\partial x^2}\right] + \frac{\partial}{\partial x}\left[F_c \sin(\delta - \Gamma)\right]$$

and for torsional motion,

$$\frac{d}{dt}\left(\frac{\partial L}{\partial \dot{\theta}_T}\right) - \frac{\partial L}{\partial \theta_T} = M_{\theta_T} + \frac{\partial}{\partial x}\left[GJ_x \frac{\partial \theta_T}{\partial x}\right] dx \qquad (24)$$

These then are the simultaneous equations which are to be solved for the two linear displacements, w and h, and the angular displacement, θ_t. The cross section of a typical blade is shown in Figure 14. Generally the three motions of the blade will be coupled since the center of gravity of each section, its elastic axes, and the center of pressure are not coincident. If the

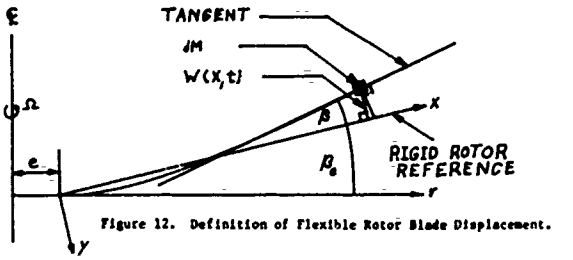

Figure 12. Definition of Flexible Rotor Blade Displacement.

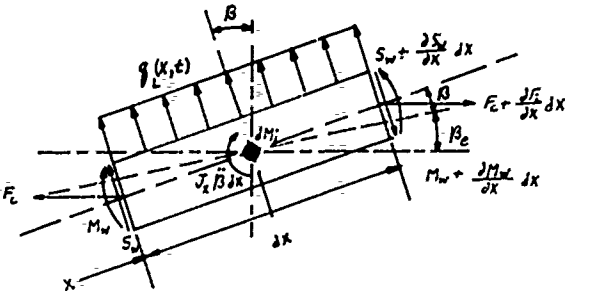

Figure 13. Equilibrium of Blade Element.

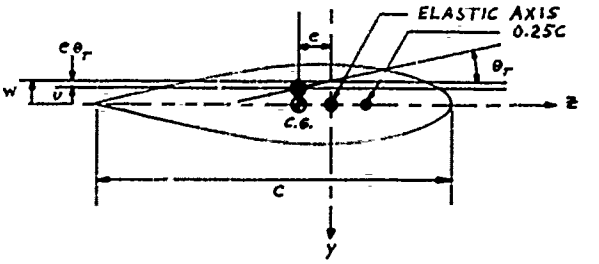

Figure 14. Typical Blade Section

elastic axis is displaced upward an amount w and the section is twisted through an angle of θ_t than the displacement of the CG from Figure 14 will be

$$v = w - e\theta_t$$

This coupling between the linear and angular displacement must be considered when writing the kinetic energy for the linear flapping motion. For example,

$$T_{BL} = \frac{1}{2}\int_e^R m V_B^2\, dx$$

where:

$$V_B = \left[(r - e)\dot{\delta}_e + \dot{v}\right]$$

$$= (r - e)\dot{\delta}_e + \frac{\partial w}{\partial t} - e\frac{\partial \theta_T}{\partial t}$$

Fortunately it has been shown by others that for a slender beam, the three dynamic equations (22), (23), and (24) can be uncoupled

before solving for w, h, and θ_t. In order to obtain the kinetic energies associated with the blade motions the blade will be divided into lumped masses and then a normal mode approach assumed of the form

$$w(x,t) = \sum_{i=1}^{m} \phi_i(x)\, q_i(t)$$

$$h(x,t) = \sum_{i=m+1}^{n} \phi_i(x)\, q_i(t)$$

$$e_o \theta_T(x,t) = \sum_{i=n+1}^{s} d_i(x)\, q_i(t)$$

where e_o is an arbitrary length defined so as to maintain consistent dimensions for the ϕ_i terms. $\phi_i(x)$ is the spanwise dependent function and $q_i(t)$ is the time dependent generalized coordinate. These functions which must satisfy the boundary conditions for the three types of displacements can be obtained from the uncoupled natural modes of the beam. Thus the equations are reduced to an Eigen-value problem which can be solved by the usual matrix method to obtain the natural frequencies and Eigenvectors for the generalized coordinates $q_i(t)$. In order to calculate the blade motion from these equations the blade will be started initially from rest at the static droop position. The instantaneous aerodynamic forces and moments acting on each blade section will be determined from a consideration of the local instantaneous velocities acting at the blade section. Ultimately it is hoped that this program can be combined with a free wake analyses of the rotor blade. It is realized however that such a program will be very time consuming and it may therefore take a considerable effort to evolve one which is economically feasible. In the interim some sort of a strip method, probably using a uniform downwash assumption, will be utilized to calculate the aerodynamic loads. In any event it is planned to account for reverse flow effects, blade dynamic stall and Mach number.

Studies of a Jet Flap for Rotor Control

In order to reduce the excessive flapping and coning associated with large helicopter rotors both analytical and experimental studies are underway to investigate the practicability of applying a controllable jet flap to such a rotor. It is not planned, at least at this time, to actually drive the rotor with the jet flap but rather to provide only enough jet blowing for the required control forces. The position of such a jet flap would be controlled automatically by sensing both the blade acceleration and its local angle-of-attack. These signals would be fed back to the jet flap in order to provide aerodynamic forces which would oppose the motion of the blade.

At the present time, because of its potential simplicity, the possibility of using a fluidic control system is being investigated. The same pressure sources which supply the flow for the jet flap could be used to power the fluidic device. One such possible scheme is pictured in Figure 15. Here the jet flap is basically a digital or bistable fluid amplifier. When a control flow, q_c, is applied through the lower control port the jet flap will separate from the bottom surface exiting through the top channel thus producing an upward deflection of the jet. A similar jet flap design considered by Eastman (Reference 12) was shown to require a control flow equal to approximately 11% of the primary flow at the jet flap. The stagnation pressure required in the control flow is also approximately the same fraction of the stagnation pressure in the mean jet; thus, there should be no difficulty in obtaining the required control power from the main plenum chamber.

There are two possible ways that a signal related to an angle-of-attack of a blade section can be obtained. First consideration is being given to measuring the difference in pressures between

Figure 15

JET FLAP DEVICE

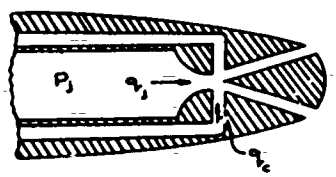

corresponding points on the upper and lower surfaces of the airfoil. Secondly, since the acceleration will be needed anyway, one might integrate this signal in order to obtain an output proportional to the vertical velocity of the blade. One difficulty here, however, might be the fact that this velocity is only one factor which determines the angle-of-attack. The acceleration sensor is envisioned as a jet of air which deflects under acceleration. The deflected jet thus enters one of two receivers and is then amplified to control the jet flap. The final control scheme which is devised will be tested in our 4 x 5 foot wind tunnel at a velocity of approximately 100 ft/sec. using a two-dimensional, jet-flapped airfoil model. From some preliminary considerations on the size of large helicopters it appears as if a range of reduced frequencies of from $\omega c/V = .06$ up to approximately .5 should be investigated. C_μ values as high as .6 should probably be studied corresponding to conditions on a retreating blade.

In addition to the experimental studies an analytical investigation to predict the performance of an oscillating 3-dimensional jet flap is being undertaken. Using a matched asymptotic expansion approach, the work of Tokuda (Reference 14) for the steady three-dimensional jet flapped wing is being extended to the unsteady case. Figure 16 illustrates the geometry of the problem.

The inner region is close to the wing, i.e. $X = \theta(\frac{1}{A})$ assuming a large aspect ratio wing whereas the outer region implies $X = \theta(1)$ away from the wing. The approach in this case is to expand the unsteady velocity potential and downwash in the regions using the reciprocal of aspect ratio as the small parameter. The so called

Figure 16

JET-FLAPPED WING

SIDE VIEW

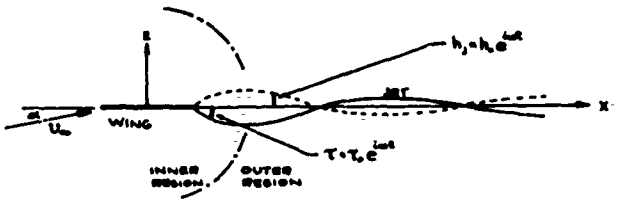

TOP VIEW

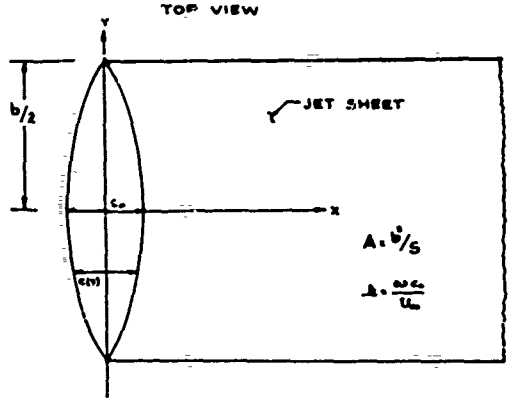

Inner and outer expansions are matched in the intermediate region along the X axis. Since the flow is assumed incompressible, Laplace's equation governs the problem.

$$\phi_{xx} + \phi_{yy} + \phi_{zz} = 0 \qquad (25)$$

The downwash boundary conditions are given as:

$$\text{on the wing } w_w(x,y,0,t) = 0 \quad -\frac{c(y)}{2} < X < \frac{c(y)}{2} \qquad (26)$$

$$\text{at the trailing edge } w_t(x,y,0,t) = U_\infty \tau_o e^{i\omega t} \quad X = C \qquad (27)$$

assuming small τ_o

$$\text{on the jet } w_j(x,y,0,t) = \frac{\partial h_j}{\partial t} + U_\infty \frac{\partial h_j}{\partial x} \qquad (27a)$$

$$= h_o(x,y) i\omega e^{i\omega t} + U_\infty \frac{\partial h_j}{\partial x} \qquad (27b)$$

The third boundary condition is arrived at from the assumption of small transverse momentum in the jet sheet (momentum in the y direction). The contention is that the edge of the jet does not begin to roll up until it is far enough downstream that it has a small effect upon the induced downwash in the near wake. Mashell and Spence (Ref. 15) give the pressure difference across the three dimensional jet sheet as,

$$p_l - p_u = k_x J(y)$$

k_x = curvature in streamwise direction

$J(y)$ = jet momentum flux per unit span

The y co-ordinate enters only as a parameter. The singularity due to flow discontinuity at the trailing edge has a small effect. Also, far from the wing and jet the flow must be uniform.

$$\phi \sim U_\infty X + U_\infty \alpha Z \qquad (28)$$

$$\text{as } X^2 + Y^2 + Z^2 \to \infty \; Z \neq 0$$

Outer flow:

To an observer in the outer region the large aspect ratio wing appears as a lifting line with a trailing jet sheet. The boundary condition on the jet sheet is satisfied directly whereas that on the wing must be satisfied through matching with the inner solution. The outer expansion is written as

$$\phi^o(x,y,z,t,\ 1/A) = \phi_1^o + \frac{1}{A}\phi_2^o + \frac{1}{A}2\ \phi_3^o + \ldots\ldots$$

$$\omega^o(x,y,z,t,\ 1/A) = \omega_1^o + \frac{1}{A}\omega_2^o + \frac{1}{A^2}\omega_3^o + \ldots\ldots \qquad (29)$$

At a fixed field point in the outer region there is no disturbance from the wing in the limit of very large aspect ratio so,

$$\phi_1^o = U_\infty X + U_\infty \alpha Y$$

$$\omega_1^o = U_\infty \alpha \qquad (30)$$

Inner flow:

In the inner region the velocity potential and the x and z axes are stretched as follows,

$$X = AX,\ Z = AZ,$$

$$A\Phi = \phi(x,y,z,t,\ 1/A)$$

$$\phi(x,y,z,t,\ 1/A) = \phi_1 + \frac{1}{A}\ \phi_2 + \qquad (31)$$

$$\omega(x,y,z,t,\ 1/A) = \omega_1 + \frac{1}{A}\ \omega_2 +$$

Laplace's equation becomes

$$\phi_{xx} + \phi_{zz} + \frac{1}{A^2}\phi_{yy} = 0 \qquad (32)$$

To obtain the first order inner solution, fix a field point x, y, z and let $A \to \infty$. From equation (32) the velocity potential is seen to satisfy the two-dimensional problem. Spence (Reference 16) has solved this problem and gives the jet height above the mean line as a function of x, in this case the inner variable,

$$h_j(X) = \mu \frac{c}{2} \tau_o\ (x/c/2)^{-1/2}\ h(\bar{X})\ e^{i\omega t} \qquad (33)$$

where $\bar{X} = \frac{X - c/2}{\mu c/2}$

$$\mu = \frac{1}{4} c_j = \frac{1}{4}\ \frac{1}{\frac{1}{2}\rho U_\infty^2 c}$$

$\mu \ll 1$ realistic assumption made for convenience

$$h(\bar{X}) = [\bar{X} + \frac{1}{2}\ (\frac{\bar{X}^2}{\bar{X}})\ \ln \bar{X} + \theta(\bar{X}^2)\ ] \qquad (34)$$

Using the following equation,

$$w = U_\infty \frac{\partial h}{\partial x} + \frac{\partial h}{\partial t}$$

the first order inner downwash on the x axis is found as,

$$w_1 = \mu \frac{c}{2} \gamma_0 \left(\frac{x}{c/2}\right)^{-1/2} \left[\bar{x} + \frac{1}{2}\left(\frac{\bar{x}^2}{\pi}\right) \ln \bar{x} + \ldots \right] ike^{ikt}$$

$$- \frac{1}{2}\left(\frac{x}{c/2}\right)^{-3/2} \mu\gamma_0 \left[\bar{x} + \frac{1}{2}\left(\frac{\bar{x}^2}{\pi}\right) \ln \bar{x} + \theta(\bar{x}^2) \right] e^{ikt}$$

$$+ \gamma_0 \left(\frac{x}{c/2}\right)^{-1/2} \left[1 + \frac{\bar{x}}{\pi} \ln \bar{x} + \right] e^{ikt} \qquad (35)$$

Equations (37) and (35) satisfy the boundary conditions at the trailing edge. This first order inner downwash will influence the second order outer downwash, w_2, through the matching process. This is presently being pursued. Only the first three orders should be necessary for accurate results from which the unsteady lift and drag can be determined. Effects of thickness and camber can also be included by appropriately altering the boundary conditions.

This work will be extended to include a partial span jet flap and further a transverse (y direction) shear flow will be introduced to better represent the environment of the helicopter rotor.

Acknowledgment

The author would like to acknowledge the contributions to this paper which were made by Mr. Michael Rudy, Mr. John Pepin and Mr. Glen Potter. These gentlemen are all graduate students in the Department of Aerospace engineering who are actively engaged on the projects described herein.

References

1. Surendraiah, M., An Experimental Study of Rotor Blade-Vortex Interaction, NASA CR-1573, May 1970 (also M.S. Thesis, The Penna. State University., Dec. 1969).

2. Padakannaya, R., Experimental Study of Rotor Blade-Vortex Interaction, Pa. State U. Report PSU Aerop. 71-1, March 1971.

3. Rudhman, W. E., A Numerical Solution of the Unsteady Airfoil with Application to the Vortex Interaction Problem, M.S. Thesis, Pa. State U., December 1970.

4. Johnson, W., Application of a Lifting-Surface Theory to the Calculation of Helicopter Airloads, 27th National V/STOL Forum, American Helicopter Society, preprint no. 510, May, 1971.

5. Cox, C. R., Field-Scale Helicopter Rotor Noise Measurements in Ames 40 x 80 Foot Wind Tunnel, Bell Helicopter Company, Rpt. 576-099-032, Sept. 29, 1967.

6. Schlegel, R., King, R., and Mull, H., Helicopter Rotor Noise Generation and Propagation, USAAVLABS Technical Report 66-4, October 1966.

7. Bisplinghoff, R. L., Ashley, H., and Halfman, R. L., Aeroelasticity, Addison-Wesley Publishing Co., Inc., 1957.

8. Hurty, W. C., Rubinstein, M. F., Dynamics of Structures, Prentice-Hall, Inc., 1964.

9. Sissingh, G. J., Kuczynski, W. A., Effect of Blade Torsion on The Dynamics of the Flapping Motion, Journal American Helicopter Society, April 1970.

10. Young, M. I., On the Kinematics and Dynamics of Lead-Lag Rotor Systems, Journal Am. Helicopter Society, Vol. 7, No. 3, July 1962.

11. Houbolt, J. C., Brooks, G. W., Differential Equations of Motion for Combined Flapwise Bending, Chordwise Bending, and Torsion of Twisted Non-Uniform Rotor Blades, NACA TN 3905, 1957.

12. Eastman, N., Missile Control by Fluidics, Third Cranfield Fluidic Conference, May 1968.

13. Aerial Very Heavy Lift Concepts for the 1990 Army, Report of the United States Army Advanced Materiel Concepts Agency, Washington, D.C., August 1969.

14. Tokuda, N., An Asymptotic Theory of the Jet Flap in Three Dimensions, J. of Fluid Mech., Vol. 46, Part 4, 705-726. 1971.

15. Maskell, E. C., and Spence, D. A., A Theory of the Jet Flap in Three Dimensions, Proc. Roy. Soc. A 251, 407-425. 1959.

16. Spence, D. A., The Flow Past a Thin Wing with an Oscillating Jet Flap, Proc. Roy. Soc. Vol. 257 A1085, 445-477.

17. Ashley, H., and Landahl, M. T., Aerodynamics of Wings and Bodies, Addison-Wesley, 1968.

18. Van Dyke, M. D. Perturbation Methods in Fluid Mechanics. New York: Academic Press, 1964.

AN EXPERIMENTAL STUDY OF HELICOPTER ROTOR IMPULSIVE NOISE

by

WILLIAM R. BAUSCH & RONALD G. SCHLEGEL

Sikorsky Aircraft
Division of United Aircraft Corporation
Stratford, Connecticut, U. S. A.

INTRODUCTION

The helicopter generates noise of both mechanical and aerodynamic origin. Mechanical noise, such as that due to the gearboxes, bearings, hydraulic systems, etc., is in most cases important only at locations near the helicopter. Of the aerodynamic sources, such as the main and tail rotors and the engine compressors, main rotor generated impulsive noise (when it occurs) can be by far the most predominant noise, exceeding even piston engine exhaust noise (as has been shown recently by Cox and Lynn, Reference 1). While the other aerodynamic sources of helicopter noise (rotor rotational noise, rotor vortex noise, turbine engine compressor noise, etc.) have been studied in quite some detail during the past few years, rotor impulsive noise (RIN) has been generally referred to as a unique and separate phenomenon and has been largely ignored until very recently. The present paper gives results of a study of RIN, sponsored by the U. S. Army AMRDL, that sought to identify the mechanisms causing RIN, to determine if RIN is primarily rotational or broadband, and to check the ability of an existing acoustic analysis to calculate characteristics of RIN. Reference (2) contains more detailed descriptions of the experimental program, the acoustic analysis, and the correlation study.

Noise and rotor airloads were measured simultaneously for flight conditions of hover, 120 kt., 150 kt, and 170 kt. The flight test vehicle was a CH-53A helicopter configured for a neutral center of gravity and nominal gross weight of 35,000 pounds. One main rotor blade carried flush-mounted pressure transducers at 5 chordwise stations for each of 5 spanwise stations. Figure 1 shows the configuration of the aircraft and of the instrumented rotor blade. The frequency response of the airborne measurement system permitted 30 harmonics of airload to be extracted from the data with an accuracy of ±2% of full scale on vibratory measurements and ±3% of full scale on steady measurements.

During the flight test, RIN was observed only during hover and 170 knot flight. Principal conclusions are 1) that RIN is a form of rotational noise, 2) that hover RIN is essentially an aerodynamic process involving the interaction of the main rotor with its own and/or tail rotor vortices, 3) that high-speed RIN is caused by the combination of a moving source acoustic process and an aerodynamic process associated with blade drag, and 4) that an existing acoustic analysis predicts qualitative differences between flight conditions with and without RIN, but that quantitative correlation of RIN is deficient due to (1) the lack of profile drag and moving source terms in the analysis and (2) the current inability to predict the higher harmonics of airload necessary to predict the higher acoustic harmonics.

GENERAL DISCUSSION

Several investigators (References 1, 3, and 4) have postulated that the observed character of impulsive noise from rotors is due to severe amplitude modulation of broadband noise. While this phenomenon can be observed during RIN conditions, it is highly unlikely that it is the sole cause of the impulsive acoustic waveforms which are perceived by an observer as impulsive noise. RIN occurs at the rotor blade passage frequency and is primarily a harmonic phenomenon whose origin appears to be ordered rotational noise rather than random broadband noise. A Fourier analysis of periodic impulsive noise produces a frequency spectrum with very high harmonic content and relatively little amplitude decay with frequency. This has recently been demonstrated analytically by Lowson and Ollerhead (Reference 5) and Leverton (Reference 6), and experimentally by King and Schlegel (Reference 7). King and Schlegel found that during nonimpulsive noise conditions, blade airloading harmonics decay with harmonic order, λ, approximately as $1/\lambda^{1.4}$ to $1/\lambda^{1.6}$ while during impulsive noise conditions the airloads decay about as $1/\lambda^{0.6}$. The increased high frequency airloading harmonic levels for the impulsive noise case result in increased high frequency sound harmonic levels, yielding the observed "slap". Furthermore, the phasing of the sound harmonics is important in determining the impulsive nature of the observed sound; for example, a harmonic spectrum with harmonics phase shifted by 90 degrees with respect to the fundamental may be more impulsive than one with all harmonics in phase. In a recent paper, Sadler and Loewy (Reference 8) indicate that the high frequency content of RIN may be primarily associated with vortex (broadband) noise. This, too, appears to be highly unlikely since vortex noise is random in amplitude, frequency, and phase. Consequently, it does not contain the necessary harmonic content and phase coherence necessary to define an impulsive sound.

The effect on acoustic waveform of harmonic amplitude and phase is shown in Figures (2) and (3). Figure (2) compares waveforms for noise harmonic falloffs of 3 dB/ octave and 10 dB/octave, from which we conclude that RIN requires a rotational noise spectrum that is rich in harmonics. Figure (3) shows the radical change in waveform that is caused by shifting the phase of all harmonics 90 degrees from those of Figure (2).

HOVER RIN

The statement that impulsive noise during hover involves strong blade/wake interactions is supported by the flight data. Comparison of airload amplitude-vs-frequency spectra shows that many more harmonics are present for the RIN case than for the RIN-free case. This increase in high frequency loading raises the higher harmonics of noise, thereby satisfying one requirement for RIN. The location of the main rotor blades at the instant of impulse generation corresponds to the azimuthal region of maximum airload fluctuation during hover. This was determined by relating acoustic impulses recorded at 3 locations inside the helicopter to the locations of the rotor blades at the instant that the noise was generated.

Interactions of rotor blades with aerodynamic wakes cause the rapid airload fluctuations that produce RIN during hover. Clark and Leiper (Reference 9) demonstrated analytically that a vortex frequently will rise above the rotor disc plane before starting down during ideal hover of a 6-bladed main rotor, but this behavior does not guarantee blade/vortex intersections. Intersections frequently occur in a real hover because the wake responds to reflections from the ground plane and small wind disturbances which induce blade flapping and further changes in the wake structure. Figure (4) shows how blade/wake intersections affect the azimuthal variation of airloads during hover. In this case, the impinging vortices came from the tail rotor during hover OGE with the tail rotor upwind of the main rotor in a 10 knot ambient wind. Intersections of main rotor blades with main rotor tip vortices were not indicated from the data of this particular flight test.

HIGH-SPEED RIN

The impulsive noise observed during 170-knot flight appears to be primarily an acoustic event, rather than an aerodynamic event as was the case during hover. The airload amplitude - frequency spectra for cruise with and without RIN showed no strong differences, and acoustic impulses were not detected inside the helicopter.

Stationary observers on the ground heard RIN only at large distances in front of the helicopter. These observations lead to the conclusion that motion of the noise source toward an observer is a major source of high-speed RIN.

This form of RIN was originally thought to be due to the formation of weak local shock waves on the advancing blade. As mentioned by Ollerhead and Lowson (Reference 10) and discussed by Leverton (Reference 6), an observer can hear such a shock wave only if the blade speed is supersonic. If the blade speed is subsonic, the shock wave can not propagate to an observer's ear. However, the formation of local shocks can affect rotor noise levels by influencing the local airloading acting on the blade. High-speed RIN as discussed in Reference 10 is basically an acoustic effect resulting from the coalescence of the harmonic wave fronts at high source translational speeds and can be explained by the Lowson/Ollerhead theory. The predicted increase in levels of higher-order noise harmonics with increasing tip speed is independent of the loading spectrum and satisfies one of the requirements for RIN. The highly directional characteristic of high-speed RIN noted by observers on the ground track is an acoustic effect which results from the forward speed correction where the distance term, r, is modified to reflect the rotor's Mach number toward an observer by substituting $r(1-M_r)$ in the argument of the Bessel functions, thus influencing the directivity characteristics. This effect can be seen in Figure 5, taken from Reference 5. As forward speed increases, the radiated sound becomes highly directional in the forward direction, particularly for the higher harmonics. This means that the RIN experienced by a helicopter at high speeds will be radiated perferentially forward with the maximum at about 15-20 degrees below the plane of the rotor. This effect was shown experimentally by Cox (Reference 11) in full-scale wind tunnel tests. Thus, the acoustic effect of a high tip Mach number is at least partially responsible for the generation of the impulsive noise and the aircraft forward speed accounts for the highly directional character of this type of RIN.

The aerodynamic forces used in current acoustic theory to predict rotational noise are the in-plane (induced drag) and out-of-plane (thrust) components of the blade section lift. The profile drag is ignored, since it is generally small compared to the other terms. When advancing tip speeds exceed a critical Mach number, however, the drag increases rapidly due to drag divergence. This increased drag may be a significant contributor to the radiated noise. In a recent paper, Arndt and Borgman (Reference 12) examined the effect of drag divergence on the radiated noise. The effect of this drag term is to increase the levels of the higher harmonics of noise, a necessary condition for impulsive noise. While Arndt and Borgman indicate that the addition of this term to the Lowson/Ollerhead noise equation enhances correlation, they unfortunately do not show to what degree. For small angles of attack (such as near the tip), the lift term may be quite small and the drag terms will dominate the noise radiation. In this case, the directivity will be that of a dipole with its maximum radiation in the plane of rotation, thus further contributing to the observed directivity of high-speed RIN. An additional factor which may contribute to the observed directivity and character of RIN is thickness noise. While it is not significant for highly loaded rotors at low forward speeds, thickness noise can become significant at high forward speeds. Arndt and Borgman accounted for thickness noise by applying a forward speed correction to the theory developed by Diprose (Reference 13) for a static propeller. No attempt was made to correct for the nonuniform velocity field over the rotor disk, but the results show that the levels of the higher harmonics of rotational noise increase rapidly as tip speed increases. This effect, coupled with the in-plane directivity pattern of thickness noise will tend to enhance the severity of the observed RIN.

CORRELATION AND ANALYSIS

Measured and calculated rotor noise data were compared to determine how well an existing acoustic analysis could predict waveform and rotational noise harmonic levels for flight conditions with and without RIN. Waveforms correlated well as can be seen in Figures 6 and 7. RIN was not heard by ground observers during the 140-knot flight that resulted in Figure 6, and the waveforms reflect the absence of impulsiveness. Waveforms for 170-knots and helicopter/observer placement comparable to Figure 6 definitely appear impulsive in Figure 7, which agrees with observers reporting RIN for this flight condition.

Despite the good qualitative agreement between measured and calculated waveforms for the 170-knot case, the unsteady behavior of the calculated waveform between pulses suggests that the acoustic analysis underestimates the higher harmonics. Figure 8 gives a general indication of the correlation between measured and calculated rotational noise harmonic levels. Measured harmonic levels are consistently greater than calculated ones at distances over 1500 to 2000 feet in front of the helicopter during high-speed forward flight. Consequently, although the calculated waveforms accurately reflect the trends of measured variations with airspeed, these waveforms do not have enough higher-harmonics content to produce the measured steadiness of pressure between pulses. The inability of the analysis to predict the higher-order harmonic levels far in front of the rotor is attributed to the following factors.

1) Motion of the rotor system in the direction of an observer is not included.
2) Drag divergence aerodynamic forces are not included in determining source strength and directionality.

The acoustic analysis that was used represents the rotor system as a conical surface of dipole radiators inclined at an angle to the ground plane. At any point on this surface, the dipole radiates continuously at integer multiples of the blade passage frequency to produce the pressure field experienced by that point as a blade passes over it. Lamb's nonhomogeneous wave equation is used to transfer the acoustic pressure at the source to the pressure reaching an observer, and the total acoustic pressure field is obtained by integrating the contributions of all source dipoles on the rotor surface for all noise harmonics.

SUMMARY

In summary, a number of important conclusions have resulted from this study. The first of these is that Rotor Impulsive Noise (RIN) is characterized by an increase in sound pressure level of the higher harmonics of rotational noise, rather than increases in broadband noise amplitude and modulation, with up to 23 harmonics (425 Hertz) being measured during RIN.

The second conclusion is that cruise RIN and hover RIN of single rotor helicopters appear to be generated by different aeroacoustic mechanisms. Cruise RIN is highly directional with maximum severity occurring directly ahead of the helicopter at small angles below the plane of the main rotor, and appears to result from the combination of acoustic effects of source motion towards an observer at high subsonic tip Mach numbers and of the aerodynamic effects of drag divergence. Aerodynamic shock does not appear to be a primary contributor to cruise RIN. Hover RIN results from high frequency oscillations in airloads commonly caused by blade/wake (main and/or tail) interactions.

The acoustic analysis developed by Sikorsky Aircraft under sponsorship of the Eustis Directorate of U. S. Army AMRDL appears to be adequate to predict the harmonics and time histories of rotor noise fairly well in OGE hover and at moderate distances from the helicopter (up to 1,000-1,500 feet) during cruise

providing that high frequency harmonic blade airload data are available. The major problem here, however, is that normal data acquisition/processing techniques used in studies of helicopter airloads have not provided information in the frequency range required for good acoustic correlation. Also, currently available theoretical airloads prediction programs are incapable of predicting the higher-harmonic amplitude and phase data that are needed for predicting the higher harmonics of noise. Correlation at large distances from the helicopter (beyond 1,000-1,500 feet) tends to be poor during high speed cruise, presumably due to the analytical omission of source motion and drag divergence effects, and possible atmospheric scattering effects on the highly directional, higher frequency radiating patterns.

FUTURE RESEARCH RECOMMENDATIONS

Limited ability of theoretical airload analyses to predict higher harmonic amplitude and phase suggests that new empirical approaches are required to provide airload data for acoustic predictions. Such airload data can probably be most economically developed through the use of acoustic wind tunnel facilities, such as the one recently developed by the United Aircraft Research Laboratories and the one planned at NASA Langley.

In addition to the development of such high frequency airload prediction schemes, current analyses should be modified to include the effects of source translation as well as profile drag and drag divergence.

A final point which should be made is that although the primary emphasis currently in the military and industrial research and development programs is on the development of hardware for reduced noise, experience has shown that only a thorough understanding of the aeroacoustic mechanisms can guarantee a high probability of success. As there are a great many areas of ignorance in rotor noise generation still to be explored, continued support must be given to basic research, such as those programs supported by AROD, if we are ever to achieve quiet vehicles which are economically feasible.

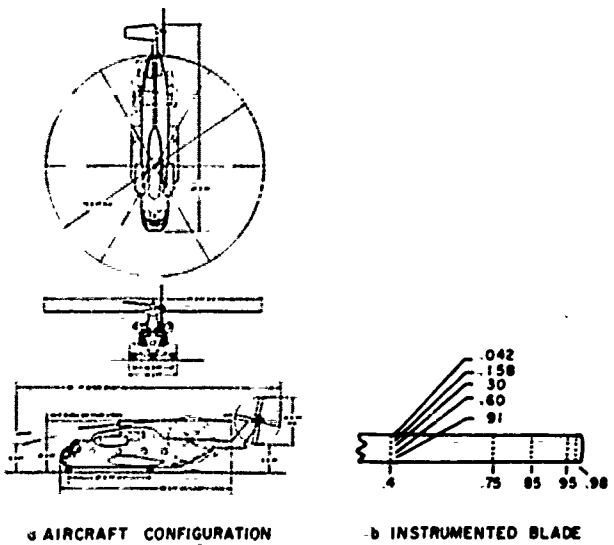

a AIRCRAFT CONFIGURATION

b INSTRUMENTED BLADE CONFIGURATION

AIRCRAFT LAYOUT AND INSTRUMENTED BLADE

Figure 1

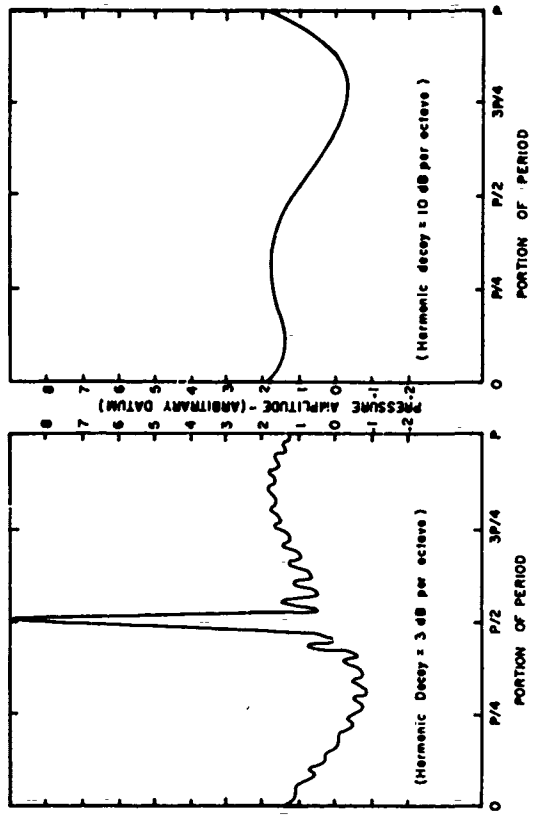

EFFECT OF HARMONIC AMPLITUDE FALLOFF ON ACOUSTIC WAVEFORM

Figure 2

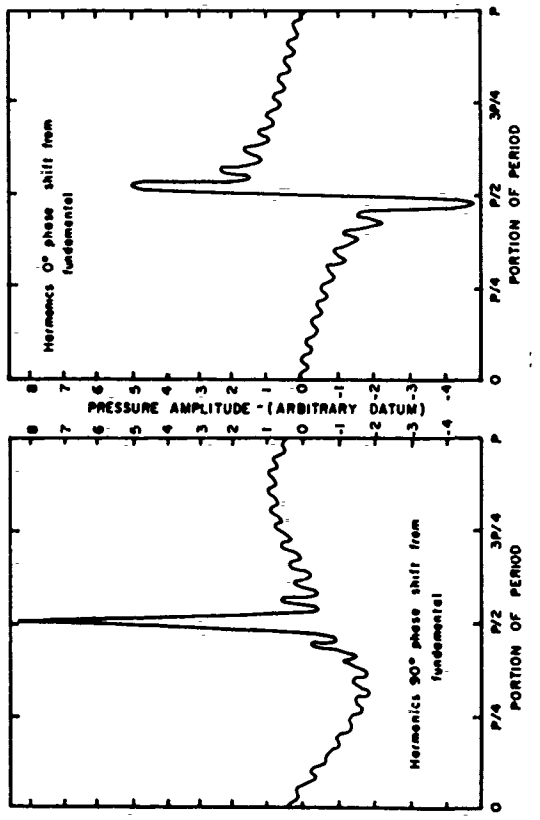

EFFECT OF HARMONIC PHASE ON ACOUSTIC WAVEFORM

Figure 3

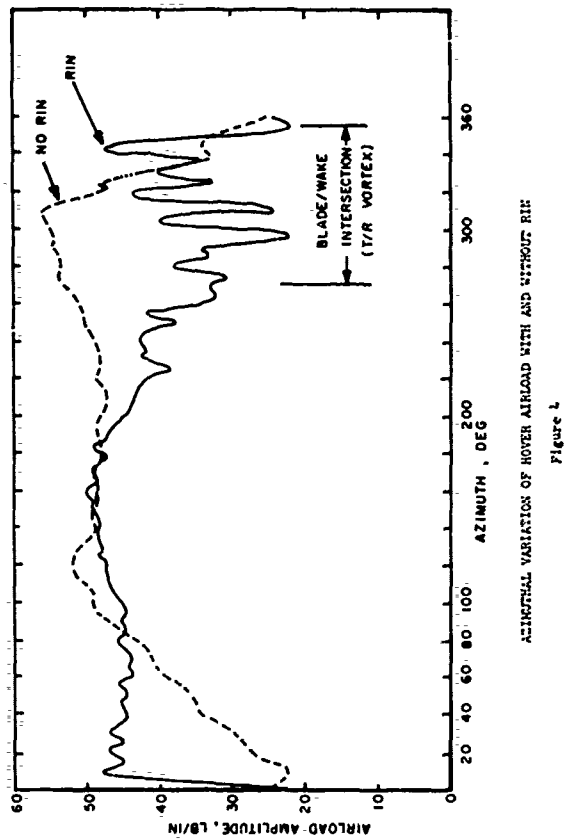

AZIMUTHAL VARIATION OF HOVER AIRLOAD WITH AND WITHOUT RIN

Figure 4

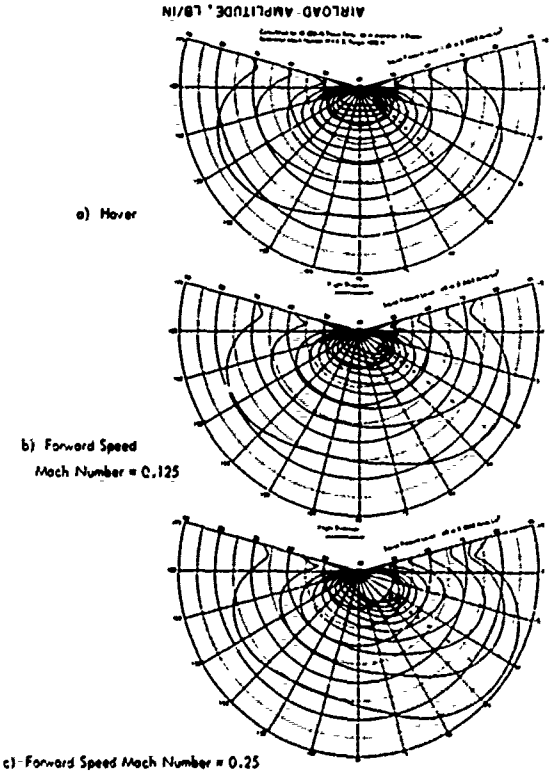

CALCULATED ROTATIONAL NOISE DIRECTIVITY

Figure 5

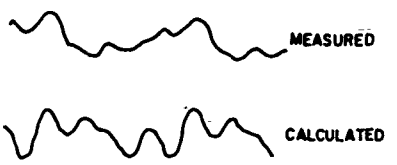

140 KT, NO RIN, HELICOPTER APPROXIMATELY 500 FT AWAY

MEASURED AND CALCULATED WAVEFORMS

Figure 6

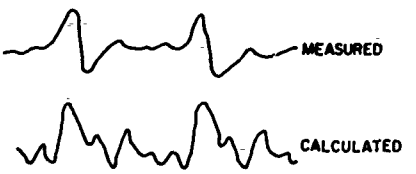

170 KT, MAXIMUM RIN, HELICOPTER 500 TO 1000 FT AWAY

MEASURED AND CALCULATED WAVEFORMS

Figure 7

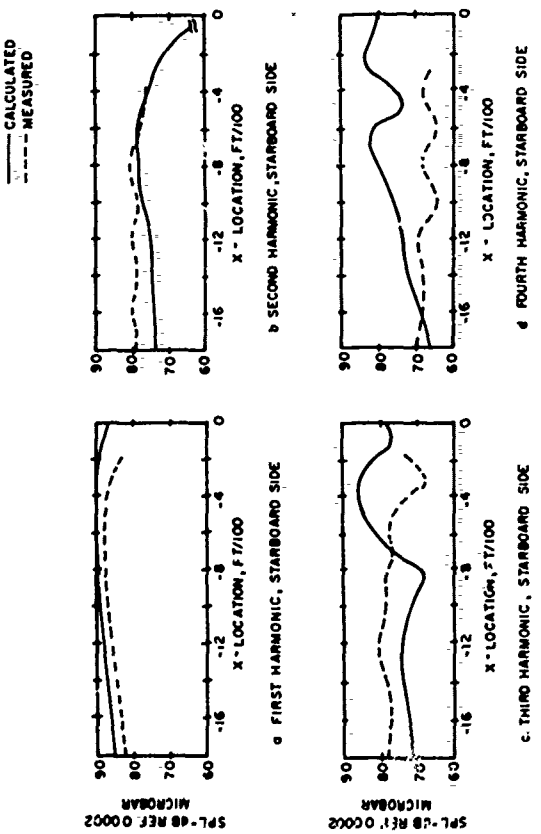

MEASURED AND CALCULATED ROTATIONAL NOISE HARMONIC LEVELS

Figure 8

REFERENCES

1. Cox, C. R., and Lynn, R. R., A STUDY OF THE ORIGIN AND MEANS OF REDUCING HELICOPTER NOISE, Bell Helicopter Company; USATCREC Technical Report 62-73, U. S. Army Transportation Research Command, Fort Eustis, Virginia, November 1962.
2. Bausch, W. E., Munch, C. L., and Schlegel, R.G., AN EXPERIMENTAL STUDY OF HELICOPTER ROTOR IMPULSIVE NOISE, Sikorsky Aircraft; USAAVLABS Technical Report 70-72, Eustis Directorate, U. S. Army Air Mobility Research and Development Laboratory, Fort Eustis, Virginia, to be published during 1971.
3. Schlegel, R. G.,King, R. J., and Mull, H. R., HELICOPTER ROTOR NOISE GENERATION AND PROPAGATION, Sikorsky Aircraft; USAAVLABS Technical Report 66-4, U. S. Army Aviation Materiel Laboratories, Fort Eustis, Virginia, October 1966, AD 645834.
4. Davidson, I. M., and Hargest, T. H., HELICOPTER NOISE, J1. Royal Aero Soc., Vol. 69, May 1965.
5. Lowson,M. V., and Ollerhead, J. B., STUDIES OF HELICOPTER ROTOR NOISE, Wyle Laboratories; USAAVLABS Technical Report 68-60, U. S. Army Aviation Materiel Laboratories, Fort Eustis, Virginia, January 1969, AD 684394.
6. Leverton, J. W., HELICOPTER NOISE - BLADE SLAP, PART 1: REVIEW AND THEORETICAL STUDY, University of Southampton; NASA Contractor Report 1221, National Aeronautics and Space Administration, Washington, D.C., October 1968.
7. King, R. J., and Schlegel, R. G., PREDICTION METHODS AND TRENDS FOR HELICOPTER ROTOR NOISE, Proc. Third CAL/AVLABS Symposium, 18-20 June 1969, Buffalo, New York.
8. Sadler, S. G., and Loewy, R. G., THE IMPORTANCE OF VORTEX SHEDDING EFFECTS ON HELICOPTER ROTOR NOISE WITH AND WITHOUT BLADE SLAP, Proc. Third CAL/AVLABS Symposium, 18-20 June 1969, Buffalo, New York.
9. Clark,D. R., and Leiper, A.C., THE FREE WAKE ANALYSIS. A METHOD FOR THE PREDICTION OF HELICOPTER ROTOR HOVERING PERFORMANCE, J1. Am. Helicopter Soc., Vol. 25, No. 1, January 1970.
10. Ollerhead, J. B., and Lowson, M. V., PROBLEMS OF HELICOPTER NOISE ESTIMATION AND REDUCTION, AIAA Paper No. 69-195, AIAA AHS VTOL Research Design, and Operations Meeting, February 1969.
11. Cox, C. R., ROTOR NOISE MEASUREMENTS IN WIND TUNNELS, Proc. Third CAL/AVLABS Symposium, 18-20 June 1969, Buffalo, New York
12. Arndt, R. E. A., and Borgman, D.C., NOISE RADIATION FROM HELICOPTER ROTORS OPERATING AT HIGH TIP MACH NUMBERS, presented at 16th Annual National Forum of the Am. Helicopter Soc., Washington, D.C., June 1970, Amer. Helicopter Soc. Preprint No. 402.
13. Diprose, K. V., SOME PROPELLER NOISE CALCULATIONS SHOWING THE EFFECT OF THICKNESS AND PLANFORM, RAE Tech M. S. 19, 1955.

A SYSTEMS STUDY OF NOISE REQUIREMENTS ON THE DESIGN OF V/STOL AIRCRAFT

Robert W. Simpson
Henry B. Faulkner
Anthony P. Hays

FLIGHT TRANSPORTATION LABORATORY
Massachusetts Institute of Technology

1.0 Introduction

The reduction of helicopter noise in military operations has two main purposes:

1) Avoidance of detection, or delay of detection to increase the surprise element of an operation
2) Minimization of noise levels in the region of friendly forces to reduce communication loss due to operations.

The chief elements of helicopter noise are due to vortex and rotational noise from the main rotor and tail rotor, and engine noise. One method of reducing the effect of helicopter noise is to reduce the noise at the source, using techniques such as slowing down the rotors, adding more blades, and using engine and gearbox noise suppression techniques. The first section of this paper will show the penalties in performance and payload (as measured by operating cost) which result from using this approach.

An alternative method of reducing the effect of aircraft noise is to modify the flight profiles in position and speed. The ability of the aircraft to fly the modified profiles may be constrained by its available thrust, acceleration limits, etc., and some small penalty may be incurred in fuel or time of flight. The second section of this paper describes a method for finding noise optimal trajectories for a helicopter takeoff and climbout.

2.0 Helicopter Design for Minimum Noise Generation

The process for preliminary design of air vehicles can be computerized such that fast, parametric variations can be obtained. These computer programs are now a design tool used to find optimal configurations for required vehicle performance in terms of payload, range, speed, etc. At the Flight Transportation Laboratory, we are extending our design programs to include the noise generation of a given vehicle (as best we can estimate it) as one of the performance measures of the vehicle. We then can meet other design objectives at varying levels of noise, or can search for optimal designs for a specified noise level. The following section briefly describes one such computer program, for helicopters, and shows some of the noise tradeoffs one can study using the program.

2.1 Description of the Helicopter Design Program

a) The Design Logic

The helicopter computer design program is fully described in FTL Technical Memo 71-3 (Reference 1). Briefly, the purpose of this program is to provide a rapid means of investigating tradeoffs between design parameters and various figures of merit, such as direct operating cost and noise generation. This program considers only conventional pure helicopters.

The program begins by reading input data such as design payload, range, speed, etc. and generating constants, including atmospheric data, for later use. Calculations regarding hover performance are done for a hot day, all other calculations assume a standard day.

Then the program goes into a design procedure which is an iteration on gross weight. Initially a gross weight is estimated based on the design payload; on succeeding iterations the previous gross weight is used. The rotor is then designed considering both cruise and hover. Next the fuselage is sized and parasite drag is calculated. Then the power plant and drive system is sized to the maximum of cruise and hover requirements. If hover rpm is less than cruise rpm then the installed power required for cruise is increased accordingly. This completes the selection of design parameters.

The vehicle is then flown through the design mission to find the fuel consumed. Ten phases in the mission profile are considered: hover, vertical climb, acceleration to advance ratio .325, unaccelerated climb, acceleration to cruise, cruise, undecelerated descent, deceleration to advance ratio .325, deceleration to hover, and vertical descent. The time, distance and fuel consumed in each phase is calculated. A table of rotor lift to drag ratio vs. advance ratio and thrust coefficient to solidity ratio is used to estimate performance above advance ratio .325. This table was derived from Ref. 2.

Then the component weights are calculated, resulting in a new gross weight. If the difference between new and old gross weights is greater than 10 lbs., the design procedure goes through another cycle. When the iteration is complete the parameters describing the final design are output.

b) Vehicle Operating Cost

Then the vehicle is flown through various mission lengths that are less than the design range, with appropriate cruise altitudes and speeds. The time, distance, and fuel consumed for each phase of each mission is calculated, output, and stored for use in the calculation of direct operating cost (DOC).

Then the program calculates DOC's, broken down by categories, for each stage length and prints this out. The DOC is now calculated according to the Lockheed VTOL formula (Refs. 3, 4).

c) Vehicle Noise Generation

Finally, the program makes calculations regarding the noise generated by the vehicle. Vortex noise is calculated using the well established formula taken from reference 5 for an observer at 300 feet distance:

$$L_p = 10 \log_{10} \frac{7.62 \times 10^{-10} T^2 (V_{tip})^2}{2 A_B}$$

where L_p = overall sound pressure level, db
T = thrust, lb.
V_{tip} = rotor tip speed, ft/sec
ρ = air density, slugs/ft^3
A_B = total rotor blade area, ft^2

Simple inverse square law attenuation is assumed for observers at other distances. Directivity effects are not

considered. This formula is applied to all flight conditions. In cruise the advancing blade tip speed is used.

Contrary to most trajectory optimization problems using dynamic programming, controls are applied at a given state and stage to find the optimum path from the initial conditions to that state, rather than applying controls forward in time and finding the optimal path to the terminal conditions. The main reason for this is that the initial conditions are more precisely defined than the terminal conditions.

3.1.2 Dynamic Model of the Aircraft

A dynamic model of the aircraft is shown in Figure 9. δ and T (and hence the noise generated) are calculated in terms of the state variables, $\dot{x}$ and $\dot{h}$, and control variables $\Delta\dot{x}$ and $\Delta\dot{h}$.

The system constraints with this program are

$0 \leq \dot{x} \leq 250$ ft/sec

$0 \leq \dot{h} \leq 90$ ft/sec

-10 ft/sec$^2 \leq \ddot{x} \leq 10$ ft/sec^2

-10 ft/sec$^2 \leq \ddot{h} \leq 10$ ft/sec^2

Power limitation $P \leq P_{max}$

Other constraints, such as maximum height, could easily be added but have not been implemented at this stage.

Initial conditions are

$x = 0$ $\quad \dot{x} = 0$

$h = 0$ $\quad \dot{h} = 0$

Terminal conditions are

$x = x_{term}$

$h = h_{term}$

$t = t_{term}$

Rotational noise was hand-calculated for a sample case using the method of Ollerhead and Lowson, Ref. 6, and another method developed in the Flight Transportation Laboratory (Ref. 7). Both results indicated that rotational noise was not significant for helicopters with low tip speeds, and thus it has not been included in the program.

The standard takeoff profile assumed throughout the helicopter design program is shown in Fig. 1. The landing profile is just the reverse. During the acceleration phase the vehicle tries to accelerate horizontally at the allowable acceleration, and if it has more than enough power to do this, it uses the excess power to climb. Hence the profile varies depending on how much power is available and the maximum acceleration allowed. During the climb phase the vehicle climbs at constant forward speed. The observers are always in the plane of the takeoff profile. Varying the height of vertical climb has the effect of shifting the noise profile up or down. Reducing the maximum acceleration causes greater excess power to be available for climb and hence has the effect of tilting the path upward during acceleration.

As the vehicle accelerates from rest to its vertical rate of climb, thrust is greater than weight and hence extra noise is generated. The noise resulting from maximum thrust is calculated and assumed to represent the noise in the first few seconds of the takeoff profile.

The noise is calculated at 15 points during the takeoff profile and output along with the time, altitude and horizontal distance corresponding to each point. This can be

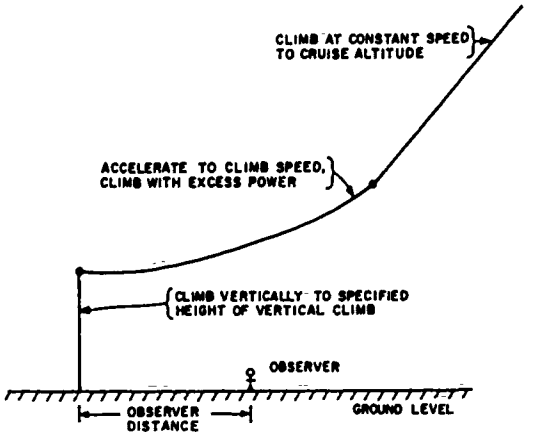

FIGURE 1 SCHEMATIC OF TAKEOFF PROFILE

repeated for observers at different distances from the takeoff point. Noise on the ground due to the vehicle cruising at cruise altitude directly overhead is also calculated.

2.2 Typical Results

2.2.1 Helicopter Noise Tradeoffs

A study of the tradeoff between noise generated and DOC, using the helicopter computer design program, has been started. The initial results are shown in Figures 2, 3 and 4. DOC is plotted vs. perceived noise level in hover for an 16,000 lb. payload tandem helicopter. The DOC is for a multiple hop trip with hops of 5, 20 and 100 miles for a total of 125 miles.

Other symbols on the graphs are as follows:

C_T = rotor thrust coefficient

σ = rotor solidity

M_{at} = advancing tip Mach number in cruise

V_{cr} = cruise speed, mph

DR = design range, miles

V_{th} = blade tip speed in hover, ft/sec

V_{tcr} = blade tip speed in cruise, ft/sec

DL = disc loading, lbs/ft^2

The formula for the calculation of rotor vortex noise at 300 ft from Ref. 5 may be written as follows for the hover condition:

$$L_p = 10 \log (3.04 \times 10^{-9} (V_{th})^6 A_B C_L^2)$$

where

A_B = blade area

$$A_B = \frac{W_{gr}}{DL}$$

W_{gr} = vehicles gross weight

C_L = average blade lift coefficient

$$C_L \cong 6 (C_T/\sigma)_{hover}$$

In order to reduce vortex noise in hover it is clear that we must reduce hover tip speed. However, since the same rotor develops very nearly the same thrust in hover and cruise, the following relation applies:

$$1/2 \rho_{hover} V_{th}^2 (C_T/\sigma)_{hover} = 1/2 \rho_{cruise} V_{tcr}^2 (C_T/\sigma)_{cruise}$$

A safe maximum for (C_T/σ) is 0.100. V_{tcr} is given by

$$V_{tcr} = \frac{a_{cr} M_{at}}{1 + \mu}$$

where

μ = advance ratio

a_{cr} = speed of sound at cruise altitude.

Thus we keep μ at a practical maximum of 0.50 and V_{tcr} is proportional to M_{at}. Hence, in order to reduce noise we must reduce $(C_T/\sigma)_{cruise}$ or M_{at}. These are the variations shown in Figures 2 and 3, respectively, for different values of DL. These two sets of curves assume that V_{th} and V_{tcr} are independent. This requires either: that there is no variation in engine power or specific fuel consumption with engine rpm over the appropriate range; or, that there is a transmission ratio change between cruise and hover. This assumption is optimistic. The variation in Figure 4 is equivalent to Figure 3 only with $V_{th} = V_{tcr}$, eliminating this assumption.

The propagation conditions assumed account for geometric spreading only from a nominal distance of 300 ft. There is no correction for ground reflection, effects of air absorption.

Figures 2 and 3 show about 25% increase in DOC for a 6 dB reduction in Sound Pressure Level. In general, reduction of (C_T/σ) in cruise appears to be a slightly less expensive way of reducing noise than reducing M_{at}, except for very low disc loadings. This is because DOC is quite sensitive to cruise speed, which depends directly on M_{at}. Also the optimum disc loading is shown to be about 5 for this vehicle. This is somewhat lower than current practice. However, the reduction in hover power required, and hence in engine and rotor weight, and the cost of maintaining these components, justifies a movement toward lower disc loading. The curves of Figure 4 are similar to those of Figure 3 except they are displaced upward for a given hover tip speed. This is because putting $V_{th} = V_{tcr}$ has reduced V_{tcr} and consequently cruise speed.

Unfortunately, there are no presently operating helicopters which are equivalent to the vehicles studied here. The right hand ends of the various curves indicate vehicles which are close to optimal (minimum DOC) without regard to noise. Presently operating helicopters were also designed without regard to noise, and hence, should make roughly the same noise for a given vehicle size. The helicopters under study here are assumed to incorporate 1975 technology. This is reflected in various aerodynamic and structural parameters which are input to the program. Thus present day helicopters would fall above the right hand ends of the curves. Since they have $V_{th} = V_{tcr}$, they would be plotted in Figure 4.

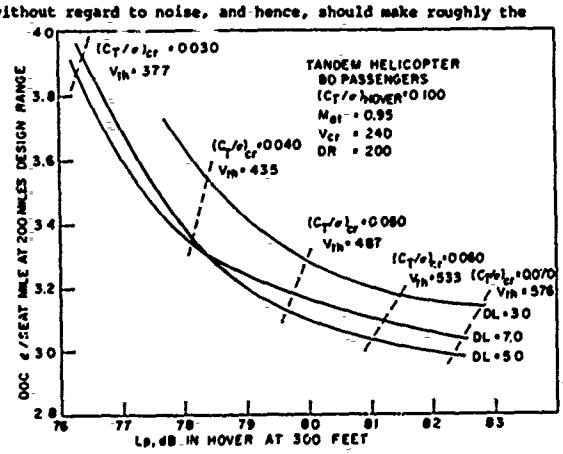

FIGURE 2 DOC VS Lp FOR VARIATIONS IN $(C_T/\sigma)_{cr}$ WITH M_{at}, $(C_T/\sigma)_{HOVER}$, V_{cr} AND DR CONSTANT

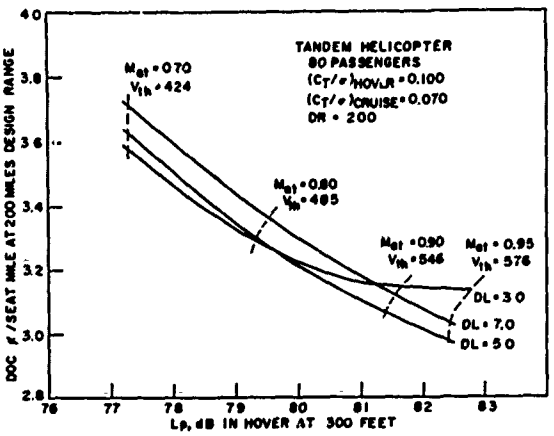

FIGURE 3 DOC VS Lp FOR VARIATIONS IN M_{at} WITH $(C_T/\sigma)_{cr}$, $(C_T/\sigma)_{HOVER}$, AND DR CONSTANT

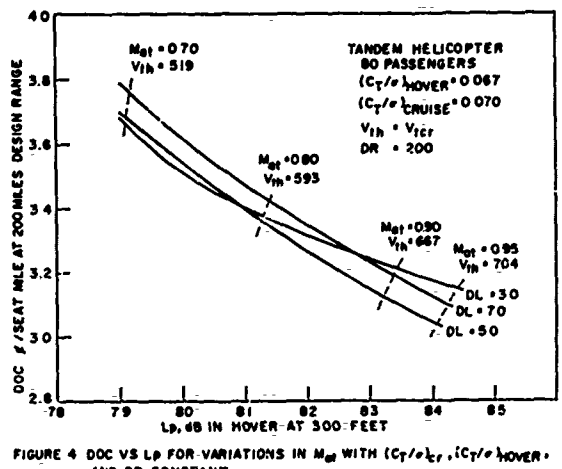

FIGURE 4 DOC VS Lp FOR VARIATIONS IN M_{at} WITH $(C_T/\sigma)_{cr}$, $(C_T/\sigma)_{HOVER}$, AND DR CONSTANT

2.2.2 Helicopter Noise Histories

Another study has examined the noise perceived by a listener under the takeoff path of three distinct helicopter designs; one representing a current helicopter, one representing a minimum operating cost vehicle designed using present state of the art technology, and the last representing a quiet vehicle designed using present state of art technology.

The three vehicles are all tandem helicopters, carrying 10,000 lbs. payload and a crew of three. They all fly takeoff and landing profiles similar to those previously described, and cruise at 5000 feet. The vehicles are compared in Table I.

The first, called R70, represents what is existing and available now. It is an approximation of the Boeing/Vertol 347, a helicopter prototype which first flew in

May 1970, except that it has less parasite drag. It has slightly more range than the other two, but does not have the ability to hover after engine failure.

The second vehicle, called MC75, is a minimum DOC vehicle designed without regard for noise. It represents what could be flying in prototype form in 1975 using the latest technology. It is an optimal vehicle given the size and flight profile. The single rotor configuration was considered for this and the third vehicle but the comparable single rotor ship was always slightly more expensive to operate and slightly noisier.

Table 1: Vehicle Comparison

	E70	MC75	Q75
Payload, lb	10,000	10,000	10,000
Cruise Speed, mph	217	252	210
Cruise Altitude, ft.	5000	5000	5000
Range with reserve, mi.	600	400	400
Gross Weight, Lb	46,140	33,813	43,003
Engine-out Hover Capability	No	Yes	Yes
Installed Power, hp	7257	5448	6913
Disc Loading, lb/ft^2	7.0	5.0	5.0
Solidity	.088	.083	.205
Number of blades	8	6	6
Tip Speed, Hover, ft/ sec	707	640	720
Tip Speed, Cruise, ft/sec	707	672	514
C_T/σ Hover	.067	.062	.100
C_T/σ Cruise	.078	.065	.045
Advance Ratio in Cruise	.45	.55	.55
Advancing Tip Mach No.	.935	.950	.750
Lift/drag Cruise	4.86	5.52	5.36
DOC @ 100 mi ¢/seat mile	3.87	3.07	4.02
L_p Takeoff @ 500 ft, dB	82	79	70
L_p Cruise @ 5000 ft, dB	64	61	56

The two configurations, however, differ by less than the accuracy of our techniques and hence no definite choice can be made.

The third vehicle, called Q75, is a minimum DOC vehicle designed to have a peak Sound Pressure Level at takeoff or landing of 70 dB at 500 feet and a peak Sound Pressure Level in cruise flyover of 56 dB at 5000 feet. The 5000 feet cruise altitude was chosen to make the vehicle comparable to the first and second vehicles, but this vehicle could cruise at 10,000 feet, making an L_p of 50 dB, with only a small penalty in DOC. This vehicle also uses 1975 technology and is optimal within the size, flight profile and noise constraints given.

The direct operating cost (DOC) of the three vehicles is shown in Fig. 5. DOC is shown in dollars per seat trip which makes a clearer presentation than cents per seat mile. Each vehicle could have 50 seats. It can be readily seen that at very short ranges the DOC is about the same for all three while at longer ranges E70 and Q75 cost about the same while MC75 is significantly cheaper.

Figures 5, 6 and 7 show the Sound Pressure Level versus time during the takeoff of the three helicopters as heard by three observers at 500, 1000 and 1500 feet distances from the takeoff point.

Various conclusions can be drawn from these curves. It is clear that Q75 is dramatically quieter, not only because it generates less noise but because it moves out of the takeoff area more rapidly. All of the curves show two peaks, one at lift off (vertical acceleration) and one approximately

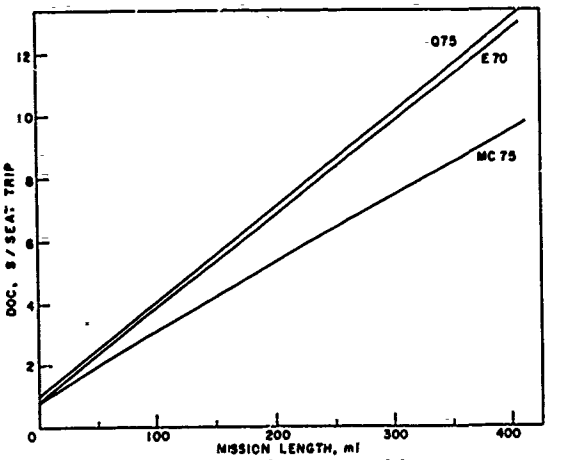

FIGURE 5 DIRECT OPERATING COSTS FOR 3 HELICOPTERS

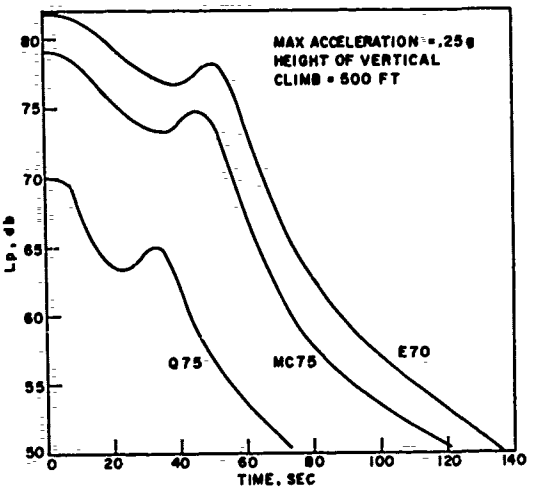

FIGURE 6 TAKEOFF NOISE VS. TIME FOR OBSERVER AT 500 FT

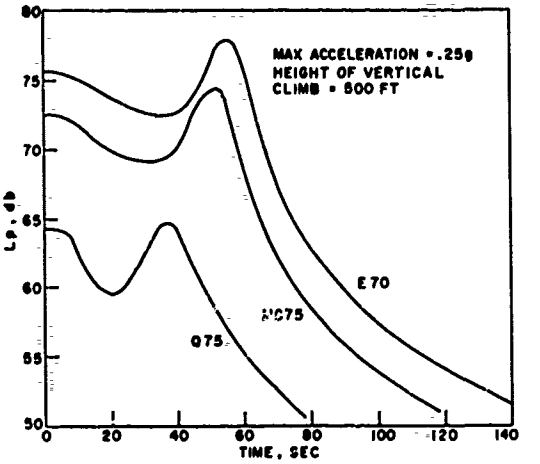

FIGURE 7 TAKEOFF NOISE VS. TIME FOR OBSERVER AT 1000 FT

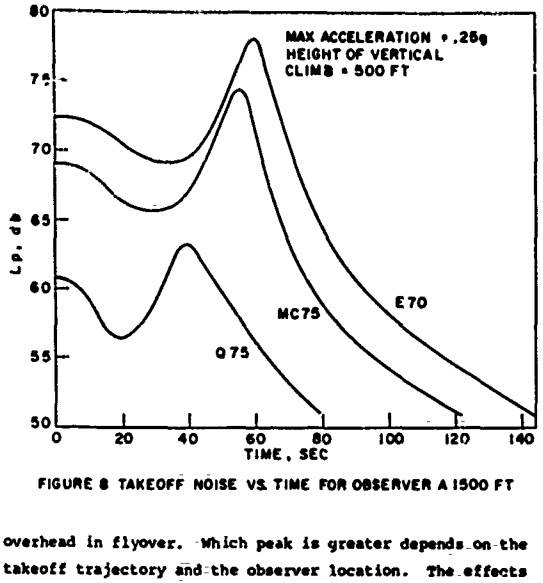

FIGURE 8 TAKEOFF NOISE VS TIME FOR OBSERVER A 1500 FT

overhead in flyover. Which peak is greater depends on the takeoff trajectory and the observer location. The effects of increasing the height of vertical climb and of tilting the flight path upward after vertical climb are similar. This raises the question of the optimal flight trajectory to minimize either annoyance or detection resulting from the noise, and the design of the aircraft capable of flying this trajectory.

3.0 Optimal Noise Takeoff Profiles for a Helicopter

For a given helicopter with its performance constraints, and noise generation characteristics, the question still remains of how to operate that helicopter such as to minimize the noise exposure (by some criteria) of a given set of listeners. If an optimal trajectory can be found, then the effects of constraints arising from vehicle performance can be investigated, and a feedback established to the vehicle design process. The following section describes the use of dynamic programming to minimize the annoyance due to noise of a helicopter in the takeoff and climbout phases of flight on a listener directly under the flight path. A more complete description may be found in References 8, 9.

3.1 The Mathematical Model

3.1.1 Use of Dynamic Programming

A detailed description of dynamic programming may be found in Reference 10; in this example the state variables have been chosen to be horizontal and vertical components of velocity, $\dot{x}$ and $\dot{h}$. Control variables are discrete differences in the values of the state variables, $\Delta\dot{x}$ and $\Delta\dot{h}$. This affords some simplification of the problem since application of controls takes the aircraft directly from one set of quantized values of state variables to another. This avoids the necessity for interpolation. As it is usually the case the stage variable is taken to be time, t, which is also quantized into discrete values of interval Δt.

Height and ground track at the terminal conditions are unconstrained.

3.1.2 Noise Generation Model and Annoyance Criteria

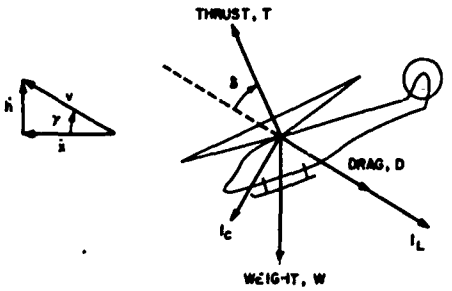

I_L AND I_C ARE COMPONENTS OF INERTIAL REACTION PARALLEL AND PERPENDICULAR TO THE FLIGHT PATH

$$I_L = \frac{W}{g} \times \dot{v} \qquad I_C = \frac{W}{g} \times v \times \dot{\gamma}$$

FIGURE 9 DYNAMIC MODEL OF AIRCRAFT

A noise generation model is required which predicts the sound pressure level in octave bandwidths at any point on a sphere of given radius centered on the aircraft. From a knowledge of attenuation due to spherical spreading, ground effect and atmospheric attenuation, the sound pressure level in octave bandwidths as heard by a listener could be determined, and the perceived noise level in PNdB calculated. This figure could then be substituted into some function relating perceived noise level and annoyance so as to find the annoyance over the given time interval.

Unfortunately such a noise model does not yet exist in analytic form so some simplifying assumptions must be made. Rotor rotational noise is a low frequency phenomenon, and although the SPL may be higher than for vortex noise, its contribution to annoyance is small. Assuming that continued use of noise suppression techniques can reduce engine, transmission and tail rotor noise to acceptable levels, main rotor vortex noise remains as the most important parameter.

This is somewhat of an oversimplification but it does mean that an easily manageable noise model can be created. Using Schlegel's equation for overall vortex noise from Appendix C of Reference 11, the sound pressure level at a radius r from a helicopter is given by (1)

$$SPL = 10\left[2\log V_{0.7} + 2\log T - \log A_b - 2\log(r/300) - 3.57\right]$$

where $V_{0.7}$ is the linear blade velocity of the 0.7 rad. section.

A_b is the total blade area (blade planform area x number of blades)

T is thrust.

Directivity effects have not been included at this stage. From a knowledge of the vortex noise frequency distribution, the perceived noise level may be calculated in terms of the overall SPL.

3.1.4 The Criterion of Annoyance

In a study by Erzburger and Lee (Ref. 12) on optimal trajectories with respect to noise for conventional aircraft, the unit of annoyance called the noy was used. This is related to PNL by

$$N_y = 10^{(PNL-40)/33.2} \qquad (2)$$

where N_T is total noisiness in noys. For noise in the urban environment there are two factors that make the noy unsuitable. The first is that noise level below 80 PNdB appears to be acceptable to the majority of the population (according to results in Ref. 13). The second is that if the background urban noise level is 80 PNdB, then any additional noise below 80 PNdB does not have much effect.

A possible alternative is to use a modified noy definition in the form

$$\text{Annoyance} = \left[10^{(PNL-80)/33.2}\right]_{PNL\geq 80} = \left[\frac{N_T}{16}\right]_{PNL\geq 80} \qquad (3)$$

In this work the following relationship was used

$$\text{Annoyance} = \left[\frac{(PNL - 80)^2}{10}\right]_{PNL\geq 80} \qquad (4)$$

This expression agrees with equation (3) to within 1 unit over the range 85 to 123 PNdB (see Figure 10).

The other effect that must be considered is the duration of the noise on annoyance. In this work the performance function to be minimized was chosen to be

$$J = \sum_{i=1}^{L} \left[\frac{\left(PNL\ (\dot{x}_i, \dot{h}_i) - 80\right)}{10}\right]^2_{PNL\geq 80} \cdot \frac{\Delta t_i}{\Delta t_{ref}} \qquad (5)$$

where J is the function to be minimized, and given the unit S-numbers

L is the number of time intervals

$\dot{x}_i$ is the horizontal velocity

$\dot{h}_i$ is the vertical velocity

Δt_i is the time interval over which PNL is measured

Δt_{ref} is some reference time interval.

Comparing this unit with that of the EPNL, which also integrates noise over a time period, there are three main differences

i) the S-number sums annoyance ($\sim 10^{\frac{PNL}{33.2}}$)

whereas the EPNL sums energy ($\sim 10^{\frac{PNL}{10}}$)

so that the duration effect is given more relative importance in the S-number formulation.

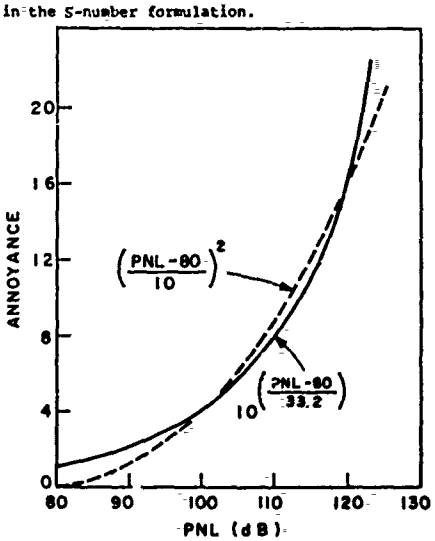

FIGURE 10 NOISE LEVEL VS. ANNOYANCE

ii) the EPNL has no explicit background noise level cutoff, whereas the S-number does.

iii) the EPNL takes the logarithm of the sum, whereas the S-number does not.

3.2 Results

3.2.1 Values of Parameters in Example

Figures 11 to 17 show the graphical output from one computer run. It is only intended to show how the program operates; it is not possible to draw any conclusions about improvements to the aircraft design from these figures. Nevertheless, they do show what the program is capable of and, more importantly, how it needs to be improved.

The parameters used in this example are as follows:

Gross weight	58,000 lb.
Blade chord	4.18 ft.
Blade thickness	.50 ft.
Rotor radius	36.4 ft.
Rotor angular velocity	14.3 rad/sec
Rotor blade angle of attack	0.07 rad.
Number of blades per rotor	3
Number of rotors	2
Fuselage equivalent flat plate area	39.5 ft^2
Distance of observer from take-off	500 ft.
Maximum allowable PNL	Unlimited
Terminal horizontal velocity	150 ft/sec.
Terminal vertical velocity	0 ft/sec.
Time to reach terminal conditions	29 sec.
Total shaft horsepower	22,000 hp.

3.2.2 Discussion of Results

Figure 11: Flight Path Profile: This figure shows the shape of the flight path profile. Program constraints prevent negative values of $\dot{x}$ or $\dot{h}$. As might be expected the aircraft takes off vertically and gradually translates to horizontal flight.

Figure 12: Height and Ground Track plotted against time: This figure serves only to reference the subsequent figures, which are plotted against time, against the flight path profile, in which time is not expressed explicitly.

Figure 13: Values of v, $\dot{x}$ and $\dot{h}$: The figure shows that the aircraft initially climbs vertically until a rate of climb of 40 ft/sec. is reached; it then starts to accelerate horizontally and the rate of climb remains constant at 50 ft/sec. The reason for this can be seen from Figure 15, which shows that at t = 5 seconds increase of rate of climb is restricted by power limitation. When the horizontal velocity has reached 60 ft/sec. the induced power has decreased sufficiently for the aircraft to increase its rate of climb to 60 ft/sec., whereafter the rate of climb remains constant for 2 seconds and then gradually decreases.

The decrease in horizontal velocity at t = 21 seconds serves to decrease the thrust, and hence noise level, while the aircraft is in audible range. From Figure 16 it can be seen that for t > 25 seconds the aircraft is out of audible range and is able to accelerate to terminal conditions without causing further annoyance. The overall reduction in annoyance gained by this manoeuver is very small and in

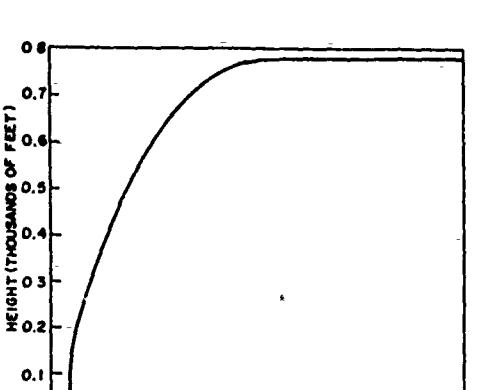

FIGURE 11 FLIGHT PATH PROFILE

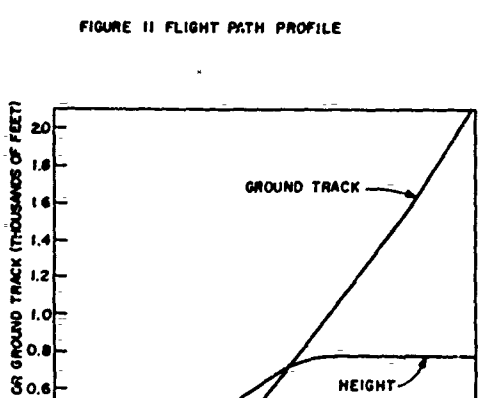

FIGURE 12 HEIGHT AND GROUND TRACK VS. TIME

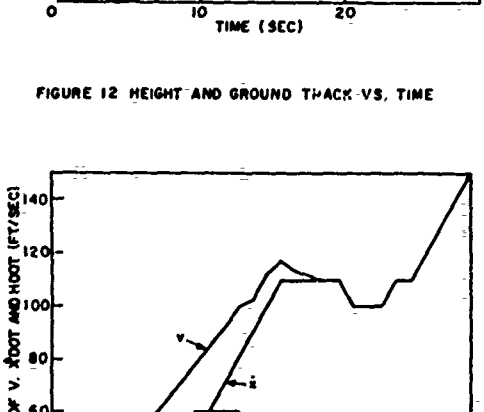

FIGURE 13. v, $\dot{x}$ AND $\dot{h}$ VS. TIME

practice would hardly be worth performing.

Figures 14 and 15; Thrust and Power Required: The plot of power requirement against time shows up one of the major limitations of the program as configured at present; aircraft performance is limited primarily by the number of control options that are available, and only secondarily by the maximum power constraint. For example, it would probably be advantageous to apply full power immediately after take-off, but the rate-of-climb control available does not use full power at the take-off conditions. The solution to this problem would be to have a greater range of controls available, so that controls utilizing maximum power could be used under all flight conditions.

Figure 16; Annoyance Produced: The curve shows the cumulative annoyance, so that the gradient of the curve indicates the level of annoyance at any given time. The curve is steep for the first 6 seconds when the highest level of thrust is applied, and less steep when thrust is reduced. The rate of cumulative annoyance finally decreases to zero as the aircraft recedes out of audible range.

3.3 Program Limitations and Extensions

3.3.1 Use of More Controls

In this dynamic programming example the control variables were numerically equal to the quantized increments in state variables. This avoided the need for interpolation procedures.

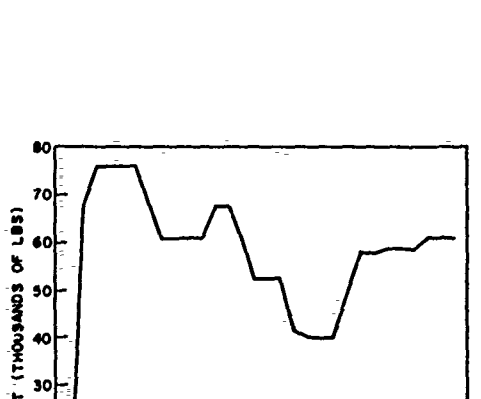

FIGURE 14 THRUST VS. TIME

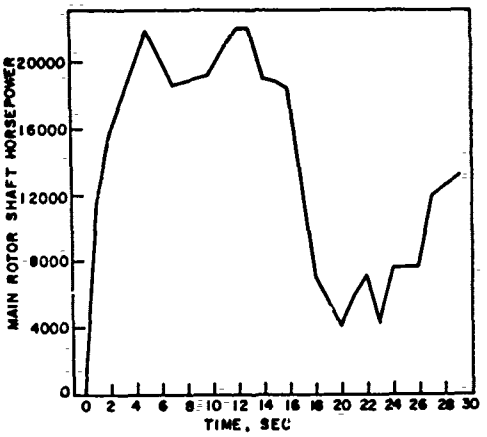

FIGURE 15 POWER VS. TIME

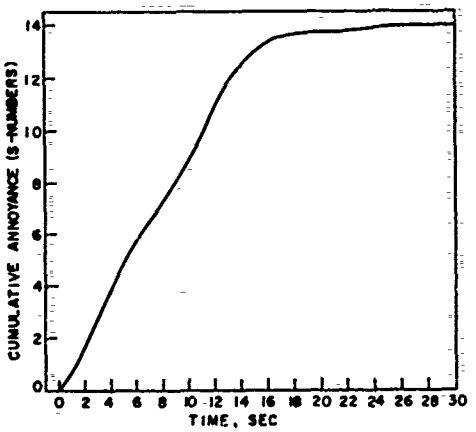

FIGURE 16 ANNOYANCE PRODUCED VS. TIME

If more controls were used the aircraft could fly at states that were not quantized increments in state variables. E.g., at present it can fly at either 20 ft/sec or 30 ft/sec but not intervening speeds.

Use of more controls would require a considerable increase in computing time but only a small increase in additional computer storage.

3.3.2 More Refined Noise Model

Reference 6 gives a directivity correction to equation (1) as

$$K_D = 10 \log \left[\frac{\cos^2 \phi + 0.1}{\cos^2 70 + 0.1} \right] \qquad (6)$$

where K_D is the correction to be applied to (1).

ϕ is the angle between listener and shaft axis. This correction can be applied without difficulty.

3.3.3 Use of More Listeners

Another useful modification to the program would be in the addition of more listeners, who could be positioned out of the plane of the flight path. Work is presently continuing on all these aspects of improvement.

4.0 Conclusions

4.1 By including noise as a measure of vehicle performance, it appears possible to design future helicopters which are significantly quieter (10-20 db) than current versions. The penalties for this quietness as measured by operating costs are in the range of 20-30%.

4.2 The optimal noise annoyance profile for a helicopter takeoff involves a vertical climb for 100 feet or more, and a substantial reduction in power as the listener is overflown.

REFERENCES

1. Helicopter Design Program Description, N. Faulkner, M. Scully, FTL Technical Memo 71-3, May 1971.
2. Generalized Rotor Performance, E. Kisielowski et al., The Boeing Co., USA AVLABS Tech. Report 66-83, Feb. 1967.
3. Helicopter DOC Comparison, M. Scully and N. Faulkner, FTL Technical Memo 71-2, Feb. 1971.
4. A Standard Method for Estimating VTOL Operating Expense, R.P. Stoessel and J.E. Gallagher, Lockheed-California Co., CA/TSA/013, October 1967.
5. Helicopter Rotor Noise Generation and Propagation, R. Schlegel et al, Sikorsky Aircraft Corp. USA AVLABS Tech. Report 66-4, October 1966.
6. Problems of Helicopter Noise Estimation and Reduction, J.B. Ollerhead and M.V. Lowson, AIAA Paper 69-195.
7. Noise Characteristics of VTOL Aircraft Elements, D. Kiang, FTL, in-Progress Report No. 3, Contract DOT-TSC-93, April 1971.
8. Noise Optimization of VTOL Takeoff and Landing Paths, A.E. Cole, MIT Department of Civil Engineering, M.S. Thesis, September 1969.
9. Noise Minimization of Helicopter Take-off and Climb-out Flight Paths using Dynamic Programming, A.P. Hays, MIT Department of Aeronautics and Astronautics, M.S. Thesis May 1971.
10. State Increment Dynamic Programming, R.E. Larson, American Elsevier Publishing Co., N.Y. 1968.
11. A Review of Aerodynamic Noise from Propellers, Rotors, and Lift Fans, J.E. Marte and D.W. Kurtz, NASA TR 32-1462, 1970.
12. Technique for Calculating Optimum Takeoff and Climbout Trajectories for Noise Abatement, K. Erzberger and H.Q. Lee, NASA TN D-5182.
13. 'Aircraft Noise - Mitigating the Nuisance', E.J. Richards, Astronautics and Aeronautics, January 1967.

Sound Attenuation Over Simulated Ground Cover *

S. P. Pao and L. B. Evans

Wyle Laboratories, 7800 Governors Drive, Huntsville, Alabama 35807

ABSTRACT

In dealing with wave propagation over land below 1000 Hz, ground attenuation is an important consideration. Very often, the actual ground surface is covered with a thick layer of vegetation which has a very high overall void to volume ratio. Such a composite boundary should be represented as layered media in order to assess the ground attenuation effect correctly. The wave attenuation characteristics under such conditions are studied in this paper. It is found through theoretical analysis that a layered boundary gives rise to strong selective absorption in certain frequency bands. Experimental data has been taken under laboratory conditions over a wide range of normalized parameters, and the results quantitatively confirm many aspects of the predictions. Both theory and experiment indicate that significant attenuation to very low frequencies can be expected for sound propagation over a deep layer of vegetation. Other results include the confirmation of a strong sound pressure gradient in the vertical direction near the layered boundary, that the excessive attenuation can increase at most 6 dB per doubling distance, and that the effectiveness of ground attenuation depends critically on the elevation angle of the sound source.

INTRODUCTION

The precise analytic nature of sound attenuation near a boundary with known acoustic impedance was first made clear in a series of studies by Rudnick [1], Ingard [2], and Lawhead and Rudnick [3]. The main application has been the estimation of ground attenuation effects on sound propagation in the atmosphere. Some subsequent analytical studies [4,5] and experiments [6,7,8] have further explored the details of this phenomenon. In these studies, the acoustic media above and below the boundary plane are assumed to be semi-infinite. Constant values are prescribed to either the impedances of the two media or the normal impedance of the boundary itself. However, in many situations with practical importance, the boundary between the upper and the lower semi-infinite acoustic media is not a simple plane, but a porous layer with finite thickness. It is natural, then, to investigate the wave attenuation characteristics near such a composite boundary.

In the analysis of the simple boundary configuration, the only geometrical parameter is the ratio of source height to the wave length. The magnitude of attenuation depends mainly on the impedance ratio, or the normal impedance, at the boundary. It was pointed out in the previous analytical studies that ground absorption arises because the sound wave propagates at nearly glancing angles of incidence, and the wave front is spherical. On the boundary, the ground attenuation increases at 6 dB per doubling the separation distance between the sound source and the point of observation. A steep sound pressure gradient exists near the boundary such that the ground attenuation effect decreases rapidly as one moves away from the boundary.

In previous experimental studies [6,7], selective absorption of sound due to ground effects has also been observed. The peak absorption band is usually located between 300-600 Hz. Two probable explanations have been offered: the interference effect of differential paths of wave propagation, and the variation of normal impedance of the boundary with respect to frequency. Evidence has been found to support both theories [4,5,6].

Owing to the special nature of wave reflections at near glancing angles of incidence, it is not possible to assign a constant value to the impedance of the entire composite boundary. A layered media representation becomes necessary in this case. It is required to specify both the acoustic impedance and the wave transmission constant of the porous transition layer. A new analysis is therefore required for estimating the magnitude and characteristics of the ground attenuation of such a layered boundary.

In addition to the analysis, an experimental study has also been undertaken to determine the attenuation characteristics of a layered boundary. The results of the experiment are intended for the verification of the theory as well as for obtaining a separate view of the problem from an independent approach. The experiment was performed under laboratory conditions such that the ground attenuation effect can be studied without the uncertainty of other complications such as wind refraction and turbulent scattering. Overall, the present study has found significant departure in several aspects of the attenuation characteristics of a layered media from those of a simple boundary. Thus, one may find the results useful in dealing with a variety of practical problems where a layered representation of the boundary is warranted.

1. FORMULATION AND ANALYSIS

The geometrical configuration for wave propagation over a layered boundary is shown in Figure 1. In this figure, the top semi-infinite layer is assumed to be air, which has a density of ρ_0, speed of sound c_0, and acoustic impedance of $\rho_0 c_0$. The middle layer is assumed to be a porous material. Its density and speed of sound are in general complex quantities. In other words, it has a complex acoustic impedance such that a plane wave transmitted from the air into this layer will be refracted into the layer with a phase shift, and will be attenuated as it propagates through this material. A third medium which represents the ground, occupies the lower half space. For the simplicity of analysis, a constant normal impedance is prescribed at the interface between the middle layer and the semi-infinite ground. Also shown in Figure 1 is a schematic of wave propagation paths through which the sound from a point source can reach an arbitrary point in the half space above the layered boundary. The interference of the waves through these paths is responsible for the boundary attenuation effect.

As pointed out in previous studies, the simple ray acoustics approach can not account for the observed ground attenuation phenomenon, and a more rigorous mathematical analysis must be followed. In the present study, the approach of Ingard [2], together with coordinate systems and symbols in that paper, has been adopted. The coordinate systems are shown in Figure 2.

A spherical wavefront which originates from a point source can be represented as an integral of its plane wave elements

$$\frac{e^{ikr}}{kr} = \left(\frac{i}{2\pi}\right)\int_0^{2\pi} d\phi \int_0^{-\frac{\pi}{2}+i\infty} e^{i\left[k_1 x + k_2 y + k_3 (h-z)\right]} \sin\theta \, d\theta \qquad (1)$$

In the above integral, the vector (k_1, k_2, k_3) identifies the wavenumber of a plane wave element, and h denotes the height of the sound source above the top of the layered boundary. The reflection of the primary wave at a boundary can evidently be represented as

* The material in this paper was presented in part at the 80th Meeting of the Acoustical Society of America, November 1970, Houston, Texas.

$$p_r = \left(\frac{i}{2\pi}\right)\int_0^{2\pi} d\phi \int_0^{\frac{\pi}{2}+i\infty} e^{i\left[k_1 x + k_2 y + k_3 (h+z)\right]} R(\phi,\theta)\sin\theta\, d\theta \qquad (2)$$

where $R(\phi, \theta)$ is the plane-wave reflection coefficient. The reflection coefficient $R(\phi, \theta)$ is a function of ϕ and θ.

It is more convenient for the purpose of integration to write Equation (2) in a new spherical coordinate system where the principal direction of the reflected ray is chosen as the reference axis [2]. The new angular variables are defined as ψ and η. Equation (2) can now be represented as

$$p_r = \left(\frac{i}{2\pi}\right)\int_0^{2\pi} d\psi \int_0^{\frac{\pi}{2}+i\infty} e^{ikr_2\cos\eta} R(\psi,\eta)\sin\eta\, d\eta \qquad (3)$$

An integral of this form can be evaluated by using the method of steepest descent [9] in the acoustic far field where the value of kr_2 is large compared to unity. Along the paths of steepest descent in the complex η-plane, a new variable can be defined such that

$$\cos\eta = 1 + it \qquad (4)$$

where t is real and positive.

The reflected wave can be then written as

$$p_r = \frac{e^{ikr_2}}{kr_2}(kr_2)\int_0^{2\pi}\int_0^{\infty} e^{-kr_2 t} R(\psi,t)\, dt\, d\psi = \frac{e^{ikr_2}}{kr_2} Q \qquad (5)$$

which has the form of a wave originating from an "image source", located at a distance h below the top of the layered boundary, with a variable strength Q.

For an arbitrarily given function of $R(\psi, \theta)$, Equation (5) can only be integrated approximately. A first asymptotic approximation has been given by Brekhovskikh [10] as

$$p_r = \frac{e^{ikr_2}}{kr_2}\left\{R(\gamma_0) + \frac{1}{ikr_2}\left(\frac{1}{2}(1-\gamma_0^2)R''(\gamma_0) - \gamma_0 R'(\gamma_0)\right)\right\} \qquad (6)$$

where $\gamma_0 = \cos\theta_0$

R' and R'' are the first and second derivates of R with respect to $\gamma = \cos\theta$. Equation (6) serves as a starting point for the present analytical investigation into ground attenuation owing to layered media.

It remains here to determine the plane-wave refraction coefficient $R(\theta)$ for a boundary with a layered configuration. The overall reflection coefficient accounts for the wave reflection at the top of the middle layer, as well as the wave which is transmitted into the middle layer, reflected by the ground, and returned into the air, (Figure 3). Hence, the overall reflection coefficient of the layered boundary can be given

$$R(\theta) = (\cos\theta - \beta_1\cos\theta_1)\Big/(\cos\theta + \beta_1\cos\theta_1) + 4\beta_1\cos\theta\cos\theta_1(\cos\theta_1 - \beta_2)\Phi\Big/\left\{(\cos\theta + \beta_1\cos\theta_1)^2(\cos\theta_1 + \beta_2)\right\} \qquad (7)$$

with $\Phi = \exp\left\{2ikh(n^2 - 1 + \cos^2\theta)^{\frac{1}{2}}\right\}$

and $\cos\theta_1 = n^{-1}\left\{n^2 - 1 + \cos^2\theta\right\}^{\frac{1}{2}}$,

where β_1 is the specific admittance ratio of the middle layer with respect to air, β_2 is the specific admittance ratio at the interface of the middle layer and the ground, and θ_1 is the refraction angle in the middle layer. The function Φ accounts for the phase difference between the two reflected wave components. This phase shift is caused by path difference and the wave transmission characteristics of the middle layer.

The instantaneous value of sound pressure in the far field can now be determined as

$$p = \frac{e^{ikr_1}}{kr_1}\left\{1 + \frac{r_1}{r_2}e^{ik(r_2 - r_1)} X \left[R(\gamma_0) + \frac{1}{ikr_2}\left(\frac{1}{2}(1-\gamma_0^2)R''(\gamma_0) - \gamma_0 R'(\gamma_0)\right)\right]\right\} \qquad (8)$$

The derivatives of $R(\theta)$ with respect to $\cos\theta$ can be obtained from Equation (7). By substituting the known expressions for $R(\theta)$, R', and R'' into Equation (6), an explicit expression can be obtained for the reflected wave. The attenuation of sound near the layered boundary can now be obtained by simply adding the incident and the reflected sound pressure fields.

The algebraic expressions involved in the computation of the sound pressure field in the upper half space is straightforward, but relatively bulky. Therefore, the results have been programmed for calculation using a digital computer. The asymptotic approximate solution is very accurate for computations of sound pressure levels in the far field, i.e., points which are more than a few wavelengths away from the sound source. For the study of ground attenuation effects, this is a practically insignificant restriction. In the computing program, all of the geometrical and acoustical parameters can be varied independently. In particular, the specific admittance ratios β_1, β_2 and the refraction index n, are assumed to be complex numbers. Some computations have been made for the limiting cases where the thickness of the middle layer approaches zero and the results agree very well with those given by Ingard [2].

II. EXPERIMENTS

The measurements of sound attenuation over a layered boundary were made on a 20 ft by 8 ft plywood platform. It serves as an idealized hard ground surface with very high acoustic impedance. A layer of porous material of uniform thickness is placed on top of this platform. The construction of the platform, the layout of the porous material, and the set-up of instrumentations, are relatively straightforward. The longest range distance available on this platform is 200 inches, and the thickness of the porous layer varies from 2 to 6 inches in the various cases. The chosen sound source is an acoustic transducer with a 3/4 in.

diameter throat openning. One-half inch Bruel and Kjaer microphones are mounted at six locations on the top and above the layer of porous material to measure the sound pressure levels in the far field.

The entire test set-up was placed in a free field environment since a large anechoic chamber was not available. However, the free field arrangement was quite satisfactory since the ambient noise level was below 45 dB, and wind and turbulence in the test area were virtually non-existent. The data was corrected for molecular absorption in air and, in most cases, this correction was very small and negligible.

From experience gained through preliminary tests, it was found that waves propagating at near glancing angles of incidence can penetrate through a porous layer and re-emerge from it only if the layer is extremely porous. Layers composed of other types of acoustic materials with higher densities may behave like semi-infinite layers. Hence, the choice of layer material for this test becomes a particularly interesting task. Basically, the suitable material should be extremely porous and yet have a stable and uniform structure such that repeatable data can be obtained with accuracy. The materials chosen for this experiment are listed below:

(1) Rubberized Horsehair Material — This is a matrix type of material composed of rubberized synthetic fibers. The density is 1.36 lb/ft^3. The estimated void to volume ratio is 97.8%. Average fiber diameters are approximately 0.004 ~ 0.01 inch. The average distance between two nonintersecting fibers is approximately 0.005 ~ 0.15 inch. However, large clear openings of 1/2 inch in diameter and depth are not uncommon. This material is originally intended for packaging of electronic instrumentation. It is commercially available in sheets of 2-inch thickness.

(2) Glass Fiber Air Filter — This is the material commonly used as air filters in heating and air-conditioning units. It is composed of long, stiff, and unbonded glass fibers. The size of the fibers is fairly uniform with a nominal diameter of 0.002 inch. The average distance between parallel fibers is approximately 0.05 inch. The density of this material is 0.52 lb/ft^3, and the void to volume ratio is approximately 99.7%. This material is commercially available in rolls of 1-inch thickness and up to 36 inches in width.

(3) Fiberglas batt — A 4-inch thick Fiberglas batt was also chosen. In spite of its extremely low density of 0.29 lb/ft^3, it has an acoustic impedance comparable to the above two materials. Moreover, the absorption factor for sound propagation in this material is relatively high.

The acoustic impedance of these materials has been measured in an impedance tube [11]. Due to the low densities of these materials, the combined normal impedance of the sample and the rigid end plate of the tube has actually been measured. It was found that the acoustic impedance characteristics of the first two materials are approximately equal. The measured impedance values are frequency dependent. For frequencies above 1000 Hz, however, the impedance reaches a constant limiting value. Attempts have been made to determine the acoustic impedance of the sample itself by decoupling the effects due to the solid backing. Some analysis indicates that the specific admittance ratio of the first two materials with respect to air is between 0.5 to 0.7. In the third material, the damping factor for wave transmission through this material is relatively high. Hence, the effect of the solid backing is much less prominant. The measured specific admittance ratio of the Fiberglas batt is approximately 0.6.

The refraction indices of these materials have not been measured. According to the data given in Beranek [12], materials in a similar density range usually have a refraction index between 1.10 and 1.25 at frequencies above 1000 Hz.

A total of twenty sets of measurements were made for various combinations of materials, layer thickness, and sound source height. In each set, microphone readings were taken at six locations in the far field over a frequency range of 1 K Hz to 20 K Hz. The scaling factor of this laboratory experimental set-up with respect to various practical field conditions ranges approximately from 1/10 to 1/100. Therefore, the tested sound frequencies would correspond to a frequency range of 10 Hz to 2000 Hz in the field. Out of these tests, a significant range of normalized conditions for sound attenuation over layered media has been encompassed. Since the tests are performed in terms of descrete frequencies and the microphone readings are recorded directly on a level recorder, the data reduction procedure was relatively simple.

III. DISCUSSION OF RESULTS

By using Equation (8), a series of case studies have been calculated to investigate the dependence of sound attenuation on various geometrical and acoustical parameters. In this study, the principal geometrical quantities are the wavelength, the middle layer thickness, and the height of sound source above the top of the middle layer. For calculations of sound pressure levels in the far field, the wavelength is chosen to normalize the coordinates, while in studies of sound absorption spectrum, the layer thickness is chosen as the reference length to normalize the frequencies. Among the three acoustical parameters, β_1 and n are more important; β_2 is usually much smaller than unity, and it has only secondary influence on the overall results. For a highly porous middle layer, β_1 is generally in the neighborhood of unity. The refraction index, n, is also close to one for isotropic porous materials with low densities. However, a porous material with special structure may have a very large refraction index.

Sound attenuation over a layered boundary is found to depend on the layer thickness. A typical case is shown in Figure 4. The sound pressure level contours in the far field for a sound source located at the top of the boundary have been computed for two different layer thicknesses. A general redistribution of sound can be seen in this figure. Of particular significance is the attenuation pattern near the boundary. On the boundary itself, the attenuation at any point can differ by about 5 dB from one case to another. The difference in sound pressure level decreases gradually as one moves away from the boundary. At line AA, the difference vanishes. In the wedge shaped region between the boundary and line AA, the difference in sound pressure level at different layer thicknesses prevails even if the sound source is located high above the boundary. However, the point of maximum difference in such cases will be located somewhere between the boundary and the line AA. Figure 4 shows also that the sound pressure gradient near the boundary is very steep.

Calculations have also been made to investigate the dependence of sound attenuation on frequency and individual acoustic parameters. For simplicity, the layer thickness, the source height, and β_2, are assumed to be constant. The source height is assumed to be one layer thickness above the boundary. Sound pressure levels in the far field are computed for given frequencies and various values of β_1 and n. It was found in these calculations that, for a given pair of values for β_1 and n, the attenuation of sound at the boundary itself remains more or less constant for all frequencies. However, at a slight distance above the boundary, a significant band absorption pattern emerges due to the variation of the sound pressure gradient for different frequencies.

At this point, a subtle descrepency between the analysis and practical ground attenuation consideration becomes apparent. In the analysis, the acoustic media in all layers are assumed to be perfectly homogeneous and stationary, and the boundaries are perfectly flat surfaces. A sound pressure gradient can always be maintained even though it may be extremely large. However, in laboratory or field measurements, slight perturbations in the speed of sound or material non-uniformity will exist. Under such conditions, the actual sound pressure level contour will not be as sharp as predicted by the analysis. One can only measure the average sound attenuation value over a portion of this computed steep sound pressure gradient. Hence, in subsequent discussions of attenuation spectrum, the value of sound attenuation due to boundary effect is taken by averaging over a distance of 0.10 of the layer thickness immediately above the boundary. The 0.10 thickness value is set arbitrarily. However, it is partially related to the fact that most of the experiments were made with layers of 4" to 6" thick, and the microphones used in these measurements were 1/2-inch diameter, which is approximately 1/10 of the layer thickness. The pressure signal sensed by the microphone is, therefore, an average value.

The dependence of the sound attenuation spectrum on the refraction index is shown in Figures 4 and 5. The specific admittance ratios are held constant. In these figures, the wavelengths are normalized with respect to the constant layer thickness. The sound attenuation due to the boundary effect is shown in decibels for a point 50 layer thicknesses away from the sound source. In Figure 5, three curves with small values of the refraction index, n, are shown. The attenuation spectrum shows clearly a peak in the low frequency range. The location of this peak depends on the value of the refraction index. For a layer of 20 ft thickness, these absorption peaks will correspond to frequencies between 50 Hz ~ 200 Hz. The dash vertical line indicates the expected absorption peak location if the middle porous layer were removed such that only the high impedance bare ground were left. For values of n between 1.20 and 2.0, the attenuation peak oscillates in the low frequency range ($kh < 40$). However, the overall attenuation spectrum shows a definite shift towards lower frequencies as n increases. In some cases, there is more than one peak. In the limiting case of a layer with a very large complex refraction index, i.e., $n \gg 2$, the layered boundary is effectively equivalent to a simple boundary with a normal impedance. The attenuation spectrum, which is an average value over a short distance near the boundary, decreases monotonically with frequency. The computed attenuation spectra for $n \gg 2$, and for $n = 2$, are shown in Figure 6. The attenuation spectrum for $n \gg 2$ shows a higher level of sound attenuation than all computed spectra at other values of n.

For a fixed value of refraction index near unity, the variation of an attenuation spectrum with respect to β_1 is quite simple. A typical set of curves is shown in Figure 7. The magnitude of attenuation increases with the specific admittance ratio while the attenuation peak remains in approximately the same location.

The experimental data obtained in this study have been reduced and normalized. The general characteristics of ground attenuation, such as the existence of a steep sound pressure gradient immediately above the boundary, and that the ground attenuation increases by 6 dB per doubling the distance from the sound source, have been clearly confirmed. The experimental data was found to be repeatable within a band of about 2 dB. The classical law of reciprocity, which implies that the value of sound attenuation remains unchanged if the positions of the sound source and the microphones are exchanged, was found to hold in this experiment. Although it had nothing to do with the objective of this study, it was a convenient reference for the verification of accuracy.

A few unique properties of sound attenuation over a layered media are also born out by this experiment. A comparison of the experimental and theoretical attenuation spectra is shown in Figure 8. Three sets of attenuation measurements with similar normalized geometrical configuration, but with different materials and layer thicknesses are shown on this figure. The agreements of the magnitude of sound attenuation and the location of the peak are very close. Although the acoustic parameters used for the theoretical curve is probably not the exact value for the acoustic materials used in the experiment, the prediction, nevertheless, shows the correct trend and order of magnitude.

By comparing the analytical curve with the data, one finds that the data is significantly below the prediction in the high frequency range. It is probably because the wave reflections become randomized such that the ground interference effect becomes ineffective. It is interesting to note that the measured absorption peak frequency is significantly below the expected "bare ground" interference peak, which is computed by using ray acoustics and is indicated by the dash line. This is particularly significant since the layered materials used in the experiment have a void to volume ratio of well over 97 percent, and large surface openings. Intuitively, one might think that such materials should have little effect on ground absorption.

Some anormalies of the dependence of sound attenuation versus distance have been measured. In Figure 9, a variation of ground absorption versus distance is shown. The values were obtained from the experiments. For the low density ground materials that were used, and for ground attenuation in distances of less than 50 wavelengths ($k x < 300$), the ground absorption and rate of increment is smaller than the classical predictions. The 6 dB per doubling distance rate is observed for distances beyond 50 wavelengths. In some sets of data,

IV. SUMMARY AND CONCLUSIONS

Several important characteristics of sound attenuation, which are unique to a layered boundary, have been found through this analytical and experimental study:

1. Selective sound attenuation in a certain frequency band has been predicted and observed for a layered boundary with constant (frequency independent) acoustic properties. Such an effect has not been considered in previous investigations in the literature.
2. A layer of extremely porous material can still offer significant attenuation to sound propagating at near glancing angles of incidence.
3. For an extremely porous layer, the sound attenuation in the near field of the sound source is usually very low. Pressure doubling may occur due to the reflected wave from the hard ground surface. However, the attenuation at distances sufficiently far away from the source will be dominated by the acoustic properties of the layered material, and significant attenuation levels are observed.

pressure doubling has also been detected in the near field at the lower frequencies.

It was found also in the analysis and the experiment that the magnitude of ground attenuation depends critically on the height of the sound source. Figure 10 shows the dependence of sound attenuation on the apparent elevation angle of the sound source as observed from a point in the far field. The data points are obtained in the experiment. If the sound source is at more than 8 degrees above the horizontal, the boundary attenuation drops below 5 dB. In many practical situations where noise control is of primary concern, the ground attenuation at large elevation angles becomes insignificant. An analytical computation, showing the effect of source height on the far field sound pressure level pattern, is given in Figure 11.

The analytical results obtained in this study seem to predict the correct trends and magnitude of sound attenuation over a layered media, and can probably be used as a basis for the development of practical ground attenuation prediction techniques for situations where a layered boundary description is warranted. Of course, a substantial amount of work has yet to be done.

ACKNOWLEDGMENT

This work was supported by the U. S. Army Research Office — Durham, North Carolina, under Contract DAHC04-70-C-0016.

REFERENCES

1. I. Rudnick, "The Propagation of an Acoustic Wave Along a Boundary," J. Acoust. Soc. Am. 19, 348 (1947).
2. K. U. Ingard, "On the Reflection of a Spherical Sound Wave from an Infinite Plane," J. Acoust. Soc. Am. 23, 329 (1951).
3. R. Lawhead, and I. Rudnick, "Acoustic Wave Propagation Along a Constant Normal Impedance Boundary," J. Acoust. Soc. Am. 23, 546 (1951).
4. U. Ingard, "On Sound Transmission Anomalies in the Atmosphere," J. Acoust. Soc. Am. 45, 1038 (L), (1969).
5. W. L. Howe, "Ground Reflection of Jet Noise," National Aeronautics and Space Administration, Report TR R-35, (1959).
6. K..U. Ingard, "Review of the Influence of Meteorological Conditions on Sound Propagation," J. Acoust. Soc. Am. 25, 405, (1953).
7. F. M. Wiener and D. N. Keast, "Experimental Study of the Propagation of Sound Over Ground," J. Acoust. Soc. Am. 31, 724 , (1959).
8. P. B. Oncley, "Low Frequency Ground Attenuation in Outdoor Noise Measurements," J. Acoust. Soc. Am. 47, 122 (A), (1970). Also, J. Sound and Vibration 13, 27, (1970).
9. E. T. Copson, Asymptotic Expansions, (Cambridge University Press, Cambridge, 1967).
10. L. M. Brekhovskikh, Waves in Layered Media, (Academic Press, New York, 1960).
11. L. L. Beranek, "Precision Measurement of Acoustic Impedance," J. Acoust. Soc. Am. 12, 3 (1940).
12. L. L. Beranek and S. Labate, "Properties of Porous Acoustic Materials," in Noise Reduction, L. L. Beranek, Ed., Chapter 12, p 271, (McGraw Hill Book Company, Inc., New York, 1960).

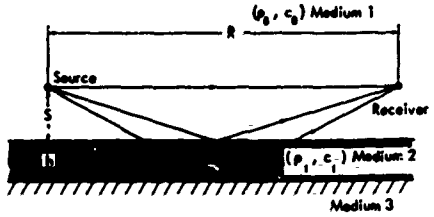

Figure 1. Reflection of a Plane Wave from Layered Media at Near-Glancing Incidence Angles

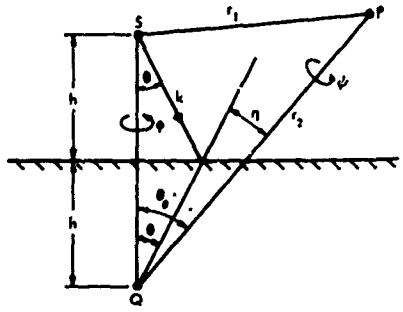

Figure 2. Coordinate Systems Employed by Ingard in his Theoretical Treatment of Ground Attenuation (Reference 2)

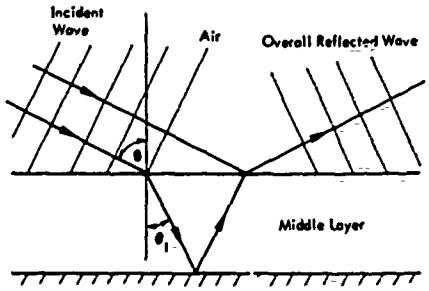

Figure 3. Reflections of a Plane Wave from a Layered Boundary

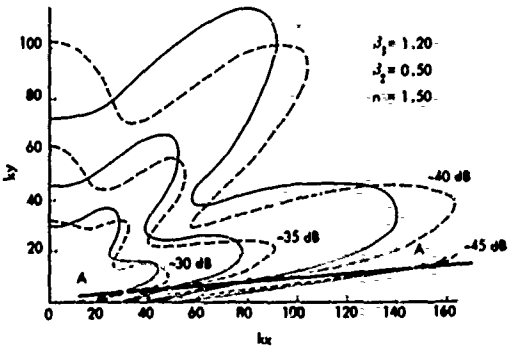

Figure 4. Ground Attenuation Directivity Pattern for two Different Ground Cover Thicknesses. The layer thickness for ——— is 0.5 wavelength, and the layer thickness for – – – – is 0.25 wavelength. The sound source is located at one wavelength above the boundary.

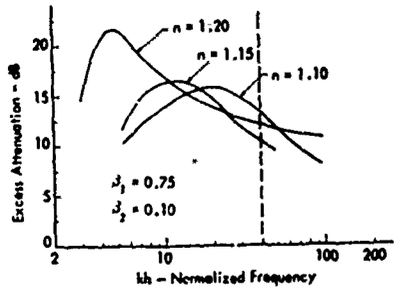

Figure 5. Ground Attenuation Spectrum as a Function of the Refraction Index. The sound source height equals the layer thickness, h. Sound attenuation values are computed for a point 50h away from the sound source. The location of absorption peak for hard ground without cover is indicated by a dashed line.

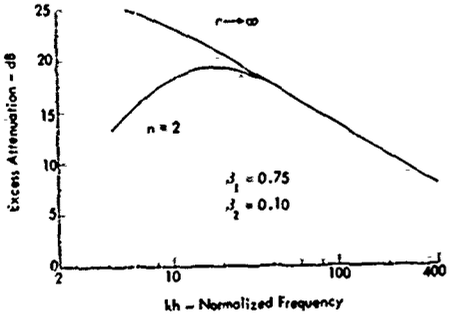

Figure 6. Ground Attenuation Spectrum for Layers with Large Refraction Indices. All the geometrical parameters are the same as in Figure 5.

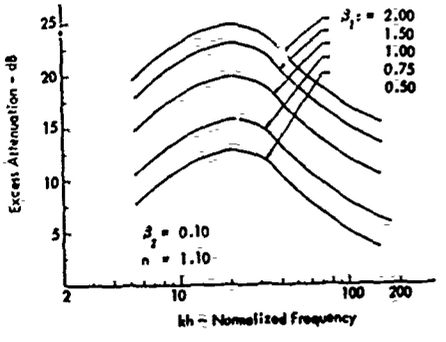

Figure 7. Ground Attenuation as a Function of the Specific Admittance Ratio of the Layer.

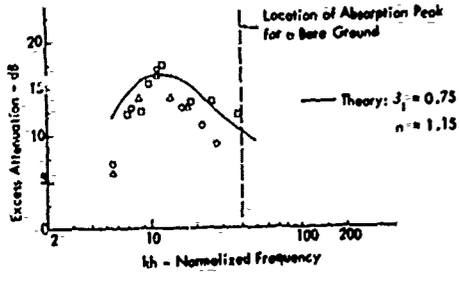

Figure 8. Comparison of Experimental Ground Attenuation Spectrum with a Theoretical Prediction. Data obtained for three ground cover materials are shown: ○ horsehair at 4-in. thickness; △ horsehair at 2-in. thickness; and □ fiber filter at 6-in. thickness.

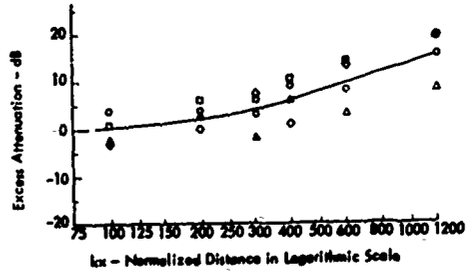

Figure 9. Ground Attenuation as a Function of Distance. Data are obtained for four types of layer materials: ○ fiberglass filter at 6-in. thickness; △ fiberglass filter at 4-in. thickness; □ horsehair at 4-in. thickness; and ◇ horsehair at 2-in. thickness.

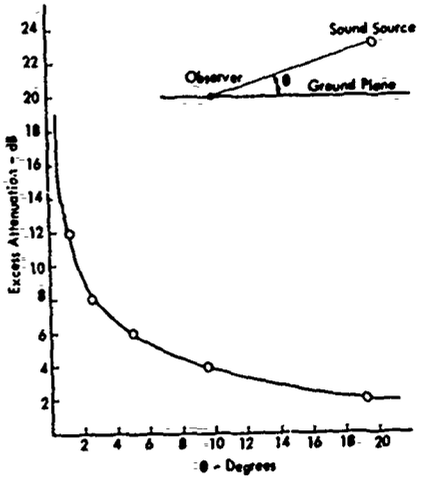

Figure 10. Ground Attenuation as a Function of Evaluation Angle of the Sound Source.

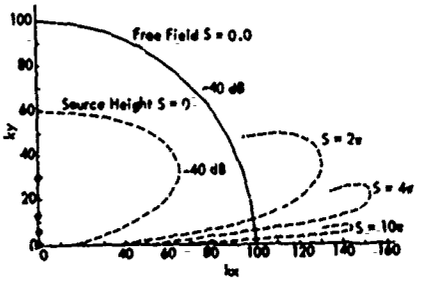

Figure 11. Attenuation Patterns near the Ground for Various Source Heights. The acoustic parameters for the layered boundary are β_1 = 1.20, β_2 = 0.50, and n = 1.50.

ATMOSPHERIC ABSORPTION OF SOUND: THEORETICAL PREDICTIONS *

L. B. Evans — Wyle Laboratories, Huntsville, Alabama 35807

H. E. Bass — University of Mississippi, Department of Physics & Astronomy University, Mississippi 38677

L.C. Sutherland — Wyle Laboratories, El Segundo, California 90245

ABSTRACT

By assuming air is composed of four gases, i.e., nitrogen, oxygen, water vapor, and carbon dioxide, and applying energy transfer rates for the binary collisions inherent in such a system, absorption of sound in the atmosphere has been predicted. The calculated curves based upon twenty-four energy transfer mechanisms are compared with experimental data over the humidity range of 0-100% relative humidity. Agreement between theory and experiment is very good. By including classical absorption and rotational relaxation effects the total atmospheric absorption is also predicted at 20° C. Calculations made for various concentrations of CO_2 indicate that low CO_2 levels (less than 0.1%) do not significantly affect absorption of audible sound at high humidities. At very low humidities, however, CO_2 is an important factor.

I. INTRODUCTION

A basic characteristic of sound propagation is the attenuation with distance due to various irreversible processes which remove energy from an acoustic wave and convert it to heat. Prediction of sound propagation in air over long distances has become a matter of increasing practical significance in several areas including:

- Prediction of community noise levels around airports
- Analysis or acoustic detection of tactical equipment or aircraft
- Evaluation of very low frequency sound in the atmosphere generated by rocket engines or from natural sources such as tidal motion, earthquakes, wind storms, etc.
- Investigation of the vertical propagation of sonic disturbances from signaling grenades or sonic booms.

Where it is necessary to evaluate sound propagation over a substantial number of wavelengths, the absorption of sound by the atmosphere must be considered. Propagation characteristics are dependent upon (a) atmospheric conditions, (b) the position of the source relative to the ground, and (c) the terrain/vegetation features adjacent to the sound path. The above listed factors which affect the intensity of the sound arriving at the observer can be classified as follows:

Spreading Losses

- Uniform spherical spreading (Inverse Square Law) losses
- Non-uniform spreading
  - reflection by finite boundaries
  - refraction by non-uniform atmosphere
  - diffraction (scattering) by non-stationary atmosphere

Absorption Losses

- Absorption by ground and ground cover
- Absorption by atmosphere
  - classical absorption
  - molecular relaxation absorption

Of these sound propagation effects, different ones may be the controlling factor for different atmospheric meteorological conditions and for varying source-receiver placement; however, for any type of condition or any type of sound propagation path, the absorption due to classical and molecular effects are fixed for a homogeneous atmosphere and are functions only of the propagation path distance, the humidity content, gas impurities, and the temperature. Before the more variable propagation effects can be accurately assessed, it is necessary, therefore, to establish the proper values for these fixed absorption losses.

Atmospheric Absorption Losses

Atmospheric absorption losses have two basic forms: (1) classical losses associated with the change of acoustical energy (or kinetic energy of molecules) into heat by fundamental gas transport properties, and (2) for polyatomic gases, relaxation losses associated with the change of kinetic or translational energy of the molecules into internal energy within the molecules themselves.

The classical losses can be further sub-divided into

- Viscous Losses
- Heat Conduction Losses — Stokes-Kirchhoff Loss
- Diffusion Losses
- Radiation Losses

Only the Stokes-Kirchhoff Losses are considered significant for air under normal atmospheric conditions. Diffusion losses contribute only about 0.3% more and radiation losses are significant only at very low frequencies.

Relaxation absorption losses in polyatomic gases are known to have the following forms.

- Thermal relaxation between translational energy and vibrational energy states of the molecules
- Thermal relaxation between a close vibrational resonance of two different molecules
- Thermal relaxation between the vibration of one molecule and the rotation of a different molecule
- Thermal relaxation between translational energy and rotational energy states of the molecules
- Electromagnetic relaxation between translational energy and allowable electronic energy states of the molecule.

As far as is known, electromagnetic relaxation is significant for only one common gas, nitric oxide, NO, and then, only at very high ultrasonic frequencies[1].

In the balance of this paper, a basic theoretical technique for predicting the total atmospheric absorption losses is presented along with supporting experimental data.

II. THEORETICAL METHOD

Investigations of sound absorption mechanisms in air have been carried out by many different laboratories since the pioneering experimental work of Pielemeier[2] in 1929 and has culminated recently in the work of Harris[3], Harris and Tempest[4], Mank[5], and Evans and Sutherland[6]. The theoretical treatment of the problem has lagged somewhat behind the experi-

* The material in this paper has been presented in part at the Helicopter Noise Symposium, Durham, North Carolina, September 28-30, 1971 and at the 82nd meeting of the Acoustical Society of America, Denver, Colorado, October 1972.

mental results. Knesers' 1933 theoretical treatment has largely been used to explain the experimental data[7]. However, it has always been recognized that this theory does not give an adequate description of the entire problem. Sutherland[8] and Piercy[9] have shown that at frequencies well below the maximum absorption there is a distinct systematic deviation from single relaxation theory. It is this area that this paper attempts to clarify.

In this paper, air is considered as a four-gas mixture, i.e., nitrogen, oxygen, carbon dioxide and water vapor. By applying the energy transfer rates for the binary collisions inherent in such a system, absorption of sound in the atmosphere is predicted. The calculated curves are based upon twenty-four energy transfer mechanisms as shown in Tables I and II.

The theoretical prediction of total sound absorption also requires calculation of the losses due to classical effects and molecular relaxation. The classical absorption can be written as

$$\alpha_{cl} = \frac{2\pi^2 f^2}{\gamma P_0 V_0}\left[\frac{4}{3}\eta + \frac{\gamma-1}{C_p}\kappa + \gamma a_d D_{12}\rho\right] \qquad (1)$$

where
- α_{cl} = total classical absorption
- P_0 = gas pressure
- f = sound frequency
- γ = effective specific heat ratio of the gas
- V_0 = sound velocity at low frequencies
- η = viscosity of the gas
- C_p = effective specific heat of the gas at constant pressure
- a_d = a molecular diffusion constant
- D_{12} = diffusion coefficient for O_2 and N_2 mixture
- ρ = gas density
- κ = thermal conductivity

For frequencies less than that at which rotational relaxation occurs this expression can be evaluated in terms of the viscosity based on measured values for the above constants[10]

$$\alpha_{cl} = \frac{2\pi^2 f^2}{\gamma P_0 V_0}\left[1.900\right]\eta \qquad (2)$$

For frequencies greater than that at which rotational relaxation occurs the general expression must be used and the effective values of the frequency dependent terms utilized[11]. Equation (2) was utilized to calculate classical losses in this study with γ taken as its low frequency value.

The absorption due to thermal relaxation between translational and rotational energy states of the molecules was calculated assuming that the rotational relaxation of each molecule was the same in air as in the pure gas. This assumes that during a collision with unlike molecules, the probability of transferring rotational energy for each molecule is independent of the collision partner. This assumption, of course, would be very poor for high frequencies. For the frequencies of interest, however, a change by a factor of 2 or 3 in the rotational relaxation time for any constituent molecule would lead to very little change in the total absorption. The effects of rotational relaxation were included by writing the effective specific heat as the sum of the contributions from the translational, (3/2R), vibrational, and rotational modes.

$$(C_v)_{effective} = \frac{3}{2}R + (C_v)_{vibration} + R\sum_{j=1}^{n} x_j \frac{(f_j-3)}{2}\frac{1}{1+i\omega\tau_j} \qquad (3)$$

where j represents the constituent molecules of air, i.e., CO_2, H_2O, O_2 and N_2; and

- x_j = concentration of molecule j
- f_j = number of degrees of freedom of molecule j
- ω = 2π times the sound frequency
- τ_j = rotational relaxation time of molecule j
- n = number of types of molecules considered.

For purposes of this study, only CO_2, N_2, O_2 and H_2O were considered; however, the method is quite general provided the above assumption regarding the effects of unlike collisions on the rotational relaxation times is valid.

The final term to be considered includes the sound loss due to the thermal relaxation between translational energy and vibrational energy states (V-T), between vibration of one molecule and the vibration of another (V-V), and between the vibration of one molecule and the rotation of the same or different molecule (V-R). The difference between (V-T) and (V-R) processes is only important when calculating energy transfer rates; so, for these calculations both processes will be considered as being (V-T). These vibrational relaxation processes are the dominant causes of loss at low acoustic frequencies.

The sound absorption due to vibrational relaxation was calculated using the method first advanced by Tanczos[12] which was expanded to a two component system by Shields[13] and later expanded by Shields and Bass[14] to allow for three-for-one (V-V) exchange between colliding molecules. The only information required to perform such calculations are the binary rate constants and the concentration of each gas present.

Shields' equations for expressing the acoustic absorption and dispersion as a function of the various energy transfer rates of importance were used as a starting point for these calculations. The only modifications required to expand the method to a four component system was a change in Equation (6) of Reference 13. The modified equations become

$$k_{10}(I) = \sum_{i=1}^{n} x_i \, MAP_0^I(I,0,A)$$

$$k_{0b}^{00}(I,J) = \sum_{i=1}^{n} x_i \, MAP_b^a(I,J,A)$$

where the terms have been defined in Reference 13. These two expressions allow the effective vibrational specific heat to be calculated which in turn can be used to determine the absorption and velocity of sound using Reference 13.

A total of 24 energy transfer processes were considered. The rates for these processes are given in Table I. Rates are labeled as $MAP_b^a(I,J,A)$. The letter A indicates the type molecules involved in the collision. An index to the numbering system used is given in Table II. MA is the number of collisions of type A occurring each second in air at one atmosphere of pressure. $P_b^a(I,J,A)$ is the probability that, during a collision between the molecules involved in type A collisions, mode I of one molecule will lose "a" quanta of vibrational energy while mode J of the same molecule or the collision partner gains "b" quanta of energy. The modes are numbered as follows:

- Mode 0 = translational mode of any molecule
- Mode 1 = symmetric stretching mode of CO_2 (ν_1 = 1388 cm^{-1})
- Mode 2 = bending mode of CO_2 (ν_2 = 667 cm^{-1}) (doubly degenerate)
- Mode 3 = asymmetric stretching mode of CO_2 (ν_3 = 2349 cm^{-1})
- Mode 4 = vibrational mode of N_2 (ν_4 = 2331 cm^{-1})
- Mode 5 = vibrational mode of O_2 (ν_5 = 1580 cm^{-1})
- Mode 6 = bending mode of H_2O (ν_6 = 1595 cm^{-1})

For example $M2P_1^1$ (4,0,2) is the rate for the (V-T) process

$$N_2^* + CO_2 \rightarrow N_2 + CO_2$$

and $M4P_1^1$ (4,5,4) is the rate for the (V-V) process

$$O_2 + N_2^* \rightarrow O_2^* + N_2$$

where * indicates a vibrationally excited mode. The symmetric and asymmetric stretching modes of H_2O were not considered since their contributions to the total specific heat is very small.

A rather large number of rates have been considered since at different humidity and frequency combinations different rates are the controlling mechanisms for the sound absorption. For example, at high humidities the effect of CO_2 is insignificant in concentrations below 1000 parts per million. However, in relatively dry air the CO_2 content controls the relaxation frequency of the mixture as shown in Figure 1. The most important rates for the study are the (V-T) and (V-V) rates for O_2/H_2O collisions; the (V-T) rate for H_2O/H_2O collisions; the (V-T) and (V-V) rates for N_2/H_2O collisions; and at low humidities the (V-T) and (V-V) rates for O_2/CO_2 interactions. It should be recognized that any of the above (V-T) rates could very well be the result of a (V-R) process followed by a rapid (R-T) process.

Although only the absorption has been discussed, the velocity could also be calculated by the same method. The velocity, however, is less sensitive to the presence of relaxation.

The power of the theoretical method used is its versatility. The same theoretical method and computer program could be used for any combination of gases. The effect of pollutants on the frequency dependence of sound absorption and the absorption of sound in alien atmospheres could readily be calculated provided the binary collision rates were known. In many cases, these rates can be found in the literature. Those not available in the literature can be measured in controlled laboratory conditions without being concerned with all the variables inherent in field measurements. The temperature dependence of the relaxation absorption can also be calculated if the temperature dependence of the individual transition rates are known. Additional laboratory measurements of the temperature dependence of the rates important in sound absorption must be made before more accurate theoretical predictions will be possible. A great deal of progress has been made towards developing theoretical expressions for energy transfer rates. Once such expressions are developed, calculations of sound absorption from molecular constants will be possible. This area clearly deserves additional attention.

III. RESULTS

The predicted curves are shown in Figures 2 through 5 along with available experimental data. Of the three sets of data, Harris and Tempest's is thought to be the most accurate. Agreement between theory and experiment is very good. The curves and data have been presented in the form, m/m_{max} versus f/f_{max} where m is the intensity attenuation coefficient and m_{max} is its value at the relaxation frequency f_{max}. By normalizing both axes, data for the various different humidities can be plotted on the same graph. In each case the experimental data has been normalized by f_{max} predicted by Monk's expression and the value of m_{max} has been computed using the Planck-Einstein relationship for the specific heat of the oxygen content. An error in f_{max} will move a data point along a 45° line; an error in m_{max} will change the vertical position of the data point on the m/m_{max} scale and hence both parameters affect the agreement between theory and experiment.

Figure 6 depicts the predicted curves of μ/μ_{max} versus f/p where μ is the absorption per wavelength. It is readily obvious from these curves that sound absorption in air is a multiple relaxation process. The curves have been normalized by the major peak which is due to the vibrational specific heat of oxygen, hence, as a result of the nitrogen relaxation μ/μ_{max} does not necessarily equal one. The minor peak is not as easily explained. It is primarily due to the nitrogen content of air; however, its position in frequency is primarily a function of the water vapor content[15].

Comparison between f_{max} and theory as a function of humidity is shown in Figure 7 along with Monk's curve[5]. It is not surprising that Monk's results and the present work are identical at high humidities since we have taken the rates which are important at high humidities from Monk's paper. However, there is considerable difference at lower humidities (Figure 1). This work approaches a value of approximately 30 Hz for the relaxation frequency at zero humidity. This agrees very well with the values reported by Piercy[16] which were extracted from very low temperature air data. There is some uncertainty in this 30 Hz prediction since the rate for O_2/CO_2 (v_2) (V-V) coupling is not well known. As shown in Figure 1 a difference of one order of magnitude in this particular rate makes approximately the same difference in f_{max} at zero humidity. For this work, $M0P_1^1$ (5, 2, 0) was chosen to be 3.0×10^3 sec^{-1} atm^{-1} to agree with Piercy's[16] results. Taylor and Bitterman[17] suggest a value of 3.0×10^4 sec^{-1} atm^{-1}. The third curve in Figure 1 emphasizes the importance of including the trace amounts (300 ppm) of CO_2. Without CO_2 the zero humidity relaxation frequency is approximately 6 Hz.

The acoustician is often faced with making corrections for atmospheric absorption and for these purposes Figure 8 is included. These curves show the total absorption (i.e., classical, vibrational, and rotational absorption) in dB/1000 ft versus f/p at 20° C. It is felt that the accuracy of these predicted curves will be well within any experimental error in field measurements and can be used without hesitation.

IV. SUMMARY

The theoretical method developed allows the acoustic absorption to be calculated to an accuracy comparable to that of present experiments. If the need for more accurate predictions of sound absorption arises, then the transition rates required in the theory must be determined more accurately, especially those involving water vapor. Further, if the theoretical method is to be expanded to alien atmospheres, the necessary binary vibrational energy transfer rates must be determined experimentally or calculated. The ability of the theoretical technique to predict the temperature dependence of the sound absorption depends upon the temperature dependence of the various vibrational rates. Again these rates involving water vapor need additional study. In order to make calculations of the absorption of sound in air, or any other calculation which requires transition rates, without "a priori" knowledge of the various transition rates, theoretical expressions for these rates must be developed. To date there has been marginal success with (V-T) calculations and with (V-R) calculations but none with (V-V) theory. These calculations also deserve additional study.

Some error may be introduced into the present calculations by exclusion of the trace amounts of H_2 and Ar which are present in the atmosphere. These constituents, particularly H_2, may have some importance at extremely low humidities. The uncertainty introduced by neglecting these two trace elements, however, is certainly no greater than that already present owing to the uncertainty in the transition rates.

These calculations were expedited by most of the needed transition rates being available in Taylor and Bitterman's[17] excellent review article on the transition rates important for CO_2 lasers. Other reviews of this nature, where the various data sets are not only recorded but their accuracy assessed, are certainly needed.

It is felt by these authors that the method and curves presented can be used to predict atmospheric sound propagation reliably at 20° C and probably safely over a 5° spread around 20° C. Not until better information is available on the temperature dependence of many of the transition rates will accurate calculations as a function of temperature be possible.

V. ACKNOWLEDGMENTS

This work was sponsored by the Army Research Office - Durham. One of us (HEB) wishes to express his gratitude to the Committee on Faculty Research of the University of Mississippi and the Office of Naval Research for support. We all express our gratitude to Dr. F. D. Shields of the University of Mississippi for making available a copy of his computer program for a binary gas mixture.

REFERENCES

1. Kneser, H.O., Bever, H.J., Kescha, H., J. Acoust. Soc. Am. 41, 1029-1031 (1967).
2. Pielemeier, W.H., Phys. Rev., 34, 1184-1203 (1929).
3. Harris, C.M., NASA CR-617; J. Acoust. Soc. Am., 40, 148-159 (1966); J. Acoust. Soc. Am., 43, 530-532 (1968); J. Acoust. Soc. Am., 49, 890-893 (1971).
4. Harris, C.M., Tempest, W., NASA CR-237; J. Acoust. Soc. Am., 36, 2390-2394 (1964).
5. Monk, R.G., J. Acoust. Soc. Am., 46, 580-586 (1969).
6. Evans, L.B. and Sutherland, L.C., Wyle Laboratories Research Staff Report WR 70-14.
7. Kneser, H.O., J. Acoust. Soc. Am., 5, 122-126 (1933).
8. Sutherland, L.C., J. Acoust. Soc. Am., 46, 86(A) (1969).
9. Piercy, J.E., J. Acoust. Soc. Am., 46, 602-604 (1969).
10. Greenspan, M., J. Acoust. Soc. Am., 31, 155-160 (1959).
11. Evans, L.B., Bass, H.E., and Winter, T.G., J. Acoust. Soc. Am., 48, 771(L) (1970).
12. Tanczos, F.I., J. Chem. Phys. 25,439-447 (1956).
13. Shields, F.D., J. Acoust. Soc. Am., 47, 1262-1268 (1970).
14. Shields, F.D., and Bass, H.E., J. Acoust. Soc. Am., 50, 382-383(L) (1971).
15. Evans, L.B., J. Acoust. Soc. Am., 50, 0000 (1971).
16. Piercy, J.E., J. Acoust. Soc. Am., 49, 110(A) (1971).
17. Taylor, R.L., Bitterman, S., Rev. Mod. Phys., 41, 26-47 (1969).
18. Knotzel, H., Akust. Z., 5, 245-256 (1940).
19. Knudsen, V.O., J. Acoust. Soc. Am., 6, 199-204 (1935).
20. Pahlman, W., Proceedings of the Third International Congress on Acoustics, Stuttgart, 1959, 532-535, L.L. Cremer, editor, (Elsevier, Amsterdam, 1961).
21. Evans, E.J., and Bazley, E.N., Acustica, 6, 238-245 (1956).
22. "Atmospheric Physics and Sound Propagation," Pennsylvania State University, September 1950.
23. Knudsen, V.O., J. Acoust. Soc. Am., 5, 112-121 (1933).
24. Dobsesse, L.P., U.S. Air Force Contract W-28-099-ac-228, February 1953.

TABLE I

Rate	Value in sec^{-1} atm^{-1}	Reference
$M0P^1_2$ (3,2,0)	6.0×10^4	a
$M0P^1_0$ (2,0,0)	3.0×10^4	a
$M0P^1_1$ (5,2,0)	3.0×10^5	a
$M0P^1_2$ (1,2,0)	4.5×10^8	a
$M1P^1_0$ (2,0,1)	1.8×10^5	a
$M1P^1_3$ (3,2,1)	1.5×10^5	a
$M1P^1_2$ (1,2,1)	4.5×10^8	a
$M2P^1_0$ (2,0,2)	3.4×10^4	a
$M2P^1_0$ (4,0,2)	1.0	a
$M2P^1_1$ (3,4,2)	1.8×10^7	a
$M2P^1_3$ (3,2,2)	6.0×10^4	a
$M2P^1_2$ (1,2,2)	4.5×10^8	a
$M3P^1_0$ (2,0,3)	4.2×10^8	b
$M4P^1_1$ (4,5,4)	1.5×10^{12}	a
$M4P^1_0$ (5,0,4)	40	a
$M4P^1_0$ (4,0,4)	1.0	a
$M5P^1_0$ (5,0,5)	63	c
$M6P^1_1$ (6,5,6)	4.6×10^7	c
$M6P^1_0$ (5,0,6)	1.1×10^6	c
$M6P^1_0$ (6,0,6)	6.0×10^4	c
$M7P^1_0$ (4,0,7)	1.0	a
$M8P^1_0$ (4,0,8)	1.13×10^5	d
$M8P^1_0$ (6,0,8)	1.4×10^6	c
$M9P^1_0$ (6,0,9)	1.0×10^9	c

a. See Reference 17.

b. Shields, F.D. and Burks, J.A., J. Acoust. Soc. Am., 43, 510-515 (1968).

c. See Reference 5.

d. See Reference 15.

e. Reference 17 gives an estimated value of $\sim 3 \times 10^6$ sec^{-1} atm^{-1}. However, for this work we have chosen a value of 3×10^5 sec^{-1} atm^{-1} which agrees with results of Reference 16.

TABLE II

Molecules Colliding - A		Molecules Colliding - A	
CO_2/O_2	0	O_2/O_2	5
CO_2/CO_2	1	O_2/H_2O	6
CO_2/N_2	2	N_2/N_2	7
CO_2/H_2O	3	N_2/H_2O	8
O_2/N_2	4	H_2O/H_2O	9

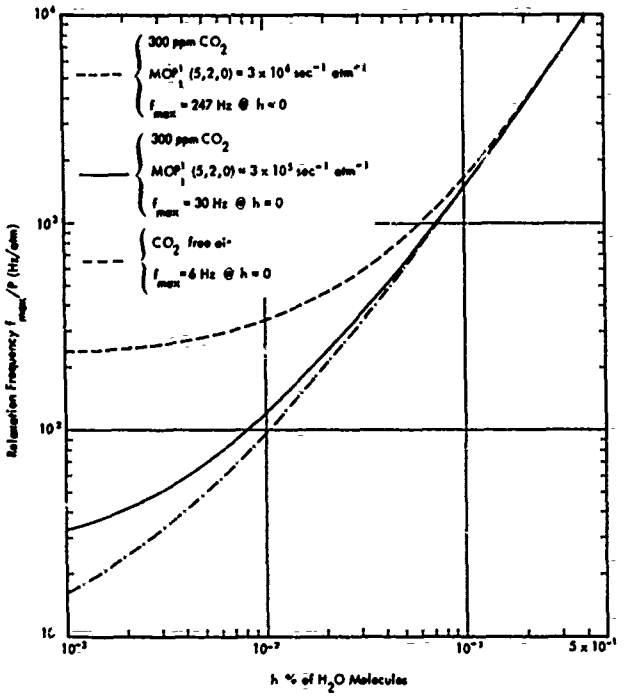

Figure 1. Low Humidity Plot of Relaxation Frequency as a Function of Percent H_2O Molecules. The solid line represents the best calculation and has been calculated with $MOP_1^1(5,2,0) = 3 \times 10^3$ sec^{-1} atm^{-1} for 300 ppm CO_2. The dashed curve represents 300 ppm CO_2 and $MOP_1^1(5,2,0) = 3 \times 10^4$ sec^{-1} atm^{-1} and has been included to emphasize the importance of this rate at low humidities. The dot-dash curve represents CO_2 free air.

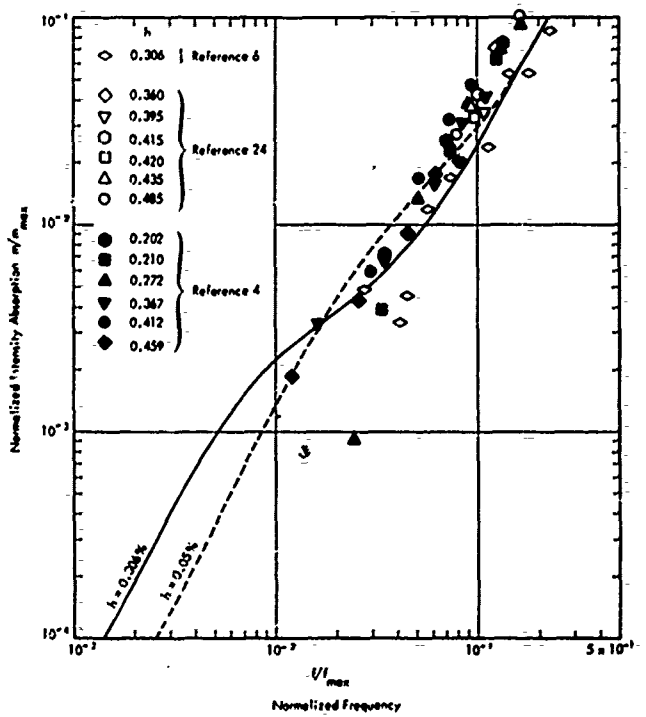

Figure 2. Normalized Intensity Absorption as a Function of Normalized Frequency for Less than 0.5% H_2O Molecules. The solid curve has been calculated for 11% Relative Humidity @ 23° C (h = .306% H_2O molecules). The dashed curve has been calculated for 1.8% Relative Humidity @ 23° C (h = 0.06% H_2O molecules).

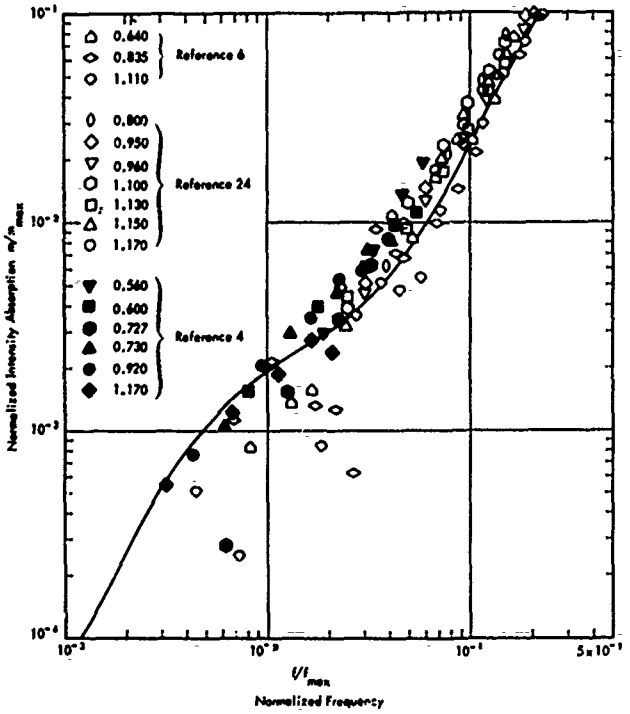

Figure 3. Normalized Intensity Absorption as a Function of Normalized Frequency for 0.5% to 1.2% H_2O Molecules. The solid curve has been calculated for 23° C and represents an average value of the calculated curves in this humidity range. The difference in the calculated values over this range is about twice the line thickness.

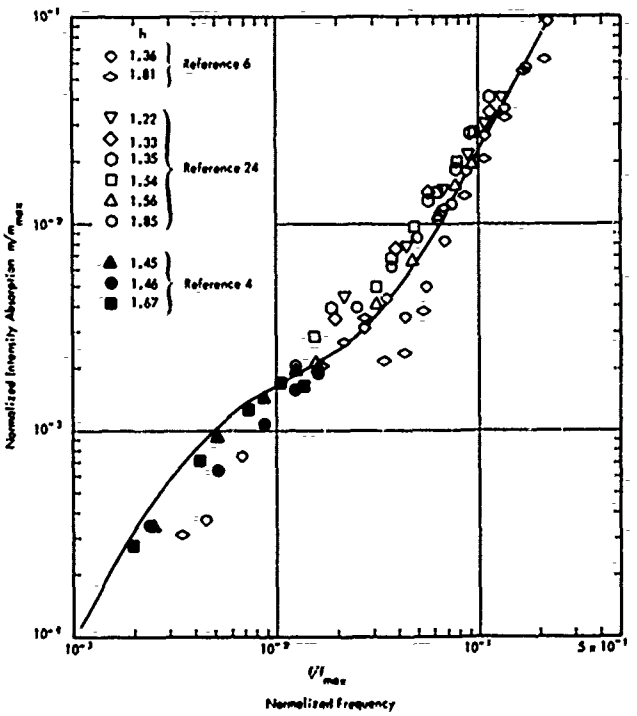

Figure 4. Normalized Intensity Absorption as a Function of Normalized Frequency for 1.2% to 1.9% H_2O Molecules. The solid curve has been calculated for 23° C and represents an average value of the calculated curves in this humidity range. The difference in the calculated values over this range is about twice the line thickness.

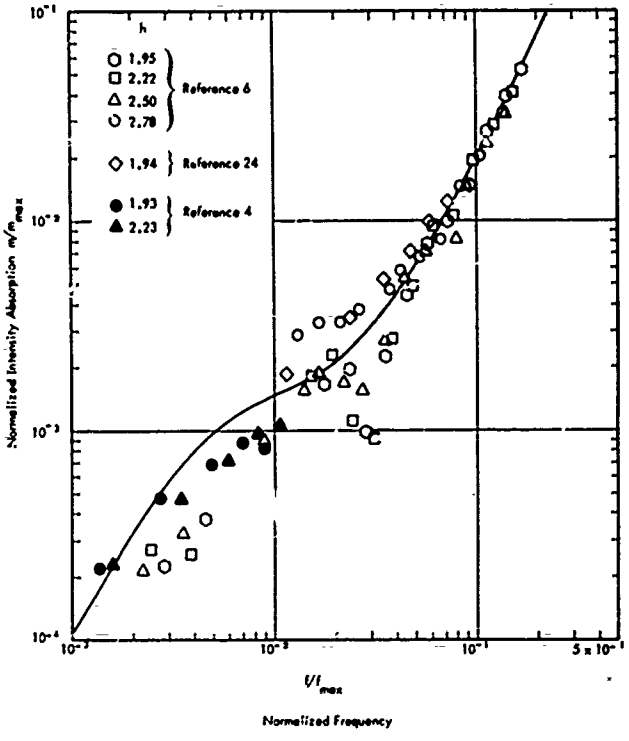

Figure 5. Normalized Intensity Absorption as a Function of Normalized Frequency for 1.9% to 2.5% H_2O Molecules. The solid curve has been calculated for 23° C and represents an average value of the calculated curves in this humidity range. The difference in the calculated values over this range is about twice the line thickness.

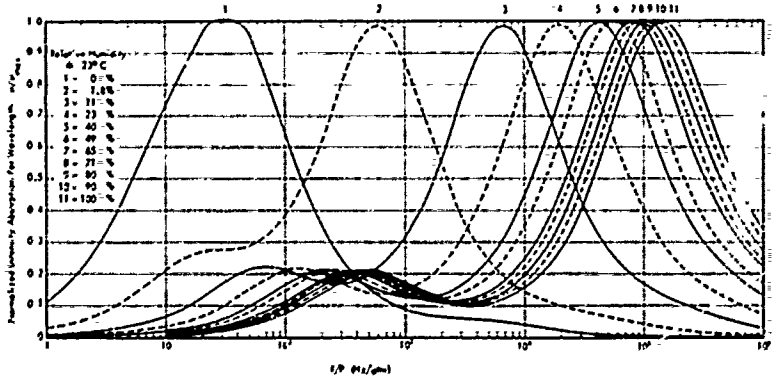

Figure 6. Normalized Molecular Absorption Per Wavelength as a Function of Frequency. The curves are calculated for the indicated relative humidities at 23° C.

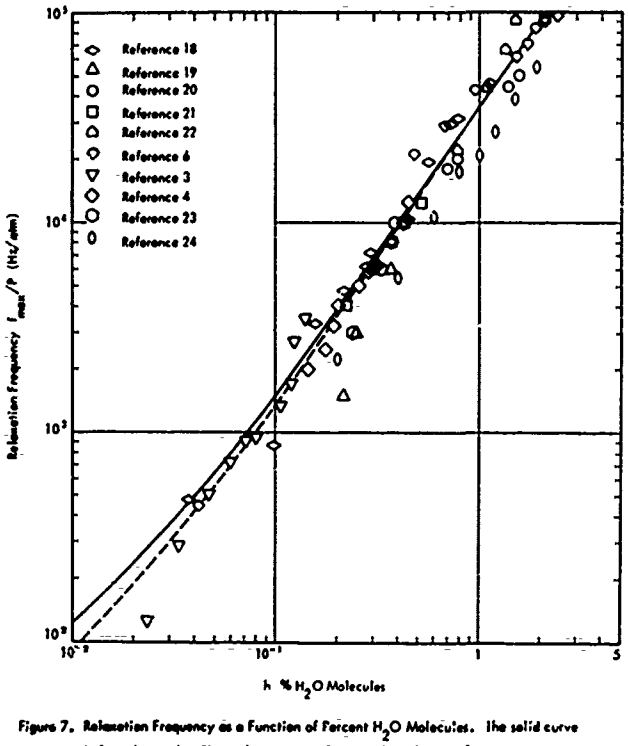

Figure 7. Relaxation Frequency as a Function of Percent H_2O Molecules. The solid curve is from this work. The dashed curve is from Monk (Reference 5).

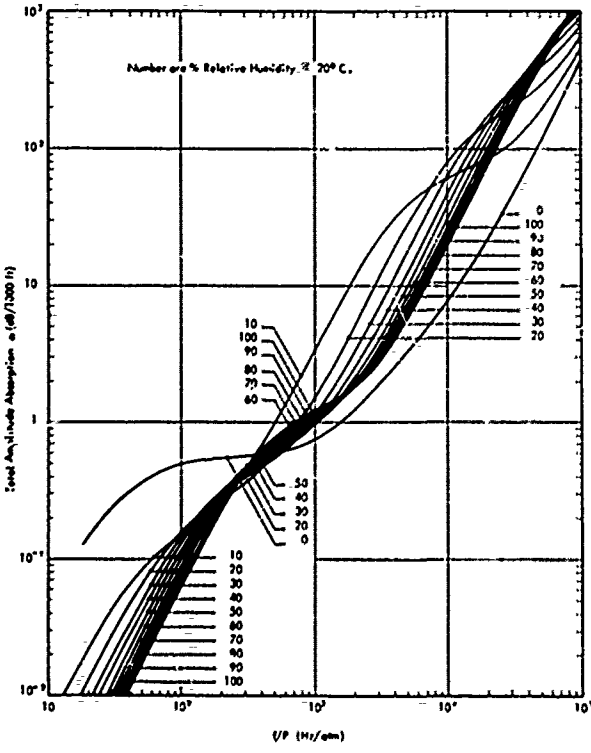

Figure 8. Total Absorption of Sound in Air as a Function of Frequency. The curves range from 0 to 100% relative humidity and are for 20° C.

Addendum to Proceedings

Helicopter Noise Symposium
28-30 September 1971

SUMMARY SESSION

Mr. Richard Ballard:

I think a summary session is very important for a couple of reasons. One is that it gives us an opportunity to sum up the papers that we have had during the last day and a half of meetings. The other thing is that it gives us a good opportunity to take a look and to assess where we have been and where we might be going. I would suggest that you give a little thought to where we are going in some of our programs and if we are really effective in solving the problem of the helicopter in the military environment. As I mentioned to you yesterday, operators are going to be reluctant to sacrifice performance to reduce noise. They are going to be reluctant to pay more for quieter helicopters with the exception of special purpose vehicles. These special purpose vehicles have a grouping of their own, so I don't think we're going to orient our efforts in that direction. Also, if we're going to reduce the noise of helicopters, we cannot do it at the expense of performance. I think we should keep these points in mind as we proceed.

We have five sessions, and I propose to let the chairman of each one o. these sessions approach it as he wishes. He may summarize the session or make his own remarks. The first session yesterday morning was chaired by Mr. Meade Mitchell and addressed the Government programs, so I will ask Mr. Mitchell to start off.

Mr. Meade Mitchell:

We have given considerable thought to trying to summarize the session we had yesterday. Generally it was a summary of the programs being sponsored by AMRDL (the Army Air Mobility Research and Development Laboratories) in conjunction with NASA. Out of that, a couple of remarks would be appropriate now from the AMRDL standpoint. It is evident that we are going to continue to invest a considerable amount of our limited resources, that is, funds, manpower and, in the case of NASA, facilities. We are going to depend pretty heavily on NASA for support as far as the Government facilities are concerned, and also on industry and universities for support of our noise program. However, it is evident that we must concentrate now on coming to an agreement amongst ourselves about defining the causes and possible solutions, and then acceptable ways of predicting noise and noise reduction methods. There are questions of how we put this in specifications from the Government's standpoint in our new systems work, how we specify what we want, and then, after we've specified it all, how we measure it.

I think there is some work to be done on coming up with an acceptable, understandable, common system of measuring noise reduction techniques. We have made some starts on this, such as under what conditions do we measure, what type of instrumentation do we use, what are the atmospheric conditions under which we are going to grade the contractor for his efforts, what kind of terrain is to be considered and things like that. It's about time we try to bring some of these aspects into focus. As we said yesterday, we are going ahead to develop systems whether or not we reduce the noise.

I am excited about some of the work that has been reported here, sponsored by ARO-D, some of the independently sponsored work, and some of the work we're trying to sponsor through the Army labs. I think we are on the verge of coming up with some techniques of predicting and eliminating noise. Now that we are beginning to understand some of the fundamental mechanisms that cause it, I think there are some design techniques that we can use. That has been evident in some of the papers presented today by Vertol. So, in summary, I think we've got to bring into focus some of these things that we are all discussing - the techniques, the measurements, and more important, the way to specify what we want without compromising performance. After we have specified, how do we grade the contractor and how do we make him stick to his contract of producing what we say we want?

I think that generally summarizes our session of yesterday. Again, I am encouraged by the things I've heard here today. It seems as though we are well on the road to a better understanding of the causes of noise and how to use them to make design improvements to reduce noise.

Aerodynamic Theory

Dr. Robert W. Truitt:

Thank you, Dick. As most of you know, I have worked with ARO-D closely over the past six or more years. And in particular, I saw the planning of Dr. Kumar in what we now see as the beginning of fruitful work in helicopter noise.

First of all, I want to say that I am impressed with the quality of papers that we had in this session. I think it's clear, and Meade Mitchell mentioned this, that there have been some important things reported here. I do think that the mission we set out to accomplish in this noise program can be realized, and I emphasize "can be" because I think it's clear to all of us that we still are a long way from answering some of the real, fundamental questions.

First of all, I want to mention the papers that were presented during this session. The first paper was a preliminary "Noise Analysis of the External Aerodynamic Diffuser Applied to Shrouded Propellers", presented by Dr. Ron Bailey and Mr. Richard Longhouse. It was brought out during the discussion of this paper that the instability of the flow due primarily to any forward motion would be caused by flow separation, that is, separation off of the shroud itself. This points to the important fact that viscosity effects are of great importance not only in the aerodynamic considerations but to noise problems as well.

The second paper was concerned with "Theoretical and Experimental Studies of Helicopter Noise Due to Blade-Vortex Interactions" and was presented by Drs. Widnall, Chu and Lee. The first type of blade-vortex interaction discussed was for the tandem rotor, where the unsteady lift on a blade is calculated using an existing linear unsteady aerodynamic theory for blade-vortex interaction. For the tip-dominated blade-vortex interaction, unsteady slender body theory is used to calculate the unsteady forces on the blade as it encounters the vortex. The theoretical model for radiated sound due to transient lift fluctuations was presented along with the predictions of the directivity, frequency spectrum, and transient acoustic signals. Agreement was found to be good compared with the experiment for small angle blade-vortex interactions. It occurred to me that perhaps one of the places where we need to consider an improvement in the approach to a problem as complicated as this is to hope that sometime we can get into the non-linear theory, particularly as you approach larger angles of attack. The inviscid slender body theory is, of course, an old standby that we always lean upon,but there are many new theories that are concerned with the viscous-transonic slender body flow which I hope we can incorporate soon.

As we move along, hopefully we can improve our theories and our ability to predict by putting in more realistic inputs from the aerodynamics point of view. Right now, transonic aerodynamics is a very popular subject. ARO-D is supporting some very interesting work in viscous transonic flow, and we are hopeful that important findings will develop from these studies. I think it would behoove us as helicopter people to keep abreast of all of this new research activity.

The third paper, given by Drs. Lyon, Mark and Pyle, was entitled "Synthesis of Helicopter Rotor Tips for Less Noise". Dr. Lyon gave a presentation of studies of rotor tip sound radiation for purposes of designing rotor tips that radiate less sound in specified frequency bands. Consideration, as you may recall, was given to radiation due to lift and thickness effects. Dr. Lyon showed that lift radiation is generally negligible in comparison with thickness radiation in specified frequency bands. Factors that affect trade-offs between choices of airfoil section and planform were discussed. Now, here again, I believe that the non-linear viscous aerodynamics that we might have as an input might be an improvement in the approach to this problem. In other words,

both the second and third papers seemed to me to require a better input than linear inviscid slender-body theory. I do not mean to imply that we won't be needing to use the wind tunnel to get a lot of answers, because theory is not going to be completely sufficient. But, some very important theoretical findings are available concerning optimum or shockless transonic airfoils. The work of Nicuwland and others may lead to optimum airfoils, bodies and wing-body combinations that will be efficient in the transonic range. They are not going to be as efficient at lower speeds, but it looks like we can hope to have some better and more efficient means to operate very near the speed of sound or certainly in the super critical range. It seems clear to me that an optimum aerodynamic body shape (meaning optimum with respect to, say, drag rise) is compatible with an optimum shape for less noise. I don't think we are going to eliminate noise but I would certainly be surprised if when you get a good aerodynamic configuration in the transonic range, you're going to have a good noise configuration too. I would like to hear what someone else in the audience has to say about that.

The fourth paper, as you recall, was given in two parts, one by Professor Sears and the other by Mr. Homicz. The first part of this presentation was related to engine noise and involved an investigation of blade forces arising from rotor-stator interaction in subsonic flow. One important conclusion was that the Kemp-Sears type of approximation can be extended to include compressibility effects by means of techniques suggested by Amiet and Sears. He also mentioned some apparent discrepancies in the results of Johnson on gust loads in subsonic two-dimensional flow. But, in particular, the extension of the Kemp-Sears theory in the compressible range involved a first-order theory for unsteady flow that was analogous to the Prandtl-Glauert correction, but it had an additional effect, that is, a first order distortion of any time-varying boundary condition, which was referred to as the gasp approximation. It is very clear that this work cannot be applied to the transonic range or even to the super critical range, because the Prandtl--Glauert theory simply breaks down. This, again, points to the fact that a better viscous-transonic approach is needed. The noise problem is most acute in this aerodynamic regime. Finally, you recall, Greg Homicz gave the second part of the presentation: "Acoustic Radiation from a Plane Surface with Application to Rotors". He developed a general approach for predicting acoustic radiation from a plane surface that exerts a fluctuating load upon the surrounding fluid. But again, if your recall, his analysis called for a linearized aerodynamic theory input. The same remarks that I made before pertain here, too.

It would now seem appropriate to have questions or comments from the audience.

Dr. Sheila Widnall:

I certainly agree with much of what you say. And when you and I talk about transonic flow, we know what that extension requires. I think many of the other people here may not realize how difficult transonic flow has always been for the aerodynamicist. It's one of those fields like turbulence, which everybody knows is very important. There have been very few strides made in transonic flow and these have always been won at great expense and great complexity. The reason that we use tools like linear aerodynamics analysis is that they allow us to predict an enoumous number of phenomena with fairly good accuracy at a fairly low cost. The transonic flow is not that kind of a problem, although I certainly agree it is a very important problem. I would also make the remark that it is known that in the case of unsteady transonic flow, the linear theory is often much better than it has any right to be. I'm sure you are familiar with the work of Martin Landahl, who did a lot of work in unsteady transonic flow. In the unsteady flow regime, you may be much better off using linear theory than you would be in the corresponding steady flow case. This has an application to what Dick Lyon is doing. He is looking at an unsteady transonic flow problem, using linear theory. Because it is unsteady, it is very likely that his results are more accurate than they would ever hope to be in a steady flow problem. So, what I am suggesting is that I do agree that transonic flow, if we could do it, is very important. One has to realize how much that is going to cost. And I put quotations around the word "cost", because I don't mean just money. I mean our ability to understand our results and our ability to obtain results, including the fact that we would have to do separate calculations for every single set of parameters, every single case would have to be investigated as a separate topic, possibly numerically. So, that is a cost in our ability to understand the results.

Dr. Robert Truitt:

I would like you to comment also on the compatibility of the best aerodynamics we can do. How do you feel about that as far as the noise is concerned?

Dr. Sheila Widnall:

Certainly the work that Harry Sternfeld and Boeing are doing shows that if you want to fly that tip at Mach numbers close to one, you might as well design it from Mach numbers close to one. Now nobody would ever design jet transport aircraft with straight wings to fly at Mach .92. There is technology in that field. Certainly supersonic or swept wings utilize planform shaping, and certainly the helicopters ought to take advantage of it. That's going to be rather slow in coming because it has to be done very carefully, but it's a direction in which to go. I do agree with you that if you do have an efficient tip shape from

the point of view of drag and performance, then I intuitively feel, as you do, that it will be more efficient from the noise point of view. Boeing correlations with critical Mach number of the airfoil section and the onset of very high impulsive loading and high impulsive noise certainly bear that out.

Dr. Fred Schmitz:

We, at Ames, have a group now doing transonic aerodynamics quite actively and the unsteady problem in particular. We are doing both theoretical and theoretical-numerical computations; that is, doing the full-blown problem. We hope to run some experiments within the next year in the wind tunnel on various operating conditions. I'm not an expert in the area, but I do know the unsteady problem is being attacked right now. And it's not just the Army; it's the Army and NASA -- a group of about six people who are attacking it. All of a sudden it's a very popular problem.

Mr. Meade Mitchell:

Bob, you triggered a thought that had been playing on my mind through the whole session -- your best shape aerodynamics would probably give you your best noise condition. There's an old adage, you know; "Where there's smoke, there's fire". I've been thinking about this, where there's noise, there's vibration. If we can reduce the noise, I think it will have a great effect on reducing the over-all vibration of the helicopter, and that's of serious concern to us right now from the standpoint of the reliability and maintainability of the machine. So, I think we can relate noise to that aspect. We have active contracts right now trying to isolate vibration or study vibration in relationship to what has been done to the reliability of parts and maintenance on the machine. I know Sikorsky has realized some improvements in their maintenance of the machine using a damper on the rotor. Of course, we can isolate vibrations, but if we can reduce them, the reduction in noise, I think, will have a great payoff too. That is a point I wanted but forgot to make.

Dr. Paul Pao:

I have a comment to make which is not related to transonic flow, but to the question of how you get noise out from a sound source in a transonic flow? In some recent analysis that I have done, I found that in transonic flow conditions with a sound source embedded in it, the local condition due to the flow gives a very serious distortion to the acoustic properties near the sound source. So the correspondence between the sound source and the far field noise are quite different from what we can see from a simple wave equation as was used in the theory. I don't know how much this property will affect the intensity of the noise but certainly it has something to do with the directivity. Transonic flow is, of course,

an extremely difficult thing, but transonic wave equations are easier to handle. So as the first step, probably we can do something in that direction.

Mr. Ronald Schlegel:

Bob, just to reiterate something I have said earlier, but in support of something you and Meade had mentioned. We find that the work we are doing right now and which is in very active progress at Sikorsky to develop quieter and more efficient rotor blades is in exactly the direction in which you're talking. We are using transonic airfoils. We do find that we can achieve very significant improvements in performance with reductions in noise level which are on the order of five to ten pndb in the range in which we're looking. We find from the vibration point of view that, in fact, as you would intuitively guess, when you reduce this separation mechanism and improve your drag characteristics on the blade the vibration levels do improve. Also, we find, in the high speed flight regimes, very significant reductions in control loads. I thinkthat a lot of this work we are doing now is really helping us finally if not to fully understand the problem, at least to probe in some of the correct directions. I'm not sure we really understand many of the mechanisms which are going on, but I think the indications from the research which we're doing are at least heading us in the right direction.

Dr. Robert Truitt:

Would you comment a little more on the optimum type shape that you're using or is that a trade secret.

Mr. Ronald Schlegel:

Well, I think the latter is probably true at this stage. I don't want to talk in detail, and frankly, I'm not qualified to talk in detail about some of the shapes which you're looking at.

Mr. William Nettles:

In the same vein in which Ron is speaking, I would like to point out that there is one thing you must keep in mind. Now, Dr. Whitcomb is doing some airfoil work, and the tendency is to use his airfoil. The helicopter blade section must operate over a very wide range of angles of attack, over a very wide range of Reynolds numbers, and over a very wide range of Mach numbers. Now, when you do that very frequently you find that if you design a blade section that will do one thing for you, make one point better, it makes the other point worse. Some recent work which Boeing is doing produced an airfoil that gives them an increase at low Mach numbers, but with the high Mach number range they have a problem. I don't mean to make a negative statement about what

you're saying because I think this is perhaps the best point being made in this conference. But in considering the comments that have been made, I think it's necessary that you keep this practical problem in mind.

Dr. Robert Truitt:

Do you speculate that you might, if you were smart enough, change the airfoil shape under different operating conditions?

Mr. William Nettles:

You mean actually change the airfoil shape as you fly?

Dr. Robert Truitt:

Yes, perhaps changing the configuration with flaps. You might be able to do that.

Mr. William Nettles:

I would not want to be negative and say no. This is something we don't want to close our minds to. Command is working on what they call a controllable twist rotor, which I find fascinating because it does all kinds of good things like this. And I know you people don't like to hear about that. But we do, in particular with the heavy lift work -- and this work is fascinating because we are trying to do something new, and we do run into this Mach number variation problem and Reynolds number problem. If you could, perhaps, come up with an airfoil change, perhaps it's worth looking at. Let me make one more point. Maybe I shouldn't say this. Dr. Truitt's comments to Sheila Widnall were very good, but then if Sheila Widnall had not done the work she has done, Dr. Truitt could not have asked the questions he asked. Now that's the problem that existed two years ago. Some of these questions couldn't be asked then, because nobody had done enough work at that point to ask it.

Mr. Richard P. White:

We have come a long way over the last three years in terms of vortex noise. I don't know if we've gone so far that we are sophisticated enough in vortex noise and understand it well enough that we've had the privilege of using it for systems studies. I thought that it was pretty good that people are really considering vortex noise. They're concerned with it in terms of flight paths, like Bob Simpson this morning. It wasn't too many years ago that if somebody said vortex noise, they would look at you and say you were out of your mind. It did start receiving some recognition as a serious area that should be understood. If you understand it, you may be able to do something

about it. There are some handy formulas. Ron Schlegel had one that worked pretty well. And Martin Lowson had one. I think the first person I can remember that used it discretely in an analysis to determine what effect it might have on the correlation between measured and predicted was based primarily on how large the rotor loading was. Dr. Loewy and Gene Sadler indicated that even with the simplified analysis they could do at this time, it gives tremendously better correlation at a high frequency in a spectrum. Also, what they determined for one helicopter seemed to apply very well to another helicopter. This led to some things, and I think it was one of the forces that led to the two programs that were sponsored by ARO-D. We heard the preliminary results of those programs yesterday. All the data have not been analyzed yet. I think the session that I had the privilege of chairing was fortunate in that it covered a wide spectrum, with some very basic research being reported in which conditions were painstakingly controlled. One controlled experiment not truly representative of all aspects of a rotor in its natural environment was work recorded by Jim Scheiman. Then we went through the full gamut of looking at the importance of vortex noise as determined from the machine we call a helicopter, working in its own environment. I think that the spectrum we have covered in this session pointed out something very interesting and something that shows a need for detailed analysis. I think the basic programs that were conducted under ARO-D sponsorship had a primary objective of doing controlled tests to demonstrate and show, hopefully conclusively, that from an airfoil type lifting section, discrete vortex shedding of the Karman vortex street type did exist and also to determine some of its basic characteristics. I think generally that those programs, within the analysis of the data that has been accomplished to date, have indicated that it does. At the same time these programs are going on, there are other investigators who have been doing some work making some measurements that have also indicated a discrete shedding on an airfoil does exist. There has been work at M.I.T. and by Dave Smith from the Air Force on the sail plane work.

It was very impressive to hear those tapes. When you come to that discrete tone, they can pick up a sail plane a quarter of a mile away. Robin Gray's very recent report with Allen Pierce indicated the extent of the noise that might be obtained by an airfoil shedding vorticity. The results of the two programs sponsored by ARO-D are somewhat preliminary because the investigators have not had the opportunity to analyze all the data they obtained. As for UARL, they are still obtaining some data. But I think some of the conclusions that were drawn or indicated yesterday are interesting to note again. There is an indication that there is a pure tone. There is indication that there may be more than one pure tone. But the frequencies associated with these tones are not what we expected. They are much higher, and they seem to be associated with the weight thickness rather than airfoil thickness. Dr. Sadler reported that in the work

he had been looking at there is some indication that the pressure fluctuation at these pure tone frequencies were correlated across the entire span of both the two-dimensional and the three-dimensional models, but they were not in the wake. That's puzzling. He also indicated in the figures he showed us that the models seemed to be vibrating at the same frequency as the pure tone, but the force output from the model through that vibration was not nearly sufficient to be the noise that was measured. Just possibly, then, that small oscillatory pressure might have correlated all the somewhat random effects we might have gotten from the shedding. It also indicated that the primary dipole associated with this is in the lift direction, not in the drag direction. We have had an indication that the laminar boundary layer associated with the pressure side of the airfoil might be one of the controlling aspects of the vortex shedding. As I've said, these are somewhat preliminary results the two investigators reported, and I think that when they look at the data in more detail and more extensively, we'll probably find other and more interesting things. I think the comparison of some of the data in results that were obtained from the basic controlled experiment to the controlled experiments of the rotor system to the somewhat uncontrolled experiments associated with a real life vehicle might shed an interesting light, and may be where we don't understand things.

I'd like to refer to the slides presented by Jim Scheiman. I thought what he showed here was very interesting. The indication from both the circular rotor and the lifting rotor with a microphone on the axis of rotation was that a peak output of the acoustic pressure occurred at roughly the same frequency. The db level from both of these is approximately the same. This is interesting because most Karman vortex-street shedding investigations have been associated with rods. I commend Jim for giving us this base point to work from. The characteristic dimension of the rod in its shedding is its diameter. If that be the case, and it seems to correlate very well, then I get the same frequency with the lifting surface. You can get strong indication that the frequency that was measured here was associated with the thickness of the airfoil and not the weight. That is different from what we got from the basic experiment with the fixed wing or models in the wind tunnel.

Another slide that Jim presented showed a lifting airfoil. The measurements made on the axis of rotation and measurements made in the rotor point showed tremendous correlation in the lifting point in the axis of rotation. This is associated with measurements of vortex shedding in the lift dipole. He didn't quite show that in the rotor point. But it did show one thing: there is about 20 db difference in the peak levels, which indicates that the drag dipole is much weaker than the lift dipole. This apparently compares with the observations and conclusions reached for the isolated airfoil in the non-rotating flow field. Then Jim threw us a hooker. It was pointed out yesterday that this might be affected by the doppler effect.

The oscillatory signal seems to peak in magnitude at the frequency that has been associated with vortex shedding. I think there are a couple of reasons for this. Even a circular rod can generate lift if it is in a sheared flow. If you have an oscillatory sheared flow created by the vortex shedding and quite possibly the lifting surface, that is why the lifting surface could develop an oscillatory lift. The circular rod could not, possibly because of the characteristic dimension of the airfoil versus the rod in the sheared flow. The wavelengths are about right to be magnified by the airfoil section. Also, in the picture of the experiment that he showed, the flow was over the motor, over the strut and into the rotor. The induced flow that I might have had with the turbulences that Sevin Wright showed yesterday could cause a pressure to be developed. This might be coming from the oscillatory pressures that are developed by working the shear flow or possibly slight interactive turbulence over the strut that excites one of the natural modes of the model. Due to the doppler shift as it goes around in the rotor plane, we see a spectrum like this. There might be a reason for it. I suggest that he ought to take a look at his data to get some information on this. I don't think it is a problem of concern in terms of vortex shedding and lift. He also noted in his paper that tip shapes did not seem to have much effect. Does this indicate to you the possibility that maybe the maximum output of the noise is not associated with the high Q area? This is something that you intuitively don't expect.

There is indication in the measured data when you get all the other types of noise sources out, that the basis of vortex shedding as an important noise source is there. The papers that were presented in this session and the data that was given to us to review and analyze raise a very serious question. Generally you first do a basic, well-controlled experiment. You are given the results and analyze and understand everything that's going on. I think from the differences that we have seen between static-type rotor tests and free rotor tests, compared to real basic experiments, there seems to be too many areas of disagreement to get the meaning that we need to support ourselves in analyzing vortex noise associated with real life systems. I thought this was a very good session. We have learned a lot. From what Kevin Johnson presented, there is a strong indication that a semi-empirical method can be devised which encompasses all different types of noise and which can be used for prediction of helicopter noise of a given configuration, given the basic parameters. That's not the first time that a semi-empirical analysis that's related to basics has been able to do a very good job. But I think we have a long way to go yet before really understanding vortex noise, and I'd appreciate getting your comments along these lines.

Mr. Harry Sternfeld:

The comment I wanted to make, hoping maybe it will trigger somebody else's thinking, is that one of the things that's vexed me involves blade slap. I'm using the very general term, but I'll say specifically tandem, although the frequencies aren't very different when we get it on our single rotor tower. We get harmonic spikes. They have an envelope and they peak right up at around the same frequency that we usually associate with vortex noise. There was no lift so there shouldn't have been a vortex. In addition, that frequency doesn't seem to move around very much if we make an airfoil change or something like that. So, my comment is that the characteristic that was shown by Schieman is very similar to the characteristic we see when we get through harmonic analysis.

Mr. Richard White:

As most of you know, I'm a proponent of vortex noise. I'm glad Harry made the initial input here, and I think the work of Robin Gray is pertinent to what he is saying. What is wrong with saying, or assuming, that a Landau shock on the blade causes separation? Can I not possibly feed in that characteristic? If I get near stall, can I not get the same thing? Robin Gray indicates that maybe you can. I'll explain any noise in terms of vortex shedding, so let's keep an open mind.

Mr. Ronald Schlegel:

What I'm going to say is an open question relative to shock formation. We concluded that the formation of a local shock on the blade itself, in relating the phenomena of the acoustic dissipation to the impulsive noise in the far field, was not an important factor. However, our impulsive noise study did conclude that blade drag and drag divergence formation was very important. The work we are doing on the full scale model tends to show that for a transonic airfoil as you move the shock formation on the suction side of the blade back, you stabilize the shock. Then, in fact, the noise does go down. I wonder if anyone here has given much thought to the acoustics of the oscillating shock. In other words, what are the acoustic characteristics of the oscillating shock? What does this do to the subsequent turbulence and loading on the rest of the blade, and is the stability of the shock formation important acoustically?

Mr. Chris Bobo:

That is exactly the mechanism we are using to define impulsive noise. The vortex interaction is the trigger for moving that shock wave, and if you think of it as an impulsive change in Mach number or angle

you get, therefore, a pulse in that shock wave position. And that pulse radiates to the acoustic signal.

Mr. William Nettles:

I'm not speaking on this particular topic, but on an earlier topic that Harry made. Perhaps what I'm going to say isn't too terribly pertinent but in preparation for some of the testing we did to get you the data for your vortex noise work, we went over to West Point, Virginia, which is a very quiet area. It is a deserted air field. We did some preliminary noise measurement and when we evaluated what we got, we found that there was an unusual spike in the spectral analysis data. After further evaluation we found that it was a dog barking in the distance. Now, if I find anything in the future that comes at that particular frequency, I think I'll say maybe it's dogs barking in the distance. I have some reservation in drawing conclusions too quickly based upon that one experience. I disagree with some of what Jim said. I disagreed also with some of what Harry showed yesterday. He showed some work relative to blade-vortex intersection which was particularly interesting and was left unanswered. I recommend that we try to leave these questions unanswered until such time that we have a thorough review of what we have and a rigorous explanation.

Mr. Peter Arcidiacano:

It seems to me that it's possible that one path of speculation might indicate that there is no vortex noise: that a well streamlined body operating in turbulent free air may not, indeed, generate any vortex noise, particularly if one includes such things as surface roughness on the airfoil to perhaps eliminate the pure tone that we did observe under very specialized conditions. Certainly in the high Reynolds number ranges and even up into stall, the pure tone did disappear in this turbulent free environment. I wonder, and I'd like to suggest that perhaps a lot of what people have been calling vortex noise may in fact be turbulence generated noise.

Mr. Richard White:

I refer to the data that Dr. Sadler was analyzing which we obtained in your tunnel. We talked about this high frequency, and I had them try to generate some turbulence. They put a tripper on it. It didn't do anything. I think I have to take exception to some of what you say. However, we hope that the data that we are getting and that we, as well as you people, are analyzing will give us information to better understand what I am calling vortex noise in a rotor blade. We get very strong indications on controlled rotor tests that this is in fact there. But it does not correlate with what we are getting with our fixed wing tests.

Mr. William Nettles:

I refer to Jim Scheiman's work. With air flow, it appeared that the spectral character of the rotor was definitely changed. Instead of having that hump associated with vortex noise, we had almost a concave signature except for that one little peak, which Jim says he doesn't believe. So, I can view that as saying that turning the air on removes the wakes from the other blades, reduces the turbulence encountered by the blades and there is no vortex noise.

Dr. Sevin Wright:

One shouldn't say they believe or don't believe in vortex noise. I think first of all we should discuss what we mean by vortex noise. The sound that radiates in the upper frequencies is usually referred to as vortex noise. I think we should remove that word vortex and talk about the noise in the high frequencies. Both mechanisms exist. What you call vortex noise, I would prefer to call blade self noise - noise generated by the blade operating in clean flow conditions - that minimum noise you would get from an airfoil. The purpose of the demonstration yesterday was to show how you can increase that minimum self noise. We run the rotor in free air, no obstructions upstream, no crosswind, no blowing, and the rotor noise was minimal. As soon as we made any external disturbance on the blade, the rotor noise went up. If you look in a propeller spectrum, or a helicopter spectrum, in the high frequencies, you will find a proportion of broadband noise which I think most people credit to the shedding mechanism. It would tend to be random and would give a random output, and therefore the spectrum would be continuous. But any kind of asymmetry in the loading will produce rotational noise and a discrete spectrum. If it is periodic, then it will be discrete, or as the last speaker indicated, if the inflow in wrong, if it's incoming turbulence, then that will give rise to an increase in the broadband noise. So, it's not an argument about whether it exists or not - both forms of radiation exist. The argument really is how much of which dominates. In the absence of obvious external influences, then I think your self noise is the dominant feature.

Mr. James Scheiman:

I agree with the comments of Dr. Wright, and I think the problem is more of terminology. For example, von Karman described airfoil drag with vortex streets. If you associate vortices with airfoil drag, then fine. Also, in case of lifting on the airfoil, if you take the starting and stopping shed vortices and say that they radiate noise, and then put fluctuating lift on the airfoil, and then put fluctuating starting and stopping vortices, and if you believe Prandtl's theory, then I think it's hard to separate. You are describing the same phenomena by two different mathematical techniques. What you mean by

vortex noise is what it amounts to, I think. The other comment I have is that in addition to the testing that we did, we put some transition strips on the airfoil and we definitely had separation. These transition strips were directed towards changing the airfoil characteristics. I think it was published in a NASA-TN, which came out just a few weeks ago. But the strips caused an increase in the airfoil noise and there still is a peak in the radiation pattern. One of the problems that is bothering me right now is in the 2-dimensional testing. Why is it this has the discrete radiation whereas in 3-dimensional testing where the Strouhal shedding frequency is different along the full span, we always get one predominant frequency shedding? Why isn't it more broad? What radius dominates the other radii in determining the frequency center? Why is it that with a transition strip in it, definitely creating turbulent flow, we had a center band frequency, whereas from the 2-dimensional tests that were performed, evidently with transition or turbulence on the airfoil, there is no discrete frequency. I think these are all questions that will require further investigation.

Mr. Richard White:

I would like to take this opportunity to thank all the authors in my session for their work in preparing these papers, and in presenting them.

Aerodynamic Test

Professor Rene Miller:

Well, we'll try to sum up. I think maybe I'd like to go back to our meeting of 1968 and remind you of a curve that I showed at that time, which I think emphasizes the importance of test in the evaluation of helicopter rotor noise. This slide shows the penalty that is paid for producing noise based purely on test results. It's based on Sheila Widnall's data. It tells you that as you reduce the tip Mach number you're going to get a penalty in performance and that the main reduction in noise is going to come from reducing rotor tip speed. I think we have to bear in mind this basic problem which we have is just to cut down rotor noise. I think Colonel Buchan made the point very clear last night that we can't wait for very refined theories: we have to do something about rotor noise. There is a limit to how far you can go in reducing rotor noise by reducing rpm. This limit is actually a limit due to the geometry of the rotor. Only a certain number of blades can be put into the rotor before the weights go up asymptotically. So far we really have nothing in the past two days which indicates that we have a real means of reducing rotor noise

other than reducing tip speed and increasing the number of blades, and, of course, playing around with the separation of the rotor to reduce the impulsive noise. We should not be concerned with trying to differentiate between vortex noise and periodic noise, but should try to concentrate specifically on the problem of how to cut down the noise. So far, the only tools we have are from test results. Consequently, I think that the papers that were presented in this session on the aerodynamic test are of particular significance. I would like to draw your attention to one item which you can also see by looking at the data. The test data for rotational noise presented by Boeing and Sikorsky both show about a 10 db error between the calculated and the experimental data. The problem that we are up against is that we really have no techniques at the present time for predicting rotational noise. This is primarily because of our lack of knowledge of the high frequency content of the rotor. The paper by Sevin Wright contained the interesting statement that, as I interpret it, given the periodic forces, you can predict the noise. However, we all realize that these forces are not yet given. The paper by Harry Sternfeld showed a fascinating problem which is associated with the lack of bang at vortex interaction. A follow-on paper by Bobo on the effect of drag rise on triggering this slap was an interesting and original contribution. It would be interesting if Harry would expand his paper and play us a tape showing how, by these straightforward things that I mentioned, he has succeeded in achieving an appreciable noise reduction.

Mr. Harry Sternfeld:

I am sure you will all recognize that this is extremely spontaneous. Professor Miller and I had discussed this and we thought the two things which this tape illustrates are: (1) we've got to produce now, and (2) we know that better can be done, but we can't wait. You've heard a lot of reference to the 347, a Chinook derivative, throughout the meeting by other speakers. There will be three steps in each of these sound tape sequences. The first is the original Chinook, the A model, which had absolutely no concession for noise reduction in its design. The performance and production costs were the driving parameters. Then we came to the C model and found out that if we adjust the rotor tilt we can make improvements, particularly at high forward speed. So, the C model has different blade vortex separation. The 347 was made from the Chinook, but reduced rotor noise and elimination of rotor bang were primary program objectives. We made the aft pylon 30 inches longer and we made the fuselage 110 inches longer. That got us blade vortex separation. We put a 4-bladed rotor on it and slowed the tip speed down from about 720 to 650 feet per second. The first set of tapes is in the sequence of first the A, then the C, and then the 347. We will hover, fly at 50 knots, 120 knots and 167 knots on the 347. One of the places where the problem is not solved is in hover. The

microphone on the fly-bys is 200 feet on the right side of each aircraft. The microphone in the hover is at a 200 feet radius at the azmuth of the worst impulse noise. This azimuth changes and we can relate it to the position of the blades in the vortices. (The tapes were played and noise reductions were evident.)

Professor Rene Miller:

I think these tapes are very interesting. The need for these test data is extremely evident - we need tests badly. However, this doesn't downgrade in any way the need for theory, for unless we have the theory and analyses we really don't know what we are testing.

I had to cut the discussion off yesterday at several places. In the paper by Sevin Wright we were in the midst of discussing the classical topic of "Can the rotor noise be entirely described by periodic forces?" In the second paper, I think there was sufficient discussion unless you want to comment on the tapes we heard this morning. The third paper was an interesting survey by Barney McCormick on his work. He showed a comparison between the simplified theory and the test. These simplified theories are always attractive as a means of understanding the phenomena with which we are dealing. The discussion ended on a question as to how important the angle of a dissection was. The fourth paper that came up was by Mr. Schlegel. Now, let's continue yesterday's discussion.

Mr. William Nettles:

With regard to the data that Harry just showed us, and I'd like to address this to Sevin Wright in particular, there are two ways that Mach number can get to us. They are perhaps dependent, but they could be called quasi-independent, whatever that means. One is in the compressive effect on the aerodynamic noise source. The other is the compressibility effect on the propagation of the noise. I believe these two are essentially independent. If my contention is correct, does Dr. Wright think the increased tendency toward popping as Mach number was increased was the result of the propagation effect or compressibility effect over the airfoil itself?

Dr. Sevin Wright:

I think there were three Mach number effects there. One is the source strength or the effect of aerodynamics. Then, the effective Mach number affects the radiation cancellation mechanism. Thirdly, the effective Mach number affects the directivity and also the sound power radiated through the doppler effect. So, there are three points there.

Mr. William Nettles:

Mr. Sternfeld's tape seems to show an increasing popping characteristic when you increase the Mach number. My question concerns the cause for this.

Dr. Sevin Wright:

I think it's basically the source, the fact that it increases the intensity of the magnitude of the fluctuating lift on the blade. This increases the radiation, therefore, increasing the popping sound.

Dr. Richard Lyon:

I have to take issue with that, at least in terms of our calculations. Our studies of the effective radiation of the tip due to thickness and lift effects simultaneously have in them, explicitly in the analyses, the effect of the changing speed on the source strength and the effect of the changing speed on the radiation efficiency, which is what Sevin meant when he said the cancellation effect. Now, it's very clear in our calculations for acceleration of the blade near Mach 1 that the radiation efficiency effect far outweighs the effect of fluctuating lift or the fluctuating sources due to volume displacement on the blade. These come out as explicit terms in our analysis. We can compare one against the other and there is no question that for accelerations near Mach 1, the radiation effect is far stronger than the source strength effect. You have to evaluate the source strength at the point of maximum radiation, it has that effect, but the fact that it fluctuates in strength near that point of maximum speed does not have an effect. It's merely the acceleration and deceleration of the blade.

Dr. Sevin Wright:

I agree with you if it's a point source and you're talking about steady forces. Near Mach 1 these things tend to dominate. But I think blade slap is a particular case where it's a very local region in the disc that radiates. You can almost treat it as a stationary problem, because the blade slap impulse is not to be regarded as in motion. The point at which it occurs is a particular point in the flight path and it's not as though you're treating the problem as a constant source in motion. It only occurs a few milliseconds for each blade revolution and so the stationary approach would give you this effect without any cancellation.

Dr. Richard Lyon:

The directivity, itself, denies that assumption, because you cannot have directivity from a point source that is strongly leaning forward. It takes, in fact, a convection effect which means that the wavelength

must preserve itself over several of its own lengths in order to get sufficient coherence along the flight of the source in order to radiate directively. So, the fact that you get for the thickness effect a solid cone of only 10 degrees and for the lift effect this double cone, but still within a beam width of about 15 degrees, itself means that the source must be important over about 3 or 4 wavelengths at the frequencies you are considering. You cannot have directivity unless you have a source that is extended in phase. Now, it looks like a point source when you take a picture of it but it must preserve itself over some distance in order to have that directive effect.

Dr. Sevin Wright:

Have you measured these directivities for impulsive noise, such as blade slap? Have you shown that the dipole is in fact pushed forward? We are familiar with this idea that in forward flight, the directivities move forward. I'd like to ask Harry Sternfeld about the directivity of the recordings we heard this morning. I have not heard many tandem rotors banging but on single rotors the directivity is always pointed forward. In other words, you hear the banging on approach and it ceases overhead. And that was the point where Jim Scheiman cried "vortex noise". We heard the banging and as soon as the helicopter passed overhead the banging ceased and, in Dick White's terminology, the vortex noise was audible. The way I see that is, if you think of a simplified model of a dipole produced by this very localized loading in the disk, this dipole will be tilted, depending upon the angle of attack, and so on. You can explain this very nicely if you assume that the dipole, particularly on a single rotor, is tilted forward as a function of the blade angle of attack. The lower lobe of the dipole will be pointing forward and the upper lobe will be pointing up in the air, so, you will only hear sound in the forward direction.

Dr. Richard Lyon:

A dipole that is tilted forward has a directivity index of 6 db and I think the directivity is stronger than that.

Dr. Sevin Wright:

Along a line normal to the dipole, the radiation is 0, so you have an infinite number of db's from right angles to along the axis of the dipole.

Mr. Harry Sternfeld:

I have two pieces of information to impart. First of all with respect to directivity, if you listen carefully or if you look at a stripout of the tape as the aircraft approaches in the distance you would see

that with a tandem rotor the number of pulses is twice the blade passage period of one rotor. As the aircraft gets close to overhead but is still on the approach, you will hear that period halved. Then you can hear the squish which may be vortex noise or modulated engine noise. The length of time that the single rotor noise exists correlates quite closely with the time it takes the aircraft to travel the distance between its two rotors. So the noise is very strongly radiated forward and in the distance we're seeing it coming from the two rotors, then we have a period when we see it coming only from the one rotor and then it goes away. The other point of information I wanted to supply was that if we plot the sound pressure level against Mach number, look for a knee in the curve, and then we plot those, the shape just about follows the drag divergence curve for the airfoil and seems to be in the vicinity of Mach 0.5 to 0.6 or higher. The shape appears to be very strongly associated with the divergence curve.

Mr. James Scheiman:

I'm not sure the distinction between vortex noise and rotational noise is really clear. For example, I think Loewy and Sadler, in their theory in which they try to describe a vortex noise, show there is fluctuating lift force at the rate at which von Karman vortex streets are shed, and there is a fluctuating drag force which is twice the frequency of the fluctuating lift force. Prandtl described the whole lift on the airfoil with his lifting line theory. Now, if we say we're going to use lifting line theory to describe the lift forces on a blade or the fluctuating lift forces on a blade, then the problem is one of using the vortices to describe the fluctuating pressures on the blade or is one of using the fluctuating pressures on the blade to calculate its noise. I think we're both trying to solve the same problem, looking from different directions. I think it's wrong to say it's all vortex noise or it's all rotational noise. I don't think we understand enough about it and I think vortex noise terminology is a poor choice.

Dr. B. W. McCormick:

You mentioned that in order to predict the impulsive noise we would need to know the shape of the pulse which is producing this. I think here is an area where we need some further testing. Nobody really knows the shape of a vortex coming off a rotating blade at high Mach numbers. There haven't been any measurements. Somebody should give some thought as to how to obtain a velocity field through a vortex coming off a rotating blade at fairly high Mach numbers. Also, let me mention the effect of the intersection angle where Dr. Widnall and I seem to have a disagreement. She said at the lower values of intersection angle she obtained a higher noise level. I said that at the lower angle the pressure differences across the section tended to decrease. In the lower angle intersection case, the entire blade

is being influenced at once by the vortex and even though you may have smaller differential pressures, the noise level could certainly be higher in that case. So I'm not sure there is really a disagreement.

Mr. Ronald Schlegel:

I think in our rush yesterday we missed a few points in the study which we had conducted. I'd like to take a few minutes to hit some of its highlights. This study has just been released by AVLABS as Technical Report 70-72 of June 1971. It's a rather comprehensive study and I think it has some good data in it. As a matter of fact, it asks a lot of questions and doesn't necessarily answer as many as it asks. We were looking at rotor impulsive noise (RIN) as an impulsive noise. I want to point out the purpose and intent of the program. We had a program which was being conducted on the CH-53A to measure rotor loads. A blade that was very well instrumented with surface pressure transducers both chord-wise and radially was used. Since this is one of the few aircraft that we built that we have been able to experience rotor impulsive noise on, it offered to us an opportunity to study this phenomena. We contracted with AVLABS under the direction of John Yeates to conduct this study along with the loads study. It was really a 3-phase study. It included measuring noise concurrently with measuring the loads on the helicopter and also at the same time conducting some inside measurements of the noise generated. The second phase was a data analysis phase in which we looked at the data with greater detail than we had before. All of the data was reduced using real time analyses. We saw some things which we had never seen before, such as the fact that has been brought out today by many people that rotor impulsive noise is a manifestation of rotational noise. In other words, it is periodic noise. By doing real time analysis we are able to see that it was very ordered noise, extending well out into the 400 - 500 Hz regions. We were also able to determine that the types of impulsive noise which we got, at least on the CH-53A type of helicopter, were different for hover and cruise conditions. The hover rotor impulsive noise is more associated with blade loading vortex interaction and the cruise noise was extremely directional in the forward plane of the rotor, indicating the probability of blade Mach effects as well as profile drag. We did some modifications to our acoustic analyses which included blade motion terms. One of the things which we also tried to show was whether with this acoustic analysis we could even approach the prediction of rotor impulsive noise. We got some qualitative agreement. We found that without the inclusion of the drag and the source translational terms for the forward flight case, where we started getting into rotor impulsive noise, that we were not capable of predicting the highly directional characteristic of the sound nor were we able to predict the level to any extent. In other words, the analysis failed for high speed rotor impulsive noise.

We were not able to predict above the 4th or 5th harmonic for even normal inflow conditions such as hover very well either. As Dr. Truitt mentioned earlier, there is an awful lot of work to be done to gain a better understanding of the higher harmonics of load. Another conclusion was that when we modified the analysis to include blade slapping and coning as steady and first harmonic effects, we did not significantly improve the correlation of measured and predicted noise level.

I would like to recommend as one final thought that we make a concerted effort, possibly through some central committee which may be the AHS or another organization like ASSP, to standardize some of the terminology which we use.

Professor Rene Miller:

I don't think we want to lose sight of the fact that right now the only way to reduce rotor noise is by slowing down the rotor and increasing the number of blades. From the chart I showed, we see that 10 db reduction is going to cost 20% - 30% increase in gross weight. You can tolerate that on a commercial vehicle because direct operating cost doesn't change much with gross weight for many reasons. We obviously can't tolerate it for military aircraft. The important thought I would like to leave on this session is that what we need right now more than anything else is not so much a better definition of the terms, but more tests which give us other tools than cutting down the rotor speed, such as blade tips and revised loading distribution on the blade, to reduce noise. Much of the work that is going on now on non-rigid weights will give some indication on how to do this. We need more tests and more theory on how to interpret these tests, but we have to find some other way of reducing noise than just reducing tip speed. I think it is important to recognize, too, that we have other vehicles than the helicopter coming along, which have entirely different noise characteristics. I'm thinking of the tilt rotor and the tilt wing. We do have to get test data to try and get a better handle on how to reduce the noise.

Environmental and System Studies

Dr. Franklin Hart:

Let's briefly look at the section on environment and systems studies. One item early in the program was identified as detectability and annoyance. There were three main sections under that heading. One was ground and environmental attenuation in masking, utilizing existing theories. The types of recommended tests involved were field tests to be made under different environmental conditions involving troops and aircraft. Another area was strictly subjective response and a third was criteria. Under the heading of systems analysis, the

topics were vulnerability vs. noise reduction, management of effectiveness of noise reduction and development of Army criteria and the penalties involved. I think you can see, based on what we had in this combined session, that this area is perhaps lagging in terms of total effort being given to all of the areas that have been identified as being prominent. Particularly, we are talking about annoyance and detection, and these things are not the same. Which should you give priority to? I am not sure we have gotten to the point here where we can really ask all the right questions.

The first of the three papers presented was given by Bob Simpson. Here he was talking about direct operating costs vs. noise and procedures for achieving operational reductions. He utilized the term vortex noise. He did have an analytical term there that he could put into his program, and I think we should keep in mind that that was the essential point. Also, I believe he indicated that on the data he used the annoyance, the PNL, was something like 10 plus the sound pressure level. This is a very restricted look at the total noise of the aircraft. This is certainly no criticism because all of these things can be built into the model when he has the right analytical predictions techniques.

In the second paper, Pao covered sound attenuation over simulated ground cover. He showed that there were selective frequency bands where you get more attenuation. The discussion following the paper started on the fact that he used a simple source and how these predictions change if you use a more realistic sound source, as for example a helicopter.

The last paper, by Dr. Evans, was on atmospheric absorption of sound. Nitrogen was identified as a more important part of the absorption than previously reported. It was also pointed out that some of the people working in the field would like to have the data cover at least one additional octave band beyond what he had in the paper. Also, he discussed how he is going to bring temperature into the atmospheric absorption picture. The problem of human factors, which we like to think about in systems has received little attention here. This area of environmental considerations and systems analysis is not receiving the effort that some of the other areas are. Now, I think it would be well to ask for points of discussion on Bob Simpson's paper.

Dr. Richard Lyon:

You pointed out that there are loudness criteria and there are detection criteria. If we do achieve V/STOL aircraft at perceived noise levels of 95 db at 500 feet, that means that at a quarter of a mile away they are in an urban background noise. Perhaps the proper question then is one for criteria. That is, maybe you can

detect it but can you classify it. I bring that up because there is a very interesting set of tapes by Hamilton Standard on the DHC-7 flying past at a distance of, I think, a quarter of a mile in the presence of urban background. There is a freeway nearby, and when the DHC-7 goes by, it is clearly audible but it sounds like a truck. That is, if you don't know it's there you cannot tell that it's an airplane. When we begin to get these aircraft quieter, from a commercial point of view the criteria may include classification.

Mr. William Nettles:

The fact of the matter is that detection is a problem. But as far as the Army is concerned, I think they are beginning to realize that the man working around a helicopter, the man flying in a helicopter, whether he is crew or passenger, must be thought of as well. I believe the Army is beginning to recognize this as more of a problem, particularly when they are working on something like the heavy-lift-helicopter where men will be working on the ground below the helicopter. One of the interesting points is that anything that you do to quiet in the detection end will probably help you in the other end as well. So I think the Army is giving consideration to this other problem.

Mr. Richard White:

I'm going to use this last session and Simpson's paper as an excuse to say something else. What we have been working on is getting rid of the problem area of the tip vortex. We have been notably successful is small model experiments and have obtained almost negligible degradation of performance. We are going to test a large tip section of the HU-1-D blade. If we are successful with the full scale blade section, we hope this can be followed by a whirl tower test, running under conditions of rotor blade slap to demonstrate that we did get rid of the high induced effect because we have gotten rid of the vorticity.

Mr. Harry Sternfeld:

I just want to read into the record that Langley is doing quite a bit of work in the Human Factors area. They are sponsoring Sikorsky's program on vibration and noise on pilots. We have been involved in programs on subjective response to V/STOL noise and so have other people. So there is an agency which is working on this in conjunction with the Army and independently. This should be at least recognized.

Mr. Richard Lewis:

We, at the Aviation Systems Test Activity, are conducting a very comprehensive series of tests in conjunction with the people at AVLABS,

in which we are going to be measuring in-flight vibrations on all of the fleet aircraft. We have also done some work of great importance to the Army on the effect on crew environment during weapons firing. I think you know that most of the aircraft are flown with doors off. We have measured sound levels on the OH6 during firing of very small weapons (the 5.56 and 7.62) in excess of 150 db in the cockpit. This is another area that may be of great interest in the future.

(Call for discussion on Ground Attenuation and Atmospheric Absorption)

Dr. L. B. Evans:

I would like to comment that when you try to correct your data and use our curves, be aware that these absorption coefficients are plotted as a function of frequency over pressure. For an extreme case, a half atmosphere pressure of 1000 Hz signal gets absorbed like it's 2000 Hz. If it's low humidity, this can make as much as 5 or 6 db per 1000 feet. If I am going to put out this interim report and set of tables, I would like to be sure that I have the coefficients and type of units engineers would like to use. So, let me know if anybody wants anything different from db per thousand feet. Another question. We've heard a lot about helicopter noise, but nothing about the infrasonic spectrum. Is it important? Does a helicopter put out 1 Hz signals? The reason I ask this is that Harry mentioned you could hear this one helicopter five miles away. If it puts out an infrasonic signal, you might be able to hear it 20 miles away. Does anybody have any information on this? Is the Army even interested in this type of detection? Does anybody know what the spectrum might look like?

Mr. Harry Sternfeld:

We certainly have the blade passage period, which is, if you like, infrasonic, depending on the aircraft it could be 10 Hz. So there's certainly that fundamental which falls off on the audio range. I can't speak below that - I don't know if anyone can. But certainly fundamental blade passage periods of the order of 10 - 15 are very common, so it's not unimportant.

Dr. L. B. Evans:

Very recently I have seen data from White Sands Missile Range detecting a cannon shot 47 miles upwind, and to me this is rather remarkable. They are looking at 1 Hz signals. Also, at Ft. Monmouth they detect the Saturn V first stage when it reenters the atmosphere about 1500 miles away. Again, it's 1 Hz type signals. So, perhaps there is a long range detectability factor here that we could look at.

Mr. Richard Ballard:

I would like to thank the session chairmen and others for their participation.

Mr. James Murray:

I want to thank you all for participating. There has been some suggestion that there be a follow up meeting of this nature. Any suggestion of this within the next year or two year's time is entirely dependent upon the productivity of you people, and the efficiency with which you do the work in question - whether you think it would be satisfactory to have a meeting two years from now or three years from now, ten years from now or six months from now. Any suggestions as to where it should be, how it should be or when it should be?

Dr. Sheila Widnall:

What is the relationship between this meeting and the Theme reviews that you have?

Mr. James Murray:

This is more specialized. We have over 30 projects in the helicopter area, of which this is a component part representing about 8 or 9. We'd rather break it up because it gets a little too specialized. After all, you've had four sessions here. I'm afraid the other two-thirds of the investigators in the program might not find it attractive. We would be running double sessions and I don't think we are in a position to do that at this time. My suggestion is that the next meeting should be hosted by the Ames people if they are so inclined. In that way, their people out there could participate a little bit more directly.